

Design and implementation of a bacterial signaling circuit

Milena Dimitrova Lazova

The work described in this thesis was performed at the FOM Institute AMOLF, Science Park 104, 1098 XG Amsterdam, The Netherlands. This work is part of the research program of the Foundation for Fundamental Research on Matter (FOM), which is financially supported by the Netherlands Organization for Scientific Research (NWO).



© M. D. Lazova, 2013

ISBN/EAN: 978-90-77209-71-4

A digital version of this thesis is available at www.ubvu.nl/dissertations and www.amolf.nl/publications/theses. Printed copies can be obtained by request to the library at FOM Institute AMOLF, library@amolf.nl.

Cover design by Nickola Nickolov.

Printed by CPI Wöhrmann Print Service(WPS), The Netherlands



VRIJE UNIVERSITEIT

Design and implementation of a bacterial signaling circuit

ACADEMISCH PROEFSCHRIFT

ter verkrijging van de graad Doctor aan
de Vrije Universiteit Amsterdam,
op gezag van de rector magnificus
prof.dr. F.A. van der Duyn Schouten,
in het openbaar te verdedigen
ten overstaan van de promotiecommissie
van de faculteit der Exacte Wetenschappen
op dinsdag 11 juni 2013 om 11.45 uur
in de aula van de universiteit,
De Boelelaan 1105

door

Milena Dimitrova Lazova

geboren te Sofia, Bulgarije

promotor: prof.dr. P.R. ten Wolde
copromotor: dr. T.S. Shimizu

To my grandmother

This thesis was reviewed by:

prof.dr. K.J. Hellingwerf
prof.dr. V. Sourjik
dr. Y.J.M. Bollen
dr. R.T. Dame
dr. Y. Tu

Publications covered in this thesis:

Lazova, M. D., Ahmed, T., Bellomo, D., Stocker, R., and Shimizu, T. S., Response rescaling in bacterial chemotaxis. *Proc Natl Acad Sci U S A* **108** (33), 13870 (2011).
(Chapter 2)

Lazova, M. D.*, Butler, M. T.*, Shimizu, T. S., and Harshey, R. M., *Salmonella* chemoreceptors McpB and McpC mediate a repellent response to L-cystine: a potential mechanism to avoid oxidative conditions. *Mol Microbiol* **84** (4), 697 (2012).
*authors contributed equally
(Chapter 4)

Lazova, M. D., Menolascina, F., Sontag, E. D., Stocker, R., and Shimizu, T. S., Chemotactic control physiology determines the behavioral strategy of enteric bacteria. (in preparation).
(Chapter 3)

Lazova, M. D. and Shimizu, T. S., Role of the phospho-regulated scaffolding protein CheV in *Salmonella typhimurium* (in preparation).
(Chapter 5)

Lazova, M. D.*, Rosier B. T.*, and Shimizu, T. S., Multiple pathways of cystine-induced repellent responses in *Salmonella typhimurium* (in preparation).
*authors contributed equally
(Appendix A)

Other publications by the same author:

van Hemert, F.*, Lazova, M. D.*, Snaar-Jagaska, B. E., and Schmidt, T., Mobility of G proteins is heterogeneous and polarized during chemotaxis. *J Cell Sci* **123** (Pt 17), 2922 (2010).
*authors contributed equally

Contents

| | |
|---|----|
| Chapter 1. Introduction | 11 |
| 1.1. Environmental sensing and intracellular signaling networks | 12 |
| 1.2. Tactic responses | 13 |
| 1.3. Motility and chemotaxis of enteric bacteria | 15 |
| 1.4. Molecular organization of the chemotaxis system | 17 |
| 1.5. Functional organization of the chemotaxis system | 19 |
| 1.6. <i>In vivo</i> fluorescence resonance energy transfer (FRET) studies of the chemotactic signaling response | 22 |
| 1.7. This thesis | 25 |
| Chapter 2. Response rescaling in bacterial chemotaxis | 27 |
| 2.1. Introduction | 28 |
| 2.2. Weber's law and fold-change detection (FCD) | 30 |
| 2.3. Dynamic range of FCD in <i>E. coli</i> chemotactic signaling | 31 |
| 2.4. FCD in population behavior of swimming <i>E. coli</i> | 33 |
| 2.5. Mechanistic requirements for Weber's law and FCD | 35 |
| 2.6. Invariance of the chemotactic adaptation timescale | 38 |
| 2.7. Discussion | 40 |
| 2.8. Materials and methods | 42 |
| 2.9. Acknowledgements | 50 |
| Chapter 3. Network-level variability in bacterial chemotaxis | 51 |
| 3.1. Introduction | 52 |
| 3.2. Receptor-kinase response in <i>S. typhimurium</i> | 58 |
| 3.3. Methylation-level adaptation in <i>S. typhimurium</i> | 60 |
| 3.4. Network-level adaptation in <i>S. typhimurium</i> | 63 |
| 3.5. Role of CheV on network-level properties of <i>S. typhimurium</i> chemotaxis | 65 |
| 3.6. Differences in chemotaxis performance of <i>S. typhimurium</i> and <i>E. coli</i> in spatial gradients | 67 |
| 3.7. Sensitivity modulation of <i>S. typhimurium</i> and <i>E. coli</i> chemotaxis response | 71 |
| 3.8. Tar-independent MeAsp response in <i>S. typhimurium</i> | 74 |

| | |
|---|-----|
| 3.9. Differences between the Tar receptors of <i>E. coli</i> and <i>S. typhimurium</i> contribute to the different shape of the sensitivity modulation profiles | 75 |
| 3.10. Discussion | 76 |
| 3.11. Materials and methods | 80 |
| 3.12. Acknowledgements | 90 |
| Chapter 4. Cystine-induced repellent chemotactic response of <i>Salmonella</i> : a potential mechanism to avoid oxidative conditions | 91 |
| 4.1. Introduction | 92 |
| 4.2. McpB and McpC mediate a response to cystine and cysteine in soft-agar assays | 96 |
| 4.3. Capillary assays do not show an attractant response to cystine | 99 |
| 4.4. FRET experiments reveal responses of opposite sign to the cystine / cysteine redox pair | 100 |
| 4.5. The repellent response to cystine is mediated by McpB and McpC | 102 |
| 4.6. Roles of McpB and McpC in cystine sensing | 105 |
| 4.7. The attractant response to cysteine is mediated by Tsr and Tar | 107 |
| 4.8. Function of the C-terminal pentapeptide of McpB | 107 |
| 4.9. Discussion | 110 |
| 4.10. Materials and methods | 114 |
| 4.11. Acknowledgements | 121 |
| Chapter 5. The phospho-regulated scaffolding protein CheV affects chemoreceptor clustering of <i>Salmonella typhimurium</i> | 123 |
| 5.1. Introduction | 124 |
| 5.2. CheV enhances the spreading of methylation-deficient cells in soft-agar assays | 128 |
| 5.3. Role of CheV in adaptation to MeAsp | 130 |
| 5.4. Phosphorylation-independent localization of CheV at the cell poles | 132 |
| 5.5. The number of receptor clusters is smaller in <i>cheV</i> mutant cells | 134 |
| 5.6. Discussion | 137 |
| 5.7. Materials and methods | 140 |
| 5.8. Acknowledgements | 144 |
| Chapter 6. Concluding remarks and outlook | 145 |
| 6.1. Fold-change detection in biological sensory systems | 146 |

| | |
|---|-----|
| 6.2. Quantitative comparative physiology of microorganisms | 148 |
| 6.3. Opposite chemotactic responses to a redox pair | 153 |
| 6.4. Phosphorylation-dependent feedbacks in bacterial chemotaxis | 156 |
| 6.5. Acknowledgements | 157 |
| Appendix A. Multiple pathways of opposite chemotaxis responses to the cystine / cysteine redox pair in <i>Salmonella typhimurium</i> | 159 |
| A.1. Introduction | 160 |
| A.2. Dose-response relation of the Tar / Tsr -mediated attractant response to cysteine | 162 |
| A.3. The magnitude of the repellent response to cystine is proportional to the logarithm of cystine concentration | 165 |
| A.4. McpB / C knockouts do not affect the shape of cystine dose-response curve in <i>S. typhimurium</i> LT2 | 167 |
| A.5. The response to another oxidized redox component, benzoquinone, is similar to the cystine response at low concentrations | 168 |
| A.6. The sign of the response to mixed cystine / cysteine solutions depends on their redox potential | 170 |
| A.7. Discussion | 171 |
| A.8. Materials and methods | 173 |
| A.9. Acknowledgements | 176 |
| Appendix B. Comparative analysis of the chemotaxis system of natural <i>Escherichia coli</i> isolates | 177 |
| B.1. Introduction | 178 |
| B.2. Diversity of soft-agar plate phenotypes of natural <i>E. coli</i> isolates | 182 |
| B.3. <i>E. coli</i> isolates with distinct chemotaxis characteristics and motility | 184 |
| B.4. Sequence analysis of the <i>meche</i> operon | 185 |
| B.5. Discussion | 189 |
| B.6. Materials and Methods | 191 |
| B.7. Acknowledgements | 195 |
| Appendix C. Effect of CheB phosphorylation feedback on adaptation kinetics in bacterial chemotaxis | 197 |
| C.1. Introduction | 198 |
| C.2. Shape of $F(a)$ in <i>E. coli</i> with disrupted phosphorylation feedback, characterized using temporal step stimuli | 201 |

| | |
|--|-----|
| C.3. Shape of $F(a)$ in <i>E. coli</i> with disrupted phosphorylation feedback, characterized using exponential ramp stimuli | 202 |
| C.4. Discussion | 205 |
| C.5. Materials and methods | 207 |
| C.6. Acknowledgements | 209 |
| Bibliography | 211 |
| Summary | 231 |
| Samenvatting | 235 |
| Acknowledgements | 239 |
| Curriculum Vitae | 243 |

Chapter 1

Introduction

Living cells sense and respond to changes in their surroundings by networks of molecules that detect environmental cues and process that information. Arguably the simplest biological signaling network is the chemotaxis system of *Escherichia coli*, which has become a paradigm for the molecular understanding of biological signaling and a model system for quantitative experimental and theoretical studies of sensory responses. In this thesis we performed physiological studies of *E. coli* and the closely related species *Salmonella typhimurium*, investigating the signaling and behavioral strategies that arise as a consequence of the design and implementation of the chemotaxis signaling circuit.

Chapter 1

1.1. Environmental sensing and intracellular signaling networks

Living organisms exhibit a number of characteristics that distinguish them from lifeless matter. The fundamental unit of life is the cell: the smallest structure capable of basic life processes, such as growth, metabolism and reproduction. A cell can represent a living organism itself, or it can be a part of a multicellular organism. A defining feature of living organisms is their ability to sense and respond to changes in their surroundings. Organisms detect environmental cues using sensory systems, which can be represented by complex organ structures or molecular receptors that transfer the information into the cell, where the information is processed and a response is generated. Possible responses include changes in the gene expression or behavioral responses that commonly involve movement of the organism.

Cells have developed networks of molecules that link the input from the receptors to behavioral output ²⁹. These molecular circuits are usually composed of multiple proteins, and each of them has a specific role in the signal transduction process. Some proteins act as transmembrane or soluble receptors that sense the signals; others are messengers or response regulators, the functions of which are to transfer the signals to the protein or protein complex that will generate the behavioral response. Other proteins that act as structural or interaction platforms, and can also take part in regulation of the signaling process, are the signaling scaffold proteins ²⁹⁰. Sensory pathways in eukaryotes usually rely on serine, threonine or tyrosine protein kinases, whereas prokaryotic sensory pathways most often involve histidine-aspartate phosphorelay systems that involve a dimeric histidine kinase and a response regulator protein ²⁶⁶. Despite the complexity of biological signaling networks in terms of their molecular organization, they can often be described in terms of functional modules ⁹⁹, which facilitates characterization of the dynamics of their function.

Bacteria provide an ideal ground for studying signaling networks from their genetic structure, protein-protein interactions, systems-level function, to behavioral outputs. The availability of genomic information ^{34,100,160,179,257} and ease of genetic manipulations ⁶² facilitates the discovery and

functional analysis of bacterial network components. Bacteria are amenable to microscopy and functional studies of their signaling systems, and reproduce rapidly, allowing experimental studies of processes that occur in different time scales, such as intracellular and intercellular signaling, behavioral responses and evolutionary processes. In particular, the chemotaxis circuit of *E. coli*, arguably the simplest and best characterized bacterial signaling network, has served as an important paradigm in the understanding of biological signaling^{19,244,266}. The *E. coli* chemotaxis circuit is used as a model system in this thesis.

1.2. Tactic responses

A cell or an organism orients in gradients of chemical or physical stimuli in the environment by altering the direction of its movement. This behavioral response is called taxis, and depending on the type of stimulus it can be classified into different categories (Table 1.1). The tactic response can be monotonic, towards increasing or decreasing values of the stimulus (attractant or repellent response)²⁶⁶ or non-monotonic, towards an optimum intermediate level of the stimulus¹¹³.

| Taxis | Stimulus | Organisms/ cells |
|---|--|---|
| Chemotaxis, including aerotaxis, pH taxis | Chemicals (organic and inorganic), including O ₂ , H ⁺ | Bacteria ²⁶⁶ , unicellular eukaryotes ¹⁰⁹ , nematodes ²⁶⁹ , sperm cells ⁷⁴ , macrophages ¹¹⁷ |
| Redox taxis | Redox potential | Bacteria ²⁸ |
| Thermotaxis | Temperature | Bacteria ²¹⁰ , nematodes ¹⁷⁷ , amoebae ¹⁰⁵ |
| Phototaxis | Light | Bacteria ²⁷⁸ , protozoans ⁶⁸ |
| Gravitaxis | Gravity | Protozoans ⁹⁷ |
| Rheotaxis | Fluid flow | Bacteria ¹⁵⁷ , fish ¹⁹³ , sperm cells ¹⁷² |
| Osmotaxis | Osmotic pressure | Bacteria ⁵ |
| Galvanotaxis | Electrical current | Bacteria ⁶ , protozoans ¹⁶ |
| Magnetotaxis | Magnetic field | Bacteria ⁶⁷ |

Table 1.1. Examples of tactic responses. Groups of organisms or cells that exhibit these tactic behaviours are shown in the last column.

Bacteria can sense and respond to various chemicals (nutrients^{4,170}, toxins⁷⁷, protons²⁸⁴, oxygen³¹ etc.), as well as other stimuli (temperature²¹⁰, redox potential²⁸, blue light²⁷⁸, fluid flow¹⁵⁷, osmolarity⁵, electric and

Chapter 1

magnetic fields ^{6,67} etc) via their chemotaxis signaling systems ^{2,4,5,210}. Motility of microorganisms was observed as early as 17th century by Anthony van Leeuwenhoek; however the first systematic investigations of directed chemotactic migration of bacteria were made by Wilhelm Pfeffer in the end of the 19th century ¹⁷¹. Pfeffer studied the attractant response of *Bacterium termo* (rod-shaped bacteria, isolated from putrid fluids) towards meat extract. In the same time Theodor Engelmann described the directed migration of *Bacterium termo* towards oxygen ⁷¹.

Chemotaxis of bacteria is involved in more complex behaviors and processes, such as biofilm formation, symbiotic associations and pathogenicity ²⁶⁶. The development of surface-attached biofilms depends on motility and chemotaxis of bacteria ^{213,285}. Chemotaxis is also important for some symbiotic associations, such as the association between nitrogen-fixing bacteria and legume plants ⁴⁸. Motility and chemotaxis play an important role in invasion and colonization of the host in many bacterial species, such as *Helicobacter pylori* ¹⁹⁷, *Vibrio anguillarum* ¹⁸⁸ and *Vibrio cholerae* ⁴⁷. Understanding bacterial chemotaxis can facilitate the development of biomedical strategies, such as using bacteria to controllably deliver therapeutics to the different tissues in the body ⁶¹.

Molecular investigations of bacterial chemotaxis and motility began in the 1960's with the pioneering work of Julius Adler ¹⁰¹. Adler applied behavioral assays, biochemical and genetic approaches to study the motile response and the underlying molecular mechanisms of *E. coli* chemotaxis ^{1,2,4-6}. He demonstrated that chemotaxis of *E. coli* does not require metabolism or transport of the sensed compound, but instead the response is generated by recognizing the chemical itself by a specific system for recognition and response. Adler's work initiated the contemporary studies of bacterial chemotaxis, which were greatly expanded in the seventies by the groups of Daniel Koshland, Jr., Melvin Simon, and Howard Berg ¹⁰¹. Bacterial chemotaxis has been a subject of increasing scientific interest in the following decades. The chemotaxis system of *E. coli* has become a preferred model system for theoretical and experimental studies of sensory responses ^{120,121,223,225,260}. Other studies of bacterial chemotaxis highlighted the diverse mechanisms of the chemotactic signaling and behavior in various prokaryotic organisms ^{254,281,283}.

1.3. Motility and chemotaxis of enteric bacteria

E. coli and its closely related species *Salmonella typhimurium* swim using organelles called flagella. Each flagellum is a semi-rigid helical filament of repetitive protein (flagellin) units that is several micrometers long but only ~20 nm in diameter, and rotates with rates on the order of 100 Hz²⁶¹. The flagellar filaments exist in different polymorphic forms with distinct curvature and twist²⁶¹. The filaments are linked by a hook to the flagellar motor: a remarkably complex structure consisting of about 50 protein components, which expression is tightly regulated^{152,266}. The flagellar motors of *E. coli* and *S. typhimurium* are driven by proton flux: the free energy stored in the electrochemical proton gradient across the cytoplasmic membrane is converted into mechanical work¹⁶⁴. The protons move through force-generating units, called Mot complexes, which are anchored to the peptidoglycan layer to form the stator of the flagellar motor complex, and interact with a ring of FliG units (rotor) on the cytoplasmic side to drive rotation²⁶⁶. The proton-driven flagellar machinery enables bacteria to swim at speeds of 15-100 $\mu\text{m}/\text{min}$ ²⁶.

Each bacterium has several flagella, usually 5-8 per cell. When all the flagella rotate counterclockwise (CCW) the flagella form a bundle that propels the cell forwards, i.e. the cell "runs". If one or more flagella change the direction of their rotation to clockwise (CW) the flagellar bundle is disrupted and the bacterium changes its swimming direction, i.e. the cell "tumbles". In this way bacteria swimming in a homogeneous environment perform a random walk²⁵ (Figure 1.1A). Typical run time for *E. coli* is ~1 s, whereas a tumble lasts ~0.1 s¹¹⁴. The direction of the motion during a run fluctuates due to rotational diffusion of the bacteria²³².

If the bacteria are placed in a gradient of a chemoattractant, the frequency of the tumbling events decreases³⁵, leading to prolonged runs and therefore the bacteria move in the direction of increasing chemoattractant concentrations (Figure 1.1B). Alternatively, increasing of the concentration of a chemorepellent leads to more frequent tumbles: bacteria change their direction more often, searching for a more favourable environment. Thus bacteria perform temporal comparisons, determining if

Chapter 1

the conditions are getting better or worse: if they are getting better the bacteria keep swimming, otherwise they change direction.

The flagellar motility of *E. coli* and *S. typhimurium* is just one of many types of bacterial locomotion that exist in nature. Other flagellated bacteria use different motility strategies, e.g. *Vibrio alginoliticus* have a single flagellum and change direction by flicking its flagellum leading to “run, reverse and flick” swimming rather than “run and tumble” swimming observed in *E. coli* ²⁵¹. Bacterial species that move on surfaces often use gliding or twitching that can involve type-IV pili extending from the poles, bind to the surface and pull the cell forward ⁴⁵.

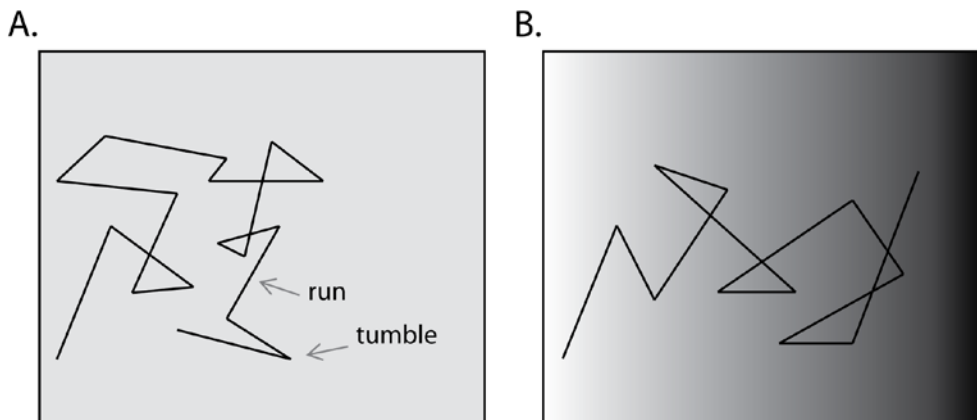


Figure 1.1. Schematic representation of a bacterial trajectory in absence and presence of a gradient of chemoattractant. The trajectory is represented in 2D for simplicity. The straight fragments represent runs, which are separated by tumble events (changing direction). **(A)** Random walk in a homogeneous environment. **(B)** Biased random walk in the presence of a chemoattractant gradient (represented in grey scale, a darker color corresponds to a higher concentration). The runs are prolonged in the direction of the gradient.

Various chemotaxis assays have been developed to evaluate the chemotaxis performance of *E. coli* and other microorganisms in spatial gradients of chemoeffectors ^{2,4,7,8,25,156,276}. Soft-agar assays are commonly used to evaluate the chemotaxis response to metabolizable chemoattractants ²⁷⁶. Bacteria are inoculated in a semi-solid agar containing the chemoattractant

of interest, which also serves as a nutrient for the bacteria. The growing colony of bacteria consumes the chemoattractant, and thus generates a radial gradient of the chemoattractant that triggers an outward migration of the bacteria ²⁷⁶. Another commonly used assay for chemotaxis is the capillary assay: a capillary that contains a chemoattractant is submerged in a solution containing the bacteria; the bacteria that accumulate in the capillary are subsequently counted to quantify the strength of the chemotaxis response ^{2,171}. Agar-based and capillary-based assays evaluating the negative response to chemorepellents have also been developed ²⁵⁹.

Quantitative studies of bacterial motility and chemotaxis have been greatly facilitated by the development of microfluidics technology, which allows generating precisely controlled gradients of chemoeffectors and observing the behavior of bacteria in these gradients at high spatial and temporal resolution ⁸. Microfluidic experiments in combination with theoretical and computational studies of the chemotactic response, enabled investigations of the behavioral strategies used by bacteria, and explaining the observed strategies using the information for the underlying control physiology of the chemotaxis response ^{137,156,158}.

1.4. Molecular organization of the chemotaxis system

The frequency of clockwise rotation of the flagellar motors of *E. coli* and *S. typhimurium* is determined by the activity of the chemotaxis signaling network (Figure 1.2) ²⁶⁶. Chemoeffector molecules are detected by transmembrane chemoreceptors, called methyl-accepting chemotaxis proteins (MCPs). Bacteria express MCPs with different specificities and affinities for ligands. The most commonly used laboratory strains of *E. coli* K12 and *S. typhimurium* LT2 have five and nine chemoreceptor species respectively ^{30,129,154,170}. However, variations exist even within each species: e.g. uropathogenic strains of *E. coli* lack two out of five chemoreceptors present in *E. coli* K12 ¹³³. MCPs exist as dimers and are coupled to the dimers of the histidine kinase CheA via scaffolding proteins: CheW in *E. coli* ²⁶⁶ and CheW and CheV in *S. typhimurium* ^{10,86,267}. Each monomer of CheA transfers the γ -phosphoryl group of an ATP molecule, bound to its kinase domain to a His residue on the opposing monomer. This phosphoryl

Chapter 1

group then can be transferred to an Asp residue of the response regulator CheY, which transduces the signal to the flagellar motors and biases the direction of their rotation. In the absence of phosphorylated CheY, the flagellar motors rotate counterclockwise⁷⁵. Phosphorylated CheY molecules bind to FliM molecules in the switch complexes of the flagellar motors, biasing the rotation of the motors towards the clockwise direction³³. The phosphatase CheZ accelerates CheY dephosphorylation and allows a rapid termination of the signal¹⁶¹. CheA also transfers its phosphoryl groups to other molecules of the chemotaxis system that has phospho-receiver domain: the methylesterase / deamidase CheB²³³ and the scaffolding protein CheV¹⁰ (although CheV phosphorylation has not been shown experimentally in *S. typhimurium*).

An increased concentration of chemoattractant (or decreased concentration of chemorepellent) inhibits the CheA autophosphorylation activity, thus the concentration of phosphorylated CheY decreases and respectively the probability of switching the flagellar motors to clockwise direction decreases, causing prolonged runs. The methyltransferase CheR methylates the receptors at multiple sites increasing their ability to stimulate CheA autophosphorylation. In this way the CheA autophosphorylation returns to prestimulus level even in the continued presence of chemoattractant, *i.e.* the bacteria adapt to the stimulus. Another enzyme, the methylesterase / deamidase CheB removes methyl or glutamyl groups from the chemoreceptors, reducing their ability to induce CheA autophosphorylation. Thus, CheR and CheB introduce a negative feedback in the chemotaxis system^{243,266}. There is also phosphorylation-dependent negative feedback on the activity of CheB: CheA phosphorylates CheB, stimulating its methylesterase activity¹⁵.

Additional chemotaxis proteins that are not present in the *E. coli* and *S. typhimurium*: the phosphatases CheX and CheC, and the deamidase CheD, exist in other bacterial species²⁸¹. The number of chemoreceptor genes also vary significantly between different bacterial species: from 1 in *Mesorhizobium loti* to >60 in *Magnetospirillum magnetotacticum*²⁶⁶.

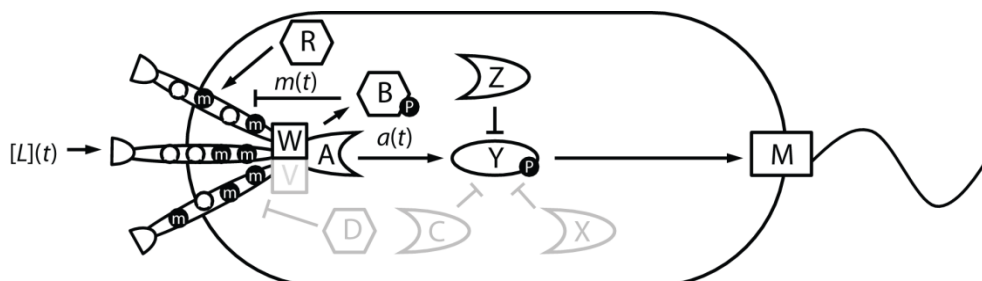


Figure 1.2. Molecular organization of the bacterial chemotaxis network. The transmembrane chemoreceptor clusters regulate the autophosphorylation activity of the kinase CheA (A), coupled to the receptors via scaffolding proteins CheW (W) and CheV (V) (CheW exists in both *E. coli* and *S. typhimurium*, whereas CheV is present in *S. typhimurium* but not in *E. coli*). CheA phosphorylates the response regulator CheY (Y), whereas CheZ (Z) accelerates its dephosphorylation. Phosphorylated CheY interacts with the flagellar motor (M) biasing its rotation in a clockwise direction. The adaptation enzymes CheR (R) and CheB (B) are involved in reversible methylation of the chemoreceptors at multiple sites. CheB methyltransferase activity is activated by phosphorylation by CheA. The ligand input, kinase output and methylation feedback are indicated with $[L](t)$, $a(t)$ and $m(t)$ respectively. Components that do not exist in *E. coli* but exist in other bacteria are indicated in gray: the scaffolding protein CheV (V), the phosphatases CheC (C) and CheX (X), and the deamidase CheD (D) ²⁸¹.

1.5. Functional organization of the chemotaxis system

The chemotaxis signaling pathway of *E. coli* is very well understood at the molecular level: structural and biochemical data are available for every step of the pathway ²⁶⁶. Thus, it has provided an ideal system for quantitative theoretical and experimental studies, which enabled better understanding of functional properties of chemotaxis and other sensory systems such as signal amplification, perfect adaptation, and wide dynamic range ^{14,78,113,114,137,158,185,186,192,222,225,226,232,234,240-242,260,263-266}. For example, experiments and computational modeling showed that cooperative interactions between the clustered chemoreceptors can explain the high sensitivity of the chemotaxis response of *E. coli* ^{42,168}.

Chapter 1

A coarse-grained model that describes the chemotaxis system as a modular system (Figure 1.3) has been recently developed ²⁶⁰, and it has been shown to explain consistently the experimental data for *E. coli*'s signaling response to time-varying chemoeffector stimuli ²²⁶. In this model the molecular details are omitted and the chemotaxis system is simplified to two modules: a receptor module, representing the activity of the receptor-kinase complexes, which detect signals from the environment and generate excitatory response, and an adaptation module, representing the methylation-dependent feedback by CheR and CheB to maintain the steady-state activity of CheA independent of the background concentration of the stimulus ²⁶⁰. The system-level dynamics of the chemotaxis signaling response is described by three dynamic variables: the concentration of the chemoeffector, $[L](t)$, the activity of the kinase representing the output of the system, $a(t)$, and the methylation level of the chemoreceptors, $m(t)$. The timescales for ligand binding (τ_l), kinase response (τ_a), and receptor methylation (τ_m) are well separated: $\tau_m \gg \tau_a \gg \tau_l$. The pathway kinetics is studied at the methylation timescale ²⁶⁰, which is most relevant to the bacterial motility since the typical run time is ~ 1 s. The ligand binding and kinase response timescales are treated with a quasi-equilibrium approximation ²⁶⁰.

The three dynamic variables are linked by two transfer functions. The transfer function G of the receptor module, $G([L], m) = a$, takes $[L](t)$ and $m(t)$ as inputs to produce an output $a(t)$, connecting the linear pathway downstream of the kinase toward motor output. This transfer function represents the cooperative modulation of CheA activity by chemoreceptors. G can be expressed by using a two-state model, in which the dependence on m and $[L]$ can be accounted for specifying a functional form of the free energy difference, f_t , between active and inactive receptor clusters:

$$G(m, [L]) = (1 + e^{f_t})^{-1},$$

where f_t is an additive function of two linearly independent terms:

$$f_t([L], m) = N(f_L([L]) + f_m(m)),$$

where $f_L([L])$ depends on the ligand binding and is characterized by the dissociation constants K_A and K_I of the active and inactive receptors, $f_m(m)$ depends linearly on the methylation level of the receptors and determines the kinase activity in the absence of ligand, and the amplification factor N

corresponds to the number of ligand-binding receptor dimers in a functional receptor cluster^{226,260}.

The transfer function F of the adaptation module, $F(a) = dm/dt$, converts $a(t)$ to rate of change of methylation level, dm/dt , and integrates it over time²⁶⁰. This transfer function represents the net methylation rate (methylation rate-demethylation rate) driven by the activities of CheR and CheB. Perfect adaptation of the kinase activity, i.e. adapting to the same level a_0 at steady-state, regardless of the background ligand concentration^{22,167,286}, is a property embedded in the design of the chemotaxis signaling system as $F(a)$ has a single fixed point at $a=a_0$ ²⁶⁰. Note that imperfect adaptation has also been observed for some chemoeffectors, and explained with the finite number of methylation sites possessed by the chemoreceptors^{132,163}.

The model of reference²⁶⁰ is used in this thesis to explain the experimental results obtained for both *E. coli* and *S. typhimurium*, which have very similar chemotactic networks⁶⁶.

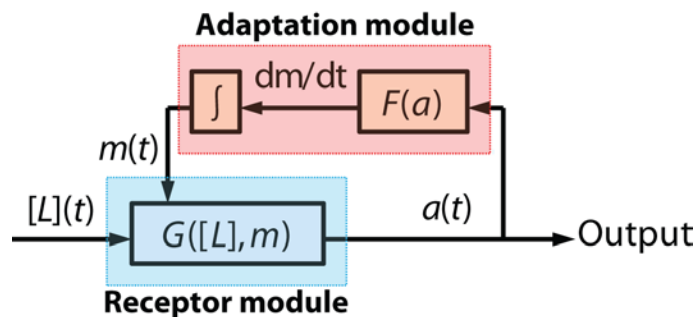


Figure 1.3. Modular organization of the bacterial chemotaxis network. The block diagram represents the functional modules rather than molecular components of the network (adapted from reference²²⁶). The dynamic variables are viewed as inputs or outputs (represented along wires) of two discrete functional modules (represented as boxes). The input-output relationship of the receptor and adaptation modules are described by functions $G([L], m)$ and $F(a)$ respectively.

Chapter 1

1.6. *In vivo* fluorescence resonance energy transfer (FRET) studies of the chemotactic signaling response

Understanding of the quantitative features of the chemotaxis signaling has been greatly facilitated by the development of experimental techniques that enabled following the signal processing dynamics in live bacteria^{224,242,264}. Most of these methods rely on fluorescence resonance energy transfer (FRET) between components of the chemotaxis pathway, which permit monitoring the activity-dependent interactions between these components in real time in live cells²⁴².

FRET assays rely on a nonradiative distance-dependent energy transfer from one fluorescent molecule, called donor, to another fluorescent molecule, called acceptor²⁷⁷. FRET measurements are widely used in biology to study interactions between proteins or parts of the same protein since the FRET technique is non-invasive, and allows observations of these interactions in real time^{17,181,207,239,242,277}. *In vivo* labeling with fluorescent dyes is difficult in bacteria due to their small size and low permeability of the cellular envelope; thus the most commonly used approach for bacterial FRET studies is genetically fusing fluorescence proteins (donor and acceptor) to the protein pair of interest. The efficiency of energy transfer, E_{FRET} , depends strongly on the distance between the donor and acceptor fluorophores: $E_{FRET} = R_0^6 / (R^6 + R_0^6)$, where R is the distance between the fluorophores and R_0 is the Förster radius, representing the distance at which the energy transfer between the donor and the acceptor have 50% efficiency²⁴². R_0 for the cyan and yellow fluorescence protein pair (CFP/YFP) in the bacterial cytoplasm is 4.9 nm, and very little energy transfer occurs if the donor and the acceptor are >10 nm apart²⁴².

The most widely used FRET assay for studying the chemotactic signaling dynamics in *E. coli* utilizes a FRET pair consisting of CheZ-CFP and CheY-YFP fusion proteins, serving as a donor and acceptor respectively^{185,192,239-242,284} (Figure 1.4A). The steady-state concentration of the phosphorylated CheY (CheY-P), and the concentration of the CheZ·CheY-P complex respectively, is determined by the balance between the phosphorylation of CheY by CheA and dephosphorylation of CheY-P by CheZ. These two enzymatic reactions have equal rates at steady-state, thus

the activity of the kinase CheA, $a(t)$, is proportional to the concentration of the protein complex CheZ-CheY-P. This concentration, which can be determined by FRET, therefore serves as a measure of the kinase output $a(t)$ on time scales that are shorter than the relaxation time of CheY phosphorylation cycle.

Upon a step addition of attractant (or a removal of repellent) the FRET level decreases, indicating a decrease in the kinase activity (Figure 1.4B). A step addition of repellent (or a removal of attractant) induces an opposite effect (Figure 1.4C). In adaptation-proficient bacteria, the kinase activity recovers toward the pre-stimulus level due to the activity of the methylation / demethylation pair of enzymes, CheR and CheB.

The described FRET system can be used to monitor the signaling activity of the chemotaxis pathway of single cells or populations of cells, attached to a coverslip, using fluorescence microscopy²⁴². In this thesis, we implemented population-based FRET measurements, which provide better sensitivity and temporal resolution compared to single-cell FRET measurements. Since the fluorescence emission is collected from hundreds of cells, attached to a coverslip, using sensitive photomultiplier tubes, we used relatively low intensities to excite fluorescence so as to minimize the photobleaching and photodamage to the cells, while achieving high signal-to-noise ratios. Input profiles smoothly varying in time were achieved by mixing a concentrated solution of chemoeffector with motility buffer using a fluid-mixing device of a design described in reference²²⁶. Using different time-varying inputs (temporal steps, up and down ramps, or sinusoids) has allowed characterization of both the receptor and adaptation modules of the chemotactic signaling system of *E. coli*²²⁶, and in this thesis we have explored in a similar manner the response of *S. typhimurium*.

Chapter 1

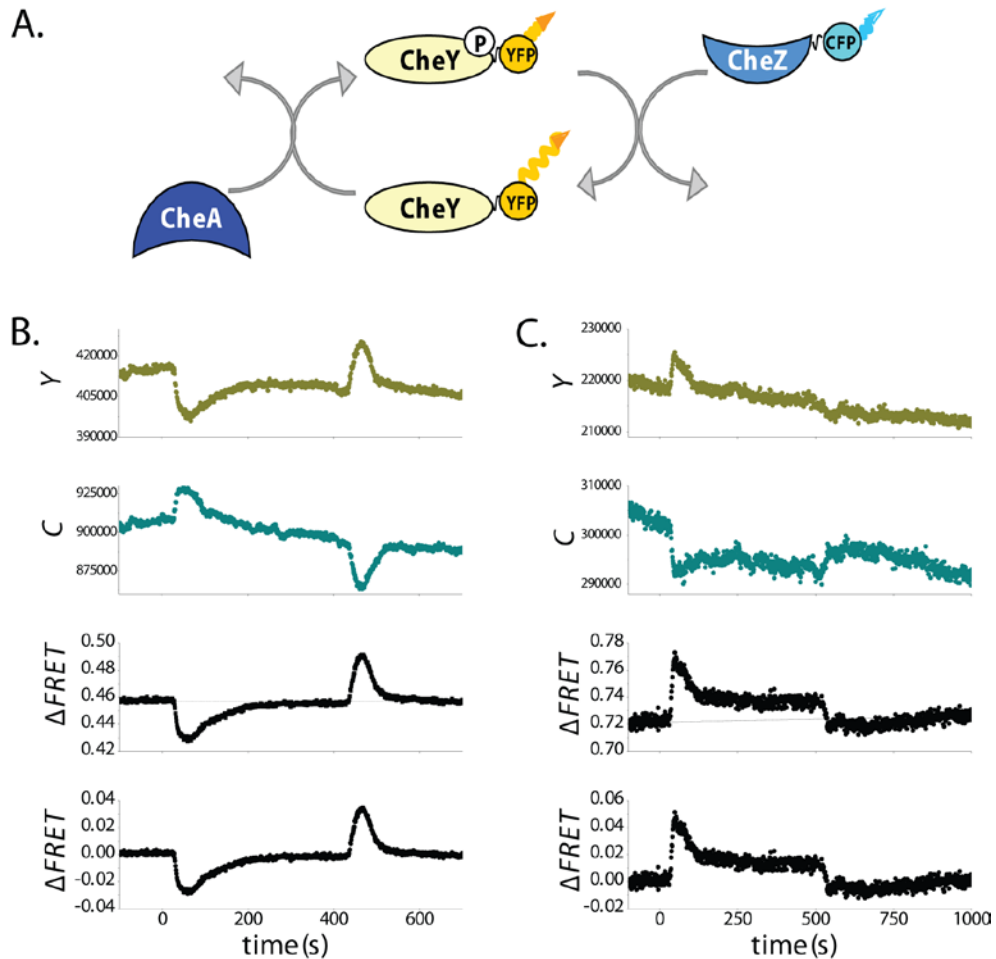


Figure 1.4. Description of the FRET system and typical responses to a chemoattractant and a chemorepellent. (A) Schematic representation of the FRET system used in this thesis. (B) and (C) From top to bottom: changes in the yellow (Y) fluorescence channel, cyan (C) fluorescence channel, Y/C ratio and Y/C ratio corrected for baseline drift: (B) at 0 s a chemoattractant (200 μ M cystine) is added, removed after 400s; (C) at 0 s a chemorepellent (200 μ M cystine) is added, removed after 500 s.

1.7. This thesis

The scope of this thesis has been to understand the design and implementation of the sensory system controlling the chemotaxis response of the enterobacteria *E. coli* and *S. typhimurium*. We characterized the input-output relationships of the chemotactic signaling response using FRET and studied the behavioral responses of bacteria in spatial gradients using microfluidics. We identified novel response strategies (Chapter 2), and performed a complete systems-level comparison of chemotactic signaling and behavior of *S. typhimurium* and *E. coli* (Chapter 3). We furthermore studied the response to previously uncharacterized chemoeffectors (Chapter 4) and the function of previously uncharacterized chemoreceptors (Chapter 4, Appendix A) and scaffolding proteins (Chapter 5), as outlined below.

In Chapter 2 we showed the first experimental proof that a sensory system implements a fold-change detection (FCD) strategy, *i.e.* responding faithfully to the shape of the input profile irrespective of its absolute intensity. We used *in vivo* FRET measurements on immobilized populations of *E. coli* to study the response-rescaling properties of chemotactic signaling, and showed that the entire time series of the response during stimulation with complex temporal waveforms depends only on fold-changes in input and not on its absolute level. Intensity-independent responses to spatial gradients were also observed using microfluidics-based assay of swimming bacteria. By theoretical analysis we identified a set of sufficient conditions for FCD.

In Chapter 3 we performed a FRET-based systems-level characterization of the chemotactic signaling transfer functions of *S. typhimurium* LT2, a closely related species to the model organism *E. coli* K12. The comparison of chemotactic signaling in the two species revealed conserved and divergent features. *S. typhimurium* showed a lower apparent cooperativity of its response to the chemoattractant α -methylaspartate (MeAsp), and a faster kinetics of adaptation. We evaluated the consequences of the differences in the signaling on the chemotactic behavior in spatial gradients created in microfluidic platforms. We were able to predict the behavioral response of bacteria from the transfer

Chapter 1

functions of their sensory response, which could provide a basis for studying organism's behavioral strategies at the level of physiological measurements. In Appendix B we set the foundations of a future comparative physiology study of the chemotactic properties of natural *E. coli* strains.

In Chapter 4 and Appendix A, we studied the chemotactic signaling response of *S. typhimurium* to the cystine / cysteine redox pair. In Chapter 4 we used *in vivo* FRET to show that the previously uncharacterized chemoreceptors McpB and McpC mediate a repellent response to the oxidized form, cystine, in *S. typhimurium* 14028, whereas Tsr and Tar mediate an attractant response to the reduced form, cysteine. In Appendix A, we measured the dose-dependent response to both cysteine and cystine, and discovered McpB / C-independent responses to cystine in *S. typhimurium* LT2 that are likely to be redox-dependent.

In Chapter 5 we tested the role of the phosphorylatable scaffolding protein CheV in the chemotaxis system of *S. typhimurium*. We observed CheV-dependent methylation-independent weak partial adaptation to MeAsp. Imaging revealed that the CheV molecules form clusters localized predominantly at the cell poles, and the number of the receptor clusters decreases in *cheV* knockout, and to a lesser extent, in the phosphorylation-deficient CheV mutants.

In Appendix C, we explored another phospho-dependent interaction: the phosphorylation-dependent feedback on CheB methylesterase activity on the kinetics of chemoreceptor methylation. We found that the strong nonlinearity in the transfer function characterizing the adaptation module in *E. coli* could be a consequence of the phosphorylation feedback on CheB activity.

In Chapter 6, we summarized our findings, and proposed experiments (including preliminary data) that can provide a continuation of the research topics explored in this thesis.

Chapter 2

Response rescaling in bacterial chemotaxis

Sensory systems rescale their response sensitivity upon adaptation according to simple strategies that recur in processes as diverse as single-cell signaling, neural network responses, and whole-organism perception. Here, we study response rescaling in *Escherichia coli* chemotaxis, where adaptation dynamically tunes the cells' motile response during searches for nutrients. Using *in vivo* FRET measurements on immobilized cells, we demonstrate that the design of this prokaryotic signaling network follows the fold-change-detection (FCD) strategy – responding faithfully to the shape of the input profile irrespective of its absolute intensity – hitherto demonstrated only in eukaryotic cell sensory systems. Using a microfluidics-based assay for free swimming cells, we confirm intensity-independent gradient responses at the behavioral level. By theoretical analysis, we identify a set of sufficient conditions for FCD in *E. coli* chemotaxis, which lead to the prediction that the adaptation timescale is invariant with respect to the background input level. Additional FRET experiments confirm that the adaptation timescale is invariant over a ~10,000-fold range of background concentrations. These observations in a highly optimized bacterial system support the concept that FCD represents a robust sensing strategy for spatial searches.

This chapter has been published:

Lazova, M. D., Ahmed, T., Bellomo, D., Stocker, R., and Shimizu, T. S., Response rescaling in bacterial chemotaxis. *Proc Natl Acad Sci U S A* **108** (33), 13870 (2011).

Chapter 2

2.1. Introduction

Maximizing the information content of perceived signals is a non-trivial problem for biological systems, as it requires adaptive tuning of sensory responses to match the statistics of input signals¹³⁵. Remarkably, strategies for inferring the likely distribution of inputs from recent experience appear to be ‘hard coded’ in many adaptive sensory systems, leading to well-defined relationships between the current response sensitivity and recent background inputs²⁴⁷. The most prevalent of such relationships is Weber’s law, which prescribes that the magnitude of the immediate sensory response, Δr , following a small step change in input, Δs , is proportional to the ratio of the step size, Δs , to the background input level, s_0 , *i.e.*, $\Delta r(\Delta s, s_0) = k \Delta s / s_0$, where k is a constant⁸¹. The underlying sensing strategy exploits a scenario commonplace in nature, where both the uninformative background intensity, s_0 , and informative deviations from it, Δs , are proportionately scaled by a common source of signal power that fluctuates slowly in time – for example, sunlight which sets the brightness of images at different times of day²⁰³. Weber’s law ensures that the response, Δr , remains invariant when both the stimulus, Δs , and the background, s_0 , are rescaled by the same factor γ , *i.e.* $\Delta r(\Delta s, s_0) = \Delta r(\gamma \Delta s, \gamma s_0)$. This obviates the need to optimize the stimulus-response relation at every level of signal power.

Recently, a response rescaling strategy that applies to a broader class of input stimuli, called fold-change detection (FCD), has been described in a number of eukaryotic cell sensory systems^{58,91,92}. FCD is conceptually similar to Weber’s law – it yields invariant responses under proportionate scaling of the stimulus with the background – but it applies to the entire time series of the response, $\Delta r(t)$, to a stimulus time series, $\Delta s(t)$, not only to the instantaneous response following a step stimulus. In addition, FCD is not limited to small-amplitude stimuli, but applies also to time-varying stimuli of arbitrary amplitude and waveform. Thus, the FCD strategy prescribes scale-invariant responses to the complete input time series, $\Delta r(\Delta s(t), s_0, t) = \Delta r(\gamma \Delta s(t), \gamma s_0, t)$, and as such imposes more stringent design constraints on sensory systems than does Weber’s law²³¹. It has been hypothesized that FCD is a desirable property for sensory

Response rescaling in bacterial chemotaxis

systems guiding spatial searches by motile organisms ²³¹, but whether and how any naturally occurring spatial guidance system implements the FCD strategy remains unknown.

Here, we study response rescaling in the signaling network of *E. coli* chemotaxis, which guides this bacterium's search for nutrients and is arguably the simplest sensory network known to exhibit adaptation over a broad dynamic range. Pioneering work by Adler and colleagues in the 1970's ¹⁷¹, as well as more recent work ¹¹⁵, has demonstrated logarithmic sensing behavior reminiscent of Weber's law in *E. coli*'s chemosensory system, which senses chemoeffector gradients as the bacterium samples its environment by swimming. Gradient sensing is achieved through temporal comparisons ²¹⁸ mediated by fast and slow molecular processes ²⁶⁵. On a rapid timescale, chemoeffector binding to transmembrane receptors produces an excitatory response, by modifying the activity of an intracellular signal that is relayed to the flagellar motor. On a slower timescale, enzyme-mediated covalent modification of the receptors restores pathway activity towards the pre-stimulus level, while also rescaling the sensitivity of receptors to ligand molecules ¹⁰².

The manner in which *E. coli* rescales its fast chemoreceptor response has been characterized in some detail by fluorescence resonance energy transfer (FRET) measurements of intracellular signaling. Using small-step stimulation by chemoeffectors, the response sensitivity was found to remain high at a nearly constant level over a broad range of background concentrations ²⁴¹, confirming that Weber's law holds at the level of the rapid chemoreceptor response. Yet, biologically relevant inputs often vary slowly over time, because the high diffusivity ($D \sim 10^{-9}$ m²/s) of small-molecule chemoeffectors leads to smooth concentration profiles in typical environments. To test whether *E. coli* demonstrates FCD in rescaling its chemotactic response to such smoothly varying inputs, we combine here FRET experiments encompassing both timescales of intracellular signaling with microfluidics-based assays of migration behavior. These experiments demonstrate that the dynamic output of the chemotaxis pathway activity is invariant under proportionate scaling of a time-varying stimulus with the background over a broad dynamic range. Thus, the *E. coli* chemotaxis system demonstrates FCD, as recently predicted on theoretical grounds ²³¹.

Chapter 2

By analyzing a theoretical model of *E. coli* chemotaxis²⁶⁰, we find that FCD imposes more stringent constraints on the design of the signaling system than does Weber’s law, and identify a set of sufficient conditions for FCD in terms of the molecular parameters of the system.

2.2. Weber’s law and fold-change detection (FCD)

The output response of the chemotaxis system can be characterized by a single variable, $a(t)$, that corresponds to the activity of a central kinase, CheA, controlled by clustered chemoreceptors. CheA activity determines the concentration of the phosphorylated response regulator protein CheY, which in turn controls cell swimming behavior^{265,266}. A FRET pair, consisting of CheY, and its phosphatase, CheZ, fused to yellow and cyan fluorescent proteins (YFP and CFP), respectively²⁴², provides a real-time readout proportional to $a(t)$ for timescales greater than the relaxation time of the CheY phosphorylation cycle. In addition to enabling studies on receptor sensitivity^{76,240,241}, this FRET system has been combined with time-varying stimuli to measure the *in vivo* kinetics of the adaptation enzymes CheR and CheB²²⁶, which provide negative feedback through covalent receptor modification (reversible methylation at multiple sites) and determine the slower timescale of the adaptation response, τ_m .

To study how the temporal response of chemotactic signaling depends upon the background level, we conducted FRET experiments in which bacteria, adapted to a background concentration $[L]_0$ of the non-metabolizable attractant α -methyl-aspartate (MeAsp), were subjected to a time-varying stimulus $\Delta[L](t)$. The stimulus was applied by modulating the input in time, as $[L](t) = [L]_0 + \Delta[L](t)$, using a fluid mixing apparatus. Figure 2.1A shows results from an experiment in which the stimuli, $\Delta[L]_i(t)$, differed in amplitude but the inputs, $[L]_i(t)$, had otherwise identical waveforms, *i.e.* $[L]_i(t) \equiv [L]_{0,i}\lambda(t)$, where $[L]_{0,i}$ is the i -th background concentration. The dimensionless waveform $\lambda(t)$ was held constant between all stimuli in this experiment, so that the stimulus-to-background ratio, $\Delta[L]_i(t)/[L]_{0,i} = (\lambda(t) - 1)$, was invariant. For this scenario, we found that the response time series, $\Delta FRET(t)$, was very similar over a broad range of background concentrations ($[L]_0 = 0.018$ – 2.903 mM). In contrast, in

Response rescaling in bacterial chemotaxis

the experiment of Figure 2.1B the sequence of stimuli, $\Delta[L]_i(t)$, was the same as the last four stimuli in the experiment of Figure 2.1A but the background level was held constant at $[L]_0 = 0.229$ mM. In this case, the FRET response to each stimulus in the sequence differed in both amplitude and waveform. Thus, the response to time-varying stimuli is not determined by the absolute difference from the background, $[L](t) - [L]_0$, but rather by the fold change over the background, $[L](t)/[L]_0$, indicating that chemotactic signaling in *E. coli* exhibits FCD.

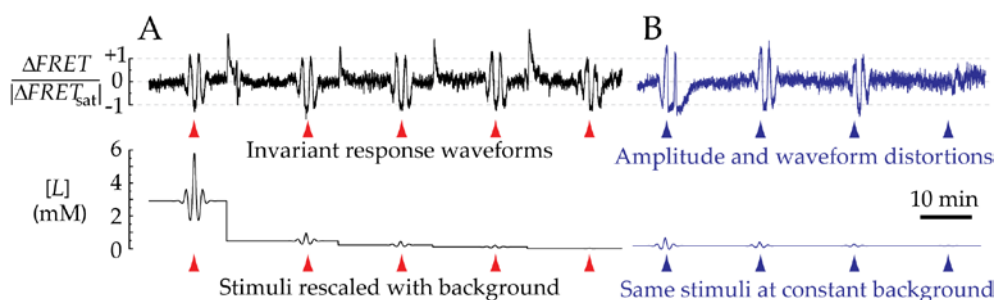


Figure 2.1. *E. coli* chemotaxis displays FCD. FRET response (top), $\Delta FRET$, normalized by the magnitude of the response to saturating stimuli ($|\Delta FRET_{sat}|$), of cells exposed to time-varying concentrations of MeAsp (bottom). **(A)** Response to five stimuli, $\Delta[L]_i(t)$, of identical waveforms and amplitudes scaled by the same factor as the background concentrations $[L]_{0,i} = (2.903, 0.478, 0.229, 0.109, 0.018)$ mM. **(B)** The last four stimuli, $i = (2, 3, 4, 5)$ were repeated while the background was kept constant (0.229 mM). (The first stimulus, at $i = 1$, could not be applied at this background because $[L]_0 + \Delta[L]_1(t)$ would reach negative values at $[L]_{0,1} = 2.903$ mM.)

2.3. Dynamic range of FCD in *E. coli* chemotactic signaling

To probe the dynamic range over which FCD holds, we compared the temporal response profiles at different background concentrations in experiments of the type shown in Figure 2.1A. One can use any function for $\lambda(t)$ to test for FCD, which, by definition, holds for arbitrary input waveforms. We chose an oscillatory waveform with a frequency $\nu = 0.01$ Hz, close to the characteristic frequency of the system's adaptation kinetics, $\nu_m \approx 0.006$ Hz (at 22° C; ²²⁶), with a Gaussian amplitude modulation to probe both the low-amplitude regime, where the stimulus-response relation is

Chapter 2

expected to be linear (*i.e.*, $\Delta FRET \propto \Delta[L]$), and the high-amplitude regime, where the stimulus-response relation saturates (*i.e.*, $\Delta FRET \rightarrow \Delta FRET_{\text{sat}}$). Figure 2.2 shows the FRET response time series over a $\sim 30,000$ fold range of background concentrations. We identified four concentration regimes. For $[L]_0 < 0.018$ mM (Figure 2.2A), the response amplitude increased with the background concentration. We detected two adjacent but distinct regimes where FCD holds locally: at intermediate ($[L]_0 = 0.018\text{--}0.229$ mM; Figure 2.2B) and high ($[L]_0 = 0.815\text{--}10.345$ mM; Figure 2.2C) background concentrations, responses were invariant in both amplitude and waveform. We hereafter refer to these regimes as FCD1 and FCD2, respectively, and to the low concentration regime, where the response amplitude depended on the background level (Figure 2.2A), as “no FCD” regime. At very high concentrations (>10.345 mM; Figure 2.2D), osmotic stress perturbs the chemoreceptors²⁶³ and this regime is not considered further.

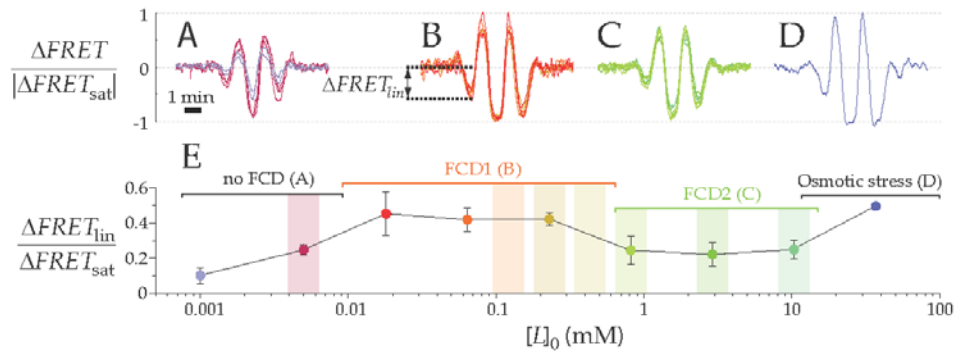


Figure 2.2. Dynamic range of FCD. (A–D) FRET response to a stimulus waveform (Figure 2.4B, blue curve) for different background concentrations $[L]_0 =$ (A) 0.001 and 0.005 mM; (B) 0.018, 0.064 and 0.229 mM; (C) 0.815, 2.903 and 10.345 mM; (D) 36.871 mM. Two replicates for each concentration are shown. (E) Response amplitude, $\Delta FRET_{\text{lin}}$, for the same cases, computed as the peak in the linear response regime (see panel B). Vertical bars indicate the concentration ranges used in microfluidic gradient experiments (Figure 2.3).

Response rescaling in bacterial chemotaxis

The two FCD regimes differ in the response magnitude, most notably in the low-amplitude regime of the response, where $\Delta FRET \ll \Delta FRET_{\text{sat}}$ (Figure 2.2B, C). Therefore, we characterized the amplitude of the first negative peak, $\Delta FRET_{\text{lin}}$ (see Figure 2.2B), which was always much smaller than $\Delta FRET_{\text{sat}}$ and thus provides a good approximation of the response within the linear regime of the stimulus-response relation. $\Delta FRET_{\text{lin}}$ depends only weakly on background concentration (Figure 2.2E), with a <2-fold difference over a ~2000-fold concentration interval ($[L]_0 = 0.005\text{--}10.345\text{ mM}$). Interestingly, this dependence of amplitude on background concentration closely resembles the previously reported²⁴¹ step-response sensitivity of chemoreceptors (defined as $(\Delta a/a_0)/(\Delta [L]/[L]_0)$, where a_0 is the steady-state kinase output), suggesting that the dependence arises within the fast timescale chemoreceptor response.

2.4. FCD in population behavior of swimming *E. coli*

If the chemotactic signaling response is invariant under rescaling of temporal gradients by the same factor as the background level, a swimming *E. coli* cell might do equally well at climbing different spatial gradients when these are similarly rescaled. A single bacterium's trajectory is difficult to follow experimentally over extended times. However, the spatial distribution of an ensemble of cells is readily imaged over long periods. If FCD holds on the behavioral level, the spatial distribution of the population is predicted to evolve identically in different chemoeffector gradients, as long as bacteria are pre-adapted to concentrations scaled by the same factor as the fold-change in the gradients' magnitude.

To test this prediction, we studied the migration of swimming cells in spatial gradients of MeAsp, established in a microfluidic system (Figure 2.3A) of a type described before^{7,52,115}. The device, consisting of polydimethylsiloxane (PDMS) and agarose, creates and maintains a steady linear MeAsp gradient. Bacteria are introduced into a $W = 600\text{ }\mu\text{m}$ wide "test channel" patterned in the PDMS layer, which has one face open to the underlying agarose layer. A linear gradient is pre-established within the agarose by flowing buffer with different MeAsp concentrations in the two

Chapter 2

flanking channels, higher in the “source channel” and lower in the “sink channel” (Figure 2.3A). A gradient mirroring that of the underlying agarose layer rapidly develops within the test channel, because of its small depth. We followed the migration of cell populations in the test channel by video-microscopy. Typical images of cell trajectories demonstrate that bacteria are initially uniformly distributed (Figure 2.3B, upper panel), but subsequently accumulate on the side closest to the source channel (Figure 2.3B, lower panel). Analysis of sequences of images yielded the bacterial distribution, $B(x)$, along the gradient.

We tested seven different gradients, each time rescaling the steepness of the gradient by the same factor as the mean concentration, $[L]_m$ (the shaded bars in Figure 2.2E). Figure 2.3C shows the temporal evolution of the spatial distributions of bacteria, $B(x)$. The left column corresponds to $[L]_m = 0.005$ mM, within the “no FCD” regime. As expected from the low amplitude of the FRET response in this range (Figure 2.2E), the chemotactic accumulation was weak. For $[L]_m$ within each FCD regime (middle and right columns) the entire temporal evolution of $B(x)$ was invariant, despite the ~ 12 -fold variation in $[L]_m$ among experiments. The accumulation was stronger within the FCD1 regime than within the FCD2 regime, consistent with the difference in sensitivity measured by FRET (Figure 2.2E).

The invariance of the distributions is demonstrated more quantitatively in Figure 2.3D, where we plot the time series of a dimensionless figure of merit, chemotactic migration coefficient (CMC)¹⁵⁶. The latter is defined as $CMC(t) \equiv \frac{\langle x \rangle(t) - W/2}{W/2}$, where $\langle x \rangle(t) \equiv \int xB(x, t)dx$ is the population-averaged spatial coordinate of the bacteria, x (along the chemoeffector gradient), measuring the mean displacement of the population from the center of the channel. The $CMC(t)$ time series are nearly identical for gradients within each FCD regime (Figure 2.3D). Taken together with the FRET data, these results demonstrate that within each concentration regime where intracellular signaling responses are invariant, the chemotactic performance in spatial gradients is also invariant. Thus, the FCD property extends from intracellular signaling to the behavior of swimming cells.

Response rescaling in bacterial chemotaxis

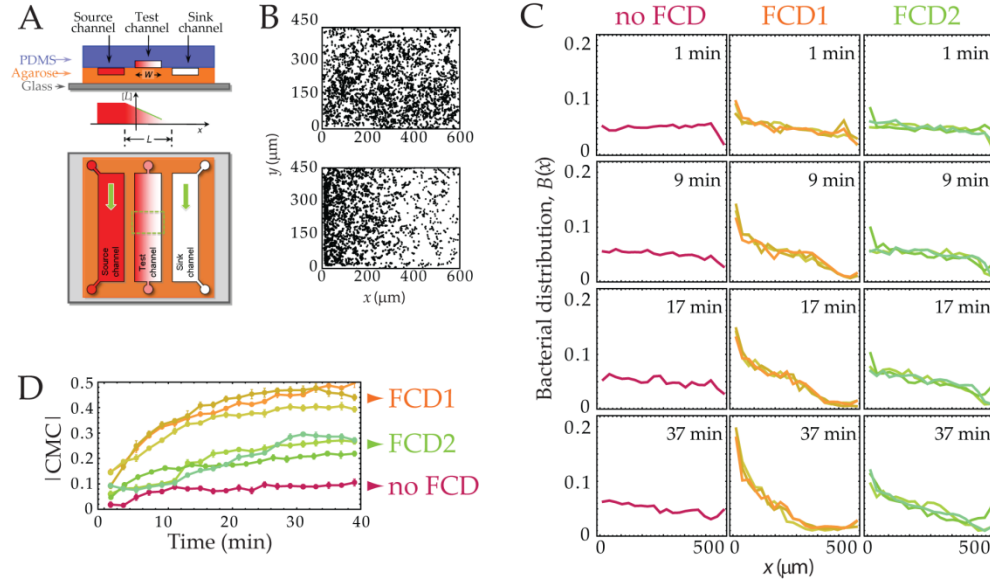


Figure 2.3. FCD demonstrated for swimming cells. (A) Schematic of the microfluidic device used to create a steady linear MeAsp gradient, of magnitude $\nabla[L]$ (see text). (B) Spatial distribution of chemotactic cells at the start of an experiment (top) and 19 minutes after establishment of a $\nabla[L] = 0.15$ mM/mm gradient along $-x$ (bottom). (C) Time evolution of the bacterial distribution in gradients of differing magnitude, but identical fold-change. In each experiment, bacteria were pre-adapted to a concentration $[L]_m$ such that $\nabla[L]/[L]_m$ was constant ($2/3$ mm $^{-1}$). The values of $[L]_m$ (0.005, 0.120, 0.229, 0.430, 0.815, 2.903, and 10.345 mM) are also indicated in Figure 2.2E. (D) Time series of the absolute value of the chemotactic migration coefficient ($|CMC|$; see text).

2.5. Mechanistic requirements for Weber's law and FCD

To gain insight into the mechanistic requirements for FCD, we analyzed a coarse-grained model of the chemotaxis network that has successfully explained a large body of quantitative experiments on chemotactic signaling²⁶⁰. This model was shown to satisfy the general mathematical requirements for FCD, but those conditions alone do not fully constrain the possible molecular mechanisms²³¹. Here we identify specific relationships between molecular parameters that lead to FCD-type response rescaling predicted to yield observable consequences. From a functional perspective, this model can be described as a negative feedback loop (Figure 2.4A) in which the ligand concentration, $[L](t)$, is the input, the

Chapter 2

receptor-kinase activity, $a(t)$, is the output, and the average receptor methylation level, $m(t)$, is the feedback signal. The relationships between these variables are mediated by two transfer functions: $F(a)$, representing enzyme-driven methylation kinetics, and $G([L],m)$, representing cooperative kinase activation by chemoreceptors. The dependence of $G([L],m)$ on ligand concentration and methylation level is through a free energy difference, $f_i([L],m)$, between active and inactive states of the receptor-kinase complex, described by an allosteric two-state model of the Monod-Wyman-Changeux (MWC) type¹⁷⁶.

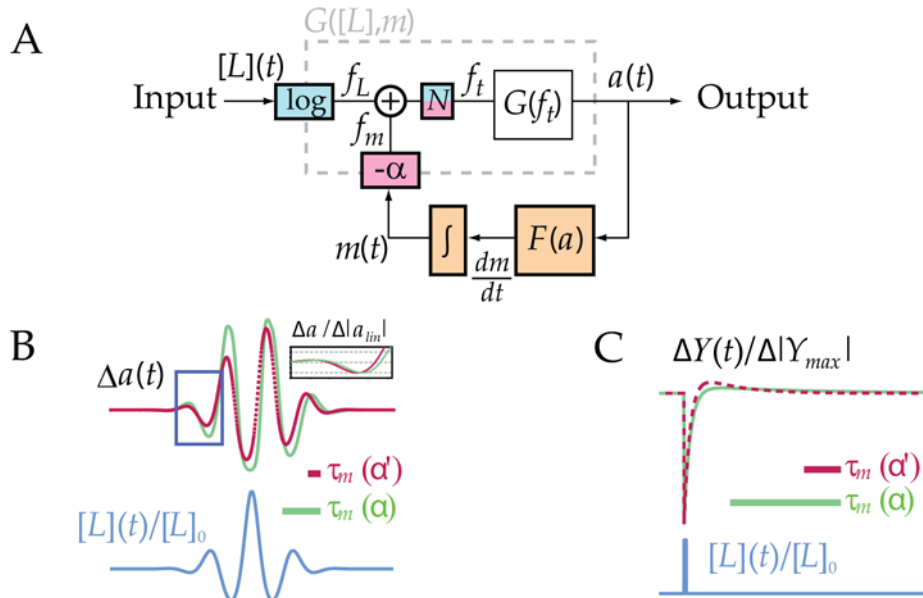


Figure 2.4. Requirements for FCD response rescaling. (A) Block diagram of the integral feedback network of *E. coli* chemotaxis. The receptor-kinase transfer function $G([L],m)$ constantly compares the ligand input $[L](t)$ with the methylation-feedback $m(t)$. Through another transfer function $F(a)$, the output $a(t)$ controls the rate of change of $m(t)$, yielding an integral-form feedback, which guarantees exact adaptation given appropriate conditions on $F(a)$. (B-C) Waveform distortions for sinusoidal (B) and impulse (C) stimuli, $[L](t)/[L]_0$ (blue curves), for a three-fold change in the response timescale, $\tau_m(\alpha)$, upon adaptation from one input level (green curves) to another (magenta curves). (B: Inset) Small-amplitude portion of the response (blue boxed region), with each response normalized by its amplitude. Note that the phase shift in the response in (B) and shape change in the impulse response in (C) are due to the difference in τ_m .

Response rescaling in bacterial chemotaxis

This model was previously used to explain Weber's-law-type response rescaling for step stimuli ²⁶⁰, which yielded a set of sufficient conditions on mechanistic parameters of this model. We find here that requiring FCD imposes an additional constraint on the design of the chemotaxis network, beyond those necessary for Weber's law, yielding the following as sufficient conditions for FCD:

- I. Exact adaptation: the steady-state output, $a_0 = \text{const}$
- II. Logarithmic coupling of ligand input, $[L]$, to the free energy, f_t :

$$\partial f_t / \partial \ln[L] = \text{const}$$
- III. Linear coupling of methylation feedback, m , to the free energy, f_t :

$$\partial f_t / \partial m = \text{const}$$

All three of these constancy conditions must hold under changes in $[L]_0$. Exact adaptation (condition I; orange in Figure 2.4A) requires that the dynamics of the kinase activity, $a(t)$, has a unique globally stable fixed point. This is guaranteed by the integral feedback architecture of this pathway ²⁸⁶, provided that the transfer function, $F(a)$, is determined uniquely by the kinase activity, a , and crosses zero only once with a negative slope ²⁶⁰. The remaining two conditions are constraints on the total free energy, which can be decomposed as $f_t([L], m) = N(f_L([L]) + f_m(m))$, where $f_L([L])$ represents the contribution from ligand binding, $f_m(m)$ represents that from methylation, and N is the size of the cooperative receptor cluster. Logarithmic input coupling (condition II; blue in Figure 2.4A) means that the ligand effect on the total free energy, f_t , is proportional to the logarithm of ligand concentration. In MWC-type allosteric models, the assumption that both ligand-binding and the active \leftrightarrow inactive transitions are thermally driven means that the ligand effect on activity depends on the distinct dissociation constants for the active and inactive states, K_A and K_I , through the relation $f_L([L]) = \ln(1 + [L]/K_I) - \ln(1 + [L]/K_A)$. Therefore condition II is satisfied for MWC models when the ligand concentration is in the range $K_I \ll [L] \ll K_A$ (where $f_L([L]) \sim \ln[L]$), given that the receptor cluster size, N , is also constant. Linear feedback coupling (condition III; pink in Figure 2.4A) signifies that the methylation effect on the total free energy, f_t , is directly proportional to the current methylation level, m .

Chapter 2

Of these three conditions for FCD, conditions I and II are sufficient for Weber's law for step stimuli ²⁶⁰. Thus, the only additional requirement for FCD is condition III, that the slope of the methylation-dependent free-energy must be a constant, i.e. $f_m(m)$ must be a linear function of m . Such a linear dependence was discovered in FRET experiments using step stimuli ²²⁶, where the function $f_m(m) = \alpha(m^* - m)$ yielded good fits to the data with $\alpha \approx 2$ and $m^* \approx 0.5$. The requirement for a constant α can be understood intuitively by examining the dynamics of this model, predicting that the characteristic timescale of adaptation, τ_m (defined as the relaxation time for the decay of the response, $\Delta a(t)$, after a small step change in the input) is inversely proportional to α : $\tau_m = (Na_0(1 - a_0)\alpha F'(a_0))^{-1}$. Thus, changes in α are expected to lead to distortions in the output waveform. In Figure 2.4B, C we illustrate the consequences of breaking this condition by numerical integration of a model that satisfies conditions I and II, but not condition III. For both smoothly varying stimuli (Figure 2.4B) and impulsive stimuli (Figure 2.4C), the response, $\Delta a(t)$, to the same input waveform, $\lambda(t) (= [L](t)/[L]_0)$, differs for two distinct feedback coupling coefficients α and α' (as could result from a nonlinear $f_m(m)$ when adapted to two different background concentrations). Thus, conditions I and II are not sufficient for FCD, even though this system will demonstrate response rescaling to step stimuli according to Weber's law.

2.6. Invariance of the chemotactic adaptation timescale

Our analysis of the requirements for FCD implies that the adaptation timescale, τ_m , is constant within each of the two FCD regimes identified in the FRET data (Figure 2.2). However, this observation does not rule out the possibility that τ_m depends on the background concentration over a broader range than each FCD regime. We reasoned that appreciable changes in τ_m would be observable as distortions in the output waveforms because this timescale directly determines the characteristic cutoff frequency, $\nu_m = (2\pi\tau_m)^{-1}$, for the linear signal filtering performed by the chemotaxis pathway ^{226,260}. Therefore, we compared the output waveforms between the two FCD regimes, as well as the "no FCD" regime, by superimposing the FRET response time series shown in Figure 2.2,

Response rescaling in bacterial chemotaxis

averaged within each of the three regimes (Figure 2.5A). The linear filtering analysis applies only for the small-amplitude regime of output, so inferring properties of τ_m from output waveform comparisons is only valid for the initial interval prior to saturation. When normalized by $|\Delta FRET_{lin}|$, responses within this interval (boxed region in Figure 2.5A) from all three regimes collapse onto a single output waveform (Figure 2.5A, *Inset*). Since large changes in τ_m would result in distortions of the output waveform, this collapse suggests the adaptation timescale, τ_m , is essentially invariant over the entire $\sim 10,000$ -fold range of background concentrations spanned by these three regimes (Figure 2.4B inset).

To test more directly the invariance of τ_m , we subjected cells to exponential sinusoid inputs, $[L](t) = [L]_0 \exp[A_L \sin(2\pi\nu t)]$, perceived as pure sinusoids with amplitude A_L and frequency ν under logarithmic input coupling^{226,260}. We recorded the response phase delay φ_D by fitting another sinusoid, $a(t) = a_0 + |A| \cos(2\pi\nu t - \varphi_D)$, to the FRET response time series. At a fixed background concentration, the dependence of φ_D on ν was shown²²⁶ to follow that expected for a linear filter, $\varphi_D(\nu) = \pi - \tan^{-1}(\nu_m/\nu)$, so any dependence of $\tau_m = (2\pi\nu_m)^{-1}$ on $[L]_0$ can be detected as a change in φ_D upon stimulation at frequency ν . We measured this dependence at $\nu = 0.006$ Hz (Figure 2.5B). The change in φ_D , if any, was very small ($\sim 0.02\pi$ per decade), corresponding to a $<20\%$ increase in τ_m over a $>1,000$ -fold increase in $[L]_0$. Thus, both the time- and frequency-domain data strongly indicate that the adaptation timescale remains constant over a broad range of background concentrations¹³⁷.

Chapter 2

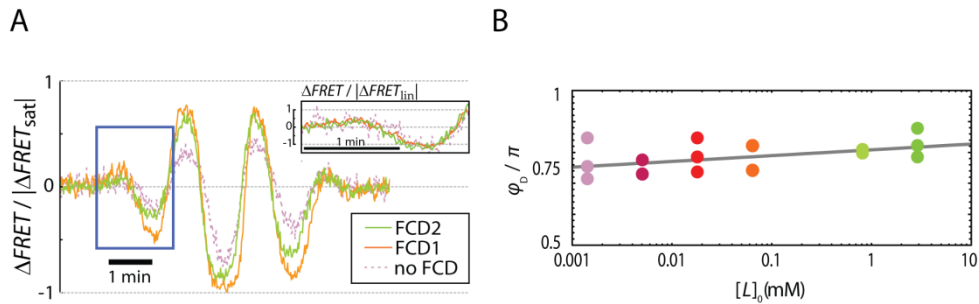


Figure 2.5. Invariance of the adaptation timescale over a ~10,000-fold range. (A) Overlaid view of output waveforms for the different background concentrations, separately averaged within the “FCD1”, “FCD2” and “no FCD” regimes. The boxed region indicates the linear regime of the response. **(Inset)** The linear-regime response is invariant when rescaled by $|\Delta FRET_{in}|$ (Figure 2.2B). **(B)** Phase delays, φ_0 , for responses to exponential sinusoids with $\nu = 0.006$ Hz and $A_L = 0.2$, for $[L]_0 = 0.001, 0.005, 0.018, 0.064, 0.815$ and 2.903 mM.

2.7. Discussion

We have shown that response rescaling in *E. coli* follows not only Weber’s law at short times after stimulation, but also FCD over the entire response time series, in agreement with a recent theoretical prediction²³¹. Unexpectedly, we identified two distinct FCD regimes which share a common adaptation timescale, but differ in their response amplitudes. As noted in a previous study of receptor sensitivity²⁴¹, a plausible explanation for these changes in the response amplitude for MeAsp is that more than one receptor species is involved in the response to MeAsp. Future experiments using mutant strains with altered receptor complements could shed light on this question (see Chapter 3).

The manner in which bacteria respond to temporal gradients is captured most succinctly by the system’s response to impulsive stimuli (Figure 2.4C), whose characteristic biphasic shape demonstrates how inputs from different times in the past are weighed to produce the output at every instant. The particular shape of this time-dependent response function is expected to be under strong selection, as it determines how time derivatives are computed by the bacterium and, as such, encodes the basic

chemotactic strategy. The optimal response function for a given environment will depend on the typical distribution of nutrient sources and the shapes of the concentration fields they generate by diffusion. Much theoretical work has been devoted to the effects on chemotaxis of different response functions under a variety of environmental conditions^{41,50,55,63,214}, based on the impulse response obtained in classic experiments^{36,218} that measured the response of flagellar rotation in cells tethered to a surface through their flagella. Our observation that the adaptation timescale is invariant with respect to the background level of input (Figure 2.5) validates the approach of using impulse response functions of the same shape to study gradient responses over the entire range of $[L]_0$ tested here, provided that the dependence of the amplitude of response on $[L]_0$ (Figure 2.2E) is taken into account.

How might FCD benefit a chemotactic bacterium? Shoval et al.²³¹ suggested that FCD could be advantageous in searching for nutrient sources. Their argument is based on the observation that typical environmental gradients generated by diffusion or convection from a source can have complex spatial profiles, but their characteristic shapes – when divided by the source strength – are invariant, *i.e.* the time-dependent spatial profile of the chemoeffector can be decomposed as $[L]([\mathcal{L}]_0, \vec{x}, t) = [\mathcal{L}]_0 \lambda(\vec{x}, t)$, where $[\mathcal{L}]_0$ is the chemoeffector concentration at the source and $\lambda(\vec{x}, t)$ is a dimensionless profile that depends on the spatial coordinate, \vec{x} , and time, t , but not $[\mathcal{L}]_0$. In this context, FCD enables a bacterium to focus on the shape of the profile as a signal encoding the source location, irrespective of the source strength. Such a strategy could be optimal when “any source is a good source”, that is, the payoff for reaching even a weak nutrient source exceeds that for discriminating between the richness of nutrient sources. The search for nutrient patches by bacteria in the ocean, where microscale sources of dissolved organics are far between and highly variable in intensity²⁵², represents a tangible example of such a scenario. Comparatively little is known about the natural habitats of enteric bacteria such as *E. coli*, but the fact that this species, noted for its highly optimized physiology, demonstrates FCD invites further studies about phases in its life cycle and ecology that favor this robust search strategy.

Chapter 2

Our results provide the first experimental demonstration of FCD in a sensory network guiding a spatial search, and of the consequences of FCD on organism- and population-level behavior. Given the arsenal of experimental and theoretical tools available for characterizing this minimal sensory network and its behavioral output, bacterial chemotaxis can serve as an ideal model system for further studies of FCD-type response rescaling, from the level of molecular mechanisms to its physiological and ecological implications.

2.8. Materials and methods

In vivo FRET measurements and data analysis

FRET microscopy of bacterial populations was performed²⁴². The FRET donor–acceptor pair (CheZ-CFP and CheY-YFP) was expressed from a plasmid pVS88²⁴⁰ in a $\Delta(\textit{cheY-cheZ})$ *E. coli* RP437. Cells, attached to a poly-L-lysine-coated coverslip, were situated at the top face of a bespoke flow cell²⁷, and kept under constant flow (~ 2 ml/min) of motility buffer (10 mM potassium phosphate, 0.1 mM EDTA, 1 μ M methionine, 10 mM lactic acid, pH 7), generated by a peristaltic pump (Rainin Dynamax RP1). Cells were subjected to time-varying input modulations, generated by mixing a concentrated solution of the chemoeffector α -methyl-DL-aspartate (MeAsp; Sigma Aldrich) and motility buffer by a fluid mixer of a type described before^{35,226}. The output concentration $[L](t)$ from the mixing chamber was controlled by modulating the in-flow rate, α , of the concentrated MeAsp using a computer-controlled syringe pump (Harvard Apparatus, PHD2000), whereas the in-flow rate of the motility buffer, β , was kept constant. Thus, $[L](t) = [L]^* \alpha(t) / [\alpha(t) + \beta]$, where $[L]^*$ is the MeAsp concentration in the syringe.

In the experiments shown on Figure 2.2 the background concentrations $[L]_0$ were equally spaced on a logarithmic scale by a factor $\gamma = (K_I K_A)^{1/4}$, centered about $[L]_{1/2} = (K_I K_A)^{1/2}$, where K_I and K_A are the dissociation constants for the inactive and active receptor states respectively. Cells, adapted to the i -th background, $[L]_{0,i} = \gamma^i [L]_{1/2}$, were subjected to an input $[L]_i(t) = \gamma^i S(t)$, where $S(t) = [L]_{1/2} \lambda(t)$, and in the

experiments of Figure 2.1, 2.2, and 2.5A, $\lambda(t) = \exp(Ae^{-\delta^2(t-t_c)^2} \sin 2\pi\nu t)$, that is a sinusoidal waveform with frequency ν multiplied by a Gaussian pulse envelope with a peak of amplitude e^A at time t_c and a decay parameter δ . The frequency $\nu = 0.01$ Hz was chosen to be close to the characteristic frequency, ν_m , of the system's adaptation kinetics²²⁶. Thus, changes in the adaptation kinetics would reveal themselves as phase shifts in the response. On the other hand, because receptor responses occur on much faster time scales, changes in receptor sensitivity would affect only the response amplitude, and not its waveform.

An upright microscope (Nikon FN1) was equipped with an oil immersion objective (Nikon CFI Plan Fluor, 40x/1.3). The sample was illuminated by a metal halide arc lamp with closed-loop feedback (EXFO X-Cite *exacte*) through an excitation bandpass filter (Semrock, FF01-438/24-25) and a dichroic mirror (Semrock, FF458-Di01). The epifluorescent emission was split by a second dichroic mirror (Semrock, FF509-FDi01) into donor (cyan, C) and acceptor (yellow, Y) channels and collected by two photon-counting photomultipliers (Hamamatsu H7422P-40) through bandpass filters (Semrock FF01-483/32 and FF01-542/27 for the C and Y channels, respectively). Detector output from the two channels were recorded through a data acquisition card (National Instruments) installed on a PC running custom-written software.

After background subtraction, the ratio between the acceptor and donor channel ($R = Y/C$) was used to compute the change in FRET efficiency upon stimulation: $\Delta FRET = \frac{R_{pre} + \Delta R - R_0}{R_{pre} + \Delta R + |\Delta Y/\Delta C|} - \frac{R_{pre} - R_0}{R_{pre} + |\Delta Y/\Delta C|}$, where where $\Delta R = R - R_{pre}$ is the ratio change, R_0 is the acceptor to donor ratio in absence of FRET, R_{pre} is the acceptor to donor ratio before stimulation, and $|\Delta Y/\Delta C|$ is the constant absolute ratio between the changes in the acceptor and donor signals per FRET pair ($|\Delta Y/\Delta C| \approx 0.6$)²⁴². Under the conditions of the measurements $R_{pre} + |\Delta Y/\Delta C| \gg \Delta R$. Thus $\Delta FRET \sim \Delta R$, and we expressed $\Delta FRET$ for simplicity in arbitrary units of ΔR . $\Delta FRET(t)$ was normalized to the absolute magnitude of the response to saturating step stimuli $|\Delta FRET_{sat}|$, to compensate for variations due to different absolute signal levels between the experiments.

Chapter 2

Microfluidic experiments and data analysis

Microfluidic chemotaxis experiments were performed in a hydrogel-based gradient generator (Figure 2.3A) ⁷, inspired by a design pioneered by Wu and colleagues ⁵². A 1 mm thick agarose layer was sandwiched between a glass slide and a polydimethylsiloxane (PDMS; Sylgard 184, Dow Corning) layer. The microdevice consisted of three parallel channels, each 600 μm wide. Two 100 μm deep feeder channels (“source” and “sink” channels) were patterned in agarose and one 50 μm deep test channel in PDMS. The test channel was fabricated using standard soft lithography techniques ²⁷². The agarose layer was made from a 3% (w/v) solution of Ultra Pure Agarose (Invitrogen) in motility buffer, heated for 30 s in a 1250 W microwave oven and poured over a silicon wafer with positive reliefs of the feeder channels. After being allowed to gel at room temperature, the agarose layer was cut to size and used immediately or stored in motility buffer. Flexible polyethylene tubing (Cole-Parmer) and metal connectors (New England Small Tube Corp) were used to connect the inlets of the source and sink channels with two 0.5 ml glass syringes (Hamilton Company), driven by a syringe pump (PHD 2000, Harvard Apparatus), and the inlet of the test channel with a 1 ml plastic syringe (BD), operated manually.

A constant flow rate of 1 $\mu\text{l}/\text{min}$ was maintained in the feeder channels, with two different concentrations of α -methyl DL aspartic acid (MeAsp; Sigma Aldrich) in the source and sink channel. Diffusion from the source to the sink, which are $L = 1$ mm apart (edge-to-edge), establishes a gradient across the agarose in ~ 20 min, and the concentration in the test channel reflects that in the underlying agarose. Because of the small height of the test channel, $H = 50$ μm , after introduction of the bacteria a gradient mirroring that of the underlying agarose rapidly develops in the test channel, within a time $H^2/2D < 10$ s (assuming a typical small-molecule diffusion coefficient for MeAsp, $D = 5 \times 10^{-10}$ $\text{m}^2 \text{s}^{-1}$). The gradient within the test channel was previously verified to be linear, with a magnitude equal to 69% of the gradient predicted assuming an exactly linear decay between source and sink channels ⁷. The MeAsp concentrations in the source and

sink channels were varied between 0.005 and 10.345 mM, to generate gradients between 0.003 and 6.9 mM/mm.

After a suspension of *E. coli* RP437 ($OD_{600} \approx 0.5$) was manually injected in the test channel by suction, the inlet and outlet of the test channel were sealed with coverslips to prevent residual flow and evaporation. Chemotaxis experiments were conducted using a computer-controlled inverted microscope (TE2000-E, Nikon), equipped with a CCD camera (PCO 1600, Cooke). Bacteria were observed at test channel mid-depth, using phase contrast microscopy and a 20 \times objective. The subsequent chemotactic behavior of cell populations was followed by video microscopy²²¹. Sequences of 200 frames sequence were captured at 10 frames per second every 2 min, from 1 to 39 min after injection of bacteria. Image analysis, using IPlab and MATLAB, was performed to determine bacterial positions in each frame. First, each frame was subtracted from the following one, to focus only on motile cells. Then motile bacteria were located in each frame as peaks in a monochrome intensity field. Bacterial positions were determined over all frames in a movie and binned to yield the the cell distribution $B(x)$ along the direction of the gradient.

FCD requires linear feedback coupling

In the model of Tu et al.²⁶⁰, the dynamics of the chemotaxis pathway is captured by two equations:

$$\frac{dm}{dt} = F(a), \quad (1)$$

which describes the rate of change of the average receptor methylation level, m , as a function of the activity of the receptor-kinase complex, a , and

$$a = G([L], m) = G(f_t([L], m)) = (1 + e^{f_t([L], m)})^{-1}, \quad (2)$$

which determines the receptor-kinase activity at every moment in time, given the current level of ligand input, $[L]$, and methylation feedback, m , via the free energy difference between the active and inactive states,

$$f_t([L], m) = N(f_L([L]) + f_m(m)), \quad (3)$$

where N is the number of ligand-binding receptor units cooperatively associated with each kinase molecule. If the free-energy contribution from

Chapter 2

methylation feedback, $f_m(m)$, is removed, the remaining ligand-dependent part of this model for receptor kinase activity, equation (2), is formally equivalent to the Monod-Wyman-Changeux (MWC) model of allosteric proteins, widely used in biochemistry ¹⁷⁶, and is also a limiting case of the Ising model of statistical physics ^{72,120,165}. As in the classical MWC model ¹⁷⁶, the effect of ligand depends on the active and inactive states for the receptor having distinct affinities for ligand, leading to the expression

$$f_L([L]) = \ln \frac{1+[L]/K_I}{1+[L]/K_A} \quad (4)$$

where K_I and K_A are the dissociation constants for the inactive and active receptor states, respectively. The methylation-dependent free energy, $f_m(m)$, is a feature that is not present in the classical MWC model, but has been shown experimentally to be well-approximated by a linear function,

$$f_m(m) = \alpha(m^* - m), \quad (5)$$

where α is the slope of $f_m(m)$, and m^* is the offset methylation level at which $f_m(m) = 0$.

This model for *E. coli* chemotactic signaling is thus completely described by the MWC parameters N , K_I and K_A , which have been estimated in numerous studies utilizing data from FRET experiments with step stimuli ^{76,120,165,166,226,240,264}, and the shapes of the functions $F(a)$ and $f_m(m)$, which were recently characterized by experiments with time-varying stimuli ²²⁶. The picture that emerges from these studies is that both $f_L(\ln[L])$ and $f_m(m)$ are linear over a broad range. The linearity of $f_L(\ln[L])$ in the range $K_I \ll [L] \ll K_A$ follows from equation (4) with a large ratio between K_A and K_I values obtained in MWC-model fits to step-response data ^{166,226}.

It has been shown previously ²⁶⁰ that for Weber's-law-type response rescaling for step stimuli, this model requires: I exact adaptation, satisfied by equation (1), and II a significantly extended linear regime of $f_L(\ln[L])$, which is achieved by the aforementioned large separation between the two dissociation constants: $K_I = 0.018$ mM, $K_A = 2.903$ mM for MeAsp binding to the aspartate receptor Tar ^{166,226}. Here, we demonstrate that FCD requires, in addition to I and II, a third condition, namely III that the methylation-dependent part of the receptor free energy, $f_m(m)$, is also linear.

Consider a system adapted to a background concentration $[L]_0$ at time t_0 . Because the output time series $a(t)$ is determined solely by the free

Response rescaling in bacterial chemotaxis

energy, f_t , according to equation (2), demonstrating invariance in this free energy as a function of time, $f_t(t)$, under multiplication of the input $[L](t) = [L]_0 + \Delta[L](t)$ by a scalar constant γ suffices to prove FCD. Due to exact adaptation, the adapted state activity $a([L]_0, t_0) = a_0$, and hence also $f_t(t_0)$, is independent of the background level of input, $[L]_0$. On the other hand, solving equation (3) for the m makes clear that the adapted-state methylation level m_0 does depend on $[L]_0$.

$$m_0([L]_0) = f_m^{-1}(f_t(t_0)/N - f_L([L]_0)), \quad (6)$$

where $f_m^{-1}(f)$ represents the inverse function of $f_m(m)$. Expressing the free-energy response time series as $\Delta f_t(t) = f_t(t) - f_t(t_0)$, we can write

$$\Delta f_t(t) = \Delta f_m(m(t)) + \Delta f_L([L](t)) \quad (7)$$

where $\Delta f_m(m(t)) = f_m(m(t)) - f_m(m_0)$; $\Delta f_L([L](t)) = f_L([L](t)) - f_L([L]_0)$. Within the range $K_i \ll [L] \ll K_A$, $\Delta f_L([L](t)) = \Delta f_L(\gamma[L](t))$, where γ is constant, because $f_L([L]) \sim \ln[L]$ in this range (equation 4). Requiring the time evolution of the total free energy, $\Delta f_t(t)$, to be invariant in equation (7) therefore requires the time evolution of $\Delta f_m(m(t))$ to also be invariant, *i.e.*,

$$\Delta f_m(m(t)) = f_m(m_0 + \Delta m(t)) - f_m(m_0) = \text{constant}, \text{ at any time, } t, \quad (8)$$

where $\Delta m(t) = \Delta m([L](t); t) \equiv m(t) - m_0([L]_0)$ is the time-dependent response to $[L](t)$ in the methylation level m . But if FCD holds, $\Delta m(t)$ is itself invariant under multiplication of the input by a factor γ , that is, $\Delta m(\gamma[L](t); t) = \Delta m([L](t); t)$, because it evolves according to the time integral of equation 1: $\Delta m([L](t); t) = \int_{t_0}^t F(a([L](t); t)) dt$, and $a(\gamma[L](t); t) = a([L](t); t)$ as required by FCD. On the other hand, m_0 depends explicitly on $[L]_0$ according to equation (6). Taking the derivative of equation (8) with respect to m_0 , we see that FCD also requires

$$f'_m(m_0 + \Delta m([L](t); t)) - f'_m(m_0) = 0 \quad (9)$$

For equation (9) to be true for an arbitrary input time series $[L](t)$, the local slope of $f_m(m)$ must be the same everywhere, that is, $f_m(m)$ must be a linear function.

Chapter 2

Alternative proof for the linear feedback coupling requirement

A more general and elegant proof of the linear $f_m(m)$ requirement for FCD has been communicated to us by Prof. Dr. Eduardo Sontag. This approach appeals to a general theorem for FCD developed in refs. ²³¹ and ²³⁰, which, applied to the system of equations. (1) and (2), requires that, for FCD to hold, there must exist a function $R(p, m)$ that solves the following partial differential equation (a) with boundary condition (b):

$$(a) \quad \frac{\partial R}{\partial m}(p, m)F(a) = F(a) \text{ for all } p, a, m;$$

$$(b) \quad G(p[L], R(p, m)) = G([L], m) \text{ for all } p, a, m.$$

From (a) it follows that for all p, m , $\frac{\partial R}{\partial m}(p, m) = 1$, which gives $R(p, m) = m + r(p)$ for some function $r(p)$. This in turn implies from (b) that:

$$f_L(p[L]) + f_m(m + r(p)) = f_L([L]) + f_m(m) \text{ for all } [L], m, p. \quad (10)$$

Taking $\partial/\partial p$ in equation (10), we have

$$[L]f'_L(p[L]) + r'(p)f'_m(m + r(p)) = 0 \text{ for all } [L], m, p. \quad (11)$$

And therefore, unless f_L is constant, there is at least some $p = p_0$ such that $r'(p_0) \neq 0$. (Because for some p_0 and $[L]_0$, $[L]_0 f'_L(p_0[L]_0) \neq 0$.) Now taking a derivative $\partial/\partial m$ in equation (11), we have $r'(p)f''_m(m + r(p)) = 0$ for all m, p , so that, in particular, $f''_m(m + q) = 0$ for all m , where $q = r(p_0)$. It follows that $f''_m(m) = 0$, so $f_m(m)$ is linear.

FCD implies an invariant adaptation timescale

Linearizing the equations (1) and (2) about the steady-state activity, a_0 , we get

$$\frac{d\Delta m}{dt} = F'(a_0)\Delta a, \quad (12)$$

$$\Delta a = \frac{\partial a}{\partial m}\Delta m + \frac{\partial a}{\partial [L]}\Delta [L], \quad (13)$$

Adaptation kinetics can be characterized by the relaxation of activity after the application of a brief pulse of ligand, where the chemoeffector jump, $\Delta [L]$, has returned to zero (*i.e.* the relaxation of the

slow overshoot in Figure 2.4C). Differentiating equation (13) with respect to time, and substituting equation (12) yields

$$\frac{d\Delta a}{dt} = \frac{\partial a}{\partial m} F'(a_0) \Delta a = -\Delta a / \tau_m, \quad (14)$$

where we define

$$\tau_m \equiv - \left(F'(a_0) \frac{\partial a}{\partial m} \right)^{-1} = - \left(F'(a_0) \frac{\partial a}{\partial f_t} \frac{\partial f_t}{\partial f_m} \frac{\partial f_m}{\partial m} \right)^{-1} = \left(-\alpha N a_0 (1 - a_0) F'(a_0) \right)^{-1} \quad (15)$$

as the characteristic timescale of adaptation.

By inspecting this solution (equation 15), we can verify that the conditions for FCD imply an adaptation timescale that is insensitive to the background ligand concentration, $[L]_0$. Condition I (exact adaptation) ensures that the steady-state activity, a_0 , and the methylation kinetics $F(a)$ are both invariant. Condition II (logarithmic input coupling) demands that $\frac{\partial f_t}{\partial \ln[L]} = N \frac{\partial f_L}{\partial \ln[L]}$ is constant, which means that N is constant within the range $K_I \ll [L] \ll K_A$, where $\frac{\partial f_L}{\partial \ln[L]}$ reduces to unity. Finally, condition III (linear feedback coupling) ensures that the remaining factor on the right hand side of equation (15), α , is also constant, confirming that τ_m is invariant under changes in $[L]_0$.

Waveform distortion due to changes in the adaptation timescale

We illustrated, through simple numerical simulations, the consequences of a violation of the invariance of the adaptive timescale τ_m (or equivalently of the feedback coupling coefficient α).

Figure 2.4B shows the time response to a sinusoidal waveform with Gaussian amplitude modulation (see Materials and methods). The responses depicted in Figure 2.4B were obtained by numerical integration of equations (1-3). The parameters were chosen as in ²²⁶: $N=6$, $a_0=1/3$, $m_0=0.5$, $K_I = 0.018$ mM, $K_A = 2.903$ mM. The function $F(a)$ was described by a Michaelis-Menten equation with a variable gain

$$\begin{aligned} F(a) &= V_R (1 - a) / (K_R + 1 - a) - V_R(a)a / (K_B + a) \\ V_B(a) &= V_B(0) \left(1 + \theta(a - a_B) \frac{a - a_B}{1 - a_B} r_B \right) \end{aligned} \quad (16)$$

Chapter 2

where K_R and K_B are the Michaelis constants, and V_R and $V_B(a)$ are the maximal velocities of the methylation and demethylation reactions (catalyzed by CheR and CheB respectively). $V_B(a)$ is a piecewise linear function, the value of which remains $V_B(0)$ for values of a below a_B , and above a_B increases with a slope $r_B/(1-a_B)$ up to a maximal value $(1+r_B)V_B(0)$, implemented by use of a step function, defined as $\theta(x) = 1$ for $x > 0$, $\theta(x) = 0$ otherwise. The parameters in equations (16) are as reported in ²²⁶: $V_R = 0.010 \text{ s}^{-1}$, $K_R = 0.32$, $K_B = 0.30$, $V_B(0) = 0.013 \text{ s}^{-1}$, $a_B = 0.74$, $r_B = 4.0$. The stimulus has a background concentration $[L]_0 = (K_R K_A)^{1/2} = 0.229 \text{ mM}$ and spans a time interval of 600s. The parameters of oscillatory waveform $\lambda(t)$ are $A = 0.69$, $\delta = 0.0112$, $\nu = 0.01 \text{ Hz}$, $t_c = 325$. The feedback coupling coefficient α was set to 2 (magenta curve) and 6 (green curve).

Figure 2.4C shows the response time series for an impulsive stimulus. For an ideal impulse input, $[L](t) = \delta(t)$, where $\delta(t)$ is the Dirac delta function, such a response can be described as demonstrated in ²⁶⁰ by the function

$$\begin{aligned} \Delta Y(t \geq 0) &= \Delta Y_0 \left[\frac{1}{\tau_m} e^{-\frac{t}{\tau_m}} - \frac{1}{\tau_z} e^{-\frac{t}{\tau_z}} \right] \\ \Delta Y(t < 0) &= 0 \end{aligned} \quad (17)$$

where $\Delta Y_0 = -c_a k_a \frac{\tau_z \tau_m}{\tau_m - \tau_z} > 0$ and $c_a = -N a_0 (1 - a_0)$. The time constant τ_z represents the dephosphorylation time, and k_a is an effective phospho-transfer rate from CheA to CheY ²⁶⁰. In Figure 2.4C, we choose $k_a = 10$, $N = 6$, $a_0 = 1/3$, $\tau_z = 10\text{s}$. The adaptation time scale τ_m was set to 3 s (magenta curve) and 9 s (green curve).

2.9. Acknowledgements

The microfluidics work was performed by Dr. Tanvir Ahmed in the group of Prof. Dr. Roman Stocker (Massachusetts Institute of Technology). Simulations were done by Dr. Domenico Bellomo (VU University, Amsterdam). Marco Seynen and Ilja Cerjak (AMOLF) contributed with FRET software development and instrument designs. Prof. Dr. Howard Berg brought the FCD topic to our attention.

Chapter 3

Network-level variability in bacterial chemotaxis

Most of our current knowledge about the bacterial chemotaxis network comes from studies of the model organism *Escherichia coli*. However, recent genomic studies have revealed that topologies of the chemotactic signaling networks demonstrate a great diversity across prokaryotes. We have studied the network-level properties of chemotactic signaling in response to the attractant α -methyl-aspartate in *Salmonella typhimurium*, which shares a homologous chemotactic network with *E. coli*. Using *in vivo* fluorescence resonance energy transfer (FRET) measurements with time-varying inputs, we revealed that the parameters of *S. typhimurium*'s receptor and adaptation transfer functions are different from those of *E. coli*'s. The response to α -methyl-aspartate shows three-fold lower apparent cooperativity and three-fold faster adaptation kinetics. The manner in which receptor sensitivity is modulated as a function of background concentration also differs between the two species, with *S. typhimurium* demonstrating a broader range over which the response is invariant to the absolute level of input (fold-change detection, FCD). We observed the migration of *S. typhimurium* populations in spatial gradients of attractant, created in microfluidic devices. We demonstrated differences from *E. coli* in the chemotactic drift velocity, which we relate to the underlying control physiology. Our study demonstrates how dynamical features of cell signaling networks can be evaluated in the context of organism behavior and evolution using a quantitative physiology approach.

Chapter 3

3.1. Introduction

The bacterial chemotaxis system, which allows bacteria to sense and respond to changes in chemical concentrations in the surrounding environment, is one of the best understood intracellular signaling networks. It is well characterized at the molecular level ^{238,266}, and the network-level dynamics of the model species *Escherichia coli* has been unravelled by numerous experimental and theoretical studies ^{120,137,166,192,226,240,241,260}. However, the chemotaxis system of *E. coli* represents a streamlined example of bacterial chemotaxis: recent advances in genomics and bioinformatics have revealed that the topologies of the chemotactic networks in other species, even of closely related bacteria, demonstrate a great diversity ^{254,281}. Moreover, chemotactic performance varies even among different strains of *E. coli* ¹³³, suggesting that the chemotactic signaling dynamics has been fine tuned in the recent evolutionary history.

We investigated the chemotactic signaling and behavior of *Salmonella typhimurium*: a pathogenic species that diverged from the common ancestor with *E. coli* 120 to 160 million years ago ^{136,190}. Although *S. typhimurium* and *E. coli* coexist both in their host and non-host habitats, they have different lifestyles ²⁷⁴; therefore it is likely that their chemotactic responses have been subject to distinct evolutionary optimization. The chemotaxis genes of *E. coli* and *S. typhimurium* are similar enough to permit swapping of components on a gene-by-gene basis: deletions in one species are complemented by the homologous genes from the other ⁶⁶. However, no systematic comparison of the dynamic features of chemotactic signaling of these two species has been performed to date.

At the molecular level, chemoeffector sensing and chemotactic signal transduction are achieved in a similar manner in the two species ^{243,266} (Figure 3.1). Chemoeffectors are detected by clustered transmembrane chemoreceptors, which form homodimers and are coupled to a histidine kinase (CheA). The kinase phosphorylates a response regulator CheY, which transduces the signal to the flagellar motors and bias the direction of their rotation. The dephosphorylation of CheY is accelerated by a phosphatase CheZ. Adaptation is achieved by a pair of enzymes with opposing actions, CheR and CheB, which provide a negative feedback by

Network-level variability in bacterial chemotaxis

reversible methylation of the chemoreceptors at multiple sites. Differences between chemotaxis protein species of *E. coli* and *S. typhimurium* are observed at the level of the receptor-kinase complex. In addition to the receptor types common for both species: Tar, Tsr, Trg and Aer, there are five *S. typhimurium*-specific receptors Tcp, Tip, McpA, McpB and McpC^{86,206,267,282} and one *E. coli*-specific receptor: Tap¹⁵⁴ (Table 3.1). Coupling of chemoreceptors to kinase molecules in *E. coli* is achieved by a single scaffolding protein, CheW. A second type of scaffolding protein, CheV, exists in *S. typhimurium*^{86,267}, although no direct evidence that CheV couples chemoreceptors to CheA in *S. typhimurium* has been reported¹⁰. CheV shares regions of homology in its N-terminal domain with CheW, and in its C-terminal domain with CheY, and it likely can be phosphorylated by CheA¹⁰. Although most of the chemotactic proteins can be swapped between *E. coli* and *S. typhimurium*, some functional differences exist between these proteins: for example, Tar from *E. coli* but not from *S. typhimurium* is able to sense maltose¹⁸⁰.

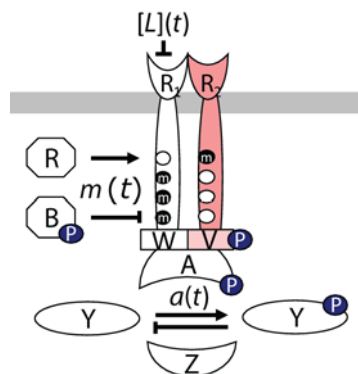


Figure 3.1. Molecular representation of chemotactic signaling network. Components that differ between *S. typhimurium* and *E. coli* are shown in color. Mixed chemoreceptor clusters regulate the activity of the kinase, CheA. Scaffolding proteins (CheW, CheV) couple the receptors and kinase molecules. The response regulator CheY that transduces the signal to the flagellar motors is phosphorylated and dephosphorylated by CheA and CheZ respectively. Receptors are methylated and demethylated / deamidated at multiple sites by the enzymes CheR and CheB respectively, and CheB activity is also feedback-regulated by phosphorylation from CheA. CheV is also likely to be phosphorylated by CheA¹⁰.

Chapter 3

| MCP | Species | Chemoeffector(s) | Reference(s) |
|-------|--|--|--------------|
| Tsr* | <i>E. coli</i> , <i>S. typhimurium</i> | Serine, glycine, oxygen, cysteine, redox | 170,202 |
| Tar* | <i>E. coli</i> , <i>S. typhimurium</i> | Aspartate, cysteine, maltose (<i>E. coli</i>), Ni ⁺ | 180,259 |
| Trg | <i>E. coli</i> , <i>S. typhimurium</i> | Ribose, galactose | 129 |
| Aer | <i>E. coli</i> , <i>S. typhimurium</i> | Oxygen, redox potential | 30,202 |
| Tap | <i>E. coli</i> | Dipeptides | 154 |
| Tcp* | <i>S. typhimurium</i> | Citrate, phenol | 282 |
| Tip | <i>S. typhimurium</i> | Unknown | 206 |
| McpA | <i>S. typhimurium</i> | Unknown | 86,267 |
| McpB* | <i>S. typhimurium</i> | Cystine | 137 |
| McpC | <i>S. typhimurium</i> | Cystine | 137 |

Table 3.1. Chemoreceptors (MCPs) in *S. typhimurium* and *E. coli*.

*Receptor contains the conserved C-terminal pentapeptide motif (NWE^T/sF).

The *E. coli* chemotaxis system can be described as a modular network: a receptor module detects environmental cues and generates an intracellular response, and an adaptation module maintains the kinase activity at a steady state indifferent to the background concentration of chemoeffector^{137,226} (see Chapter 2, Figure 2.4A). In a coarse-grained model²⁶⁰, the essential system-level properties of *E. coli* chemotaxis signaling are described by three dynamic variables: chemoeffector concentration $[L](t)$ (input), receptor-controlled kinase activity $a(t)$ (output), and average methylation level of the receptors $m(t)$ (memory), linked by two transfer functions²⁶⁰. The transition between the active and inactive state of the receptors is described by an allosteric model of the Monod-Wyman-Changeux (MWC) type¹⁷⁶. The transfer function, $G([L], m)$, represents the cooperative modulation of kinase activity by chemoreceptors, determined through the free energy difference, $f_i([L], m)$, between the active and inactive states of the receptor-kinase complex. The second transfer function, $F(a)$, represents enzyme-driven methylation kinetics (see Materials and methods).

Both transfer functions of the chemotactic signaling response to the non-metabolizable chemoattractant α -methyl-aspartate (MeAsp) have been characterized in *E. coli*, using a fluorescence resonance energy transfer (FRET) system²⁴² that provides a real time readout of the output kinase activity, $a(t)$. This FRET assay uses a donor-acceptor pair between the

Network-level variability in bacterial chemotaxis

phosphatase CheZ and the response regulator CheY, fused to yellow and cyan fluorescent proteins (YFP and CFP) respectively ^{226,240-242}. The measured FRET value is proportional to the intracellular concentration of the complex formed between CheZ and phosphorylated CheY, [CheZ·CheY-P], which is determined by the balance between CheY phosphorylation by CheA and its dephosphorylation by CheZ, which have equal rates at steady state. Therefore, the kinase (CheA) activity, $a(t)$, is proportional to [CheZ·CheY-P], and this FRET pair provides a real-time readout of the chemotaxis pathway output $a(t)$ on time scales slower than the relaxation time of the CheY phosphorylation cycle.

Measurements of the amplitude of the initial rapid FRET response to step stimuli allowed characterization of the sensitivity ²⁴¹ and cooperativity ^{76,240} of the *E. coli* receptor module. The methylation kinetics has been studied in *E. coli* by applying temporal exponential ramp stimuli matching the adaptation time scale ²²⁶. The frequency response of the chemotaxis system has been characterized by monitoring the FRET response to oscillatory input signals ²²⁶. Response dynamics has been also measured at different background concentrations of chemoeffector, showing that *E. coli* chemotaxis follows the fold-change detection (FCD) strategy, that is, it responds faithfully to the shape of the input profile irrespective of its absolute intensity ^{137,231} (see Chapter 2). The high degree of conservation between *S. typhimurium* and *E. coli* chemotaxis proteins ^{10,66} permits the utilization of the same FRET assay to probe properties of *S. typhimurium* chemotaxis signaling, as exemplified in Chapter 4 ¹³⁸.

The behavioral performance of *E. coli* in spatial chemoeffector gradients has also been investigated ^{7,8,28,156,276}. Microfluidic technology facilitated studies of the quantitative properties of bacterial chemotaxis performance by enabling the generation of precisely controlled gradients of chemoeffectors, and observations of bacterial behavior at high spatial and temporal resolution ⁸. For example, cell tracking in controlled microenvironments allowed quantification of population-scale transport parameters in *E. coli* ⁹, and diffusion-based microfluidic devices have been developed to generate steady gradients of arbitrary shape ⁷. Such devices were used to observe *E. coli* distributions in linear gradients rescaled by

Chapter 3

their mean concentration and showed that the FCD property holds also in the behavioral chemotactic response¹³⁷.

We examined here the chemotaxis system of *S. typhimurium*, using FRET and microfluidic experiments and the modeling framework developed for *E. coli* chemotaxis. We find that the quantitative parameters that characterize these two transfer functions of the chemotaxis response in *E. coli* and *S. typhimurium* are not conserved. The chemoreceptor response to MeAsp of *S. typhimurium* is less cooperative and the sensitivity of the response has a different dependence on the background level of chemoeffector. *S. typhimurium* shows faster kinetics of receptor methylation, and differences in network-level adaptation properties lead to a higher characteristic frequency below which *S. typhimurium* can compute time derivatives of the input signal. We show that the differences in the control physiology affect the transient and steady-state chemotaxis performance. Using receptor-mutant strains, we demonstrate that the differences between *S. typhimurium* and *E. coli* chemotaxis properties can be ascribed to differences in the receptor population composition, as well as the characteristics of the individual receptors. Our comparison of the dynamical features of *S. typhimurium* and *E. coli* chemotactic signaling and behavior is of fundamental interest as it provides a snapshot of the evolution of bacterial chemotaxis.

3.2. Receptor-kinase response in *S. typhimurium*

To test *S. typhimurium*'s receptor sensitivity to MeAsp, we applied sequential steps of MeAsp, $\Delta[L]$, to populations of cells adapted to a background level $[L]_0$, and measured the amplitude of the initial rapid excitatory response, $\Delta FRET_i$. Figure 3.2A illustrates an example of such an experiment. Like in *E. coli*, the adaptation to MeAsp in *S. typhimurium* is perfect: the steady-state kinase activity of adapted cells is the same as the kinase activity prior to stimulation^{12,241} (Figure 3.2B, see also FRET response time series in Figure 3.2A). However, the steady-state kinase activity, a_0 , in *S. typhimurium*, $a_0^{St} = 0.4$, is higher than a_0 for *E. coli* measured under identical conditions ($a_0^{Ec} = 0.33$)²²⁶. (The superscript Ec is

Network-level variability in bacterial chemotaxis

used for *E. coli* components and parameters and the superscript St – for *S. typhimurium* components and parameters throughout the text.)

We adapted *S. typhimurium* populations to 14 different background levels, $[L]_0$, and constructed dose-response curves of the kinase activity, a , as a function of the total attractant concentration $[L] = [L]_0 + \Delta[L]$ (Figure 3.2C). The sigmoid dose-response curves we fit by a Hill function, $a = a_l + (a_h - a_l) \frac{[L]^{n_H}}{[L]^{n_H} + [K_{1/2}]^{n_H}}$, where $K_{1/2}$ is the ligand concentration of the half-maximum of the response, n_H is the Hill coefficient, and a_l and a_h are the lowest and the highest kinase activity in the dose-response curve. The $K_{1/2}$ values, which provide an estimate for the receptor sensitivity, scale proportionately with the background level over a 1000-fold concentration range (0.03-30 mM $[L]_0$): $\log K_{1/2} \propto \log [L]_0$ with a slope ≈ 1 (Figure 3.2D). In contrast to *E. coli*, where the apparent cooperativity of the response is not constant but peaks in the range $[L]_0 = (0.02 - 3)$ mM, where $n_H > 2$ ^{166,241}, *S. typhimurium* shows a low and nearly constant apparent cooperativity of its MeAsp response: $n_H = 1.3 \pm 0.2$ across the entire range of tested background concentrations (Figure 3.2E). It has been previously shown that within the concentration range 0.02 - 3 mM $[L]_0$ the instantaneous chemotactic kinase response of *E. coli* follows Weber's law^{171,247} (see Chapter 2), *i.e.* it is proportional to the ratio of the change in ligand concentration, $\Delta[L]$, to the background concentration of ligand, $[L]_0$: $\Delta a([L], [L]_0) = k \Delta [L] / [L]_0$. The proportionality constant k is called the Weber-Fechner constant, and in the limit of small $\Delta[L]$, is equivalent to $k = \left. \frac{da}{d \ln [L]} \right|_{[L]=[L]_0}$ ²⁶⁰. From fits to the data of Figure 3.2C, we showed that $\left. \frac{da}{d \ln [L]} \right|_{[L]=[L]_0}$ for *S. typhimurium* is nearly constant in the range $[L]_0 = (0.03 - 30)$ mM (Figure 3.2F). Thus, the *S. typhimurium* chemotaxis network also follows Weber's law, and this property holds over a concentration range spanning three orders of magnitude.

Chapter 3

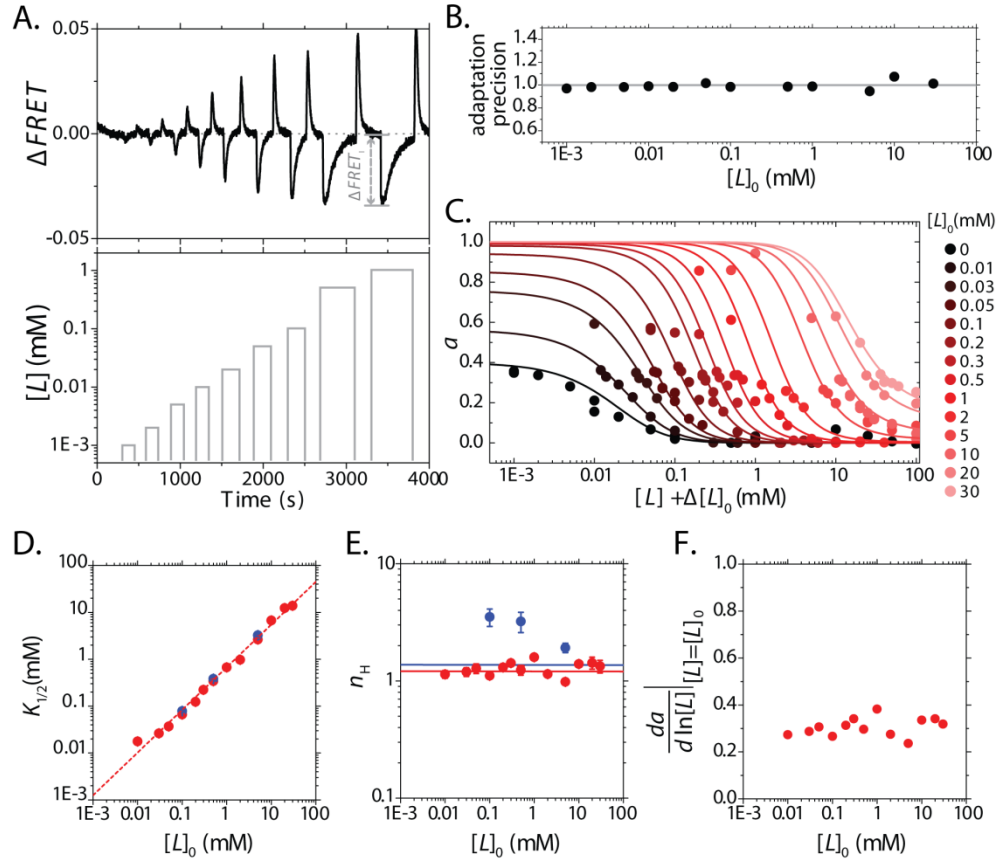


Figure 3.2. Dose-response measurements in wild type *S. typhimurium*. (A) FRET response (top) to step changes in $[L]$ (bottom). (B) Precision of adaptation to different MeAsp concentrations. Adaptation precision is determined as the ratio between the prestimulus value of the kinase activity and the new constant value of kinase activity, reached after adaptation. Perfect adaptation (adaptation precision of 1) is indicated by the gray line. (C) Dose-response data of the kinase activity, a , to steps of MeAsp, applied to cells, adapted at different background concentrations of MeAsp, $[L]_0$. Fits using the MWC model of equations (1), (2), and (3) are shown with parameters $N = 2$, $K_I = 0.026$ mM and $K_A = 27.889$ mM. (D) Concentration of half-maximum response ($K_{1/2}$) and (E) Hill coefficient (n_H) and at different $[L]_0$ for *S. typhimurium* (red) and *E. coli* (blue, data from ²³⁹). In (D), a linear fit with a slope 0.97 ± 0.1 of $K_{1/2}$ values of *S. typhimurium* is shown. Lines in (E) indicate n_H for $[L]_0 = 0$ for *S. typhimurium* (red, 1.1 ± 0.1) and *E. coli* (blue, 1.2 ± 0.1) (F) The local slope of the kinase activity with respect to the logarithm of ligand concentration for *S. typhimurium* at $a = a_0$ and $[L] = [L]_0$, demonstrating Weber's law (see text).

Network-level variability in bacterial chemotaxis

The effect of receptor cooperativity on the transfer function $a = G([L], m)$ is well described in *E. coli* by an MWC-type allosteric model,

$$a = G([L], m) = G(f_t([L], m)) = (1 + e^{f_t([L], m)})^{-1} \quad (1)$$

where f_t is the total free energy, expressed in units of $k_B T$, of the receptor-kinase complex. f_t is an additive function of two linearly independent terms²⁶⁰:

$$f_t([L], m) = N(f_L([L]) + f_m(m)) \quad (2)$$

where N is the number of ligand-binding receptor units in a functional cluster, $f_L([L])$ represents the free energy contribution from ligand binding and $f_m(m)$ is the contribution from receptor methylation (see Materials and methods).

In *E. coli*, the ligand-dependent fraction of total free energy

$$f_L([L]) = \ln \left[\frac{1+[L]/K_I}{1+[L]/K_A} \right], \quad (3)$$

where K_I and K_A are the dissociation constants of the inactive and active receptor states, respectively, is linear in $\log[L]$ over the concentration range $K_I \ll [L] \ll K_A$, where $K_I^{Ec} = 0.018$ mM, $K_A^{Ec} = 2.903$ mM, and the cooperativity of the main receptor for MeAsp, Tar, is high ($N^{Ec} = 6$)¹⁶⁶. *S. typhimurium*'s dose-response curves are well fit by the aforementioned functional form for a (equations (1), (2) and (3)), assuming fixed values for N , K_I and K_A over the whole range of background concentrations²⁶⁰, with parameters $K_I^{St} = 0.026$ mM and $K_A^{St} = 27.889$ mM and $N^{St} = 2$ (Figure 3.2C). The three-fold lower N in *S. typhimurium* could be a consequence of the larger number of receptor species (see Table 3.1), decreasing the number of ligand-binding receptors per cluster, as it has been shown previously that cooperativity increases in pure receptor populations in *E. coli*²⁴⁰. Using *S. typhimurium* cells expressing as the sole receptor species TarSt, we found that the cooperativity of the response observed in pure Tar populations in *S. typhimurium* also increases (Figure 3.3A).

The methylation-dependent free energy in *E. coli* is well-approximated by a linear function, $f_m(m) = \alpha(m^* - m)$, where the offset methylation level $m^* \approx 0.5$ ²²⁶ and the free energy contribution per methylation increment $\alpha \approx 2$ $k_B T$ (see Materials and methods). Using adaptation-deficient $\Delta cheR \Delta cheB$ *S. typhimurium* cells, expressing as the

Chapter 3

sole receptor species Tar^{St} at a fixed modification state (see Materials and methods, Figure 3.3A) so as to fix the methylation-dependent free energy, f_m , we found that the change of f_m per modification increment is linear, similarly to *E. coli* (Figure 3.3B).

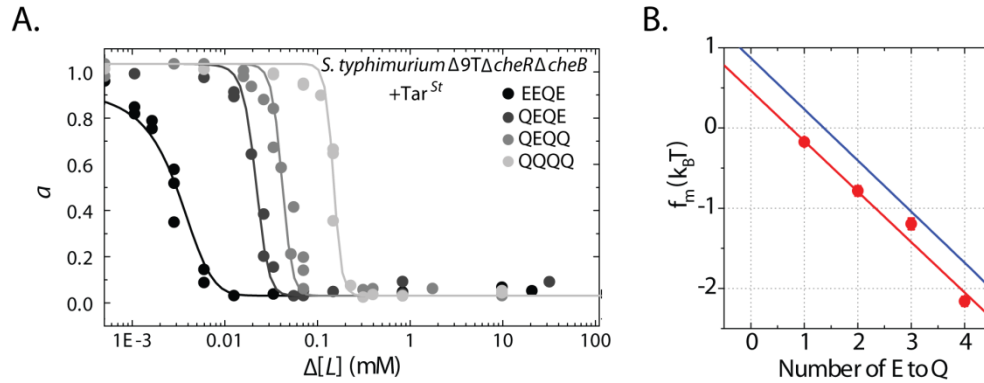


Figure 3.3. Effect of Tar modification in *S. typhimurium*. (A) Dose-response curves for Tar^{St} with a different number of glutamines (Q) per monomer (a modification that mimics methylated glutamate Em), expressed in adaptation deficient $\Delta 9\text{T} \Delta \text{cheR} \Delta \text{cheB}$ *S. typhimurium* cells, in which all nine receptors are deleted from the chromosome. Tar^{St} expression was induced with $1.4 \mu\text{M}$ sodium salicylate. Fits using the MWC model of equations (1), (2), and (3) are shown with parameters $N = 12$, $K_I = 0.026 \text{ mM}$ and $K_A = 27.889 \text{ mM}$. (B) Methylation-dependent free energy f_m of Tar^{St} as a function of the number of glutamines (Q) at the four modification sites per monomer, *i.e.* the methylation increment. The blue line is a linear fit to data from ²²⁶ for $\Delta \text{tar} \Delta \text{tap} \Delta \text{tsr}$ *E. coli*, expressing Tar^{Ec} in different modification states.

3.3. Methylation-level adaptation in *S. typhimurium*

The dynamics of the adaptation module of *E. coli* was recently mapped by FRET measurements using temporal exponential ramp stimuli of the form $[L](t) = [L]_0 e^{rt}$, where r is the ramp rate, t is the time, and $[L]_0$ is the background concentration of MeAsp, to which the cells were pre-adapted before applying a stimulus $L(t)$ ²²⁶. Upon sustained temporal exponential ramp stimulation the methylation feedback signal eventually cancels the change in the ligand input signal exactly, leading to a kinase

output, a_c , that is constant in time ²²⁶. The dependence of the constant output a_c as a function of the ramp rate r represents the sensitivity of the steady-state kinase activity to sustained gradients, and the shape of the feedback transfer function

$$\frac{dm}{dt} = F(a) \quad (4)$$

can be inferred from the curve $a_c(r)$, which we refer to here as the gradient-sensitivity curve. The changes in the ligand-dependent and methylation-dependent free energy cancel each other, i.e. $\frac{df_L}{dt} + \frac{df_m}{dt} = r - \alpha F(a_c) = 0$ (see reference ²²⁶), where $\alpha = \frac{df_m}{dm}$ is the free energy change per methylation increment, thus $F(a_c) = \frac{r}{\alpha}$ can be obtained from the gradient-sensitivity curve by inverting $a_c(r) = F^{-1}(r/\alpha)$, i.e. rescaling the abscissa and inverting the axes about ($r = 0, a_c = a_0$) ²²⁶.

We probed the gradient sensitivity of *S. typhimurium*, applying up ($r > 0$) and down ($r < 0$) exponential ramp stimuli to cells, adapted to $[L]_0 = 0.229$ mM MeAsp (a concentration that belongs to the region of maximal sensitivity for *E. coli*, and was used for analogous experiments in *E. coli* ²²⁶), using a computer-controlled fluid mixer ^{35,226}. Figure 3.4A shows an example of up- and down-ramps ($r = \pm 0.01$), in which constant kinase activities a_c are reached. We plotted a_c as a function of the ramp rate to obtain a gradient-sensitivity curve (Figure 3.4B). The slope $\Delta a_c / \Delta r$ near $r = 0$ is less steep than that of *E. coli* by a factor of approximately three: $\Delta a_c / \Delta r \approx 11$ s for *S. typhimurium*, whereas for *E. coli* under identical conditions $\Delta a_c / \Delta r \approx 30$ s ²²⁶. Thus, a_c responds more sensitively to shallow gradients in *E. coli* than in *S. typhimurium*.

From the gradient-sensitivity curve, we obtained the feedback transfer function $F(a)$, which reveals the methylation kinetics for *S. typhimurium* (Figure 3.4C). The shape of $F(a)$ in *S. typhimurium* is similar to that in *E. coli*. It is a non-linear monotonically decreasing function, which has a single fixed point at $a = a_0$ with a_0 given by $F(a_0) = 0$. The conditions (i) $F'(a_0) < 0$ and (ii) $da/dm > 0$ show that this fixed point is stable ²²⁶. Thus, regardless of the background ligand concentration $[L]_0$, the kinase activity always returns to the same steady-state level a_0 . The slope near $a = a_0$ determines how fast the system relaxes to the steady state after small changes in a . Thus, this slope provides a measure for the strength of

Chapter 3

the methylation-dependent negative feedback in the chemotaxis system. A shallow slope $F'(a_0) \approx -0.01 \text{ (s)}^{-1}$ was measured in *E. coli* ²²⁶. The three-fold steeper slope $F'(a_0) \approx -0.03 \text{ (s)}^{-1}$ that we measured in *S. typhimurium* under identical conditions indicates that the methylation-dependent negative feedback in *S. typhimurium* is three-fold stronger.

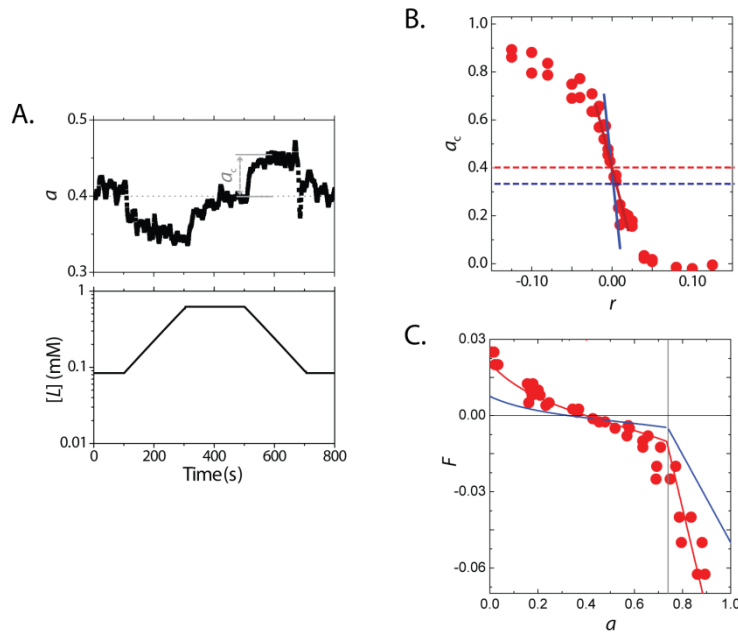


Figure 3.4. Gradient-sensitivity curve and feedback transfer function $F(a)$ in *S. typhimurium*. (A) Kinase activity response of *S. typhimurium* (top) to exponential ramp stimuli with ramp rate $r = \pm 0.01 \text{ s}^{-1}$ (bottom). (B) Gradient-sensitivity curve of wild type *S. typhimurium*, evaluated by measuring the constant kinase activity a_c reached during exponential ramps with rate r . The slope of near $r=0$ is $\Delta a_c / \Delta r \approx -11 \text{ s}$. The slope for *E. coli* ($\approx -30 \text{ s}$) is shown by a blue line (data from reference ²²⁶). Dashed lines show the steady-state kinase activity (a_0) in *E. coli* (blue) and *S. typhimurium* (red) (C) The feedback transfer function $F(a)$ of *S. typhimurium* is mapped using the data from Figure 3.4B (see text). The slope near steady state $F'(a_0)$ in *S. typhimurium* is $\approx -0.03 \text{ (s)}^{-1}$, whereas in *E. coli* the slope $F'(a_0) \approx -0.01 \text{ (s)}^{-1}$ (blue line, *E. coli* data is taken from reference ²²⁶).

3.4. Network-level adaptation in *S. typhimurium*

Calibration of the response functions of the receptor and adaptation modules allows an estimate of the characteristic frequency, ν_m , which sets an upper bound on the frequency range over which the chemotaxis network is able to take time derivatives of the chemoeffector input ²²⁶:

$$\nu_m = \frac{-\alpha F'(a_0) N a_0 (1-a_0)}{2\pi} \quad (5)$$

For *E. coli* $N = 6$, $F'(a_0) = -0.01 \text{ (s)}^{-1}$, $a_0 = 0.33$, and $\alpha = 2$, yielding $\nu_m \approx 0.004 \text{ Hz}$, which is in good agreement with the value experimentally determined using FRET measurements with exponential sinewave inputs, $\nu_m \approx 0.006 \text{ Hz}$ ²²⁶. This characteristic frequency is a network-level adaptation property of the chemotaxis system, as it involves parameters of both modules of the network, and is inversely proportional to the adaptation timescale, τ_m , of the chemotaxis response ²⁶⁰:

$$\tau_m = \frac{1}{2\pi\nu_m} \quad (6)$$

From the calibration of the transfer functions $G([L], m)$ and $F(a)$ (Figures 3.2, 3.3 and 3.4), we estimated the values for the transfer function parameters for *S. typhimurium*: $N = 2$, $F'(a_0) = -0.03 \text{ (s)}^{-1}$, $a_0 = 0.4$, and $\alpha = 2$. Using equation (5), these values lead to a predicted value of the characteristic frequency $\nu_m \approx 0.005 \text{ Hz}$.

We tested experimentally the frequency response of populations of *S. typhimurium* adapted to 0.229 mM MeAsp using temporal exponential sinusoid inputs $[L](t) = [L]_0 \exp(A_L \sin(2\pi\nu t))$ with a fixed input amplitude $A_L = 0.2$, $[L]_0 = 0.229 \text{ mM}$, and frequencies ν ranging between 0.002 and 0.05 Hz. For stimulus variation within the range $K_I \ll [L]_0 \ll K_A$, the change in ligand-dependent free energy $\Delta f_L = f_L([L](t)) - f_L([L]_0)$ follows the logarithm of the ligand concentration, and the kinase outputs to exponential sinewave stimuli are pure sinusoids with frequencies ν matching the frequency of input modulation, and amplitudes $|A|$ and phase delays φ_D dependent on the frequency of input modulation ²⁶⁰ (Figure 3.5A). Both $|A|$ and φ_D can be solved for by linearizing equations (1) and (4) around $a = a_0$, which gives ²²⁶ $\varphi_D(\nu) = \pi - \tan^{-1}(\nu_m/\nu)$ and $|A| = \frac{N a_0 (1-a_0)}{\sqrt{1+(\nu_m/\nu)^2}} A_L$.

Chapter 3

Figure 3.5B shows the frequency dependence of the phase delay, ϕ_0/π , and normalized amplitude of the FRET response, $|A|/|A_{\max}|$ for *S. typhimurium*, where A_{\max} is the amplitude of the output sinewave with maximal amplitude. Fits to the both amplitude and phase response data revealed for *S. typhimurium* a characteristic frequency $\nu_m = 0.017 \pm 0.002$ Hz, nearly three times higher than that of *E. coli*. Interestingly, the measured value for ν_m^{St} differs from that predicted ($\nu_m \approx 0.005$ Hz, see above) from measurements of the transfer functions of receptor and adaptation modules of *S. typhimurium*.

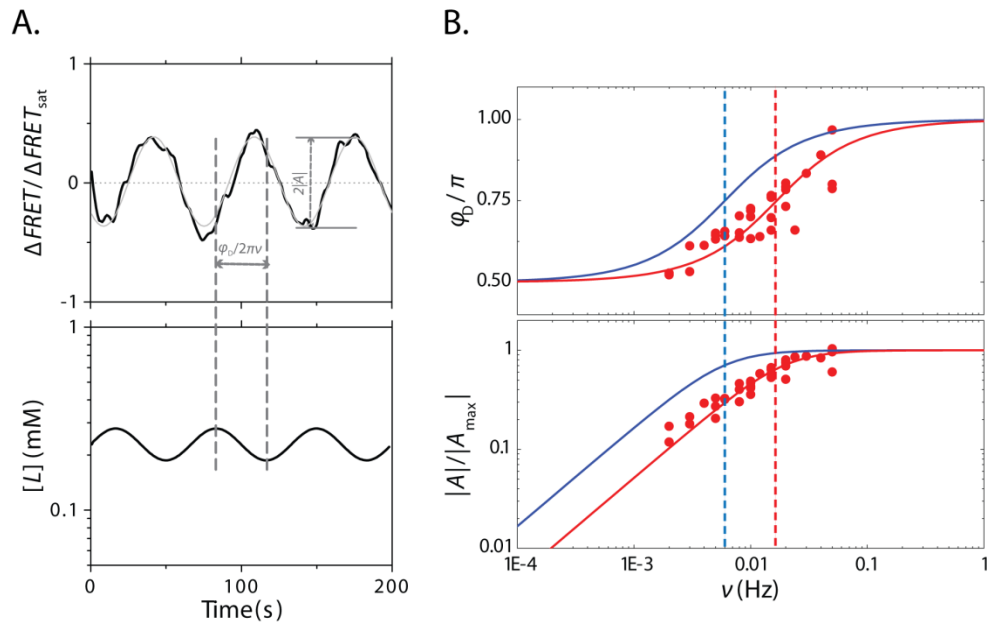


Figure 3.5. Frequency response of *S. typhimurium*. (A) Normalized FRET response (top) to exponential sinewave stimuli with frequencies $\nu = 0.015$ Hz and 0.024 Hz and amplitude $A_L = 0.2$ and $[L]_0 = 0.229$ mM (bottom). (B) Bode plot for wild type *S. typhimurium*, showing the phase delay (top) and the normalized amplitudes (bottom) of the output sinusoids as a function of the driving frequency ν . The red curve is a fit to *S. typhimurium* data and the blue curve is a fit to *E. coli* data from ²²⁶. The characteristic frequencies for *S. typhimurium* (red) and *E. coli* (blue) are indicated with dashed lines.

3.5 Role of CheV on network-level properties of *S. typhimurium* chemotaxis

The hybrid protein CheV, which has an N-terminal domain homologous to the scaffolding protein CheW, and C-terminal regulatory domain homologous to CheY and hence is likely to be phosphorylated, exists in *S. typhimurium* but not in *E. coli*¹⁰ (see Chapter 5). Thus CheV might be involved in the differences in the transfer functions $F(a)$ and $G([L],m)$, as well as the frequency response we observed between the two species. For example, CheV phosphorylation could provide a mechanism for methylation-independent feedback in *S. typhimurium*, leading to faster or slower network-level adaptation.

We measured the dependence of the rapid response to step changes in $[MeAsp]$ for different background concentrations of MeAsp in $\Delta cheV$ *S. typhimurium* (Figure 3.6A), in the same manner by which we measured this response in wild type *S. typhimurium* (Figure 3.2C). We fit these dose-response data of the $\Delta cheV$ strain using the MWC model of equations (1), (2), and (3), and obtained parameters $N = 2$, $K_I = 0.015$ mM and $K_A = 20.207$ mM, which are very similar to those obtained from the data for the wild type strain.

We also applied exponential sinewave inputs of different frequencies to determine the characteristic frequency ν_m of the $\Delta cheV$ *S. typhimurium* frequency response. Fits of both amplitude and phase delay data (Figure 3.6B) gave $\nu_m \approx 0.016$ Hz, which is very similar to the ν_m measured for wild type *S. typhimurium*. Thus neither the higher characteristic frequency of the response, nor the lower cooperativity of the response of *S. typhimurium* compared to *E. coli* can be explained by the presence of the *S. typhimurium*-specific protein CheV (see Chapter 5 for further experiments on the effects of CheV in the chemotactic signaling of *S. typhimurium*).

Chapter 3

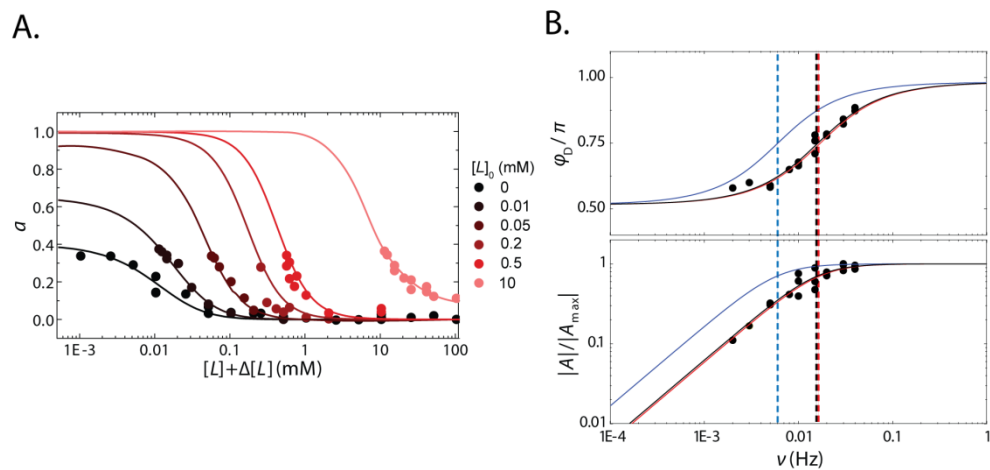


Figure 3.6. Kinase response of $\Delta cheV$ *S. typhimurium*. (A) Dose-response data of the kinase activity (a) to steps of MeAsp, applied to $\Delta cheV$ *S. typhimurium* cells, adapted at different background concentrations of MeAsp, $[L]_0$. Fits using the MWC model of equations (1), (2), and (3) are shown with parameters $N = 2$, $K_I = 0.015$ mM and $K_A = 20.207$ mM. (B) Bode plot for $\Delta cheV$ *S. typhimurium* (black points), showing the phase delay (top) and the normalized amplitudes (bottom) of the output sinusoids as a function of the driving frequency ν (see text). Red and blue curves are fits to data for wild type *S. typhimurium* and wild type *E. coli*, respectively. The characteristic frequencies for $\Delta cheV$ *S. typhimurium* (black), wild type *S. typhimurium* (red) and wild type *E. coli* (blue) are indicated with dashed lines.

3.6. Differences in chemotactic performance of *S. typhimurium* and *E. coli* in spatial gradients

The transfer functions of chemotactic signaling determine the organism's chemotactic performance¹¹⁴, thus it is of interest to ask how the observed differences in receptor-kinase response and adaptation kinetics of *S. typhimurium* and *E. coli* affect their chemotactic performance in identical microenvironments. The behavioral response of *E. coli* was recently probed in steady linear gradients of MeAsp with the magnitude of the gradient $\nabla[L]$ rescaled by the mean concentration $[L]_0$, i.e. $\nabla[L]/[L]_0 = \text{const}$ ¹³⁷.

We tested the *S. typhimurium* response in steady linear gradients of MeAsp created in a similar manner using a microfluidic platform of a design described in reference⁷ (Figure 3.7A). The platform consisted of a polydimethylsiloxane (PDMS) layer, in which "source", "sink", and "test" channels were patterned, and one face opened towards an agarose hydrogel. MeAsp solutions with different concentrations were flowed through the source and the sink channels, such that $\nabla[L]/[L]_0 = 0.7 \text{ mm}^{-1}$, and $[L]_0$ was varied over the range 0.005 - 36.871 mM. Diffusion of MeAsp within the agarose layer, sandwiched between a glass slide and the PDMS layer, lead to establishment of a stable linear gradient in the agarose hydrogel, which is rapidly mirrored in the test channel after injection of the bacterial suspension⁷ (Materials and methods).

We recorded the time evolution of the distribution of *S. typhimurium* populations within the test channel using time-lapse video microscopy. We determined the positions of the bacteria in the channel to yield the distribution of the bacteria along the spatial coordinate x in time t , $B(x, t)$. (For simplicity we consider a one-dimensional system along coordinate x throughout this study.) To estimate the strength of the chemotactic response in different gradients, we computed the chemotaxis migration coefficient (CMC), a dimensionless metric, for one hundred equally spaced time frames for each experiment. CMC represents the mean displacement of the population from the center of the channel¹⁵⁶, normalized by the channel half-width:

$$CMC(t) \equiv \frac{\langle x \rangle(t) - W/2}{W/2} \quad (7)$$

Chapter 3

where W is the width of the test channel (600 μm) and $\langle x \rangle(t)$ is the population-averaged spatial coordinate of the bacteria along the chemoeffector gradient. We used the absolute value $|CMC|(t)$ to quantify the dynamics of the chemotaxis response. Figure 3.7B shows the time evolution of $|CMC|$ for each of the eight tested gradients of MeAsp. For each gradient, $|CMC|$ increases until it reaches a steady state, $|CMC|_{ss}$.

The steady-state $|CMC|$ profile, $|CMC|_{ss}$, as a function of the mean concentration of the gradient, showed a characteristic inverted U-shape for *S. typhimurium* (Figure 3.7C). $|CMC|_{ss}$ was high and nearly invariant ($|CMC|=0.37\pm 0.04$) in the range $[L]_0=(0.064 - 10.345)$ mM, whereas for smaller or larger $[L]_0$, $|CMC|_{ss}$ decreases monotonically. In contrast, the *E. coli* $|CMC|_{ss}$ profile showed two nearly flat plateaus, in the ranges $[L]_0=(0.12 - 0.43)$ mM and $(0.815 - 10.345)$ mM: these two plateaus correspond to the concentration regimes in which the response of pre-adapted bacterial populations to fold-changes in the input are invariant to changes in the background, described earlier as “FCD regimes”¹³⁷ (Chapter 2). Our results show that the fold-change detection (FCD) property, *i.e.* invariance of the response to relative gradients $\nabla[L]/[L]_0$, irrespective of the absolute magnitude of $\nabla[L]$ or $[L]_0$, holds in *S. typhimurium* within a single FCD regime of background concentrations, $[L]_0=(0.064 - 10.345)$ mM.

At steady state, the distribution of the bacteria is well described by an exponential distribution $B(x)_{ss} = B_0 e^{-x/\lambda_{ss}}$, where B_0 is the cell density at $x=0$, and $\lambda_{ss} = \langle x \rangle_{ss}$ is the mean position of the bacterial population (Figure 3.7D; see Materials and methods). λ_{ss} can be expressed as $\lambda = D_B/v_D$, where v_D is the drift velocity of the bacterial population, and D_B is the random motility coefficient of the cells in an absence of attractant¹¹⁵. From equation (7) it follows that

$$|CMC|_{ss} \equiv |2\lambda_{ss}/W - 1| = |2D_B/(v_D W) - 1| \quad (8)$$

Thus $(1/\lambda)_{ss}$ is proportional to v_D and has a hyperbolic dependence on $|CMC|_{ss}$, *i.e.* $(1/\lambda)_{ss} = 2/(2W - W|CMC|_{ss}) = v_D/D_B$. We plotted $(1/\lambda)_{ss}$ as a function of the background level $[L]_0$, for both *S. typhimurium* and *E. coli* (Figure 3.7C *Inset*), and this also revealed a single plateau shape for *S. typhimurium* and two plateaus for *E. coli*.

Network-level variability in bacterial chemotaxis

In order to compare the transient chemotactic response between *S. typhimurium* and *E. coli*, we calculated the times τ_{50} and τ_{90} , in which the swimming populations of cells reached respectively 50% and 90% of the steady-state $|CMC|$ levels, $|CMC|_{ss}$ (Figure 3.7E and Figure 3.7E *Inset* respectively). We calculated also τ_{50} and τ_{90} for *E. coli*, using the data of reference¹³⁸. The two species show a large difference in the mean time to reach steady state: $\langle \tau_{50} \rangle = 105 \pm 38$ s for *S. typhimurium*, whereas $\langle \tau_{50} \rangle = 489 \pm 248$ s for *E. coli*. The respective $\langle \tau_{90} \rangle$ values are 322 ± 68 s and 1157 ± 335 s.

Recent theoretical studies by Yuhai Tu's group have shown that the drift velocity, v_D , of numerically simulated bacterial populations is phenomenologically well described by a simple relation, *i.e.* $v_D = CG/(1 + G/G_c)$: it depends linearly on the gradient G , until it reaches a maximal value v_D^{\max} beyond a critical gradient G_c ^{114,232}. v_D^{\max} and G_c are proportional to the square root of the methylation rate constant K_R ¹¹⁴ (corresponding to $F'(a_0)$ in our notation²⁶⁰), which could provide an explanation of the smaller values of τ_{50} and τ_{90} of *S. typhimurium* compared to that of *E. coli* (we determined that the methylation rate in *S. typhimurium* is three-fold lower than that of *E. coli*, see Figure 3.4). The dependence of $|CMC|_{ss}$ on $[L]_0$ that reflects the dependence of v_D on $[L]_0$ suggests that the gradients that we used in our experiments have steepness smaller or comparable to G_c . The reason why τ_{50} and τ_{90} , reflecting the transient drift velocity, are nearly constant in *S. typhimurium* requires further investigation. The larger spread in the τ_{50} and τ_{90} values for *E. coli* might reflect the larger variation in the drift velocities at different $[L]_0$, expected from the data shown on Figure 3.7C. Note that the *E. coli* data come from single experiments per gradient¹³⁷ whereas 3-5 repeats per gradient were performed for *S. typhimurium*, which is also likely to explain the greater spread in the *E. coli* data.

Chapter 3

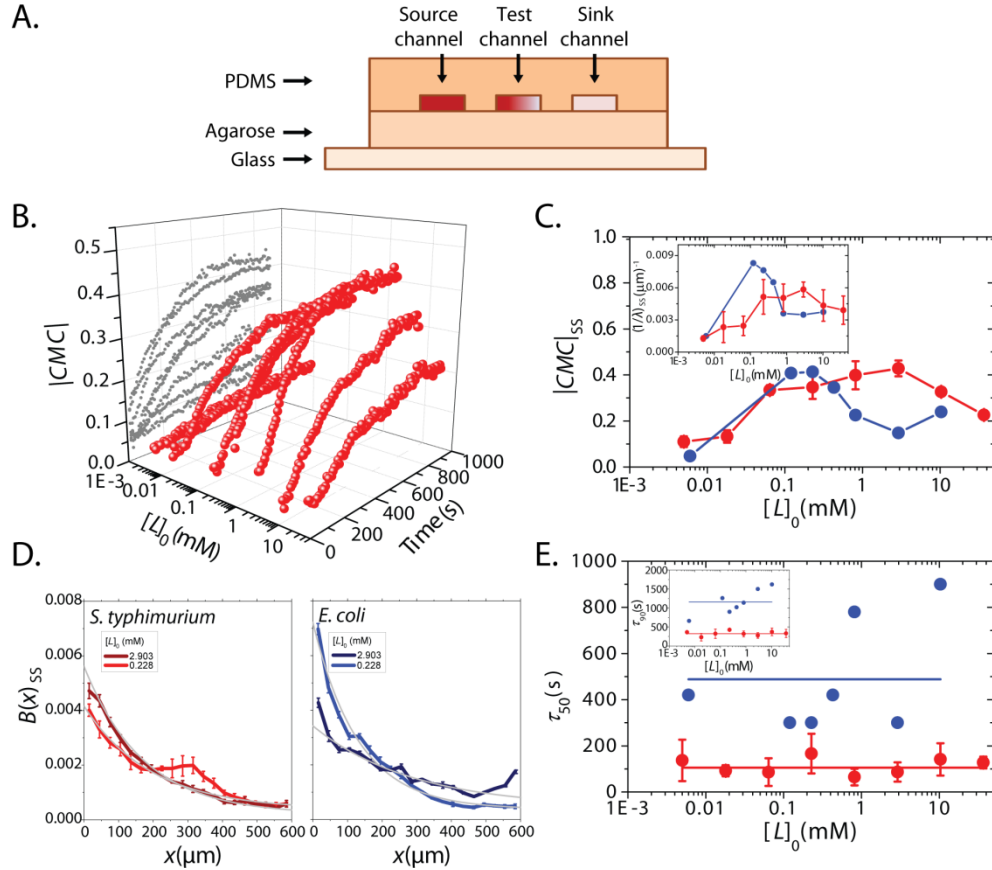


Figure 3.7. Chemotactic behavior of *S. typhimurium* in steady linear gradients of MeAsp. (A) Schematic cross-section of the diffusion-based microfluidics gradient generator (see text). (B) 3D plot of the chemotaxis migration coefficient $|CMC|(t, [L]_0)$. The projections (gray) show the time evolution of the chemotactic response. (C) Steady-state levels of $|CMC|$, $|CMC|_{ss}$, for *S. typhimurium* (red) and *E. coli* (blue) in rescaled gradients of MeAsp. *Inset*: inverse value of the decay constant λ_{ss} taken from exponential fits to steady-state distributions $B(x)_{ss}$ of both species (see (D)). (D) Examples of $B(x)_{ss}$ of *S. typhimurium* and *E. coli* for different gradients (see legends). Exponential fits to $B(x)_{ss}$ from which λ_{ss} values are obtained are shown in gray (note that not all the fits are well constrained). (E) Times, τ_{50} , in which the swimming populations of *S. typhimurium* (red) and *E. coli* (blue) populations reached 50% of $|CMC|_{ss}$ in the rescaled gradients of MeAsp with different mean concentration, $[L]_0$. *Inset*: Times, τ_{90} , in which the same populations reached 90% of $|CMC|_{ss}$. The lines indicate the mean values of τ_{50} and τ_{90} . Error bars in represent standard deviation from 3-5 repeats.

3.7. Sensitivity modulation of *S. typhimurium* and *E. coli* chemotactic response

We sought to explain the differences in the behavioral performance of *S. typhimurium* and *E. coli* in terms of the differences in the underlying control physiology. We define $\psi([L]_0) \equiv \left. \frac{\partial f_t}{\partial \ln[L]} \right|_{[L]=[L]_0}$ as the ‘sensitivity modulation profile’ of the kinase response. The dependence of both the change of kinase activity upon temporal ligand stimulation and drift velocity of cells in spatial gradients is proportional to $\psi([L]_0)$, i.e. $\Delta a \propto \psi([L]_0)$ and $v_D \propto \psi([L]_0)$ (see Materials and methods):

$$\Delta a = -a_0(1 - a_0)\psi([L]_0)\frac{\Delta[L]}{[L]_0} \quad (9),$$

$$v_D \approx \frac{v^2\tau H(1-a_0)\psi([L]_0)}{2+\frac{\tau}{\tau_m}} \frac{d \ln[L]}{dx} \quad (10),$$

where a_0 is the steady-state kinase activity, v is the mean run speed, τ is the average run length, H is the Hill coefficient of the flagellar motor response and τ_m is the adaptation time scale of the chemotactic response^{114,115,260}.

Our FRET setup allowed us to determine experimentally the shape of $\psi([L]_0)$. We pre-adapted immobilized bacterial populations to different background levels of MeAsp within the range $[L]_0 = (0.001 - 36.871)$ mM, and probed $\psi([L]_0)$ for both *S. typhimurium* and *E. coli* using exponential sinewave stimuli with an amplitude $A_L = 0.2$ and frequency close to characteristic frequency ν_m of the respective species (Figure 3.8A; $\nu = 0.015$ Hz for *S. typhimurium* and $\nu = 0.006$ Hz for *E. coli*, see section 3.4). The absolute amplitude $|A|$ of the sinusoidal response can be expressed as a function of $\psi([L]_0)$ by linearizing equations (1) and (4) around the steady state $a = a_0$ and solving for $|A|$:

$$|A|([L]_0) = \frac{\psi([L]_0)a_0(1-a_0)}{\sqrt{1+(\nu_m/\nu)^2}} A_L \quad (11)$$

In the experiments shown on Figure 3.8, $\nu \approx \nu_m$, thus $\psi([L]_0) = \frac{|A|([L]_0)}{a_0(1-a_0)\frac{A_L}{\sqrt{2}}}$.

For both species the phase delay φ_D does not change over the tested range of background concentrations (Figure 3.8B): it has a mean value of $(0.72 \pm 0.02)\pi$ for *S. typhimurium* and $(0.78 \pm 0.02)\pi$ for *E. coli*, showing that the adaptation timescale τ_m (see equation (6)) is invariant with the background

Chapter 3

level over the entire range of tested concentrations. However, in both species the amplitudes of the kinase response depend on the background concentration, $[L]_0$, leading to different shapes of $\psi([L]_0)$. For *S. typhimurium*, $\psi([L]_0)$ forms a single peak, where a plateau of nearly constant amplitudes is observed in the range $[L]_0 = (0.064 - 2.903)$ mM (Figure 3.8C left). In contrast, two adjacent plateaus of nearly invariant $\psi([L]_0)$, in the ranges $[L]_0 = (0.018 - 0.229)$ mM and $(0.815 - 10.345)$ mM, are observed for *E. coli* (Figure 3.8C right). The plateaus correspond to the FCD regimes of invariant responses described in Chapter 2¹³⁷, although the transition between the plateaus is somewhat smoother than in the data reported in Chapter 2¹³⁷.

The sensitivity modulation $\psi([L]_0)$ is defined as the change of the free energy f_t with the logarithm of ligand concentration $[L]$ at $[L] = [L]_0$:

$$\psi([L]_0) = \frac{\partial f_t}{\partial \ln[L]} = N \left(\frac{[L]_0}{[L]_0 + K_I} - \frac{[L]_0}{[L]_0 + K_A} \right) \quad (12)$$

Thus, the profile of $\psi([L]_0)$ for ligand binding to a single receptor species has the shape of a single peak, where the width of the peak depends on the separation between the dissociation constants of the inactive and active receptor states, K_I and K_A , and the number of ligand-binding receptor units per cluster, N , determines the height of the peak. We found that $\psi([L]_0)$ for *S. typhimurium* could be well fit using equation (12) with parameters $N = 4$, $K_I = 0.014$ mM, $K_A = 23$ mM (Figure 3.8C left, dotted line). Surprisingly, N is two-fold higher than that predicted from the measurements of the receptor sensitivity using step stimuli (Figure 3.2). Using $N = 4$, and the other parameters obtained from the characterization of the chemotactic transfer functions, the predicted characteristic frequency of *S. typhimurium* from equation (5) is ~ 0.010 Hz. This value is still lower but closer to that measured experimentally (~ 0.017 Hz).

In *E. coli* we observed two adjacent plateaus in both behavioral (Figure 3.7C) and signaling (Figure 3.8C) data suggesting that $\psi([L]_0)$ has a more complex shape. FRET measurements of receptor sensitivity in *E. coli* using step stimuli²⁴¹ showed that the serine receptor, Tsr^{Ec}, likely also binds MeAsp at high concentrations, with dissociation constants $K_{I2} \approx 100$ mM and $K_{A2} \gg 100$ mM¹²⁰. Thus the second plateau could correspond to the transition regime between Tar-dependent and Tsr-dependent peaks. Tsr-

Network-level variability in bacterial chemotaxis

dependent responses are hard to measure experimentally because concentrations of MeAsp > 10 mM were reported to mechanically perturb receptors in *E. coli* via the osmotic pressure they induce²⁶³. However, a two receptor species MWC model (see Materials and methods) fits well the experimental data for *E. coli*'s $\psi([L]_0)$ with parameters $a_0 = 0.33$, $N_1 = N_2 = 7$, $K_{I1} = 0.005$ mM, $K_{A1} = 0.7$ mM, $K_{I2} = 10$ mM, $K_{A2} = 10^4$ mM (Figure 3.8C right).

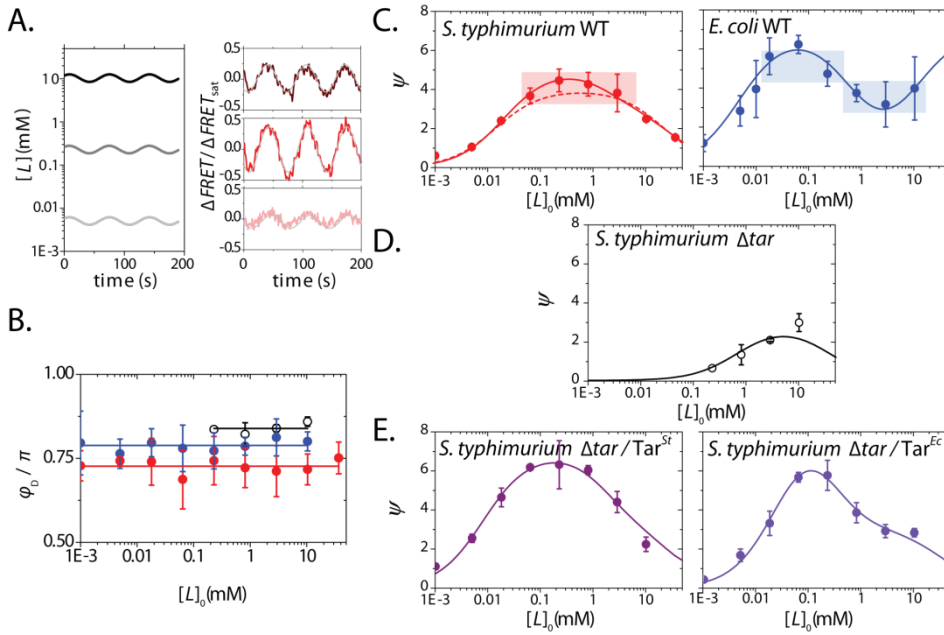


Figure 3.8. Sensitivity modulation profile $\psi([L]_0)$ in wild type and mutant strains. (A) An example of exponential sinusoid inputs with amplitude rescaled with $[L]_0$ ($\nu = 0.015$ Hz, $[L]_0 = 0.005, 0.229, \text{ and } 10.345$ mM) (left). For each input, the normalized FRET output for WT *S. typhimurium* is shown (right). (B) Phase delays of the output sinusoids for stimuli of the type shown in (A) with a driving frequency of $\nu = 0.015$ Hz for *S. typhimurium* (WT – red, Δtar – open points), and $\nu = 0.006$ Hz for WT *E. coli* (blue). The solid lines represent the mean values for each strain. (C-E) $\psi([L]_0)$ in response to inputs of the type shown in (A) for (C) WT *S. typhimurium* (red) and WT *E. coli* (blue), (D) Δtar *S. typhimurium* (open points), (E) Δtar *S. typhimurium*, complemented with Tar^{St} (purple, NaSal induction level of $1.4 \mu\text{M}$) or Tar^{Ec} (violet, $1.4 \mu\text{M}$ NaSal). The plateaus of invariant responses are indicated by the shaded rectangles. Error bars represent standard deviation from 3-5 repeats. The fitted parameters are indicated within the text.

3.8. Tar-independent MeAsp response in *S. typhimurium*

To test whether the shape of the sensitivity modulation profile $\psi([L]_0)$ of wild type *S. typhimurium* is determined by a single chemoreceptor, we probed the response of Δtar *S. typhimurium* cells that lack the main chemoreceptor for MeAsp, Tar (see Table 3.1). We used exponential sinewave stimuli of the type shown on Figure 3.8A. Responses of Δtar *S. typhimurium* to MeAsp were detected starting at relatively low background concentrations of MeAsp, $[L]_0$, with a threshold ~ 0.229 mM (Figure 3.8D). The steady-state kinase activity a_0 was ~ 0.4 , similar to that of wild type *S. typhimurium*. We have not tested background concentrations higher than 36.871 mM because the osmotic shock they induce is likely to mechanically perturb receptors in *S. typhimurium* as has been observed in *E. coli* ²⁶³. A fit using equation (12) with parameters $N = 3$, $K_I = 0.743$ mM, $K_A = 36.388$ mM is shown on Figure 3.8D (see section 3.9).

The phase delays of the output sinewaves remained nearly constant, with a mean $\sim 0.84 \pm 0.02$, which is $\sim 14\%$ higher than the phase delay observed for wild type *S. typhimurium* (Figure 3.9B). Since $\varphi_D = \pi - \tan^{-1}(v_m/v)$ ²²⁶, we calculated that the characteristic frequency of the chemotactic response of Δtar *S. typhimurium* is $v_m = 0.004$ Hz, ~ 4 -fold lower than that of wild type *S. typhimurium* (note that both strains have $a_0 \approx 0.4$). Thus, the Tar-independent response has a longer adaptation timescale, *i.e.* smaller characteristic frequency, than that for TarSt.

The Tar-independent response to MeAsp could be mediated either via chemoreceptors or alternative pathways ¹⁸⁵. In the presence of the methylation enzymes CheR and CheB, Δtar *S. typhimurium* cells do adapt perfectly to MeAsp steps (Figure 3.9A), whereas minor partial adaptation is observed in $\Delta cheR \Delta cheB$ knockout cells (Figure 3.9B; see also Chapter 5 that discusses possible methylation-independent mechanisms of partial adaptation in *S. typhimurium*). These results indicate that adaptation in the Tar-independent response depends on the activities of CheR and CheB, presumably by methylation / demethylation of chemoreceptors.

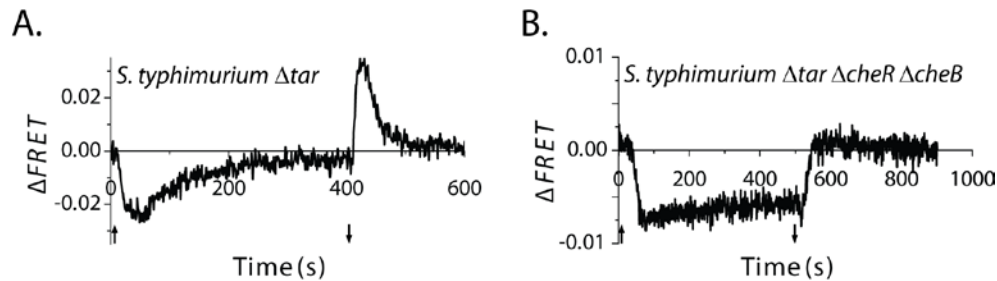


Figure 3.9. Time series of the FRET response of Δtar *S. typhimurium* strains. (A) Response of CheR CheB + strain to 10 mM MeAsp. (B) Response of $\Delta cheR \Delta cheB$ strain to 10 mM MeAsp. The attractant is added and removed at 0 and 400 s, and 0 and 500 s, respectively (addition and removal are indicated with up and down arrows).

3.9. Differences between the Tar receptors of *E. coli* and *S. typhimurium* contribute to the different shape of the sensitivity modulation profiles

Differences in the population of chemoreceptor species (see Table 3.1), or in the properties of the Tar receptors of *E. coli* and *S. typhimurium* could affect the shape of the sensitivity modulation profile $\psi([L]_0)$, which determines the background dependence of the kinase response upon temporal modulation of ligand concentration, and drift velocity of cells in spatial gradients. At the receptor-population level, high concentrations of MeAsp are thought to be sensed not only by Tar, but also by Tsr in *E. coli*²³⁹, and we have found evidence for a pathway independent of Tar in *S. typhimurium* (Figure 3.8D). The Tar-independent receptor response in *S. typhimurium* does not manifest itself as second plateau in the receptor-sensitivity profile $\psi([L]_0)$, as observed in *E. coli*. This reflects the fact that the responsive concentration range of the Tar-independent pathway in *S. typhimurium* is not well separated from that of the Tar-mediated pathway, leading to partially overlapping sensitivity peaks for the two pathways.

To test whether differences in the Tar receptor itself contribute to differences in the sensitivity modulation profiles, we expressed in Δtar *S. typhimurium* cells either TarSt or Tar^{Ec} from a plasmid with sodium salicylate (NaSal) inducible promoter (Figure 3.8E; for both strains $a_0 \approx 0.2$).

Chapter 3

Δtar *S. typhimurium*, complemented with Tar^{St} , showed a singly-peaked sensitivity profile similar to that of wild type *S. typhimurium*. We obtained fits of the data for wild type *S. typhimurium*, Δtar *S. typhimurium* complemented with Tar^{St} , and Δtar *S. typhimurium* with the two-species MWC model, using the same parameters $N_2 = 3$, $K_{I2} = 0.74$ mM, and $K_{A2} = 36.39$ mM for species 2. For species 1, *i.e.* Tar, the parameters obtained for wild type *S. typhimurium* are $N_1 = 5$, $K_{I1} = 0.020$ mM, and $K_{A1} = 1.20$ mM, and for the strain, expressing Tar^{St} from a plasmid, $N_1 = 7$, $K_{I1} = 0.008$ mM, and $K_{A1} = 1.34$ mM ($N_1 = 0$ for Δtar *S. typhimurium*). The lower N_1 in wild type is likely to be a consequence of lower number of Tar^{St} ²⁴⁰.

Δtar *S. typhimurium*, complemented with Tar^{Ec} , showed a sensitivity profile with two plateaus (at (0.064-0.229) mM and (0.815-10.345) mM $[L]_0$) resembling more closely the response of *E. coli*. The data could be fit by a two-species MWC model, using for species 2 the same parameters that we used to fit the Δtar *S. typhimurium* data (Figure 3.8D), *i.e.* $N_1 = 7$, $K_{I1} = 0.031$ mM, $K_{A1} = 0.29$ mM, $N_2 = 3$, $K_{I2} = 0.74$ mM, $K_{A2} = 36.39$ mM (Figure 3.8E left). Note that the dissociation constants for species 1 differ from those for wild type *E. coli* ($N_1 = 7$, $K_{I1} = 0.005$ mM, $K_{A1} = 0.7$ mM).

3.10. Discussion

We have provided the first, to our knowledge, systematic comparison of chemotaxis signaling dynamics and behavior between *S. typhimurium* and *E. coli*. Despite the similarity of their chemotaxis systems at the molecular level, the two species show substantial quantitative differences in their network-level chemotactic signaling characteristics and behavioral responses.

We used *in vivo* FRET combined with time-varying stimuli to characterize both transfer functions of the modular network: $G([L], m)$, which determines how the receptor module detects chemoeffector signals and generates the excitatory response, and $F(a)$, which describes the dynamics of the adaptation module that maintain the steady-state kinase activity invariant to the background chemoeffector concentration. We determined conserved features of the response between *E. coli* and *S. typhimurium*: perfect adaptation to MeAsp, invariant adaptation time

scale over a broad range of background concentrations, and linear dependence of the modification-dependent free energy on the number of modified glutamates. However, many quantitative features of the signal detection and processing and behavioral responses differ between the two species. We discuss below the mechanistic origin of each of these features.

The apparent cooperativity of the response to MeAsp is low and constant in *S. typhimurium* over more than four orders of magnitude of background concentrations (Figure 3.2), whereas the apparent cooperativity in *E. coli* is not constant and nearly three-fold higher in the background concentration range centered at the geometric mean of the dissociation constants of active and inactive chemoreceptor Tar^{166,241}. This weaker signal amplification at the level of the receptor-kinase complex in *S. typhimurium* could be a consequence of a smaller number of ligand-binding receptor units associated with each kinase molecule, e.g. because of the larger number of receptor species in *S. typhimurium*, leading to a smaller relative number of MeAsp binding receptors in the overall receptor population. Indeed we showed that for pure Tar populations in cells that express Tar as the sole chemoreceptor, the cooperativity of the response is augmented (see Figure 3.3).

In *S. typhimurium* the time scales of adaptation, both evaluated at the level of methylation kinetics by mapping $F(a)$ using exponential ramp stimuli (Figure 3.4), and at the level of the network by measuring the frequency response (Figure 3.5), are three-fold shorter than those observed in *E. coli*. The mechanistic origin of the faster adaptation to MeAsp of *S. typhimurium* likely lies in the properties of the populations of adaptation enzymes, CheR and CheB. However, using the parameters of the two transfer functions obtained for *S. typhimurium*, we were not able to predict the experimentally measured network-level adaptation timescale: according to equations (5) and (6), the three-fold lower cooperativity factor N of the response in *S. typhimurium* should cancel out the three-fold faster methylation kinetics. Thus, additional factors not represented in the model²⁶⁰ might contribute to the faster network-level adaptation timescale (i.e. higher characteristic frequency of the response) in wild type *S. typhimurium*. We ruled out the involvement of the *S. typhimurium* protein CheV in this

Chapter 3

discrepancy, by showing that it does not affect either the cooperativity or the characteristic frequency of the response (Figure 3.6).

We observed differences between the sensitivity modulation profiles of *E. coli* and *S. typhimurium*, which determine the kinase-activity and drift-velocity dependence on the background level (see equations (9) and (10)). We have demonstrated that both a Tar-independent response and the properties of the Tar receptor itself contribute to the differences between the sensitivity-modulation profiles of the two species (Figure 3.8D, E). The Tar-independent response in *S. typhimurium* could be receptor-independent or mediated by one or more chemoreceptors. The fact that only minor partial adaptation is observed in $\Delta tar \Delta cheR \Delta cheB$ cells (Figure 3.9B) suggests that the Tar-independent response does involve methylation / demethylation of chemoreceptors.

The model described in reference ²⁶⁰ assumes that each receptor dimer binds a single ligand molecule. Bieman and Koshland ³² indeed demonstrated that aspartate binds to *E. coli* Tar dimers with half-of-sites negative cooperativity, i.e. if one of the binding sites in the dimer is occupied, the second cannot bind aspartate. However, these authors also showed that the negative cooperativity of *S. typhimurium* Tar dimers is weaker, i.e. if one of the binding sites in the dimer is occupied, the second binds aspartate with lower affinity. If the two sets of dissociation constants, K_{I1} , K_{A1} and K_{I2} , K_{A2} , of the two binding sites are separated sufficiently, the actual cooperativity of the response could be higher than the apparent one ($N=2$), determined using the standard MWC model, which assumes a single binding site in each of N dimers in a complex.

Differences in the sensitivity profile between *S. typhimurium* and *E. coli* can explain differences in the behavioral response between the two species (Figure 3.7). Both the steady state chemotactic migration coefficients, $|CMC|_{ss}$, and the inverse values of the exponential decay constants λ_{ss} of the steady-state distributions $B(x)_{ss}$, $(1/\lambda)_{ss}$ serve as a proxy for the drift velocity v_D . Thus, as expected from the measured sensitivity profiles for *S. typhimurium* and *E. coli* and the v_D dependence on the sensitivity profile (equation (10)), $|CMC|_{ss}$ and $(1/\lambda)_{ss}$ for *S. typhimurium* show a single broad peak, whereas $|CMC|_{ss}$ and $(1/\lambda)_{ss}$ for *E. coli* – two adjacent plateaus (Figure 3.7C and Figure 3.7C *Inset*, note that the small difference in shape

Network-level variability in bacterial chemotaxis

can be explained with the non-linear dependence of $|CMC|_{ss}$ on v_D). These profiles are in very good agreement with the profiles of kinase activity measured with FRET (Figure 3.8C).

The single plateau in *S. typhimurium* and two plateaus in *E. coli* observed at both the signaling (Figure 3.8C) and behavioral (Figure 3.7C) levels can be considered as fold-change detection (FCD) regimes: concentration ranges in which the entire time evolution of the response is invariant upon multiplication of both the stimulus and the background by a scalar constant^{137,231} (see Chapter 2). The conditions for FCD regarding the main MeAsp receptor Tar, namely perfect adaptation (i), logarithmic sensing (ii) and linearity of the methylation-dependent free energy of the receptor-kinase complex (iii)¹³⁷, were also shown to hold in both species. Thus, the FCD property has been conserved in the two species, suggesting that it might provide a selective advantage to the bacteria.

What are the ecological implications of the observed differences in *S. typhimurium* and *E. coli* chemotactic signaling and migration behavior? The two species descended from a common ancestor, so the observed differences must reflect the consequences of natural selection in the relatively recent evolutionary history of the two species. Both species have two habitats: host (animals, primary habitat) and non-host (water, soil etc, secondary habitat)²⁷⁴. *S. typhimurium* actively cycles between host and non-host environments, whereas *E. coli* has a low rate of survival in non-host environments and lower probability of colonizing a new host^{106,274}. Although such natural environments are not well characterized and therefore difficult to reproduce in experiments, differences in chemotactic characteristics might reflect the optimization of chemotaxis in enteric bacteria to different conditions. Future ecological studies in enteric bacteria could shed light on the ecological significance of the differences in chemotaxis that we have observed between *S. typhimurium* and *E. coli*.

Chapter 3

3.11. Materials and methods

Bacterial strains and plasmids

The strains and plasmids used in this study are listed in Table 3.2.

In-frame chromosomal gene deletions were created using an allele replacement procedure, based on a modification of Datsenko and Wanner's method⁶², that does not leave a scar. It is based on an insertion cassette that contains the lethal *ccdB* gene under the control of a L-rhamnose-inducible promoter. This cassette is later removed by selection on rhamnose-minimal plates²⁸⁸. *Salmonella*'s resident plasmid pSLT contains *ccdA* and *ccdB* genes and thus interfere with the positive selection strategy described above. Therefore it was displaced prior to allele replacements using Kit10 from *Salmonella* Genetics Stock Collection (SGSC): a plasmid pLL6, which is from the same compatibility group as pSLT, is transformed in the strain of interest, pSLT is cured, and pLL6 is subsequently removed using temperature selection¹¹⁸.

Salmonella Tar (TarSt) constructs were designed by PCR amplification of genomic *tarSt* using primers that include AseI and BamHI restriction sites for ligating into NdeI and BamHI restriction sites on the sodium salicylate-inducible plasmid pKG116 (AseI and NdeI create compatible ends; this strategy was selected because of the presence of an NdeI site within *tarSt* sequence). TarSt mutants, in which glutamates in the methylation sites are replaced with glutamines, are created using site-directed mutagenesis using overlap PCR.

| Plasmid | Gene(s) | Resistance | Induction | Source |
|---------|--------------------------------|-----------------|-------------------|----------------|
| pVS88 | <i>cheZ-ecfp / cheY-eyfp</i> | ampicillin | IPTG | ²⁴⁰ |
| pKG116 | Cloning vector | chloramphenicol | Sodium salicylate | J.S. Parkinson |
| pVS123 | <i>tar^{Ec}</i> [QEQE] | chloramphenicol | Sodium salicylate | ²⁴⁰ |
| pML18 | <i>tarSt</i> [QEQE] | chloramphenicol | Sodium salicylate | This work |
| pML20 | <i>tarSt</i> [QEQQ] | chloramphenicol | Sodium salicylate | This work |
| pML21 | <i>tarSt</i> [QEEE] | chloramphenicol | Sodium salicylate | This work |
| pML22 | <i>tarSt</i> [QQQQ] | chloramphenicol | Sodium salicylate | This work |
| pML23 | <i>tarSt</i> [EEEE] | chloramphenicol | Sodium salicylate | This work |

Network-level variability in bacterial chemotaxis

| Strain | Relevant genotype | Source |
|---------|---|--|
| LT2 | wild type <i>S. typhimurium</i> (official designation, <i>Salmonella enterica</i> serovar Typhimurium) | <i>Salmonella</i> Genetic Stock Center |
| TSS500 | LT2 $\Delta cheY \Delta cheZ$ | This work |
| TSS515 | LT2 $\Delta cheV \Delta cheY \Delta cheZ$ | This work |
| TSS878 | LT2 $\Delta tar \Delta cheY \Delta cheZ$ | This work |
| TSS1038 | LT2 $\Delta tar \Delta cheR \Delta cheB \Delta cheY \Delta cheZ$ | This work |
| 14028 | wild type <i>S. typhimurium</i> ATCC strain | R.M. Harshey |
| TSS863 | 14028 $\Delta 9T$, i.e. $\Delta tar \Delta tsr \Delta tcp \Delta trg \Delta mcpA \Delta mcpB \Delta mcpC \Delta aer \Delta tsr \Delta cheR \Delta cheB \Delta cheY \Delta cheZ::Kan$ | This work |
| RP437 | <i>E. coli</i> wild type for chemotaxis | 195 |
| VS104 | RP437 $\Delta cheY \Delta cheZ$ | 241 |

Table 3.2. Strains and plasmids used in this work. Δ and $::$ refer to deletion of, or deletion / substitution within the indicated gene, respectively. Kan refer to substitution with kanamycin-resistance cassette.

Growth conditions

Cells were grown at 250 rpm at 33.5°C in a rotary shaker to mid-exponential phase ($OD_{600} \sim 0.5$) in tryptone broth (TB; 1% tryptone, 0.5% NaCl, pH 7.0) supplemented with appropriate antibiotics (100 μ g/ml ampicillin, 34 μ g/ml chloramphenicol) and inducers (150 μ M IPTG, sodium salicylate, NaSal, with concentrations, indicated in the text). Cells were harvested by centrifugation, washed twice and resuspended in motility buffer (10 mM potassium phosphate, 0.1 mM EDTA, 1 μ M methionine, 10 mM lactic acid, pH 7), and stored at 4°C for 1-5 h prior to the experiment.

In vivo FRET measurements and data analysis

FRET microscopy of immobilized bacterial populations was performed as described earlier²⁴². The FRET donor-acceptor pair - CheZ-CFP and CheY-YFP - was expressed from a plasmid pVS88²⁴⁰. FRET fusion proteins were expressed in $\Delta cheY \Delta cheZ$ strains.

Chapter 3

Cells were attached to a poly-*L*-lysine-coated microscope coverslip, seated at the top face of a flow cell ²⁷, and kept under constant flow of motility buffer, generated by either a peristaltic pump (Rainin Dynamax RP1) or syringe pump (Harvard Apparatus, PHD2000). The flow cell was mounted on an upright microscope (Nikon FN1), equipped with an oil immersion objective (Nikon CFI Plan Fluor, 40x/1.3). The sample was illuminated by a metal halide arc lamp with closed-loop feedback (EXFO X-Cite *exacte*) through an excitation bandpass filter (Semrock, FF01-438/24-25) and a dichroic mirror (Semrock, FF458-Di01). The epifluorescent emission was split by a second dichroic mirror (Semrock, FF509-FDi01) into donor (cyan, C) and acceptor (yellow, Y) channels and collected through emission bandpass filters (Semrock FF01-483/32 and FF01-542/27 for the C and Y channels, respectively) by two photon-counting photomultipliers (Hamamatsu H7422P-40).

Signal intensities of the donor and acceptor channels were recorded through a data acquisition card (National Instruments) installed on a PC running custom-written software. After subtraction of coverslip background, the ratio R between the two channels, $R = Y/C$ provided an indicator of FRET activity robust to fluctuations in excitation intensity. The change in FRET efficiency upon stimulation, $\Delta FRET$, was computed at every time point from the donor and acceptor fluorescence $\Delta FRET = \frac{R_{pre+\Delta R}-R_0}{R_{pre+\Delta R}+|\Delta Y/\Delta C|} - \frac{R_{pre}-R_0}{R_{pre}+|\Delta Y/\Delta C|}$, where $\Delta R = R - R_{pre}$ is the ratio change, R_0 is the acceptor to donor ratio in absence of FRET, R_{pre} is the pre-stimulus acceptor to donor ratio, and $|\Delta Y/\Delta C|$ (≈ 0.6 for our setup) is the constant absolute ratio between the changes in the acceptor and donor signals per FRET pair ²⁴². However, under our FRET measurement conditions, $R_{pre} + |\Delta Y/\Delta C| \gg \Delta R$; thus $\Delta FRET \sim \Delta R$. For simplicity we expressed $\Delta FRET$ in arbitrary units of ΔR throughout the study.

$\Delta FRET(t)$ was normalized to the absolute magnitude of the response to addition of a saturating attractant step, $|\Delta FRET_{sat}^{add}|$, to compensate for variations between different experiments. The steady-state kinase activity, a_0 , was calculated as $a_0 = \frac{|\Delta FRET_{sat}^{add}|}{|\Delta FRET_{sat}^{add}| + |\Delta FRET_{sat}^{remove}|}$, where $\Delta FRET_{sat}^{remove}$ is the response to removal of a saturating attractant step after the cells have been

Network-level variability in bacterial chemotaxis

completely adapted. The kinase activity $a = a_0 + \Delta a$, where $\Delta a = \frac{\Delta FRET}{|\Delta FRET_{sat}^{add}| + |\Delta FRET_{sat}^{remove}|}$ is the kinase activity change in every point in time.

In dose-response measurements to the non-metabolizable chemoeffector α -methyl-*DL*-aspartic acid (MeAsp; Sigma Aldrich) bacteria were adapted to a background level of MeAsp, $[L]_0$, and by using a fluidic switch (Hamilton, valve HV 3-2) that could rapidly select between input flow channels with different concentrations $[L]$, cells were exposed to a sequence of steps of addition and removal of MeAsp of increasing magnitude. A Hill function, $a = a_l + (a_h - a_l) \frac{[L]^{n_H}}{[L]^{n_H} + [K_{1/2}]^{n_H}}$, where $K_{1/2}$ is the ligand concentration of the half-maximum of the response, n_H is the Hill coefficient, and a_l and a_h are the lowest and the highest kinase activity in the dose-response curve, was fit to each dose-response curve.

To subject the cells to input modulations, smoothly varying in time, the control of the temporal profile of chemoeffector stimulus was achieved by mixing a concentrated solution of chemoeffector and motility buffer in a fluid mixer of a type described before²²⁶. The mixing chamber was a cylinder with internal volume $V_{mix} \approx 100 \mu\text{l}$, with two input channels and two output channels. The in-flow rate, β_1 , of the concentrated MeAsp was modulated using a computer-controlled syringe pump (Harvard Apparatus, PHD2000). The in-flow rate of the buffer, β_2 ($\beta_2 \gg \beta_1$), was kept constant ($\sim 2 \text{ ml/min}$) throughout the experiment. Thus, the output chemoeffector concentration $[L](t) = [L]^* \frac{\beta_1(t)}{\beta_1(t) + \beta_2}$, where $[L]^*$ is the MeAsp concentration in the syringe. $[L](t)$ is proportional to β_1 as long as the latter is varied smoothly over time scales much greater than the mixing time, $\tau_{mix} \equiv \frac{V_{mix}}{\beta_1 + \beta_2}$.

Microfluidics experiments and data analysis

Microfluidics experiments were performed in a hydrogel-based gradient generator device with a design identical to “Design 1” described in reference⁷. The device consisted of three parallel channels, each $600 \mu\text{m}$ wide, with $200 \mu\text{m}$ spacing between the channels. Both the flanking channels (“source” and “sink”) and the “test” channel ($150 \mu\text{m}$ deep) were

Chapter 3

patterned in a layer of a polydimethylsiloxane (PDMS) (Sylgard 184). The PDMS layer was placed on top of a 1-mm-thick agarose hydrogel layer (3% wt/vol agarose in motility buffer), which was positioned on top of a glass slide. Outlets of the source and sink channels were connected by metal connectors and flexible polyethylene tubing to two plastic syringes of 3 ml, driven by a syringe pump (Harvard Apparatus, PHD 2000). A constant flow rate of 1 $\mu\text{l}/\text{min}$ was maintained with two different concentrations of MeAsp in the source and the sink. Diffusion between the two feeder channels, separated edge to edge by a distance $L = 1$ mm, leads to an establishment of a gradient across the agarose in ~ 20 min.

Before injection, bacteria were pre-adapted for at least 15 min to the mean concentration of the source and the sink channels (i.e. the mean concentration in the test channel, $[L]_{\text{mean}}$). After injection of bacterial suspension and immediate termination of the residual flow using T-shaped switch (Hamilton, valve HV 3-2), a gradient mirroring that in the underlying agarose layer is rapidly established in the test channel (the height of the test channel is $H = 150$ μm , and the diffusion coefficient for MeAsp is assumed to be the typical one for small molecules in water, $D = 5 \times 10^{-10}$ $\text{m}^2 \text{s}^{-1}$).

The linearity of the gradient in the test channel of this device was previously verified ⁷. In each gradient the ratio between the concentrations of MeAsp in the source, $[L]_{\text{source}}$, and in the sink, $[L]_{\text{sink}}$, was kept constant (Table 3.3), and therefore the steepness of the expected linear gradients also remained constant. The magnitude of the actual gradient was estimated to be $\sim 40\%$ of the predicted gradient ⁷.

The distribution of the bacteria within the test channel was observed using phase-contrast microscopy. Bacteria were observed close to the agarose layer with an inverted microscope (Nikon Eclipse), using a 20x objective (phase-contrast, ELWD). Movies were recorded using an Andor Neo sCMOS camera, controlled by Nikon NIS-Elements control software at 10 frames per second for 15 min, and the image acquisition started 10-30 s after injection of the bacteria. Image analysis was performed using MATLAB. Immobile cells were removed by subtracting a mean image from each frame, followed by locating the positions of the motile cells.

Network-level variability in bacterial chemotaxis

Subsequent binning yielded the cell concentration profile, $B(x, t)$, along the direction of the gradient x at each time point t .

| $[L]_{\text{sink}}$, mM | $[L]_{\text{mean}}$, mM | $[L]_{\text{source}}$, mM | Predicted gradient $\frac{d[L]}{dx}$, mM/mm | Actual gradient $\frac{d[L]}{dx}$, mM/mm | Relative gradient $\frac{1}{[L]_{\text{mean}}} \frac{d[L]}{dx}$, 1/mm |
|-----------------------------|-----------------------------|-------------------------------|---|--|--|
| 0.002 | 0.005 | 0.008 | 0.007 | 0.003 | 0.5 |
| 0.006 | 0.018 | 0.030 | 0.024 | 0.010 | 0.5 |
| 0.021 | 0.064 | 0.107 | 0.085 | 0.034 | 0.5 |
| 0.076 | 0.228 | 0.380 | 0.304 | 0.122 | 0.5 |
| 0.271 | 0.814 | 1.357 | 1.085 | 0.434 | 0.5 |
| 0.968 | 2.903 | 4.838 | 3.871 | 1.548 | 0.5 |
| 3.449 | 10.35 | 17.24 | 13.795 | 5.518 | 0.5 |
| 12.29 | 36.87 | 61.45 | 49.161 | 19.665 | 0.5 |

Table 3.3. Concentrations of MeAsp and gradients used in the microfluidics gradient generator.

The strength of the chemotaxis response was evaluated by the absolute value of the dimensionless chemotactic migration coefficient (CMC): $|CMC|(t) \equiv \frac{|\langle x \rangle(t) - W/2|}{W/2}$, where W ($= 600 \mu\text{m}$) is the width of the test channel, and $\langle x \rangle(t)$ is the population-averaged spatial coordinate, $\int_0^W xB(x, t)dx$, of the bacteria along the chemoeffector gradient ¹⁵⁶.

The distribution of the bacteria is characterized by advection-diffusion equation $\frac{\partial B(x, t)}{\partial t} = D_B \nabla^2 B - \nabla(v_D B)$, where D_B is the random motility coefficient measuring the diffusivity of a population of bacteria resulting from their random walk behavior, and v_D is the drift velocity of the bacterial population ¹¹⁵. At steady state, $\frac{\partial B(x, t)}{\partial t} = 0$; thus $B(x)_{SS} = B_0 e^{-x/\lambda_{SS}}$, where B_0 is the cell density in the channel edge ($x = 0$) and $\lambda_{SS} = \langle x \rangle_{SS}$, where $\langle x \rangle_{SS}$ is the mean steady-state position of the bacterial population in the channel. λ_{SS} can be expressed as $\lambda_{SS} = D_B/v_D$ ¹¹⁵, therefore $|CMC|_{SS} \equiv |2\lambda_{SS}/W - 1| = |2D_B/(v_D W) - 1|$.

Chapter 3

Single receptor species MWC model for chemotaxis signaling

The dynamics of the *E. coli* chemotaxis pathway is captured by two equations ²⁶⁰, which link the three dynamic variables: input $[L](t)$, output $a(t)$ and memory $m(t)$:

$$\frac{dm}{dt} = F(a), \quad (13)$$

$$a = G([L], m) = G(f_t([L], m)) = (1 + e^{f_t([L], m)})^{-1}, \quad (14)$$

The differential equation (13) expresses the rate of change of the feedback signal, m , as a function F of the current signal output, a . Perfect adaptation follows as the function $F(a)$ has a single stable fixed point at $a = a_0$ with steady-state kinase activity a_0 given by $F(a_0) = 0$. The receptor-kinase activity, a , relaxes much rapidly ²³⁹, so its value at each moment in time is given by the algebraic equation (14). A variant of the Monod-Wyman-Changeux (MWC) allosteric model ^{176,226} has been used to prescribe a specific form of the function G , which denotes the dependence of the kinase activity, a , on the current level of ligand input, $[L]$, and methylation feedback signal, m , via the free energy difference between the active and inactive states of the receptor-kinase complex,

$$f_t([L], m) = N(f_L([L]) + f_m(m)), \quad (15)$$

where N is the number of ligand-binding receptor units cooperatively associated with each kinase molecule. As in the classical MWC model ¹⁷⁶, the effect of ligand depends on the active and inactive states for the receptor having distinct affinities for ligand, leading to the expression

$$f_L([L]) = \ln \frac{1+[L]/K_I}{1+[L]/K_A}, \quad (16)$$

where K_I and K_A are the dissociation constants for the inactive and active receptor states, respectively. From equation (16), it follows that f_L is linear in $\log[L]$ within the range $K_I \ll [L] \ll K_A$ when the ratio between K_A and K_I values is large ^{166,226}.

A feature that is not present in the classical MWC model ¹⁷⁶ is the methylation-dependent free energy, $f_m(m)$. FRET-based studies in *E. coli* ²²⁶ showed that it is well-approximated by a linear function,

$$f_m(m) = \alpha(m^* - m), \quad (17)$$

Network-level variability in bacterial chemotaxis

where α is the slope of $f_m(m)$, and m^* is the offset methylation level at which $f_m(m) = 0$. $\alpha \approx 2$ and $m^* \approx 0.5$ yielded good fits to *E. coli* experimental data.

Data from wild type *E. coli* taken at room temperature was well fit by the following parameters: $N=6$, $a_0=0.33$, $K_I = 0.018$ mM, $K_A = 2.903$ mM²²⁶. The function $F(a)$ was described by a Michaelis-Menten equation with a variable gain

$$F(a) = V_R \frac{1-a}{K_R+1-a} - V_B(a) \frac{a}{K_B+a}, \quad (18)$$

where

$$V_B(a) = V_B(0) \left(1 + \theta(a - a_B) \frac{a - a_B}{1 - a_B} r_B \right), \quad (19)$$

K_R and K_B are the Michaelis constants, and V_R and $V_B(a)$ - the maximal velocities of the methylation and demethylation reactions (catalyzed by CheR and CheB respectively), and $V_B(a)$ is a piecewise linear function, the value of which remains $V_B(0)$ for values of a below a_B , and above a_B increases with a slope $\frac{r_B}{1-a_B}$ up to a maximal value $(1 + r_B)V_B(0)$, implemented by use of a step function $\theta(a - a_B)$, defined as $\theta(a - a_B) = 1$ for $a > a_B$, $\theta(a - a_B) = 0$ otherwise. For *E. coli*, the fit parameters are $V_R = 0.010$ s⁻¹, $V_B(0) = 0.013$ s⁻¹, $K_R = 0.32$, $K_B = 0.30$, $a_B = 0.74$, $r_B = 4.0$ (all concentrations are normalized, in units of the CheA concentration: K_R and K_B are dimensionless)²²⁶. For *S. typhimurium*, we fitted the data with $V_R = 0.030$ s⁻¹, $V_B(0) = 0.030$ s⁻¹, $K_R = 0.45$, $K_B = 0.30$, $a_B = 0.74$.

Chemotactic drift velocity in shallow gradients

S. typhimurium and *E. coli* in liquid media either run smoothly, or tumble, changing their swimming direction. We consider a bacterial population executing run-and-tumble motility with a mean run speed v and average run length τ_0 in a shallow gradient, i.e. a gradient $\nabla[L]$ that is small enough that a change in the kinase activity, Δa , caused by a run of length $v\tau_0$ along the gradient is much smaller than the initial kinase activity a_0 ($\Delta a/a_0 \ll 1$). The chemotactic drift velocity

$$v_d = v \frac{\tau_+ - \tau_-}{\tau_+ + \tau_-} \quad (20)$$

where τ_+ and τ_- are the average run times for bacteria swimming up and down the gradient respectively. These run durations are determined by the rotational bias of the flagellar motors:

Chapter 3

$$\langle CW \rangle = \frac{\tau_{CW}}{\tau_{CW} + \tau_{CCW}} \quad (21)$$

where τ_{CW} and τ_{CCW} are the average clockwise (CW) and counter clockwise (CCW) intervals, respectively. The rotational bias is controlled by the kinase activity, a , and is well-fit by a Hill equation:

$$\langle CW \rangle = \frac{a^H}{a^H + a_{1/2}^H} \quad (22)$$

where $a_{1/2}$ is the kinase activity at which $\langle CW \rangle = 1/2$, and H is the motor Hill coefficient^{114,115}. From equations (21) and (22) follows that:

$$\tau_{CCW} = \gamma a^{-H} \quad (23)$$

where $\gamma = \tau_{CW} a_{1/2}^H$ is a constant, assuming that τ_{CW} and $a_{1/2}$ are not affected by changes in a .

During each run, the kinase activity changes from a_0 to $a_0 + \Delta a$ if the run is in the direction up the gradient, and from a_0 to $a_0 - \Delta a$ if the run is in the direction down the gradient. Thus, using equations (20) and (23) we can write

$$v_d = v \frac{(1 - \Delta a/a_0)^H - (1 + \Delta a/a_0)^H}{(1 - \Delta a/a_0)^H + (1 + \Delta a/a_0)^H} \quad (24)$$

Considering our shallow gradient condition ($\Delta a/a_0 \ll 1$), we have $(1 \pm \Delta a/a_0)^H \approx 1 \pm H(\Delta a/a_0)$, which leads to a simple expression for the drift velocity:

$$v_d \approx -vH \frac{\Delta a}{a_0} \quad (25)$$

Note that the simple derivation for v_d given above neglects the fact that Δa is not constant in time. Nevertheless, we can approximate Δa in equation (25) by a time-averaged value $\overline{\Delta a}$, expanding $\Delta a(t) = \left(\frac{da}{dt}\right)t + \mathcal{O}(t^2)$ and averaging over the run interval τ ,

$$\overline{\Delta a} = \frac{1}{\tau} \int_0^\tau \left[\frac{da}{dt} t + \frac{1}{2} \frac{d^2 a}{dt^2} t^2 + \dots \right] dt \approx \frac{da}{dt} (\tau/2), \quad (26)$$

where the last approximate equality is valid if $\frac{da}{dt}$ is approximately constant over the time interval τ . To obtain $\frac{da}{dt}$ explicitly, we appeal once again to the shallow gradient condition and linearize the two-state MWC model²⁶⁰ (equations (1) and (4)) about $a = a_0$ to obtain its rate of change in time,

$$\frac{da}{dt} = \frac{d\Delta a(t)}{dt} = -\Delta a(t)/\tau_m + \frac{\partial a}{\partial f_t} \frac{\partial f_t}{\partial \ln[L]} v \frac{d \ln[L]}{dx}, \quad (27)$$

Network-level variability in bacterial chemotaxis

where f_t is the total free energy of the receptor-kinase complex, and $\tau_m = \left(\frac{\partial f_t}{\partial m} F'(a_0)\right)^{-1}$ identifies with the adaptation timescale defined earlier in equations (5) and (6). Further differentiation of equation (26) yields for higher time derivatives $\frac{d^{n+1}a}{dt^{n+1}} = \tau_m^{-n} \frac{d^n a}{dt^n}$ for all $n \geq 1$, so $\Delta a(\tau) = \left(\frac{da}{dt}\right)\tau + \mathcal{O}((\tau/\tau_m)^2)$. Thus, the truncation of the series upon averaging over the run interval τ is valid whenever $\tau \ll \tau_m$.

Combining equations (26) and (27), and considering that $\tau = \tau_0(1 + \Delta a/a_0)^{-H}$ and $(1 \pm \Delta a/a_0)^H \approx 1 \pm H(\Delta a/a_0)$ for $\Delta a/a_0 \ll 1$, we obtain

$$\overline{\Delta a} = \left[-\overline{\Delta a}(t)/\tau_m + \frac{\partial a}{\partial f_t} \frac{\partial f_t}{\partial \ln[L]} v \frac{d \ln[L]}{dx} \right] \frac{\tau_0}{2(1+H\frac{\overline{\Delta a}}{a_0})}, \quad (28)$$

which is a quadratic equation for $\overline{\Delta a}$ and has solutions $\overline{\Delta a} = -\beta/2 \pm \sqrt{(\beta/2)^2 - \delta}$ with $\beta = \frac{a_0}{H} \left(1 + \frac{\tau_0}{\tau_m}\right)$ and $\delta = \frac{N}{H} a_0^2 (1 - a_0) v (\tau_0/2) \frac{d \ln[L]}{dx}$. Further, if $\frac{d \ln[L]}{dx} \ll (1 + \frac{\tau_0}{\tau_m})^2 / (4HN(1 - a_0)v\tau_0/2)$, then $(\beta/2)^2 \gg \delta$ and the nonnegative solution reduces to $\overline{\Delta a} \approx -\delta/\beta$, yielding

$$\overline{\Delta a} \approx \frac{-a_0(1-a_0)\psi([L]_0)v\tau_0}{2+\frac{\tau_0}{\tau_m}} \cdot \frac{d \ln[L]}{dx}, \quad (29)$$

where $\psi([L]_0)$ is the sensitivity-modulation profile of the receptor module, defined in equation (12).

Finally, using $\overline{\Delta a}$ from equation (29) for Δa in equation (25), we obtain an expression for the drift velocity in the shallow-gradient limit:

$$v_D \approx \frac{v^2 \tau_0 H (1 - a_0) \psi([L]_0)}{2 + \frac{\tau_0}{\tau_m}} \cdot \frac{d \ln[L]}{dx}. \quad (30)$$

Two receptor species MWC model for chemotaxis signaling

If the ligand is sensed by two different receptor species within the same MWC cluster, f_t can be written as

$$f_t = N_1 \left(\ln \left[\frac{1+[L]/K_{I1}}{1+[L]/K_{A1}} \right] + f_{m1} \right) + N_2 \left(\ln \left[\frac{1+[L]/K_{I2}}{1+[L]/K_{A2}} \right] + f_{m2} \right) \quad (31)$$

where $(N_1, K_{I1}, K_{A1}, f_{m1})$ and $(N_2, K_{I2}, K_{A2}, f_{m2})$ are the number of ligand-binding receptor units, the dissociation constants for the inactive and active receptor, and the methylation-dependent free energy for the first and the

Chapter 3

second receptor species respectively. This leads to a sensitivity modulation profile

$$\psi([L]_0) = N_1 \left(\frac{[L]_0}{[L]_0 + K_{I1}} - \frac{[L]_0}{[L]_0 + K_{A1}} \right) + N_2 \left(\frac{[L]_0}{[L]_0 + K_{I2}} - \frac{[L]_0}{[L]_0 + K_{A2}} \right) \quad (32)$$

3.12. Acknowledgements

I have performed the microfluidics work presented in this chapter in the lab of Prof. Dr. Roman Stocker (Massachusetts Institute of Technology), together with Dr. Filippo Menolascina from Stocker group. Eduardo Sontag (Rutgers Institute) and Roman Stocker provided helpful comments. Simone Boskamp provided help with the cloning of the different TarSt modifications on plasmids.

Chapter 4

Cystine-induced repellent chemotactic response of *Salmonella*: a potential mechanism to avoid oxidative conditions

Chemoreceptors McpB and McpC in *Salmonella typhimurium* have been reported to promote chemotaxis in LB motility-plate assays. Of the chemicals tested as potential effectors of these receptors, the only response was towards *L*-cysteine and its oxidized form, *L*-cystine. Although enhanced radial migration in plates suggested positive chemotaxis to both amino acids, capillary assays failed to show an attractant response to either in cells, expressing only these two chemoreceptors. *In vivo* fluorescence resonance energy transfer (FRET) measurements of kinase activity revealed that in wild-type bacteria, cysteine and cystine are chemoeffectors of opposing sign, the reduced form being a chemoattractant and the oxidized form a repellent. The attractant response to cysteine was mediated primarily by Tsr, as reported earlier for *Escherichia coli*. The repellent response to cystine was mediated by McpB / C. Adaptive recovery upon cystine exposure required the methyl-transferase/-esterase pair, CheR / CheB, but restoration of kinase activity was never complete (*i.e.* imperfect adaptation). We provide a plausible explanation for the attractant-like responses to both cystine and cysteine in motility plates, and speculate that the opposing signs of response to this redox pair might afford *S. typhimurium* a mechanism to gauge and avoid oxidative environments.

This chapter has been published:

Lazova, M. D. *, Butler, M. T. *, Shimizu, T. S., and Harshey, R. M., *Salmonella* chemoreceptors McpB and McpC mediate a repellent response to *L*-cystine: a potential mechanism to avoid oxidative conditions. *Mol Microbiol* **84** (4), 697 (2012).

*authors contributed equally

Chapter 4

4.1. Introduction

Salmonella typhimurium and *Escherichia coli* show chemotaxis toward amino acids and sugars, as well as oxygen and other stimuli that change cellular energy levels (reviewed in ^{11,19,102,175,255,266}). Chemotaxis can be metabolism-independent or -dependent and requires processing of sensory input from chemoreceptors through a signaling pathway wherein the receptor-associated kinase CheA transfers phosphoryl groups to the response regulator CheY, which ultimately modulates the rotational bias of the flagellar motor. The steady-state level of the phosphorylated response regulator is determined by the balance of its production by CheA and destruction by a phosphatase CheZ. The activity of the receptor-kinase complex is feedback-regulated by the methyltransferase CheR and the methylesterase / deamidase CheB. The competing activities of CheR and CheB, involving reversible receptor methylation at multiple sites, enable cells to adapt to static chemical environments by restoring receptor-kinase output towards its pre-stimulus state.

Binding of chemoeffector molecules to transmembrane chemoreceptors, also known as methyl-accepting chemotaxis proteins (MCPs), is sufficient to initiate the metabolism-independent chemotaxis response. Ligand binding can be either direct or via a periplasmic binding protein ¹⁸⁶. Reversible ligand binding to dimeric MCPs at their periplasmic domains affects the receptors' conformational state on both sides of the cytoplasmic membrane, thereby propagating a signal into the cell. Upon crossing the membrane, signal transmission is thought to proceed through the regulatory HAMP domain ²⁹¹, the "methylation module" harboring the reversibly modified residues, and the signal-output domain that regulates the activity of CheA. Conserved pentapeptide motifs (NWE^T/sF) at the C-termini of a subset of MCPs (see Table 3.1, Chapter 3) reversibly bind CheR and CheB ^{24,144}. Another metabolism-independent chemotactic response involves carbohydrate transport via the phosphoenolpyruvate-dependent phosphotransferase system (PTS), which requires the CheA–CheY signaling pathway and one or more chemoreceptor species ^{151,185}. Metabolism-coupled chemotaxis includes redox taxis in response to changes in the redox state of the electron transport system ²⁸ and pH taxis in response to

Cystine-induced repellent chemotactic response of *Salmonella*

changes in the pH gradient across the cell membrane (proton-motive force)¹²⁴.

In *E. coli*, chemotaxis is carried out by one of four MCPs: Tsr senses serine¹⁷⁰, Tar senses aspartate and maltose¹⁸⁰, Trg senses ribose, galactose and glucose¹²⁹, and Tap senses dipeptides¹⁵⁴. Trg and Tap lack the NWE^T/sF motif and therefore require the presence of Tsr or Tar for efficient methylation-dependent adaptation to their ligands⁸³. An additional MCP-like receptor, Aer, mediates responses to changes in oxygen concentration³¹. Aer lacks the adaptive methylation module as well as a large periplasmic domain, and it senses changes in the redox potential using a cytoplasmic PAS domain^{30,270}. Structural and biochemical studies indicate that chemoreceptors oligomerize as trimers of dimers, interacting at their distal cytoplasmic tips¹⁰². The principal trimer contact residues are identical in Aer and the MCPs, suggesting that all the different receptors should be able to form mixed trimers of dimers⁹³. Chemoreceptors cluster in subpolar patches¹⁵³, and there is direct experimental evidence for inter-dimer methylation¹⁴³.

S. typhimurium lacks Tap but has additional transmembrane chemoreceptors: Tcp that senses citrate and phenol²⁸², and two recently identified receptors McpB and McpC with unknown ligand specificity^{86,267}. Two other chemoreceptor homologs with unknown function, Tip and McpA, have also been described in *S. typhimurium*: Tip is a transmembrane receptor with no recognizable periplasmic domain²⁰⁶, whereas McpA appears to be cytoplasmic⁸⁶. The *mcpC* gene is located immediately downstream of *aer*. Both genes have distinct flagellar class 3 promoters, yet insertions in *aer* are polar on *mcpC* (R. Harshey, unpublished results). The relative RNA levels of the *mcpB* and *mcpC* genes, as determined by microarray data, fall between those of the genes encoding the low-abundance receptor Trg and the high-abundance receptor Tsr, and are similar to the RNA levels seen for the *tar* gene²⁶⁷. Both chemoreceptors have a periplasmic sensory domain, a HAMP domain, a methylation module, and receptor-trimer contact sites (Figure 4.1). However, they display differences in the C-terminal pentapeptide sequence, which is NWETF in Tsr and Tar. The pentapeptide EWVSF at the C-terminus of McpB resembles NWETF at the critical positions W and F²²⁸, but the

Chapter 4

pentapeptide DTQPA at the C-terminus of McpC has no similarity to the NWETF sequence. In addition, the C-terminal 'tail' of McpC is 26 residues shorter than that of McpB (Figure 4.1).

The present study was undertaken to identify chemoeffectors sensed by McpB and McpC, which mediate enhanced radial migration on LB or tryptone soft-agar plates²⁶⁷. Here we present experimental evidence that McpB and McpC, when present as sole chemoreceptors, mediate a chemotactic response to *L*-cystine. Whereas behavior in long-time motility-plate assays shows an almost identical tactic response to both *L*-cystine and *L*-cysteine, *in vivo* fluorescence resonance energy transfer (FRET) experiments with wild-type bacteria reveal responses of opposite sign to these two chemicals that form a redox pair: cystine acts as a repellent and cysteine as an attractant. Only cystine is sensed via McpB/C. The attractant-like response to cystine in long-time behavioral assays is likely from spreading due to increased tumbling caused by a repellent response with imperfect adaptation. We discuss a possible role for the cystine response in assisting the escape of *S. typhimurium* from cellular damage-inducing oxidative environments.

Chapter 4

4.2. McpB and McpC mediate a response to cystine and cysteine in soft-agar assays

In an earlier study, progressive deletion of chemoreceptors in *S. typhimurium* 14028 had shown that a strain missing seven of the nine chemoreceptors ($\Delta 7T$) - Tsr, Tar, Trg, Tcp, Aer, McpB and McpC - does not spread in Luria-Bertani (LB) or tryptone broth (TB) soft-agar swim plates; however, a strain missing the first five receptors but retaining McpB and McpC spreads significantly²⁶⁷. We infer from these results that the two other uncharacterized receptors - Tip and McpA - do not contribute to the spreading observed in these plates. Indeed, the additional deletion of these two receptors in a $\Delta tsr \Delta tar \Delta trg \Delta tcp \Delta aer$ strain did not affect the migration phenotype as shown in Figure 4.2A (compare BC only* to BC only; strains which still retain McpA and Tip are marked with an * hereafter; for example, the strain that contains only *mcpB* and *mcpC* chemoreceptor genes is referred to as “BC only”, whereas the strain that contains only *mcpB*, *mcpC*, *tip* and *mcpA* chemoreceptor genes is referred to as “BC only*”). A strain expressing McpC alone was also capable of promoting faster spreading than the $\Delta 7T$ strain, but slower than a strain expressing McpB and McpC together; a strain expressing McpB alone migrated only marginally faster than the $\Delta 7T$ strain (Figure 4.2A, second row). McpC is encoded downstream of the genomic locus encoding Aer. However, Aer did not substantially affect the enhanced migration mediated by McpC (compare BC only* to C only* and C, Aer only*; Figure 4.2A, second row). The radial migration promoted by McpB / C was observed despite that the plates were buffered to attenuate establishment of pH gradients, suggesting that the response was to a chemical other than H⁺.

To identify chemoeffectors, we tested the response of the BC only* strain in soft-agar swim plates containing minimal-glycerol media with mixtures of amino acids, sugars, succinate / pyruvate (labeled ‘energy mix’; their metabolism creates oxygen gradients), nucleosides, and vitamins (see Materials and methods). Of the many potential attractants, only the commercial essential amino acid mixture ‘MEM’ (arginine, cystine, histidine, isoleucine, leucine, lysine, methionine, phenylalanine, threonine, tryptophan, tyrosine and valine) enhanced the migration response

Cystine-induced repellent chemotactic response of *Salmonella*

(Figure 4.2B), whereas a non-essential amino acid mixture did not (essential and non-essential refer to requirement for growth of mammalian cells). To further dissect which of the MEM components triggered chemotactic spreading, we tested the individual amino acids present in the essential MEM mix. Of these, only *L*-cystine (a dimeric amino acid, formed by oxidation of two cysteine monomers covalently linked by a disulfide bridge; referred to henceforth as simply cystine), elicited a migration response (Figure 4.2C). When cystine was omitted from the MEM mix, the migration rate of the BC only* strain was attenuated. In addition, we tested the reduced form, cysteine, and found that it enhances migration in a manner indistinguishable from cystine. Responses to serine and aspartate, which serve as major attractant ligands sensed by the chemoreceptors Tsr and Tar, respectively, are shown for comparison. The $\Delta mcpB \Delta mcpC$ strain (referred to as “ ΔBC ”), which retains seven chemoreceptors, showed the expected response to serine and aspartate (Figure 4.2C; bacteria have migrated to the edge of these plates) but did not respond to cystine or cysteine in this assay.

Chapter 4

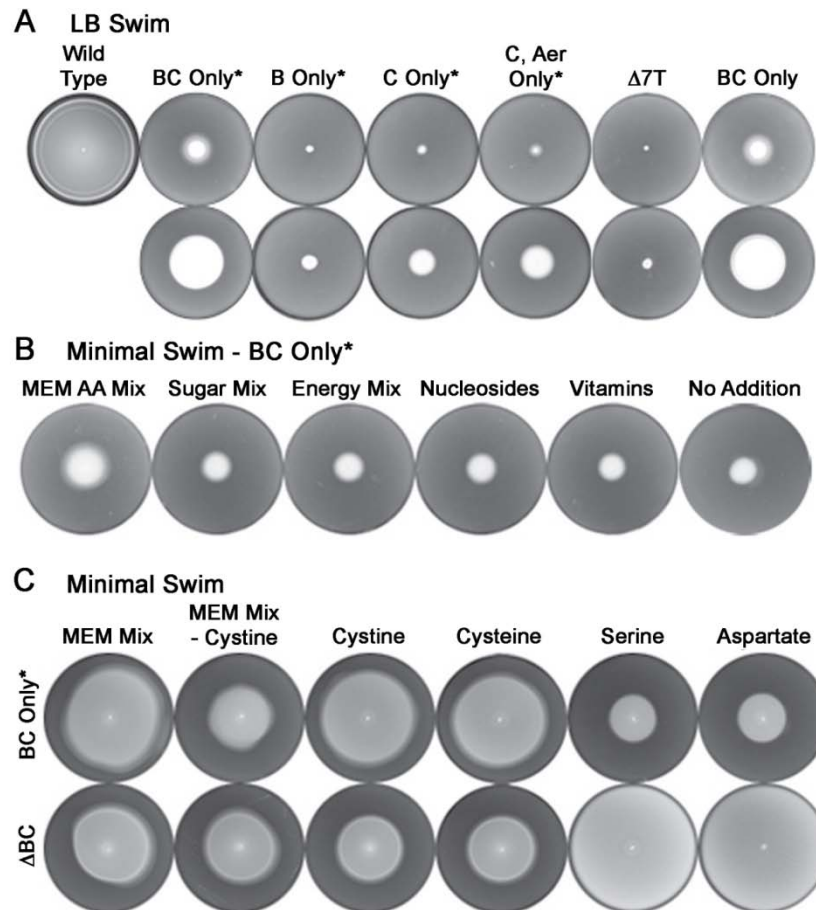


Figure 4.2. Response of *S. typhimurium* 14028 strains to chemoeffectors in soft-agar swim plates. (A) Top row: WT, BC only*, B only*, C only*, C / Aer only*, $\Delta 7T$ *, and BC only strains were inoculated at the center of LB swim plates and incubated at 37°C for 7 h. Second row: Plates were incubated for an additional 16 h at room temperature, by which time the BC only* strains colonized half the plate. **(B)** The BC only* strain was inoculated in minimal-glycerol swim media containing either the commercial MEM essential amino acid mix or the indicated nutrient mixes and incubated at 37°C for 22 h. **(C)** BC only* and ΔBC strains were inoculated in minimal-glucose swim media containing the essential MEM mix or indicated amino acids and incubated at 37°C for 22 h. The MEM mixes in this experiment were reconstructed to reflect the composition of the commercial mix.

4.3. Capillary assays do not show an attractant response to cystine

In *E. coli*, pioneering experiments by Adler and colleagues using capillary assays ¹⁷⁰, established cysteine as an attractant sensed by Tsr, whereas in the same assays cystine elicited no response. Cysteine was also reported to be an attractant for *S. typhimurium* ¹⁰³. Because oxidation / reduction reactions interconvert these two amino acids, it is unclear whether these redox species are stable over the many hours over which motility-plate assays are conducted, and the enhanced migration conferred by McpB and McpC could be due to cystine, cysteine, or a mixture of the two. We therefore performed capillary assays, which are completed within a much shorter time (< 1 h), to test the response to these amino acids ³. We ascertained that both amino acids maintained their structure in freshly prepared solutions using mass spectrometry (see Materials and methods). The response of four *S. typhimurium* 14028 strains – wild type (WT), Δ BC, BC only* and Tar only* - is shown in Figure 4.3, with the response to aspartate serving as a control (Figure 4.3A). Neither BC only* nor any other of the tested strains accumulated significantly in capillaries containing cystine, indicating the lack of an attractant response (Figure 4.3B). However, WT and Δ BC strains showed an attractant response to cysteine (Figure 4.3C). These observations suggest that neither cysteine nor cystine is an attractant sensed by McpB / C under the conditions of these capillary assays, in stark contrast to the seemingly positive chemotactic migration response of the BC only* strain in both cysteine and cystine motility plates (Figure 4.2C).

Chapter 4

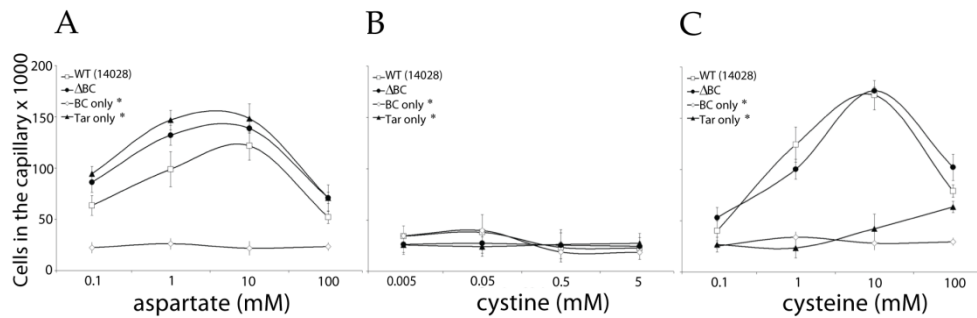


Figure 4.3. Capillary assays. The response of *S. typhimurium* 14028 strains WT, BC only*, ΔBC , and Tar only* was monitored with (A) aspartate, (B) cystine, and (C) cysteine. The cell numbers are an average of three technical repeats of the experiment. Error bars are standard deviation from the mean.

4.4. FRET experiments reveal responses of opposite sign to the cystine / cysteine redox pair

To probe the effect of cysteine and cystine on chemotactic activity, we used an *in vivo* fluorescence resonance energy transfer (FRET) assay, utilizing the donor-acceptor pair between fusions of CheZ and CheY to cyan and yellow fluorescent proteins (CFP and YFP), respectively²⁴² (Materials and methods). The FRET signal is proportional to the activity of CheA, the central kinase of the chemotaxis pathway. An analogous *in vivo* FRET system has been used in numerous studies of *E. coli* chemotactic signaling^{137,226,237,241}.

We first applied step increases in the concentration of cystine to immobilized bacterial populations kept under constant flow of motility buffer, and monitored the FRET response. Figure 4.4 (left) shows a typical time series of the FRET response to addition and removal of 100 μM cystine in *S. typhimurium* LT2 strains. Cystine caused an increase of the FRET signal, indicating a repellent response (Figure 4.4). WT responded to concentrations of cystine as low as 20 nM (see Appendix A).

Cystine-induced repellent chemotactic response of *Salmonella*

In contrast to cystine, the reduced form, cysteine, produced a decrease in the FRET signal, indicating an attractant response (Figure 4.4, right). This response of WT cells to cysteine steps was detectable in FRET down to a threshold of ~20 μ M (see Appendix A). The attractant response to cysteine is consistent with the capillary assay data shown in Figure 4.3C, as well as results from previous studies ¹⁶⁹.

In *E. coli* and *S. typhimurium*, efficient adaptation to chemoeffectors involves methylation and demethylation of specific glutamyl residues on the chemoreceptors by CheR and CheB respectively. In CheR / CheB⁺ cells (e.g. the WT strain used here), the rapid initial increase in the FRET signal upon stepping up the cystine concentration (Figure 4.4, left) was followed by a slower, partial recovery toward the pre-stimulus level; upon stepping down the concentration, a small, transient decrease of the FRET signal was observed. This result showed that the repellent response to cystine was adaptive, but that the adaptation was incomplete, i.e. imperfect adaptation ^{132,163}. In contrast, the FRET response of Δ *cheR* Δ *cheB* cells to a cystine step did not recover toward the pre-stimulus level (Figure 4.4, left), indicating that the adaptive recovery of the FRET response in WT cells was due to the activities of CheR and CheB. Similarly, an adaptive response to cysteine was observed in WT bacteria, and no adaptation occurred in Δ *cheR* Δ *cheB* cells (Figure 4.4, right). However, the adaptation of WT cells to cysteine was perfect: during the cysteine step, the FRET signal recovered precisely to the pre-stimulus level. Deleting the gene encoding the scaffolding protein CheV ¹⁰, whose homolog has been implicated in the chemotactic adaptation of *Bacillus subtilis* ¹¹⁶, showed no substantial effect on the response to cystine or cysteine (Figure 4.4 bottom panels).

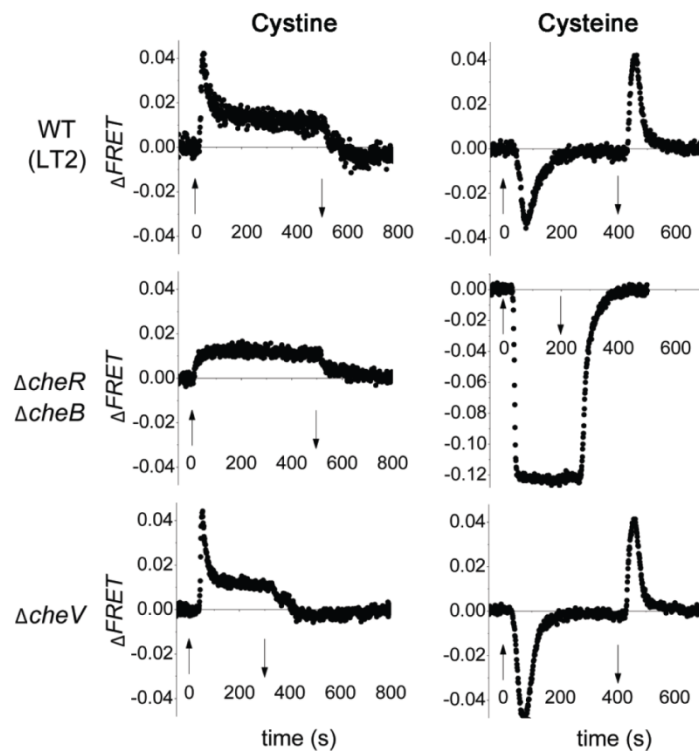


Figure 4.4. FRET response of WT and mutant *S. typhimurium* LT2 strains to cystine and cysteine. Strains used were: WT, $\Delta cheR \Delta cheB$, and $\Delta cheV$. 100 μ M cystine or cysteine steps were used in all panels except for $\Delta cheR \Delta cheB$ (right), where the cysteine step size was 100 mM. Up / down arrows indicate the time of addition / removal of chemoeffectors, respectively.

4.5. The repellent response to cystine is mediated by McpB and McpC

We performed FRET experiments in receptor knockout strains to probe whether cystine and cysteine are sensed in a McpB / C-dependent manner. Figure 4.5 (left) shows a typical time series of the FRET response to addition and removal of 100 μ M cystine in WT, ΔBC , and BC only* strains. Note that all three strains are *S. typhimurium* 14028 derivatives, in contrast to the LT2 strains shown in Figure 4.4. The differences in amplitudes in LT2 and 14028 backgrounds could be explained by the presence of unlabeled *cheY* and *cheZ* genes in 14028 strains, as well as strain-dependent variations

Cystine-induced repellent chemotactic response of *Salmonella*

in chemoreceptor expressions. This conjecture is supported in data presented in Figure 4.6. The response to cystine of *S. typhimurium* 14028 was completely abolished in the Δ BC strain. However, the BC only* strain showed a repellent response to cystine: qualitatively, the temporal profile of the response was similar to WT, although the response amplitude in the BC only* strain was smaller than that of WT (Figure 4.5, left), likely because of the diminished size of the total receptor population²³⁷. Indeed, overexpression of McpC from a plasmid in the BC only strain produced a substantially stronger response (see Figure 4.7A). In agreement with the capillary-assay results (Figure 4.3), the FRET response of the Δ BC strain to the cysteine was nearly the same as WT, but the response to cysteine was completely abolished in the BC only* strain (Figure 4.5 right). We conclude that the repellent response of *S. typhimurium* 14028 to cystine depends on McpB / C chemoreceptors. The reduced cysteine form is an attractant, but it is not sensed via McpB or McpC.

Chapter 4

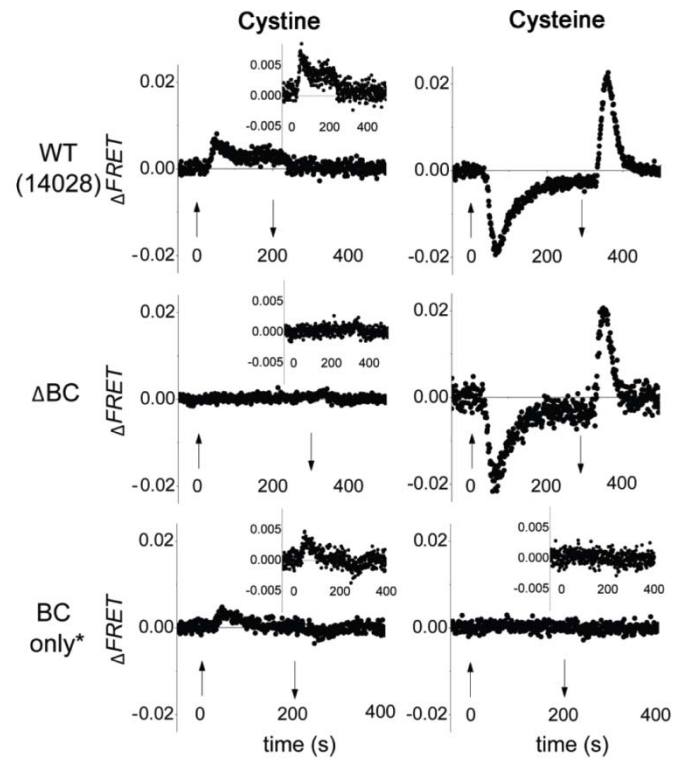


Figure 4.5. FRET response of *S. typhimurium* 14028 strains to cystine and cysteine. Strains used were: WT, Δ BC, and BC only*. 100 μ M cystine or cysteine steps were used in all panels, except for Δ BC (right), where the cysteine step was 1 mM. Insets with magnified axes are shown for strains with a weaker or no response. Three repeats are averaged for BC only* cystine and cysteine responses and for Δ BC cystine responses. The other descriptions are as in Figure 4.4.

Cystine-induced repellent chemotactic response of *Salmonella*

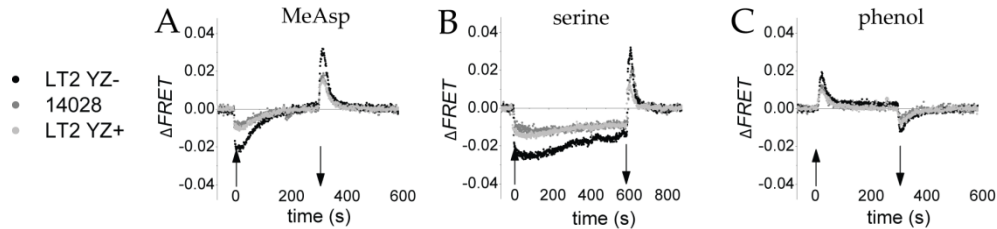


Figure 4.6. Comparison of differences in the FRET responses of *S. typhimurium* to α -methyl-aspartate (MeAsp) (A), serine (B) and phenol (C) in the presence and absence of the native (and hence unlabeled) *cheY* and *cheZ* genes. FRET responses of LT2 $\Delta cheY \Delta cheZ$ (LT2 YZ-), LT2 (LT2 YZ+) and 14028 strain to 100 μ M MeAsp, 100 μ M serine and 100 μ M phenol are shown. The LT2 YZ+ strain shows the largest amplitude of the response to all chemoeffectors. The other descriptions are as in Figure 4.4.

4.6. Roles of McpB and McpC in cystine sensing

We sought to dissect the roles of McpB and McpC in the cystine response by comparing FRET responses of mutant strains engineered for their chemoreceptor composition. For both $\Delta mcpB$ and $\Delta mcpC$ strains (referred to as ΔB and ΔC respectively), the response upon cystine addition was in the repellent direction (Figure 4.7A, top row), suggesting that each of these receptors can sense cystine in absence of the other. When both receptors are deleted, the response to cystine is abolished (Figure 4.5). However, the response upon cystine removal was atypical in the ΔC strain: the FRET signal increased upon removal instead of decreasing, as expected for removal of a repellent. A plausible explanation for this peculiar ΔC response is that one or more of the seven other receptor species are responding to traces of cystine present within the cystine solution (due to partial reduction of the dissolved cystine; see below). Next we probed the responses mediated by McpB and McpC when they were present in cells as the sole chemoreceptor species. Weak but detectable repellent responses to cystine were observed in the McpC only strain; the response of the McpB only strain was even weaker (Figure 4.7A, middle row). Overexpression of McpC in the BC only strain produced a response comparable to wild-type;

Chapter 4

however the overexpression of McpB in the BC only strain did not noticeably increase the amplitude of the response to 100 μ M cystine (Figure 4.7A, bottom row).

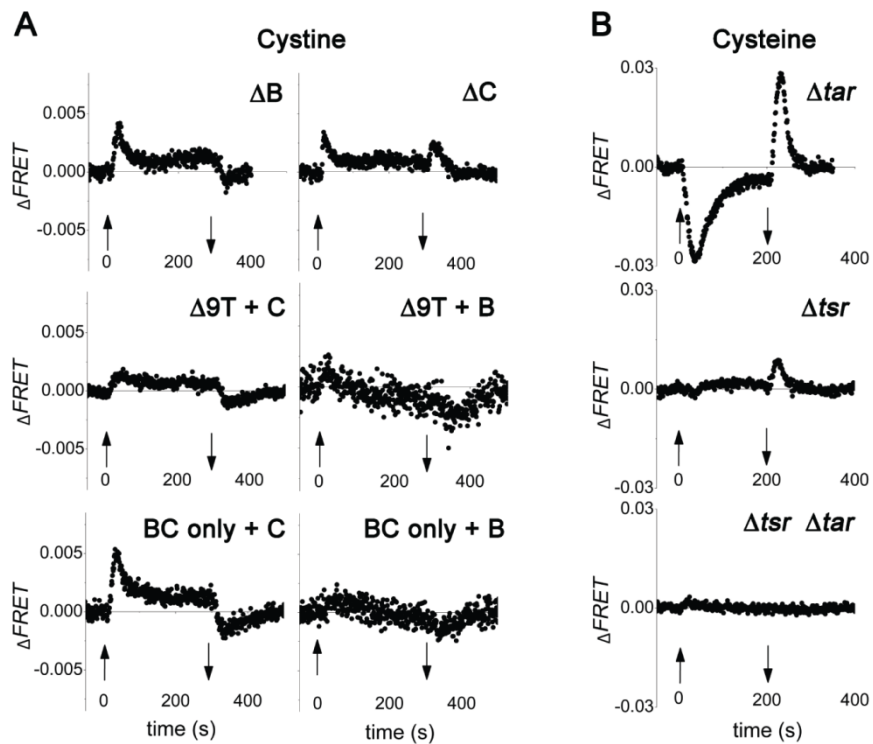


Figure 4.7. FRET responses to cystine and cysteine steps in various chemoreceptor mutants. (A) 100 μ M cystine steps were used in all panels. *S. typhimurium* 14028 strains used were: ΔB , ΔC , $\Delta 9T + C$, $\Delta 9T + B$, BC only + C, and BC only + B. McpB expression from pMB1 was induced with 0.2% *L*-arabinose, and McpC expression from pML19 was induced with 7 μ M sodium salicylate. Three repeats are averaged for all. **(B)** 100 μ M cysteine steps were used in all pretreatments. *S. typhimurium* LT2 strains used were: Δtar , Δtsr , and $\Delta tsr \Delta tar$. The other descriptions are as in Figure 4.4.

4.7. The attractant response to cysteine is mediated by Tsr and Tar

Previous studies using capillary assays demonstrated that as in *E. coli*¹⁷⁰, Tsr is likely the dominant sensor for cysteine in *S. typhimurium*¹⁰³. Figure 4.7B shows a typical time series of the FRET response upon addition and removal of 100 μ M cysteine in *S. typhimurium* LT2 strains deleted for the *tsr* and *tar* genes, singly and together. The response of the Δtar strain was similar to wild-type; however, the amplitude of the response of the Δtsr strain was strongly diminished. No attractant response to cysteine was observed in $\Delta tsr \Delta tar$ double knockout, even when cysteine concentrations up to 10 mM were tested (see Appendix A). Thus, FRET experiments confirmed the results from previous studies that Tsr is the dominant receptor for cysteine.

4.8. Function of the C-terminal pentapeptide of McpB

The strongest responses to cystine were observed when McpB and McpC were present together in both plate (Figure 4.2A) and FRET (Figure 4.7A) experiments. Similar to other MCPs, both *mcpB* and *mcpC* genes have a conserved methyl-accepting domain (Figure 4.1), and FRET experiments showed that adaptation to cystine occurs in CheR- and CheB-dependent but CheV-independent manner (Figure 4.4). This result was confirmed in both wild-type and BC only* backgrounds by motility-plate assays: deleting *cheR*, *cheB*, or *cheW* dramatically diminished migration on cystine motility plates, whereas deleting *cheV* had little effect on the cystine response (Table 4.1A, rows 1-10). McpB could provide 'adaptational assistance' to McpC by supplying the C-terminal pentapeptide sequence (referred to henceforth as 'pentapeptide') (Figure 4.1). This sequence motif, found also at the extreme C-terminus of Tsr, Tar, and Tcp but not in the low-abundance receptors Trg and Tap, is known to stimulate the activities of CheR and CheB in *E. coli*²⁴. Low-abundance receptors mediate effective taxis only in the presence of pentapeptide-containing receptors⁸². Adding a flexible linker ending in the pentapeptide to the carboxyl terminus of low-abundance receptors greatly enhances their function^{83,271}.

Chapter 4

To test whether the weaker taxis mediated by McpC alone was due to lack of a pentapeptide sequence and whether the role of McpB was to provide this sequence, we added the last 30 residues from the C-terminus of Tsr to McpC in the C only* strain and deleted the pentapeptide from McpB in the BC only* strain. A comparison of the migration of these strains in minimal-media supplemented with cystine is shown in Table 4.1B (rows 11-14). Addition of the Tsr C-terminus to C only* abrogated its activity (row 13), whereas deletion of the McpB pentapeptide in BC only* resulted in spreading similar to the C only* strain (row 14). Although loss of the stimulatory effect of McpB upon deletion of its pentapeptide is consistent with a role for McpB in adaptational assistance, it could also be due to loss of McpB activity as a result of the deletion. A similar loss of activity appears to be the case with addition of the Tsr C-terminal segment to McpC.

Next, we constructed a Tar C only* strain to test if Tar could provide adaptational assistance to McpC (Table 4.1B, rows 15-16). This strain was efficient in its response to aspartate (row 16), but did not restore the cystine response to levels seen with the BC only* strain (compare rows 15 and 11). We also assessed the contribution of Tar and Tsr expressed from plasmids (pTar and pTsr) in the C only* strain, and compared their migration in media with cystine versus aspartate and serine (Table 4.1B; rows 17-19, 20-22, and 23-25 respectively). We also introduced a plasmid pTsr^{R64C} encoding Tsr with a mutation in the serine binding pocket (R64C), which cannot sense serine but is otherwise functional⁴⁴, to determine if this aided taxis of a C only* strain in LB medium (Table 4.1B; rows 26-28). In none of these strains did motility improve to levels seen with the BC only* strain. In summary, these data show that whereas deletion of the pentapeptide in McpB eliminates its stimulatory effect, provision of Tar or Tsr does not improve McpC-mediated taxis to cystine. Therefore, if the function of McpB is to provide adaptational assistance to McpC, then the assistance must be specific, as Tsr and Tar are unable to provide it.

Cystine-induced repellent chemotactic response of *Salmonella*

| No | Strain | Incubation Time | Media | Motility |
|------------|-------------------------------|----------------------|---------------------|----------|
| A 1 | Wild Type 14028 | 7 h (37° C) | LB Swim | 10 |
| 2 | $\Delta cheB$ | 7 h (37° C)+O/N (RT) | " | 1 |
| 3 | $\Delta cheR$ | " | " | 0 |
| 4 | $\Delta cheW$ | " | " | 0 |
| 5 | $\Delta cheV$ | 7 h (37° C) | " | 9 |
| 6 | BC only* | " | " | 7 |
| 7 | BC only*, $\Delta cheB$ | 7 h (37° C)+O/N (RT) | " | 1 |
| 8 | BC only*, $\Delta cheR$ | " | " | 0 |
| 9 | BC only*, $\Delta cheW$ | " | " | 0 |
| 10 | BC only*, $\Delta cheV$ | 7 h (37° C) | " | 7 |
| B | | | | |
| 11 | BC only* | 22 h (37° C) | Minimal + Cystine | 9 |
| 12 | C only* | " | " | 4 |
| 13 | C::Tsr only* | " | " | 0 |
| 14 | B _{A5} C only* | " | " | 4 |
| 15 | Tar, C only* | " | " | 5 |
| 16 | Tar, C only* | " | Minimal + Aspartate | 10 |
| 17 | C only* | 22 h (37° C) | Minimal + Cystine | 4 |
| 18 | C only*, pTar | " | " | 4 |
| 19 | C only*, pTsr | " | " | 3 |
| 20 | C only* | " | Minimal + Aspartate | 2 |
| 21 | C only*, pTar | " | " | 6 |
| 22 | C only*, pTsr | " | " | 3 |
| 23 | C only* | " | Minimal + Serine | 2 |
| 24 | C only*, pTar | " | " | 4 |
| 25 | C only*, pTsr | " | " | 8 |
| 26 | BC only* | 7 h (37° C)+O/N (RT) | LB | 7 |
| 27 | C only* | " | " | 3 |
| 28 | C only*, pTsr ^{R64C} | " | " | 4 |

Table 4.1. Motility-plate response of *S. typhimurium* 14028 strains. (A) McpB / C function requires CheB, CheR and CheW but not CheV. Motility is expressed as relative swim colony diameter compared to wild-type (given an arbitrary value of 10) whose moving front had just reached the edge of an LB swim plate (37°C, 7 h; see Figure 4.2A). **(B)** Role of the C-terminal pentapeptide in McpB / C function. Strains were inoculated in LB or minimal media and incubated as indicated. 1 μ M IPTG was included in the plates containing pTsr and pTsr^{R64C}. pTar expresses Tar constitutively.

Chapter 4

4.9. Discussion

To our knowledge, McpB and McpC are the first chemoreceptors reported to respond to cystine. Although the cystine response was first discovered by observing enhanced migration in motility-plate assays and interpreted as an attractant response, measurement of kinase activity using *in vivo* FRET revealed a McpB / C-specific response indicative of a repellent. Below, we tie together the apparently contradictory responses of McpB / C to cystine / cysteine in motility-plate and FRET assays.

A unified interpretation of a repellent response to cystine

Imperfect adaptation. Motility-plate assays show an apparently positive response to cystine, whereas FRET assays show a repellent response. We can reconcile the behavior in motility-plate assays by the FRET data showing ‘imperfect adaptation’ to cystine. CheR / B-mediated recovery does not restore kinase activity exactly to the pre-stimulus level upon step stimulation with cystine (Figures. 4.4, 4.5, and 4.7), and such imperfect adaptation could explain the enhanced spreading of cells on cystine motility plates. As was first described by Wolfe & Berg ²⁷⁶, radial spreading of cells on soft-agar plates can occur even in strains incapable of normal chemotaxis, e.g. in adaptation-deficient $\Delta cheR \Delta cheB$ strains, or even in “guttled” strains of *E. coli* deleted for all receptors and chemotaxis genes. In such non-chemotactic strains, the rate of spreading was found to increase monotonically with the tumbling bias. So, when a chemoeffector is seen to enhance the rate of spreading in motility plates, it could be due to an attractant response to a chemical being consumed, an increase in the steady-state tumbling bias, or both. In the context of our experiments, an increase in the steady-state tumbling bias due to imperfect adaptation to the repellent cystine would be expected to increase the rate at which cells spread in the motility-plate assays. Therefore, the imperfect adaptation to cystine observed in FRET assays forms the basis of our proposal that the enhanced migration in motility-plate assays is due to an increased rate of spreading resulting from an increase in the steady-state tumbling bias, rather than a positive chemotactic response to an attractant.

Cystine-induced repellent chemotactic response of *Salmonella*

Two recent studies have provided explanations for imperfect adaptation to attractant stimuli, such as serine and aspartate^{132,163}. Although the details of these two proposed mechanisms differ, both are essentially due to effects of the finite number of methylation sites possessed by chemoreceptors. Whether such mechanisms might contribute to the observed imperfect adaptation to cystine would make for an interesting question for future investigations.

The cystine / cysteine redox pair. We showed that cystine but not cysteine is sensed by the BC only* strain (Figure 4.5). Why then do both amino acids elicit a response in motility-plate assays (Figure 4.2)? A major difference between the motility-plate, capillary and FRET assays is the time scale over which responses reveal themselves. Motility-plate assays compare colony propagation rates over hours, capillary assays reflect the accumulation of cells over minutes, and FRET assays reveal intracellular signaling responses within seconds. Because oxidation / reduction reactions interconvert cystine and cysteine, one possible explanation is that the migration response on cysteine plates is due to oxidation of cysteine to cystine during the long duration of the experiment. The similarity in the results for cystine and cysteine plates (Figure 4.2) could be explained if in both cases the cystine / cysteine ratio relaxes toward an equilibrium that is independent of the initially added form of these inter-convertible amino acids. Reports suggest that aerobic conditions would favor cystine, whereas anaerobic conditions would shift this equilibrium towards cysteine^{18,73,227}. Indeed, when the plates were incubated anaerobically, the response of the BC only* strain to both amino acids was diminished but was again identical for the two amino acids, indicating that the equilibrium has likely shifted towards cysteine and that cystine is the true chemoeffector sensed by these receptors (Figure 4.8A). (Reducing agents such as dithiothreitol or β -mercaptoethanol were not used to create reducing conditions because they are not stable for a long time in the conditions used in motility-plate assays²⁴⁶). The inference for interconversion of the cystine / cysteine redox pair was confirmed by repellent response of $\Delta tsr \Delta tar$ strain (insensitive to cysteine) to high concentrations of cysteine (see Appendix A).

We also performed a chemical-in-plug assay where the chemical gradient is formed by diffusion rather than consumption of the chemical. A

Chapter 4

hard-agar plug containing the chemical was inserted into a soft-agar minimal media plate and bacteria were allowed to migrate toward the plug after being inoculated at some distance. This assay gave results similar to those shown in Figure 4.2, confirming that McpB / C are sufficient for the taxis response to cysteine / cystine (Figure 4.8B). When this assay was conducted anaerobically (Figure 4.8B right), the response was consistent with the results in Figure 4.8A: the migration towards either amino acid was not as pronounced as under aerobic conditions. Taken together, these results suggest that the equilibrium composition of the cystine / cysteine mixture shifts towards cystine under aerobic conditions and cysteine under anaerobic conditions, so that the enhanced spreading mediated by McpB / C (which sense cystine but not cysteine) is attenuated under anaerobic conditions.

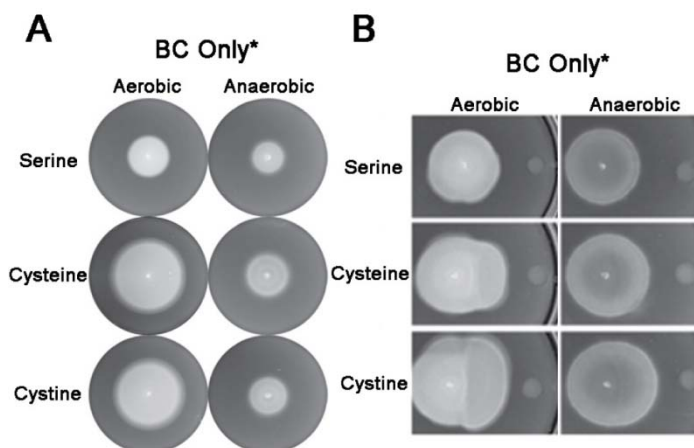


Figure 4.8. Response to cystine / cysteine in aerobic versus anaerobic conditions in long-time motility-plate assays. (A) Bacteria were inoculated in the center of minimal media plates. Growth conditions were as described in Figure 4.2C. See Materials and methods for description of the anaerobic chamber. (B) Chemical-in-plug assay. The hard-agar plugs on the right contain the test chemical, which diffuses into the soft-agar media. Bacteria were inoculated at some distance and plates incubated for 22 h at 37°C.

Cystine-induced repellent chemotactic response of *Salmonella*

Role of McpB and McpC in the cystine response

The strongest responses to cystine were observed when McpB and McpC were expressed together. However, because cystine responses were observed in the absence of either one, but not both of these receptors, apparently each receptor senses cystine. The requirement for the adaptation enzymes CheR and CheB was observed in both long- and short-time assays. McpB, which has the C-terminal pentapeptide motif that is absent in McpC, might provide adaptational assistance to McpC. However, because two other pentapeptide-harboring receptors, Tsr and Tar, failed to improve the function of McpC, it appears that the contribution of McpB to the McpC-mediated response is specific.

Physiological significance of the cystine response

Although cystine is neither a direct participant in biochemical pathways, nor incorporated into proteins, it is cystine rather than cysteine that is taken up by *E. coli* and *S. typhimurium*^{21,191}. At high concentrations, cysteine is toxic to cells and is exported to the periplasm by multiple cysteine transporters where it is converted into cystine in the oxidative environment of the periplasm. The periplasmic flagellar protein FliY binds cystine⁴⁶ and, along with two other cystine transport systems, is implicated in its transport back into the cell²¹. The cysteine / cystine shuttle system is proposed to play an important role in oxidative stress tolerance by providing reducing equivalents to the periplasm¹⁹¹. Our preliminary results ruled out that cystine is sensed through FliY, as deletion of *fliY* in the BC only* background did not alter its positive migration to cysteine or cystine in plates incubated under aerobic or anaerobic conditions, nor did deletion of *fliY* in the wild-type background alter the response in FRET experiments.

What then could be the physiological relevance of the repellent response to cystine in *S. typhimurium*? We showed in this study that oxidized and reduced forms of the cystine / cysteine redox pair elicit responses with an opposite sign: whereas cysteine is a chemoattractant, cystine acts as chemorepellent. Oxidative environments are expected to

Chapter 4

shift the equilibrium of the cysteine / cystine pair towards cystine. Therefore, the presence of cystine in the environment is likely an indicator of oxidizing conditions. Such conditions generate reactive oxygen species, which are responsible for damage to all macromolecules (DNA, lipids and proteins) ²⁰⁵. The McpB / C-mediated repellent response to cystine could provide *S. typhimurium* with an escape mechanism from such environments, either outside or within the host. In oxidative environments such as those found in macrophages ¹⁶², the response to cystine could facilitate the spread of *S. typhimurium* beyond the gastrointestinal tract in systemic disease ²¹².

4.10. Materials and methods

Bacterial strains and plasmids

The strains and plasmids used in this study are listed in Table 4.2.

| Strain | Relevant genotype | Source |
|--------|--|--------------|
| 14028 | <i>Salmonella enterica</i> serovar Typhimurium ATCC strain (wild type <i>S. typhimurium</i> 14028) | R.M. Harshey |
| SM542 | 14028 $\Delta mcpB \Delta mcpC$ | This study |
| QW265 | 14028 $\Delta mcpB$ | This study |
| SM457 | 14028 $\Delta mcpC$ | This study |
| JW20 | 14028 <i>mcpB</i> , <i>mcpC</i> only* | This study |
| MB203 | 14028 <i>mcpB</i> , <i>mcpC</i> only (<i>mcpA</i> ::Kan) | This study |
| MB1 | 14028 <i>mcpC</i> only* (<i>mcpB</i> ::Cm) | This study |
| MB2 | 14028 <i>mcpB</i> only* (<i>mcpC</i> ::Cm) | This study |
| MB211 | 14028 $\Delta 9T$ ($\Delta tsr \Delta tsr \Delta trg \Delta aer \Delta tcp \Delta mcpA \Delta mcpB \Delta mcpC \Delta tip$) | This study |
| SM469 | 14028 <i>tar</i> only* (<i>tcp</i> ::Kan) | This study |
| SM576 | 14028 <i>mcpC aer</i> only* (<i>mcpB</i> ::Cm, <i>tcp</i> ::Kan) | This study |
| SM387 | 14028 $\Delta cheB$ | This study |
| SM399 | 14028 $\Delta cheR$ | This study |
| SM423 | 14028 $\Delta cheV$::Cm | This study |
| SM464 | 14028 $\Delta cheW$ | This study |
| MB82 | 14028 <i>mcpB mcpC</i> only*, <i>cheB</i> ::Kan | This study |
| MB83 | 14028 <i>mcpB mcpC</i> only*, <i>cheR</i> ::Kan | This study |

Cystine-induced repellent chemotactic response of *Salmonella*

| MB84 | 14028 <i>mcpB</i> , <i>mcpC</i> only*, <i>cheW</i> ::Kan | This study | | |
|----------------|--|---|---------------------|-----------------|
| MB187 | 14028 <i>mcpB</i> , <i>mcpC</i> only*, <i>cheV</i> ::Kan | This study | | |
| SM162 | 14028 $\Delta 7T$ ($\Delta tsr \Delta tar \Delta trg \Delta aer \Delta mcpB \Delta mcpC \Delta tcp$::Kan) | | | |
| ST998 | 14028 <i>tar mcpC</i> only* (<i>mcpB</i> ::Cm) | This study | | |
| ST1000 | 14028 <i>mcpC</i> :: <i>tsr</i> _Tet only* (<i>mcpB</i> ::Cm) | This study | | |
| ST1001 | 14028 <i>mcpB</i> $_{\Delta 5}$, <i>mcpC</i> only* | This study | | |
| LT2 | <i>Salmonella enterica</i> serovar Typhimurium strain LT2 (wild type <i>S. typhimurium</i> LT2) | <i>Salmonella</i> Genetic Stock Center (SGSC) | | |
| TSS500 | LT2 $\Delta cheY \Delta cheZ$ | This study | | |
| TSS507 | LT2 $\Delta cheR \Delta cheB \Delta cheY \Delta cheZ$ | | | |
| TSS515 | LT2 $\Delta cheV \Delta cheY \Delta cheZ$ | | | |
| TSS868 | LT2 $\Delta tsr \Delta cheY \Delta cheZ$ | This study | | |
| TSS878 | LT2 $\Delta tar \Delta cheY \Delta cheZ$ | This study | | |
| TSS866 | LT2 $\Delta tar \Delta tsr \Delta cheY \Delta cheZ$ | This study | | |
| Plasmid | Gene(s) | Resistance | Induction | Source |
| pKG110 | cloning vector | chloramphenicol | sodium salicylate | J.S. Parkinson |
| pBAD33 | cloning vector | chloramphenicol | <i>L</i> -arabinose | ⁹⁶ |
| pML19 | <i>mcpC</i> | chloramphenicol | sodium salicylate | This work |
| pBR1 | <i>mcpB</i> | chloramphenicol | sodium salicylate | This work |
| pVS88 | <i>cheZ-ecfp / cheY-eyfp</i> | ampicillin | IPTG | ²⁴⁰ |
| pMK113 | <i>E. coli tar</i> | ampicillin | constitutive | M. D. Manson |
| pJC3 | <i>E. coli tsr</i> | ampicillin | IPTG | J. S. Parkinson |
| pJC3 (R64C) | <i>E. coli tsr</i> insensitive to serine | ampicillin | IPTG | ⁴⁴ |

Table 4.2. Strains and plasmids used in this study. Δ and :: refer to deletion of, or deletion / substitution within the indicated gene, respectively. Kan, Cm or Tet refer to substitutions with kanamycin, chloramphenicol, and tetracycline-resistance cassettes. Deletions created by the Datsenko & Wanner method ⁶² left behind a ‘scar’ sequence of ~80 base pairs in all 14028 strains. LT2-based deletion strains do not have a scar. Strains indicating ‘only’ refer to presence only of the indicated chemoreceptor gene and absence of all others. Only* indicates that the strain retains *mcpA* and *tip*. *mcpC*::*tsr* strain fuses the end of *mcpC* to the C-terminal 30 amino acid residues of *tsr* and has a Tet marker downstream. *mcpB* $_{\Delta 5}$ deletes of the last five amino acid residues in *mcpB*.

Chapter 4

Strain and plasmid construction

Deletion or insertion of genes and regulatory regions was achieved by the one-step mutagenesis procedure⁶² as described²⁶⁸. The initial deletion / substitution involved selection with either kanamycin^R (Kan), chloramphenicol^R (Cm) or tetracycline (Tet) cassettes. Except for deletion of the C-terminal pentapeptide encoding region of *mcpB*, all gene deletions were designed to remove the entire coding sequence except the first and last few amino acids, and were verified by DNA sequencing. LT2-based strains were created using a modification of the Datsenko and Wanner strategy that does not leave a scar: the insertion cassette contains the lethal gene *ccdB* under control of rhamnose inducible promoter, and is removed by positive selection on rhamnose-minimal plates²⁸⁸. The resident plasmid pSLT (containing *ccdA ccdB* operon) was displaced prior to chromosomal manipulations using Kit 10 from *Salmonella* Genetics Stock Center (SGSC).

Addition of the last 30 amino acid-encoding segment of *tsr* to the end of *mcpC* was achieved as follows: a PCR product linking the C-terminal end of *tsr* to *tet* was first generated using appropriate primers specific to *tsr* and *tet*. This product was used as a template to similarly generate a second PCR product linking the end of *mcpC* to the *tsr-tet* fusion. The *mcpC-tsr-tet* product was recombined into the C only* strain. The hybrid joint has the following sequence (the underlined residues are from *mcpC*, followed by those from *tsr*): DTQPAAREVAAVKTPAAVSSPKAAVADGSDNWETF.

In the LT2-based strains used in the FRET experiments, *cheY* and *cheZ* are deleted from the chromosome and CheY-YFP and CheZ-CFP fusions are expressed from a plasmid pVS88²⁴⁰ (except in LT2 YZ+ strain shown on Figure 4.6). Lack of competitive interaction of labeled and unlabeled CheY and CheZ proteins leads to a greater amplitude of FRET responses, compared to strains that express unlabeled CheY and CheZ. This is supported by data in Figure 4.6: the amplitudes of the initial FRET response to all tested chemicals are greater in LT2 $\Delta cheY \Delta cheZ$ than in LT2 and 14028, which contain unlabeled *cheY* and *cheZ*. Other factors that could contribute to the different response amplitudes in LT2- and 14028-based strains are possible strain-dependent and day-to-day variations in receptor expression levels, and the density of cells in the area of the coverslip from

Cystine-induced repellent chemotactic response of *Salmonella*

which FRET signals were measured (LT2-based strains attached more efficiently than did 14028-based strains, resulting in higher experiment-to-experiment variation in fluorescence levels for the 14028-based strains).

pMB1 was constructed by PCR amplification of genomic *mcpB* using primers that included *SphI* and *XbaI* restriction sites for ligating into the same sites on the expression vector pBAD33⁹⁶. A similar cloning strategy was used for the plasmid for McpC expression, pML19; however, the primers contained *NdeI* and *BamHI* sites, and the expression vector was pKG110. pMK113 expressing *E. coli* Tar was a gift from Michael Manson (Texas A & M University), and pJC3 expressing *E. coli* Tsr was a gift from Sandy Parkinson (University of Utah, Salt Lake City); expression is from the *tac* promoter in the pTrc99A vector¹³. *E. coli* Tsr(R64C) was expressed from the parent plasmid pJC3⁴⁴. The FRET donor–acceptor pair - CheZ-CFP and CheY-YFP – was expressed from a plasmid pVS88 under control of an isopropyl β -D-1-thiogalactopyranoside (IPTG)–inducible promoter²³⁷.

Motility-plate and chemical-in-plug assays

Bacteria were grown either in L-broth (LB) base (20 g/L), tryptone broth (1% Bacto tryptone, 0.5% NaCl) or in M63 minimal medium (100 mM KH₂PO₄, 15 mM (NH₄)₂SO₄, 1.8 μ M FeSO₄·7H₂O, 1 mM MgSO₄, 10 mM carbon source, adjusted to pH 7 with KOH). When testing for a response to a sugar, pre-cultures were grown with 0.2% concentration of that sugar.

Amino acid (all *L*-form) and vitamin mixtures were obtained from Invitrogen, and the nucleoside mixture was purchased from Millipore. The final amino acid concentrations in minimal-swim plates ranged from 2-20 μ M for individual amino acids from the Invitrogen MEM (Minimal Essential Medium) mix (arginine, cystine, histidine, isoleucine, leucine, lysine, methionine, phenylalanine, threonine, tryptophan, tyrosine and valine), or non-essential mix (glycine, alanine, asparagine, aspartic acid, glutamine, glutamate, proline and serine); 1 mg/L for each vitamin (choline, pantotheic acid, folic acid, nicotinamide, pyridoxal hydrochloride, riboflavin, thiamine and inositol); 30 μ M for each nucleoside (adenosine, cytidine, guanosine, thymidine and uridine). Individual amino acids were tested at 100 μ M. The sugar mix contained 50 μ M each of glucose, maltose,

Chapter 4

ribose and arabinose. The energy mix contained 75 μ M each of pyruvate and succinate.

Swim or chemotaxis plates were solidified with 0.3% agar and inoculated in the center with 2.5 μ l of an exponentially growing culture at OD₆₀₀ of 0.6. Plates were incubated for 7 h at 37° C or overnight at room temperature (RT), as indicated at Figure 4.2 and Table 4.1.

In the chemical-in-plug assays, hard-agar plugs with 10 mM chemical dissolved in minimal-glucose media and set with 2% agar were inserted with a sterile pipette tip into soft-agar (0.3%) minimal-media plates. The plates were poured at least 5 h before use and the plugs were inserted just before the plates were point-inoculated with bacteria at some distance from the plug. Plates were incubated for >20 h at 37° C.

Anaerobic motility assays were conducted in a 2.5 Liter, Oxoid AnaeroJar system AG0025. AnaeroGen sachets placed in a sealed jar rapidly absorb atmospheric oxygen with the simultaneous generation of carbon dioxide. Oxygen levels in the jar are claimed to fall below 1% within 30 minutes, and the resulting carbon dioxide levels are between 9% and 13%. The jar was set up according to manufacturer specifications.

Cystine preparation

Stock solution of 100 mM cystine (*L*-cystine, Calbiochem, Cat# 2470, 99.1%, for the plate and capillary assay experiments; *L*-cystine, Sigma Aldrich, Bioultra, \geq 99.5% for FRET experiments) was prepared in 1M HCl. The Calbiochem product has a certified synthetic origin. Sigma Bioultra is of animal origin; however, Calbiochem cystine, as well as two other Sigma products (Cat# C7602, 98.5-101.0% - from non-animal source, and Cat# 49603, TraceCERT® - from animal origin) were tested in FRET and qualitatively similar repellent responses were obtained.

Working solutions were prepared in minimal-glycerol M63 medium for the plate experiments, chemotaxis buffer (CB: 1xPBS, 0.1 mM EDTA, 0.01 mM *L*-methionine, and 10 mM DL-lactate) for the capillary assay experiments, and motility buffer (10 mM potassium phosphate, 0.1 mM EDTA, 1 μ M methionine, 10 mM lactic acid, pH 7) for FRET experiments. As the working solutions were buffered, their pH was neutral. Control

Cystine-induced repellent chemotactic response of *Salmonella*

FRET measurements with 100 μ M cystine dissolved directly in motility medium without using HCl, confirmed the repellent response.

Mass Spectrometry

LC-MS (liquid chromatography mass spectrometry) of cysteine and cystine solutions was performed at the University of Texas ICMB/CRED Protein and Metabolite Analysis Facility. An electrospray ion trap mass spectrometer (LCQ, ThermoFisher, San Jose, CA) coupled with a microbore HPLC (Magic 2002, Michrom BioResources, Auburn, CA) was used to acquire spectra. Cysteine was dissolved in water and cystine was dissolved in either formic acid or hydrochloric acid aqueous solutions. The samples were analyzed immediately. 10 μ l of each solution was injected into HPLC and directly infused into LCQ. Automated acquisition of full scan MS spectra was executed by Finnigan Excalibur™ software (ThermoFisher, San Jose, CA). The full scan range for MS was 50-300 Da. Each solution displayed only a single peak, corresponding to the expected mass for each amino acid.

Capillary Assays

Capillary assays were performed as previously described³, except that plastic gaskets (2 cm in diameter, ~1.5 mm thick) were used to create the chamber or “pond”. About one sixth (60°) of the circular gasket was removed to provide a portal for entry of the capillary tubes. Capillaries contained either chemotaxis buffer (CB) alone or CB with the indicated concentration of aspartate, cysteine or cystine. The first two amino acids were dissolved in deionized water, whereas cystine was first dissolved in 0.1M HCl and then neutralized with NaOH. Freshly prepared 100 mM stock solutions were diluted appropriately in CB prior to the capillary assay, which was run for 45 min at 37°C. The number of cells entering the capillary was determined by plating dilutions of the capillary contents on LB agar and counting colonies after 24 h incubation at 37° C.

Chapter 4

In vivo fluorescence resonance energy transfer (FRET) experiments and data analysis

The FRET pair, in which the response regulator, CheY, and its phosphatase, CheZ, are genetically fused to yellow (acceptor) and cyan (donor) fluorescence proteins (YFP and CFP) respectively, provides a measure of the concentration of the intracellular complex, formed between phosphorylated CheY (CheY-P) and CheZ. The concentration of CheZ·CheY-P complex is determined by two opposing reactions: phosphorylation of CheY by CheA, and dephosphorylation of CheY-P by CheZ. The rates of the two reactions are equal at steady-state, therefore the FRET signal is proportional to the activity of the central kinase of the chemotaxis pathway CheA, which is considered as a single output of the chemoreceptor activity^{226,241,260}. Thus, this FRET pair provides real-time readout of the activity of the bacterial chemotaxis pathway for any changes on a time scale greater than the relaxation time of CheY phosphorylation.

Bacteria were grown at 33.5°C to mid exponential phase (OD₆₀₀ ~0.5) in tryptone broth supplemented with appropriate antibiotics and inducers. Cells were harvested by centrifugation, washed twice, resuspended in motility buffer and stored at 4°C.

Prior to the experiment (1-5 h after harvesting), bacteria were immobilized on a poly-L-lysine coated coverslip. The coverslip was then situated at the top face of a flow cell²⁷, and the bacteria were kept under constant flow of motility buffer generated by a syringe pump (Harvard Apparatus, PHD2000). The same flow was used to add and remove chemoeffectors during experiments. There is a consistent ~ 25 s delay between the time when the switch was thrown to induce the step (indicated by arrows on the figures) and the time when the new solution reached the cells located in the flow cell.

An upright microscope (Nikon FN1), equipped with an oil immersion objective (Nikon CFI Plan Fluor, 40x/1.3), was used to perform FRET microscopy. The sample, situated in the flow cell, was illuminated by a metal halide arc lamp with closed-loop feedback (EXFO X-Cite *exacte*) through an excitation bandpass filter (Semrock, FF01-438/24-25) and a dichroic mirror (Semrock, FF458-Di01). The epifluorescent emission was

Cystine-induced repellent chemotactic response of *Salmonella*

split by a second dichroic mirror (Semrock, FF509-FDi01) into donor (cyan, C) and acceptor (yellow, Y) channels. Photon-counting photomultipliers (Hamamatsu H7422P-40) were used to collect the signal from C and Y channels through emission bandpass filters (Semrock FF01-483/32 for C channel and FF01-542/27 for Y channel). Signal intensities of the donor and acceptor channels were recorded through a data acquisition card (National Instruments) installed on a PC running custom-written software.

Both Y and C channels were corrected for the coverslip background. The signal from the Y channel was also corrected for leakage from CFP emission. The ratio R between the two channels, $R=Y/C$, serves as a robust indicator of FRET activity. $\Delta FRET$, the change in FRET efficiency upon stimulation at every time point, was computed as following:

$$\Delta FRET = (R_{pre+\Delta R} - R_0) / (R_{pre+\Delta R} + |\Delta Y/\Delta C|) - (R_{pre} - R_0) / (R_{pre} + |\Delta Y/\Delta C|),$$

where R_0 is the acceptor to donor ratio in absence of FRET, R_{pre} is the prestimulus acceptor to donor ratio, $\Delta R = R - R_{pre}$ is the change in the ratio upon stimulation, and $|\Delta Y/\Delta C|$ is the constant absolute ratio between the changes in the acceptor and donor signals per FRET pair²⁴². Under the applied experimental conditions, $R_{pre} + |\Delta Y/\Delta C| \gg \Delta R$; thus $\Delta FRET \sim \Delta R$. Thus for simplicity $\Delta FRET$ is expressed in arbitrary units of ΔR .

4.11. Acknowledgements

The motility-plate and chemical-in-plug assays presented in this chapter were performed by Mitchell Butler in the group of Prof. Dr. Rasika Harshey (University of Texas at Austin). The capillary assays were performed by Mitchell Butler, with the help of Dr. Manjunath Hedge from the group of Prof. Dr. Arul Jayaraman (University of Texas, A&M). 14028 strains were constructed by Susana Mariconda, Jaemin Lee and Vince Nieto from Harshey's lab.

Chapter 4

Chapter 5

The phospho-regulated scaffolding protein CheV affects chemoreceptor clustering in *Salmonella typhimurium*

The transmembrane receptors in the bacterial chemotaxis circuit interact with the central kinase CheA via scaffolding proteins CheW and CheV. CheV is a hybrid protein that contains a phosphorylatable receiver domain and plays a role in receptor clustering and adaptation to chemoeffectors in some bacterial species. Here we study the function of CheV in the chemotaxis of *Salmonella typhimurium*. In the absence of methylation-dependent adaptation, *cheV* knockout cells spread slower, and the CheV+ phenotype is restored only by expression of CheV that can be phosphorylated. *In vivo* fluorescence resonance energy transfer measurements indicate a weak but significant CheV-dependent partial adaptation to the non-metabolizable attractant α -methyl-aspartate. The adaptational recovery, however, is not affected by CheV phosphorylation. Using fluorescently-tagged CheV, we show that CheV forms clusters, predominantly localized at the cell poles, and the number and localization of these clusters does not depend on the phosphorylation state. Using YFP-CheR as a marker for receptor clusters, however, we show that the receptor cluster number decreases in *cheV* knockout cells, and has intermediate levels in a phosphorylation-deficient CheV mutant strain. The number of lateral receptor clusters also decreases in the absence of CheV. We speculate that CheV might play a role in the clustering of some of the chemoreceptor species in *S. typhimurium* and in the adaptation to chemoeffectors which these chemoreceptors can sense.

Chapter 5

5.1. Introduction

Scaffolding proteins bring together and promote interactions between different components of intracellular signaling networks ²⁹⁰. Signaling scaffolds create microenvironments in which the concentration of the participants is enriched, promote economical use of a limited set of signaling molecules without compromising specificity, and can also play active role in network-level dynamic regulation of the signaling modules involving feedbacks ^{54,178}. Scaffolding proteins are ubiquitous in eukaryotic signaling, but also play role in some signaling processes in bacteria: for example CheW and CheV are proteins that couple the transmembrane chemoreceptor arrays to a cytoplasmic layer of the complex formed by the histidine kinase CheA ¹⁰.

In the two-component chemotactic signaling system of bacteria, chemoeffectors are detected by transmembrane chemoreceptors that form allosteric complexes with histidine kinase molecules (CheA). Activated CheA gets autophosphorylated, and transfers phosphoryl groups to the response regulator CheY. Phosphorylated CheY in turn modulates the frequency of clockwise rotation of the flagellar motors ²⁶⁶. Different enzymes that accelerate CheY dephosphorylation, and enzymes that promote adaptation to chemoeffectors by reversible covalent modification (methylation) of chemoreceptors at multiple sites, exist in different bacterial species ^{201,281}. In all organisms that have chemotaxis networks defined by the presence of CheA, the kinase is coupled to the chemoreceptors by the scaffolding protein CheW, CheV or both, and these proteins are essential for the receptor-kinase interactions ^{90,102}.

CheW interactions with CheA and the chemoreceptors have been extensively studied: CheW binds *in vitro* to both with dissociation constants $\sim 6 \mu\text{M}$ and $\sim 11 \mu\text{M}$ respectively ^{39,90}, forming stable ternary complexes ^{78,216}. Chemoreceptors of different types form mixed trimers of dimers, which couple to CheA via CheW to form higher-order signaling arrays ^{119,194,240}. High levels of expression of CheW beyond the functional chemoreceptor-CheW-CheA complex stoichiometry, impair chemotactic ability of bacteria ^{146,211}. A recent study proposes that CheW-binding sites in receptor dimers overlap their trimer contact sites and overexpression of CheW saturates the

CheV affects chemoreceptor clustering in *Salmonella typhimurium*

inter-receptor-binding sites, preventing the assembly of trimers-of-dimers units⁴⁹. CheW plays a role also in the formation of higher-order receptor assemblies^{119,153}, which detailed structure has been recently revealed by cryoelectron tomography^{43,147}.

CheV is a two-domain protein (Figure 5.1A), in which the N-terminal domain is homologous to CheW (hereafter referred to as V_w). CheW residues that are crucial for the coupling with CheA and chemoreceptors have been identified^{39,146}, and multiple alignment shows that several of these residues are conserved between CheW and V_w. This observation suggests that CheV could also interact with CheA and the chemoreceptors, although such interactions have not been proven experimentally¹⁰. The C-terminal domain of CheV (hereafter referred to as REC) is homologous to regulatory proteins that are phosphorylated at a conserved aspartate residue, allowing them to switch between active and inactive conformations^{40,87,88}. The REC domains of CheV in some species, such as *Bacillus subtilis* and *Helicobacter pylori*, are phosphorylated *in vitro*^{116,197}.

The phenotypes of *cheV* knockout mutants differ between organisms, suggesting that the function and importance of CheV in different species varies¹⁰. As a hybrid protein, CheV possibly performs a coupling function associated with its V_w domain, a regulatory / adaptation-related function associated with its REC domain, or another function that individual domains alone cannot support. For example, in *B. subtilis*, CheV phosphorylation is required for normal adaptation to asparagine¹¹⁶. CheV also has a receptor-coupling function in *B. subtilis*, however, its function is partially redundant with CheW: both $\Delta cheV$ and $\Delta cheW$ knockouts but not $\Delta cheV \Delta cheW$ double knockout are chemotactic²⁰⁴. In *H. pylori*, which has three CheV proteins, loss of CheW leads to a non-chemotactic phenotype, whereas the loss of each of the three CheVs does not impair chemotaxis abilities of the cells, although their motility phenotypes are different^{149,197}. *H. pylori* lacks a methylation-dependent adaptation system, and it is possible that some of its CheV proteins are involved in a methylation-independent adaptation mechanism¹⁴⁰.

Here we study the role of CheV in chemotaxis of *S. typhimurium*. CheV has been recently identified in *S. typhimurium*^{86,267}, and deletion of

Chapter 5

cheV in wild type cells produces only very subtle phenotypic changes²⁶⁷. *S. typhimurium* cells in which the genes of the enzymes CheR and CheB involved in methylation-dependent adaptation were knocked out, form chemotactic rings in soft-agar motility assays, suggesting that a methylation-independent mechanism of adaptation might exist^{250,249}. The later discovery of CheV suggested that this protein might be involved in an adaptation that works in parallel to the methylation-dependent pathway in wild type cells. CheV is the only cytosolic component of the chemotactic network of *S. typhimurium* that does not have a homolog in the orthologous chemotaxis system of its close relative *Escherichia coli* (Figure 5.1B). However, *S. typhimurium* has more chemoreceptor species than *E. coli* (see Table 3.1, Chapter 3), so it is possible that CheV is involved only in the coupling of these chemoreceptors species not present in *E. coli* to the kinase CheA.

We investigated the phenotype of CheV mutant strains in soft-agar plates and showed that CheV, but not a phosphorylation-deficient CheV mutant can restore the phenotype of an adaptation-deficient $\Delta cheR \Delta cheB \Delta cheV$ strain to that of $\Delta cheR \Delta cheB$ strain. Our measurements of the kinase activity indicate a weak but significant partial adaptation upon stimulation with α -methyl-aspartate (MeAsp) steps in methylation-deficient cells that express CheV. Imaging reveals that fluorescently labelled CheV and its non-phosphorylatable variant CheV_{D250A} both form clusters in the presence of chemoreceptors. Moreover, knocking out *cheV* affects receptor-cluster number and localization. We discuss possible roles of CheV in chemoreceptor clustering and adaptation to chemoeffectors sensed by different chemoreceptor species.

CheV affects chemoreceptor clustering in *Salmonella typhimurium*

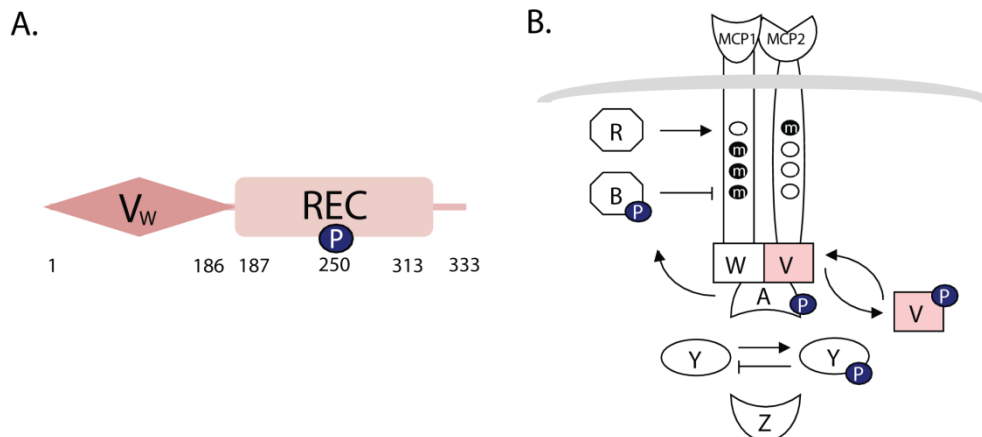


Figure 5.1. Structure of CheV and topology of *S. typhimurium* chemotactic network. (A) Domain structure of *S. typhimurium* CheV. Domain boundaries were determined using the SMART database ^{141,217}. The N-terminal domain (the amino acids 1-186), V_w , is homologous to CheW. The amino acids 187-313 form a receiver (REC) domain, which might be phosphorylated at D250. The phosphorylatable aspartate position was determined by aligning of CheV and CheY: the site of phosphorylation D57 of CheY corresponds to D250 in CheV (all the conserved residues among the CheY family of response regulators are either identical in CheV or are conservative substitutions). Multiple alignment of CheV proteins from different species show that the D250 site is conserved (M.Sc. thesis, M.E. Dougherty, 2006). (B) Chemotaxis network of *S. typhimurium*. Network topology is identical to that of *E. coli*, except for the presence of CheV (V), which could be phosphorylated by the kinase CheA (A), and could shuttle in and out of the receptor-kinase complex. The other proteins in the chemotactic network are the chemoreceptors (methyl-accepting chemotaxis proteins, MCPs), the response regulator CheY (Y) and its phosphatase CheZ (Z), the scaffolding protein CheW (W), the methyltransferase CheR (R) and methyl-erasure / deamidase CheB (B).

5.2. CheV enhances the spreading of methylation-deficient cells in soft-agar assays

To identify the role of CheV in chemotaxis of *S. typhimurium*, we performed a soft-agar assay, in which the bacteria are inoculated in tryptone broth (TB) low-concentration agar and subsequently spread outwards due to growth and chemotaxis in self-created gradients, formed by metabolizing the surrounding nutrients²⁷⁶. The phenotype of the $\Delta cheV$ knockout in a wild type background does not differ from that of wild type (Figure 5.2A). However, in knockout strains of the adaptation enzymes CheR and CheB, we noticed a phenotypic difference: whereas $\Delta cheR \Delta cheB$ strains spreads outwards, forming a single sharp ring, the $\Delta cheV \Delta cheR \Delta cheB$ spreads much slower, forming a smaller single ring which is more diffuse than that of the $\Delta cheR \Delta cheB$ strain (Figure 5.2B). A similar observation was reported earlier also by Wang et al²⁶⁷. The phenotype of the $\Delta cheR \Delta cheB$ strain is restored in $\Delta cheV \Delta cheR \Delta cheB$ expressing CheV from a plasmid (Figure 5.2C). Overexpressing CheV from a plasmid in $\Delta cheR \Delta cheB$ does not change its phenotype (Figure 5.2C). CheV, fused with yellow fluorescence protein, CheV-YFP, also complements $\Delta cheV \Delta cheR \Delta cheB$ (Figure 5.2C), similar to the untagged CheV. However, a version of the same fusion protein that bears a point mutation in the putative CheV phosphorylation site (D250), CheV_{D250A}-YFP, does not complement the $\Delta cheV$ phenotype in the $\Delta cheR \Delta cheB$ background (Figure 5.2C), suggesting that phosphorylation is essential for the function of CheV in modulating chemotactic behavior.

CheV expressed in wild type *E. coli* does not affect substantially its spreading phenotype: if anything, both wild type CheV and the non-phosphorylatable version, CheV_{D250A}, slightly increase the diameter of the outer spreading ring (Figure 5.2D). Both CheV and CheV_{D250A} fail to restore the chemotactic abilities of *cheW* knockout of *E. coli*, which does not form chemotactic rings in TB soft-agar plates. In contrast to *S. typhimurium*, *E. coli* strains that do not express the methylation and demethylation enzymes CheR and CheB, do not form chemotactic rings on TB soft-agar plates. We expressed CheV and CheV_{D250A} from a plasmid in $\Delta cheR \Delta cheB$ *E. coli*, and only the strain expressing wild type CheV showed a minor enhancement in

CheV affects chemoreceptor clustering in *Salmonella typhimurium*

spreading after three days of incubation. The aforementioned experiments with *S. typhimurium* and *E. coli* suggest that CheV plays a role in chemotaxis, and its function depends on its abilities to be phosphorylated.

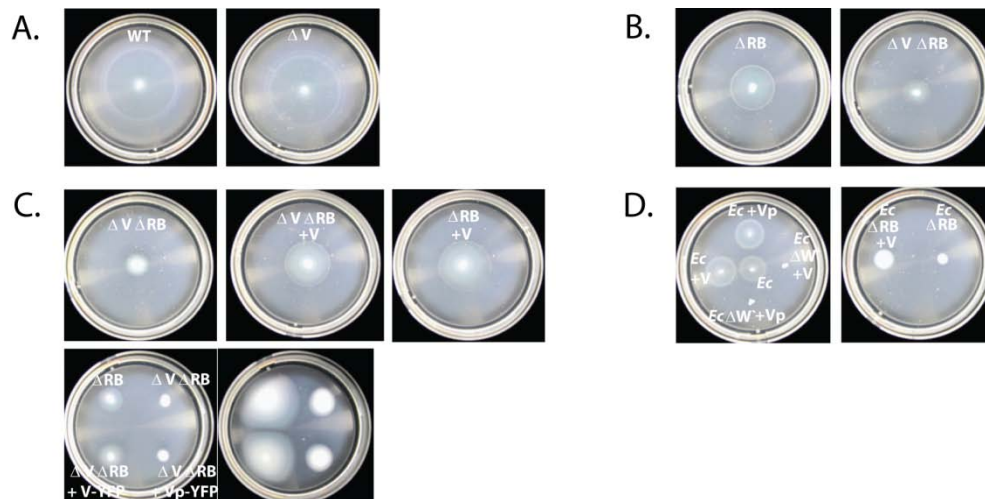


Figure 5.2. Soft-agar assays of chemotactic behavior. (A) Wild type and $\Delta cheV$ (ΔV) *S. typhimurium* after 7 h incubation. (B) $\Delta cheR \Delta cheB$ (ΔRB) and $\Delta cheV \Delta cheR \Delta cheB$ ($\Delta V \Delta RB$) *S. typhimurium* after 9 h of incubation. (C) Complementation of $\Delta V \Delta RB$ *S. typhimurium* (upper left) with CheV (V) expressed from a plasmid (upper middle) after 9 h of incubation. Upper right: CheV (V) from a plasmid was expressed in the ΔRB *S. typhimurium* and also imaged after 9 h of incubation. Lower: Complementation of $\Delta V \Delta RB$ *S. typhimurium* with CheV-YFP (V-YFP) and CheV_{D250A}-YFP (V_P-YFP) after 9 h (left) and 19h (right) of incubation. ΔRB and $\Delta V \Delta RB$ were also inoculated for comparison (D) Left: Comparison of the spreading of wild type *E. coli* (*Ec*) and *E. coli* in which CheV (V) and CheV_{D250A} (V_P) were expressed, after 7 h of incubation. $\Delta cheW$ *E. coli* (*Ec* ΔW) does not spread, and it is not complemented by either V or V_P. Right: $\Delta cheR \Delta cheB$ *E. coli* (*Ec* ΔRB) expressing V shows a minor enhancement of its spreading in soft-agar compared to *Ec* ΔRB after >72 hours of incubation (due to the prolonged incubation and high density of bacteria it is hard to determine whether the spreading is diffuse or a chemotactic ring exists).

5.3. Role of CheV in adaptation to MeAsp

The formation of chemotactic rings in $\Delta cheR \Delta cheB$ *S. typhimurium* strains has been interpreted as a methylation-independent adaptation pathway^{250,249}. Consistent with this view, experiments with tethered $\Delta cheR \Delta cheB$ cells showed partial recovery of the motor rotational bias upon stimulation with a chemoeffector step^{250,249}. CheV had not yet been discovered at the time of those studies, but later investigation of the role of CheV in methylation-deficient cells²⁶⁷ showed that $\Delta cheR \Delta cheB$ *S. typhimurium* has a near-normal tumbling bias, whereas $\Delta cheV \Delta cheR \Delta cheB$ has a higher counter clockwise bias of its motors, *i.e.* they change direction (tumble) less frequently. Tumbler cells migrate faster on soft-agar plates in chemotaxis-deficient strains²⁷⁶, which can provide an explanation of the different migration phenotype of the two strains. Another explanation for the partial adaptation of $\Delta cheR \Delta cheB$ cells could be the adaptive remodelling of the flagellar motor, recently discovered by Yuan et al²⁸⁹.

We have shown that the time scales of adaptation to MeAsp in the wild type and *cheV* knockout strain do not differ significantly: the frequency response of the two strains are nearly identical (see Chapter 3, the characteristic frequency of the frequency response is determined by the adaptation time scale of the chemotaxis system²⁶⁰). To test for adaptation of the kinase activity in the absence of receptor methylation, we applied steps of chemoeffectors to $\Delta cheR \Delta cheB$ *S. typhimurium* strains and observed the changes in the kinase (CheA) activity using *in vivo* fluorescence resonance energy transfer (FRET). The assay utilizes a FRET pair between the phosphatase CheZ and the response regulator CheY, fused to yellow and cyan fluorescent proteins (YFP and CFP) respectively, and provides a real-time readout of the kinase activity²⁴². We tested the response to a step stimulus of the non-metabolizable attractant MeAsp, and we observed a minor but reproducible adaptational recovery only in the presence of CheV. Figure 5.3A shows a typical FRET response time series of the $\Delta cheR \Delta cheB$ strain expressing wild type CheV, CheV_{D250A} or no CheV to 0.25 mM MeAsp. Both the strain expressing wild type and mutant CheV show partial adaptation recovery of ~10%. $\Delta cheV$ strain does not show partial

CheV affects chemoreceptor clustering in *Salmonella typhimurium*

adaptation even after >1500 s (Figure 5.3A), suggesting that CheV could be involved in a methylation-independent adaptation mechanism. The degree of partial adaptation in CheV-containing strains is minor and only slightly greater than the measurement noise, and occurs on a very slow time scale (>1500 s), whereas the tethering assays of Stock et al. demonstrated adaptation on a ~100 s time scale²⁵⁰.

The smaller amplitude of the response in the $\Delta cheV$ strain to 0.25 mM MeAsp suggests that the sensitivity of this strain to MeAsp could be lower. We constructed dose-response curves for $\Delta cheR \Delta cheB$ strains with and without the *cheV* gene. We measured the initial amplitude of the FRET response ($FRET_i$), normalized it to the saturated response to a mix of MeAsp and serine ($|FRET_i^{max}|$), inhibiting the two major chemoreceptors Tar and Tsr, and plotted $FRET_i/|FRET_i^{max}|$ as a function of the MeAsp concentration (Figure 5.3B, negative responses; the $|FRET_i^{max}|$ is -0.11 ± 0.05 and -0.14 ± 0.07 for the strains with and without CheV respectively). Although the shapes of the tested curves for the two strains are similar, the dose-response curve of the *cheV* knockout is shifted towards the higher concentration range, indicating lower sensitivity to MeAsp. For both strains, two dissociation constants (K_D s) are apparent, and the dose-response curves are fit by a multisite Hill model $y = y^I \frac{x^{n_H^I}}{K_D^I n_H^I + x^{n_H^I}} + y^{II} \frac{x^{n_H^{II}}}{K_D^{II} n_H^{II} + x^{n_H^{II}}}$, where x is the concentration of MeAsp, y is the normalized $FRET_i$, y^I and y^{II} are the two plateaus in the normalized $FRET_i$ level, K_D^I and K_D^{II} are the two apparent dissociation constants, and n_H^I and n_H^{II} are the two Hill coefficients. Hill coefficients of 1.1 and 1, and 1.2 and 1, are used for the fits shown on Figure 5.3B (for the plateaus reached at -0.8 and -1 and -0.7 and -1 respectively). The dissociation constants for $\Delta cheR \Delta cheB$ strain are 0.17 and 400 mM, and for the $\Delta cheV \Delta cheR \Delta cheB$ strain: 0.40 and 409 mM MeAsp. We have shown that in *S. typhimurium* more than one receptor mediates responses to MeAsp (see Chapter 3). Since the receptors in both tested strains are in the same modification state due to lack of CheR and CheB, the difference in the sensitivity could be explained by a different proportion of receptors that are coupled in receptor-scaffold-kinase complexes, for example if CheV is involved in coupling of one of the receptors involved in MeAsp sensing but not the other(s).

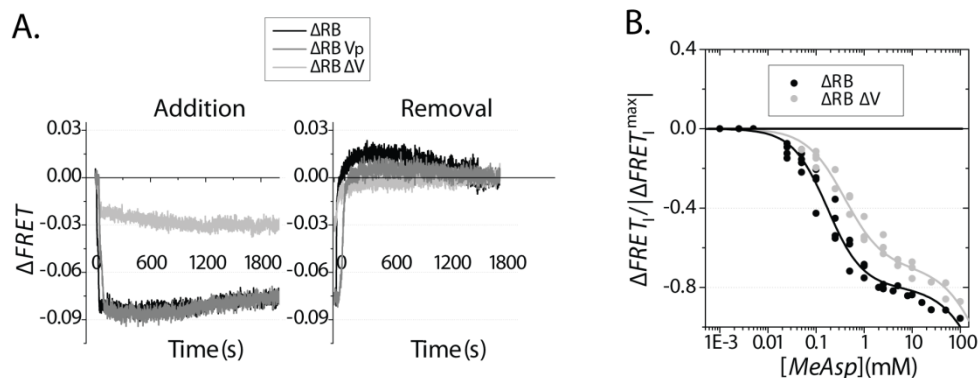


Figure 5.3. FRET response of *S. typhimurium* to chemoeffector steps. (A) Representative time series of the FRET response of $\Delta cheR \Delta cheB$ (ΔRB), $\Delta cheV \Delta cheR \Delta cheB$ ($\Delta V \Delta RB$) and $cheV_{D250A} \Delta cheR \Delta cheB$ ($V_P \Delta RB$) strains to 0.25 mM MeAsp. MeAsp is added and removed at times 0 on the left and right part of the panel, respectively. (B) Normalized initial amplitude of the FRET response ($FRET_i$) as a function of MeAsp concentration for ΔRB and $\Delta V \Delta RB$ strains. Fits to a multisite Hill equation of the MeAsp response of ΔRB and $\Delta V \Delta RB$ are shown (see text for fitted parameters).

5.4. Phosphorylation-independent localization of CheV at the cell poles

In order to explore the role of CheV in coupling and adaptation at the molecular level, we studied the localization of CheV and its non-phosphorylatable mutant CheV_{D250A}, using fluorescent fusion proteins CheV-YFP and CheV_{D250A}-YFP, expressed in $\Delta cheV \Delta cheR \Delta cheB$ *S. typhimurium*. The functionality of the CheV-YFP fusions were confirmed by the complementation of *cheV* deletion in soft-agar assays (Figure 5.2C). We observe that both CheV and CheV_{D250A} form cluster-like aggregates, but these clusters are not observed in cells in which most of the chemoreceptors are knocked out (Figure 5.4A; $\Delta 7$ refers to *S. typhimurium* strain, which has only McpA and Tip chemoreceptors). The existence of CheV-YFP clusters only in cells that contain chemoreceptors suggest that these clusters can serve as markers of chemoreceptor-scaffold-kinase complexes.

CheV affects chemoreceptor clustering in *Salmonella typhimurium*

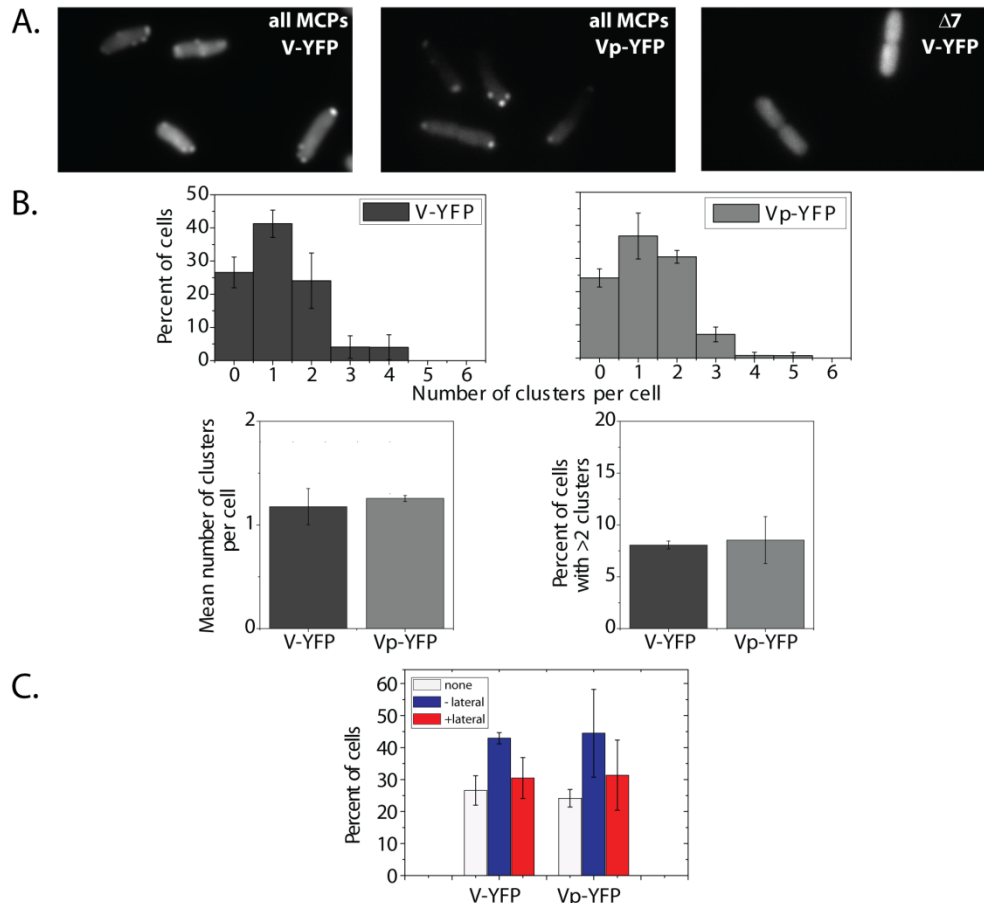


Figure 5.4. Localization and clustering of CheV-YFP and CheV_{D250A}-YFP in *S. typhimurium*. (A) Representative fluorescence microscopy images (600x) of CheV-YFP (left) and CheV_{D250A}-YFP (middle) in $\Delta cheV \Delta cheR \Delta cheB$ ($\Delta V \Delta RB$) strain. Right: Representative image of CheV-YFP in *S. typhimurium* cells, in which seven of the nine chemoreceptors are knocked out. (B) Upper row: distribution of the number of clusters formed by CheV-YFP and CheV_{D250A}-YFP in $\Delta V \Delta RB$ cells. 137 and 141 cells were analysed respectively. Lower left: mean number of receptor clusters per cell. Lower right: percent of cells with > 2 clusters. (C) Localization of clusters of CheV-YFP and CheV_{D250A}-YFP in $\Delta V \Delta RB$ cells. White, blue and red bars represent the percent of cells with no clusters, no lateral clusters and at least one lateral cluster (see text). The error bars in (B) and (C) represent the standard deviation obtained from two independent repeats (77 and 60 cells expressing CheV-YFP, and 69 and 72 cells expressing CheV_{D250A}-YFP).

Chapter 5

We evaluated the number and localization of the detectable CheV-YFP and CheV_{D250A}-YFP clusters within individual cells. 137 and 141 cells respectively were analyzed for each fusion protein in *ΔcheV ΔcheR ΔcheB S. typhimurium*. For both constructs, we determined the distribution of cluster numbers. The mean number of detected clusters per cell is ~1.2 and ~8% of the cells contain >2 clusters (Figure 5.4B). Differences, if any, are within the experimental error. To determine the position of the clusters within each cell, we divided the cells in three parts along the long axis, and considered clusters within the inner third lateral, and within the two outer thirds – polar. The distributions of the clusters among these partitions along the long cell axis were indistinguishable for the phosphorylatable and non-phosphorylatable CheV: cells containing at least one lateral cluster make up ~30% of the total population (Figure 5.4C). We conclude that the localization and number of the CheV-containing clusters does not depend on phosphorylation of the protein. However, we cannot rule out subtle differences in the number of receptors per cluster, which could be measured in future studies for example using superresolution microscopy⁹⁴ to count the number of CheV molecules per cluster.

5.5. The number of receptor clusters is smaller in *cheV* mutant cells

To obtain single-cell statistics of the number and localization of receptor clusters in the presence and absence of CheV, we used a YFP fusion of the methyltransferase CheR as a reporter¹¹⁹. CheR binds to the C-terminal conserved pentapeptide found at four of the chemoreceptors in *S. typhimurium* (Tar, Tsr, Tcp, and McpB, see Chapter 3, Table 3.1). The YFP-CheR fusion does not appear to interfere with clustering²²⁹, therefore it can be used to observe the localization of both clustered and non-clustered chemoreceptors¹¹⁹.

We imaged YFP-CheR in wild type, *ΔcheV* knockout and *cheV*_{D250A} non-phosphorylatable mutant *S. typhimurium* strains (Figure 5.5A). Fluorescence clusters are observed in all three strains; however, there are differences in the number of clusters per cell and in the cluster localization (Figure 5.5B, C). We obtained the distribution of cluster number per cell (for 507, 452, and 676 cells per strain respectively). The mean number of

CheV affects chemoreceptor clustering in *Salmonella typhimurium*

clusters is the highest in wild type cells (1.4 ± 0.1), intermediate in cells, expressing non-phosphorylatable CheV_{D250A} mutant (1.2 ± 0.1), and the lowest in $\Delta cheV$ knockout cells (0.9 ± 0.1) (Figure 5.5B; the error bars represent the standard deviation obtained from two independent repeats). The number of cells with more than two clusters is also decreasing in order of wild type, *cheV*_{D250A} strain and $\Delta cheV$ knockout strain: 14 ± 6 , 8 ± 5 , and 4 ± 0.2 percent of the total number of cells, respectively (Figure 5.5B; the error bars represent the standard deviation obtained from two independent repeats). The decrease in cluster number reflects the smaller number of lateral clusters observed in *cheV* mutant strains: $30 \pm 1\%$ of the wild type cells contain at least one lateral cluster, whereas the fractions of cells containing at least one lateral cluster is $21 \pm 3\%$ in cells that express the non-phosphorylatable CheV_{D250A} mutant, and $15 \pm 3\%$ in the $\Delta cheV$ knockout cells (Figure 5.5C). We concluded that CheV increase the chemoreceptor clustering in a phosphorylation-dependent manner, and the role of CheV in chemoreceptor clustering is particularly pronounced for the clusters with a lateral localization.

Chapter 5

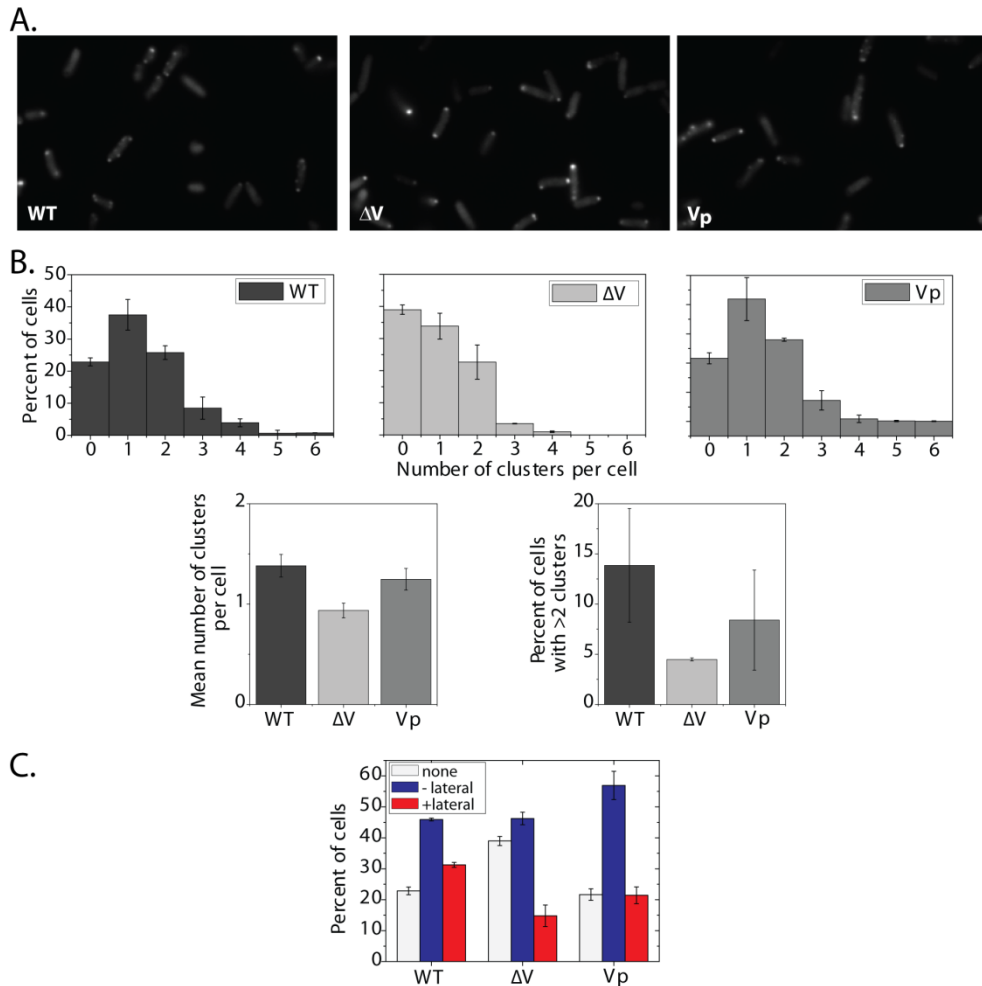


Figure 5.5. Localization and clustering of YFP-CheR. (A) Representative fluorescence microscopy images (150 \times) of YFP-CheR in wild type (WT, left), $\Delta cheV$ (ΔV , middle) and *cheV_{D250A}* (V_p , right) *S. typhimurium* strains. (B) Distribution of the number of YFP-CheR clusters in WT (upper left), ΔV (upper middle), and V_p (upper right) cells. 507, 452, and 676 cells were analysed respectively. Lower left: mean number of receptor clusters per cell. Lower right: percent of cells with more than two clusters. (C) Localization of YFP-CheR clusters in WT, ΔV , and V_p cells. The error bars in (B) and (C) represent the standard deviation obtained from two independent repeats (132 and 375, 87 and 365, and 123 and 553 cells for WT, ΔV , and V_p respectively).

5.6. Discussion

We have explored the role of the scaffolding protein CheV in adaptation and chemoreceptor clustering in *S. typhimurium*. Using classical chemotaxis soft-agar assay, we have demonstrated a phenotypic difference between CheV⁺ and CheV⁻ cells, incapable of methylation-dependent adaptation (Figure 5.2). The difference is complemented by CheV but not by its non-phosphorylatable mutant CheV_{D250A}, suggesting a role of phosphorylation in the functional role of CheV. Faster spreading in the presence of CheV could be explained either by partial adaptation dependent on CheV (Figure 5.2A), and / or by the higher counter-clockwise bias of the flagellar motors of CheV⁻ cells, which was reported previously²⁶⁷. CheV expression promotes the formation of chemotactic rings in soft-agar experiments even in methylation-deficient *E. coli* cells, which is not achieved by the mutant CheV_{D250A}. This finding suggests that CheV might be involved in the clustering or functioning of some of the receptors common to *E. coli* and *S. typhimurium*, i.e. Tar, Tsr, Trg or Aer.

We have studied the role of CheV in *S. typhimurium* chemotaxis signaling using *in vivo* FRET measurements in CheV⁺ and CheV⁻ cells (Figure 5.3). In Chapter 3 we have probed the frequency response of the chemotaxis system in CheV⁺ and CheV⁻ cells (Chapter 3, Figure 3.6), and have not observed differences in the characteristic frequency, which is inversely proportional to the adaptation time scale of the chemotaxis system²⁶⁰. Here we probed the adaptational recovery to steps of α -methyl-aspartate, and observed a partial (~10%) adaptation in CheV⁺ cells, even when the phosphorylation site of CheV is disrupted. The adaptational recovery is small, comparable with the experimental noise; thus assays of chemotactic signaling with better sensitivity could be useful for precise quantification of the degree of adaptation. However, our experiments could provide an explanation for the Stock et al. studies^{250,249} reporting methylation-independent adaptation in *S. typhimurium*. The larger degree of adaptation observed in these studies, as well as the shorter adaptation time scale, on which the adaptation was observed by Stock et al., could be attributed to an additional adaptation mechanism that occurs downstream of the kinase activity. For example, a recent study by Berg's

Chapter 5

group ²⁸⁹ reported methylation-independent adaptation at the level of the flagellar motor based on active remodelling of the composition of the flagellar motors. CheV might be involved in a similar adaptation mechanism but at the level of receptor-kinase complexes.

Another difference between the kinase activity of CheV⁺ and CheV⁻ cells is the lower sensitivity to MeAsp of the latter (Figure 5.3B). The shapes of the dose-response curves are similar, with two plateaus that suggest more than one receptor binding MeAsp (see also Chapter 3, Figure 3.9, showing Tar-independent responses to MeAsp). We speculate that CheV might affect to different degrees the coupling and clustering of the different chemoreceptors sensing MeAsp, for example if some chemoreceptor species form complexes preferentially with CheW and others - with CheV (see Chapter 6).

In order to assess the localization of CheV in *S. typhimurium* cells, we created a CheV-YFP fluorescent fusion protein, the functionality of which was confirmed using soft-agar assays. We demonstrated that both CheV-YFP and the non-phosphorylatable variant CheV_{D250A}-YFP form clusters only in cells containing the majority of the chemoreceptors (Figure 5.4). Clusters were predominantly localized in the poles of the cells. We have not identified a difference either in the cluster number or in the cluster localization using wild type CheV or its non-phosphorylatable mutant CheV_{D250A}. However, we cannot exclude subtle differences for example in the number of receptors per cluster, which could be quantified in future studies using superresolution microscopy.

We have also assessed the number and localization of receptor clusters in CheV⁺ and CheV⁻ cells, using YFP-CheR as a marker for receptor clusters (Figure 5.5). Receptor cluster number is lower in cells where *cheV* is knocked out, and also the clusters in the *cheV* knockout strain are localized predominantly in the cell poles, whereas CheV⁺ cells have also a large fraction of lateral clusters. Cells expressing non-phosphorylatable CheV_{D250A}, have more clusters than CheV⁻ cells, but fewer clusters than wild type cells; the number of lateral clusters follows the same pattern. These observations indicate that CheV plays a role in receptor cluster formation in *S. typhimurium*, and phosphorylation of CheV is likely to increase the number of CheV-coupled chemoreceptors. A differential

CheV affects chemoreceptor clustering in *Salmonella typhimurium*

distribution of phosphorylated and non-phosphorylated CheV has been recently reported in *B. subtilis*²⁷⁹: phosphorylated CheV is predominantly localized in the lateral clusters, which might also be the case in *S. typhimurium*.

CheV does not complement *cheW* knockouts either in *E. coli* (Figure 5.2D) or in *S. typhimurium* where the *cheW* deletion abrogates chemotaxis (Chapter 4, Table 4.1). Thus, CheW's and CheV's role in chemoreceptor coupling of *S. typhimurium* are not redundant. Future studies with CheV and CheW co-localization for example by labelling with fluorophores with different colors, could reveal whether CheW and CheV participate in the same or in separate clusters.

In summary, we have shown that *S. typhimurium* CheV affects the number and localization of chemoreceptor clusters in a phosphorylation-dependent manner. We speculate that such changes could be explained by dynamic remodelling of the clusters, in which CheV acts as a scaffolding protein. Adaptive remodelling of the receptor-kinase clusters could be a consequence of changes in the phosphorylation level of CheV. Since the phosphorylation of CheV is most likely performed by CheA, and CheA activity is modulated by binding of chemoeffectors to the transmembrane chemoreceptors, CheV might be involved in a phosphorylation-dependent feedback regulation of the stability of the receptor clusters. Such a novel mode of feedback might explain the partial adaptation observed in methylation-deficient *S. typhimurium* cells, and this phosphorylation-dependent regulation could be more pronounced under certain environmental conditions. One possibility is that CheV and CheW are expressed to different degrees under different conditions of growth, or in different strains. Another possibility is that CheV and CheW are involved in coupling of different subsets of chemoreceptors. Since the chemoreceptor species change their relative abundance under different growth conditions or phases of bacterial growth^{210,284}, the role of CheV and CheW may also change depending of the relative chemoreceptor species abundance. Future studies of CheV expression and localization under controlled environmental conditions could reveal more insights regarding the function of CheV in *S. typhimurium*.

Chapter 5

5.7. Materials and Methods

Bacterial strains and plasmids

All strains and plasmids used in this study are listed in Table 5.1. All *S. typhimurium* strains, except the strain, in which seven chemoreceptors are removed from the chromosome (SM162, referred to as $\Delta 7$) have LT2 background. The $\Delta 7$ strain is used in CheV clustering experiments and we verified that its parent strain, 14028, CheV clusters in a manner similar to the clustering in LT2.

In-frame deletion of genes in the strains designed for this work was achieved by allele-replacement procedure based on Datsenko and Wanner's method⁶². *S. typhimurium* LT2 resident plasmid pSLT contains a *ccdA ccdB* operon that interferes with the deletion strategy. Thus, pSLT was first displaced using Kit10 from *Salmonella* Genetics Stock Collection (SGSC): a plasmid pLL6, which is from the same compatibility group as pSLT, is transformed in the strain of interest, pSLT is cured, and pLL6 is subsequently removed using temperature selection¹¹⁸. The initial knockout step involves an insertion of a cassette providing kanamycin resistance, and also containing the lethal gene *ccdB* under the control of *L*-rhamnose inducible promoter. The cassette is removed by positive selection on *L*-rhamnose-minimal plates²⁸⁸. All allele replacements were verified by genetic sequencing.

The plasmid for CheV expression (pML13) was constructed by PCR amplification of genomic *cheV* using primers, containing *SacI* and *XbaI* restriction sites for ligation into the same sites on the expression vector pBAD33. The plasmid for CheV_{D250A} expression (pML14) was created in similar manner, but D250A mutation was introduced using overlap PCR. Induction of protein expression from pML13 and pML14 was achieved using 0.01% *L*-arabinose. The plasmid for CheV-YFP expression (pML16) was created by overlap PCR, introducing a GSGGGG linker, which contains *BamHI* site, between *cheV* and *eyfp* genes. The overlap product was ligated in the expression vector pTrc99A using *SacI* and *XbaI* sites. The plasmid for CheV_{D250A}-YFP expression (pML17) was created in similar manner, but *cheV* gene was replaced with *cheV*_{D250A}. Induction of protein

CheV affects chemoreceptor clustering in *Salmonella typhimurium*

expression from pML16 and pML17 was achieved using 2 μ M isopropyl- β -D-1-thiogalactopyranoside (IPTG). All plasmid constructs were verified by genetic sequencing.

The YFP-CheR fusion that served as a marker for receptor clusters was expressed from a plasmid pVS102¹¹⁹, using 0.01% *L*-arabinose.

The CheY-YFP and CheZ-CFP fusions for the FRET experiments were expressed from a plasmid pVS88²⁴⁰, induced with 150 μ M isopropyl β -D-1-thiogalactopyranoside (IPTG). The same amount of IPTG was used in the soft-agar assays, whenever Δ *cheY* Δ *cheZ* strains were used. In all strains used in FRET experiments, chromosomal *cheY* and *cheZ* were deleted in order to prevent a competitive interaction between labelled CheY-YFP and CheZ-CFP, and unlabelled CheY and CheZ.

| Strain | Relevant genotype | | | Source |
|---------|---|-----------------|---------------------|---|
| LT2 | <i>Salmonella enterica</i> serovar Typhimurium strain LT2 (wild type <i>S. typhimurium</i> LT2) | | | <i>Salmonella</i> Genetic Stock Center (SGSC) |
| TSS511 | LT2 Δ <i>cheV</i> | | | This work |
| TSS530 | LT2 <i>cheV</i> _{D250A} | | | This work |
| TSS519 | LT2 Δ <i>cheR</i> Δ <i>cheB</i> | | | This work |
| TSS524 | LT2 Δ <i>cheV</i> Δ <i>cheR</i> Δ <i>cheB</i> | | | This work |
| TSS507 | LT2 Δ <i>cheR</i> Δ <i>cheB</i> Δ <i>cheY</i> Δ <i>cheZ</i> | | | This work |
| TSS520 | LT2 Δ <i>cheV</i> Δ <i>cheR</i> Δ <i>cheB</i> Δ <i>cheY</i> Δ <i>cheZ</i> | | | This work |
| 14028 | wild type <i>S. typhimurium</i> ATCC strain 14028 | | | R.M. Harshey |
| SM162 | 14028 Δ <i>tar</i> Δ <i>tsr</i> Δ <i>tcp</i> Δ <i>trg</i> Δ <i>aer</i> Δ <i>mcpB</i> Δ <i>mcpC</i> | | | R.M. Harshey |
| RP437 | <i>Escherichia coli</i> wild type for chemotaxis | | | ¹⁹⁵ |
| VS149 | <i>E. coli</i> RP437 Δ <i>cheR</i> Δ <i>cheB</i> Δ <i>cheY</i> Δ <i>cheZ</i> | | | ²⁴⁰ |
| VS180 | <i>E. coli</i> RP437 Δ <i>cheW</i> Δ <i>cheY</i> Δ <i>cheZ</i> | | | ²³⁷ |
| Plasmid | Gene(s) | Resistance | Induction | Source |
| pVS88 | <i>cheZ-eyfp</i> / <i>cheY-eyfp</i> | ampicillin | IPTG | ²⁴⁰ |
| pVS102 | <i>eyfp-cheR</i> | chloramphenicol | <i>L</i> -arabinose | ¹¹⁹ |
| pBAD33 | cloning vector | chloramphenicol | <i>L</i> -arabinose | ⁹⁶ |
| pTrc99A | cloning vector | ampicillin | IPTG | ¹³ |
| pML13 | <i>cheV</i> | chloramphenicol | <i>L</i> -arabinose | This work |
| pML14 | <i>cheV</i> _{D250A} | chloramphenicol | <i>L</i> -arabinose | This work |
| pML16 | <i>cheV-eyfp</i> | ampicillin | IPTG | This work |
| pML17 | <i>cheV</i> _{D250A-eyfp} | ampicillin | IPTG | This work |

Table 5.1. Strains and plasmids used in this work.

Chapter 5

Soft-agar plate assays

Bacteria were grown overnight to saturation in tryptone broth (TB, 1% Bacto tryptone, 0.5 % sodium chloride, pH 7.0). Soft-agar (motility) plates were prepared using 25 ml TB per plate with appropriate antibiotics and inducers (Table 5.1), and solidified with 0.26% agar. Plates were left to cool down for ~2 h and 5 μ l of the tested cultures were inoculated in the plates. Plates were then incubated at 30° C (the durations of the incubations are specified in the legend of Figure 5.2), and imaged using a custom-made dark-field imaging system with a Nikon camera.

Fluorescence microscopy and image analysis

Bacteria were grown at 33.5° C to a mid-exponential phase ($OD_{600} \sim 0.5$) in TB, supplemented with appropriate antibiotics and inducers (Table 5.1). Bacteria were harvested by centrifugation, washed and resuspended twice in motility buffer (10 mM potassium phosphate buffer pH 7.0, 0.1 mM EDTA, 1 μ M L-methionine, 10 mM lactic acid, pH 7.0), and stored at 4° C 1-5 h prior to the experiment.

Bacteria were immobilized on a poly-lysine coated coverslip. The bacterial density was controlled such as individual cells can be imaged and segmented by the image analysis program. The coverslip was attached to a tunnel slide, and subsequently imaging was performed on an inverted microscope (Nikon Eclipse), equipped with oil-immersion objective (100x). For all images, additional 1.5x magnification was used. For CheV imaging experiments, an extra magnifier (4x) was also used. For fluorescence imaging, cells were excited using 515 nm laser with 50 ms exposure time.

The cluster numbers and distributions were obtained using MATLAB. After background correction, cells were segmented using morphological operations from Imaging Toolbox (MATLAB). Clusters were defined based on their intensity (at least three standard deviations greater than the mean) and size. Clusters were separated to polar and lateral in the following manner. First, the longer diameter of each cell was determined. Clusters, which projection was within the distance between the poles and

CheV affects chemoreceptor clustering in *Salmonella typhimurium*

1/3 of the longer diameter were defined as polar. The rest of the clusters were defined as lateral.

Fluorescence resonance energy transfer (FRET) experiments and data analysis

Bacteria, expressing the FRET donor-acceptor pair CheZ-CFP / CheY-YFP, were prepared in the same way as for the fluorescence imaging experiments. *In vivo* FRET microscopy on live bacterial populations was performed as described previously²⁴². This FRET assay provides a real-time readout of the kinase (CheA) activity, because it measures the concentration of the complex between the phosphorylated CheY and the phosphatase CheZ, and in steady state the activity of the phosphatase and the kinase are equal.

Bacteria, were immobilized on a poly-*L*-lysine-coated microscope coverslip, attached to the top surface of a flow cell²⁷, and kept under constant flow of motility buffer, generated by a syringe pump (Harvard Apparatus, PHD2000). Chemoeffectors were added and removed by using a fluidic switch (Hamilton, valve HV 3-2) that could rapidly select between input flow channels with different concentrations of chemoeffectors. There is a nearly constant delay of ~25 s between the time in which the change of solutions is induced by switching the valve (indicated as time 0 in the figures) and the time, when the new solution reaches the bacteria at the flow cell.

FRET microscopy on bacterial populations was performed on an upright microscope (Nikon FN1), equipped with an oil immersion objective (Nikon CFI Plan Fluor, 40x/1.3). The bacteria in the flow cell were illuminated by a metal halide arc lamp with closed-loop feedback (EXFO X-Cite *exacte*) through an excitation bandpass filter (Semrock, FF01-438/24-25) and a dichroic mirror (Semrock, FF458-Di01). The epifluorescent emission was split by a second dichroic mirror (Semrock, FF509-FDi01) into donor (cyan, C) and acceptor (yellow, Y) channels. The signals from the C and Y channels, passed through emission bandpass filters Semrock FF01-483/32 and FF01-542/27 respectively, were collected by photon-counting photomultipliers (Hamamatsu H7422P-40). Signal intensities were recorded

Chapter 5

through a data acquisition card (National Instruments) installed on a PC, running custom-written software.

The ratio R between the coverslip background-corrected Y and C fluorescence signal intensities: $R = Y/C$, provided an indicator of FRET activity, robust to fluctuations in the light intensity. The change in FRET activity upon stimulation, $\Delta FRET$, can be expressed as a function of the change in the ratio ΔR ,

$$\Delta FRET = \frac{R_{pre} + \Delta R - R_0}{R_{pre} + \Delta R + |\Delta Y/\Delta C|} - \frac{R_{pre} - R_0}{R_{pre} + |\Delta Y/\Delta C|}$$

where R_{pre} is the pre-stimulus acceptor to donor ratio, $\Delta R = R - R_{pre}$ is the ratio change, R_0 is the acceptor to donor ratio in absence of FRET, and $|\Delta Y/\Delta C|$ is the constant absolute ratio between the changes in the acceptor and donor signals per FRET pair, $|\Delta Y/\Delta C| \approx 0.6$ ²⁴². Under the measurement conditions $R_{pre} + |\Delta Y/\Delta C| \gg \Delta R$; thus $\Delta FRET \sim \Delta R$. $\Delta FRET$ is thus expressed in arbitrary units of ΔR .

5.8. Acknowledgements

Dr Sophie Roth provided help with development of image analysis code. Ilja Serjak, Marco Konijnenburg and Marco Seynen developed the dark-field imaging system.

Chapter 6

Concluding remarks and outlook

We have implemented experiments at the level of signaling and behavior to investigate the design and implementation of one of the simplest signaling circuits in nature: the chemotactic signaling system of enteric bacteria. We demonstrated the fold-change detection property of bacterial chemotaxis, systematically compared the transfer functions of chemotactic signaling and behavioral response in linear gradients of *Escherichia coli* and *Salmonella typhimurium*, and identified and characterized the opposite responses to the cystine / cysteine redox pair of *S. typhimurium*. We explored the function of the phosphorylatable scaffolding protein CheV in *S. typhimurium*, and the phosphorylation-dependent feedback on CheB in *E. coli*. Here we summarize the main findings of this thesis, comment on further questions that have been identified, and discuss experimental approaches and technological developments and that could help answer these questions. We discuss possible future studies based on our findings and potential applications of the research.

6.1. Fold-change detection in biological sensory systems

Living organisms have evolved sensory systems that allow them to detect changes in their surroundings. Arguably the best-studied bacterial sensory system is the chemotaxis circuit of *E. coli*, which shares common features with other more complex sensory systems. Among these features is the ability to adapt precisely, *i.e.* after a change in the input to a new constant level, the output gradually returns to the pre-stimulus level. Another feature of adaptive sensory systems, well-known in physiology, is that the responses follow Weber's law ²⁴⁷, $\Delta r(s, s_0) = k\Delta s/s_0$, *i.e.* the magnitude of the instantaneous response, Δr , following a small step change in input, Δs , scales proportionately to the ratio of the input change to the background input level, s_0 . The proportionality constant k is called the Weber-Fechner constant.

A more general type of adaptive response rescaling that has been recently described theoretically is fold-change detection (FCD) ²³¹: the entire shape of the response, including its amplitude and duration, depends only on fold-changes in the input and not on its absolute levels, *i.e.* $\Delta r(s(t), s_0) = \Delta r(\gamma s(t), \gamma s_0)$, where γ is constant. In Chapter 2, we provided the first experimental demonstration that FCD holds in a biological sensory system: the chemotaxis circuit of *E. coli* ¹³⁷ (Figure 6.1). Using *in vivo* FRET and microfluidics respectively, we showed that for the attractant α -methyl-aspartate (MeAsp) the FCD property holds in two adjacent but distinct regimes, both at the level of signaling and behavior. More recently, a study ¹⁵⁸ that utilized a noninvasive inference of the chemotactic response function of bacteria by analyzing bacterial trajectories in chemoeffector gradients provided further evidence that the FCD property holds over > 3 orders of magnitude for both MeAsp and glucose.

In Chapter 3, we demonstrated that FCD also holds in the MeAsp response of the closely related species *S. typhimurium*. However, the ranges over which FCD holds, are different between the two species, and we showed that the difference is determined by the sensitivity modulation profile $\psi([L]_0) \equiv \left. \frac{\partial f_t}{\partial \ln[L]} \right|_{[L]=[L]_0}$ of the kinase response. The interspecies comparison between FCD properties of *E. coli* and *S. typhimurium* could

serve as a starting point for further studies of the evolution of the FCD property in enteric bacteria, as discussed in section 6.2.

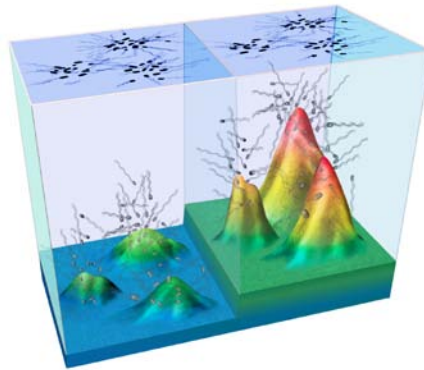


Figure 6.1. Artist representation of bacteria, executing FCD type of chemotaxis response. The nutrient gradients (represented as colored landscapes) are rescaled by the same factor as the background concentration of nutrients, to which the bacteria have been adapted. Image has been created by Gorick G, Bellomo D, Shimizu TS and Stocker R.

Sensory systems could detect multiple types of inputs; in the case of the bacterial chemotaxis system, it can detect multiple chemoeffectors, either by the same or different chemoreceptors (see examples in Table 3.1, Chapter 3). Recently, Uri Alon and colleagues have developed mathematical models to analyze how FCD-type sensory systems respond to multiple input signals⁹⁸. Alon et al. find that if both input signals bind the same receptor independently, the integrated response is multiplicative, *i.e.* the response dynamics depends only on the product of the fold changes in the two inputs.

We can test this prediction experimentally for bacterial chemotaxis by providing cells with two simultaneously varying input signals and using fluorescence resonance energy transfer (FRET) measurements of the type described in Chapter 2. The challenge in this experimental study will be to select a chemoreceptor that can bind independently two chemoeffectors. One candidate is the Tar chemoreceptor of *E. coli* that senses the attractants aspartate, cysteine and maltose, and repellents Co^{2+} and Ni^{+} ^{170,180}. However, binding of some of these ligands (e.g. aspartate and

Chapter 6

cysteine) is not independent¹⁷⁰. Also some of the ligands (maltose, Ni⁺)^{65,155} are first bound to periplasmic binding proteins, and the formed complexes are detected by the chemoreceptors, which might complicate the analysis of the experimental results. Another strategy to test FCD to multiple simultaneous inputs could be to express in *E. coli* McpS: a heterologous chemoreceptor from *Pseudomonas putida* KT2440, which has two binding sites that has been recently characterized¹⁹⁶. The membrane-proximal site of McpS binds malate and succinate, whereas its membrane-distal site binds acetate¹⁹⁶. Heterologous expression of McpS in *E. coli* would provide the possibility to utilize the existing knowledge for the chemotaxis signaling pathway of *E. coli* and characterize the properties of the *P. putida* chemoreceptor. A challenge in these experiments will be to work with acetate, which is a membrane-permeable acid⁶⁴ that could perturb the intracellular pH of the cells, affecting bacterial metabolism³⁷. Exploring other microorganisms and chemoreceptor types could provide numerous opportunities for studying FCD to single or multiple inputs.

6.2. Quantitative comparative physiology of microorganisms

The molecular composition and topologies of the chemotactic signaling networks demonstrate diversity across bacteria²⁸¹: even between *E. coli* strains, there are differences in the chemoreceptor species composition¹³³. In Chapter 3, we performed a FRET-based comparative physiology study of the transfer functions of chemotactic signaling of the two closely related species *E. coli* and *S. typhimurium*. Using FRET measurements with time-varying inputs, we showed that the parameters of receptor and adaptation transfer functions differ between the two species: *S. typhimurium* has three-fold less cooperative response to MeAsp, but the dynamic range of the MeAsp response is ten-fold broader; the adaptation in *S. typhimurium* is three-fold faster. Evaluating the response at different background concentrations of the attractant MeAsp revealed that the sensitivity modulation profile $\psi([L]_0)$, which determines both the drift velocity in steady spatial gradients of attractant and the changes of the kinase activity of chemotactic signaling response differ between the two species (Figures 3.7 and 3.8, Chapter 3).

Concluding remarks and outlook

How the observed differences in the chemotactic signaling and behavior of *S. typhimurium* and *E. coli* will affect the fitness of the bacteria in microniches in which these species coexist? Competition experiments within the same microfluidics platform could provide insights on this question. The two species can be transformed with plasmids that express fluorescent proteins of different colors. Careful selection of spectrally separated fluorescence proteins and optimization of the expression levels will allow distinguishing the bacteria from the two species in a mixed suspension. Bacterial cultures from the two species mixed into defined ratios can be injected in the test channel of a microfluidic device, e.g. of the type shown on Figure 3.7A (Chapter 3) and the distributions of the bacteria can be subsequently recorded using a fluorescence microscopy and high-speed camera. This setup will be useful for distinguishing for subtle differences in behavioral performance that are hard to detect in separate experiments with individual populations. Moreover such competition experiments might allow identification of interspecies interactions affecting the behavioral performance of bacteria.

Recent theoretical studies^{114,232} have shown that the drift velocity v_D depends linearly on the gradient of the logarithmic concentration of ligand, $G = d \ln[L]/dx$, before it saturates when G exceeds a critical value G_C (Figure 6.2)¹¹⁴. For $G < G_C$, $v_D \approx CG$; the constant $C \propto v^2 \tau$, where v is the average run speed and τ is the average run time. G_C is determined by the linear rate constant of receptor methylation $K_R (= F'(a_0)/2$ in the model of reference²⁶⁰), rotational Brownian motion, or both²³². C has been shown to be roughly independent of K_R . The saturating (maximal) drift velocity v_D^{\max} at $G \geq G_C$ is also determined by K_R : $v_D^{\max} \propto K_R^{1/2}$. The methylation rate for *E. coli* was estimated to be $K_R = 0.005 \text{ s}^{-1}$ ²²⁶, and in Chapter 3 we found that *S. typhimurium* adapts three-fold faster, i.e. $K_R = 0.015 \text{ s}^{-1}$, and the average time to reach steady state of the chemotactic migration coefficient (CMC)¹⁵⁶ is also three-fold shorter in *S. typhimurium*. The dependence of the steady-state v_D on the mean concentration of the gradient $[L]_0$, to which the bacteria were pre-adapted (Figure 3.7, Chapter 3), suggests that the gradients that we used for these experiments are less steep or comparable to G_C for both species (similar to gradient G^I on Figure 6.2). In the future, single-population or competition experiments could be used to explore

Chapter 6

different gradients selected such that the steepness is larger than the G_c of one or both species so the maximal drift velocity that the two species can reach depends on their adaptation rates (similar to gradient G^{II} on Figure 6.2). Comparing the behavioral performance under controlled conditions could elucidate the ecological significance of the observed differences in the parameters of chemotactic signaling response and behavior.

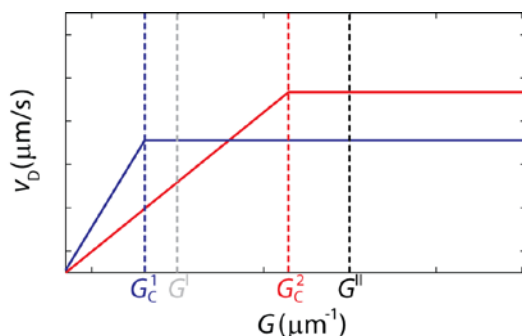


Figure 6.2. Schematic illustration of the dependence of the drift velocity v_D on the gradient of logarithmic concentration of ligand G . Blue and red curves represent two bacterial populations with different values of the critical gradient G_c (G_c^1 and G_c^2 respectively). G^I and G^{II} represent hypothetical gradients to which bacteria are exposed (see text).

In Appendix B, we discuss preliminary experiments on the ECOR collection of natural *E. coli* isolates representing much of the current genetic diversity of the species^{189,275}. We found that the chemotactic performance in self-created nutrient gradients in soft-agar plates significantly differs between ECOR strains. We identified a subset of strains that have contrasting properties of their chemotactic performance and swimming speed (Table B.2, Appendix B). We have also engineered genetically most of these strains such that they can be used for experiments using our *in vivo* FRET system²⁴² for measuring the chemotactic signaling response. Future FRET-based comparative physiology studies of the chemotactic signaling transfer functions of the selected ECOR strains, similar to the interspecies comparison that we described in Chapter 3, might allow identification of parameters that are conserved or have diverged in the recent evolution of *E. coli*, and reveal whether different properties of chemotactic signaling such as perfect adaptation, Weber's law or FCD are conserved. Strains in

Concluding remarks and outlook

which one or more of these properties are not conserved could be subjected to further behavioral tests using microfluidics⁸, and compared for their fitness (chemotactic performance) under defined gradients.

Figure 6.3 illustrates the first FRET results that we have obtained for an ECOR strain, ECOR51. This strain was selected because it belongs to a phylogenetic group B2, which is distant from group A to which *E. coli* K12 (used as a model strain for the majority of the current studies of chemotaxis) belongs (see Figure B.3, Appendix B). Interestingly, the cooperativity of the response to MeAsp of ECOR51 is three-fold lower than that of *E. coli* K12 (Figure 6.3A). The dissociation constant of the active receptors²⁶⁰ of ECOR51 appears to be ~10-fold lower than that of *E. coli* K12, however this parameter is not well constrained by our current results; further experiments with higher background concentrations $[L]_0$ would be necessary to confirm this conclusion (Figure 6.3A). The frequency response of ECOR51 at $[L]_0 = 0.229$ mM MeAsp, however, is identical to that of *E. coli* K12 (Figure 6.3B), suggesting that the system-level adaptation properties of the two strains are the same (see Chapter 3).

We have also found that the sensitivity modulation profile $\psi([L]_0)$ of ECOR51 to exponential sinewave inputs has a shape of a single broad peak (see Figure 6.3C), indicating the existence of a single FCD regime in this strain over the range $[L]_0 = (0.018-0.229)$ mM MeAsp. The main MeAsp receptor, Tar, of ECOR51 has only two residues different from that of wild type *E. coli* K12: Y131H and A184V, both in the cytoplasmic region¹⁸⁹. The different shape of the sensitivity modulation profile of ECOR51 suggests that it is likely that the properties of its chemoreceptor population differ from that of wild type *E. coli*.

Further experiments of this type with this and other ECOR strains could start a comparative physiology study that would provide an opportunity to study the design principles involved in evolutionary optimization of chemotaxis system, generating phenotypic variability while preserving the important functional features of this system.

Chapter 6

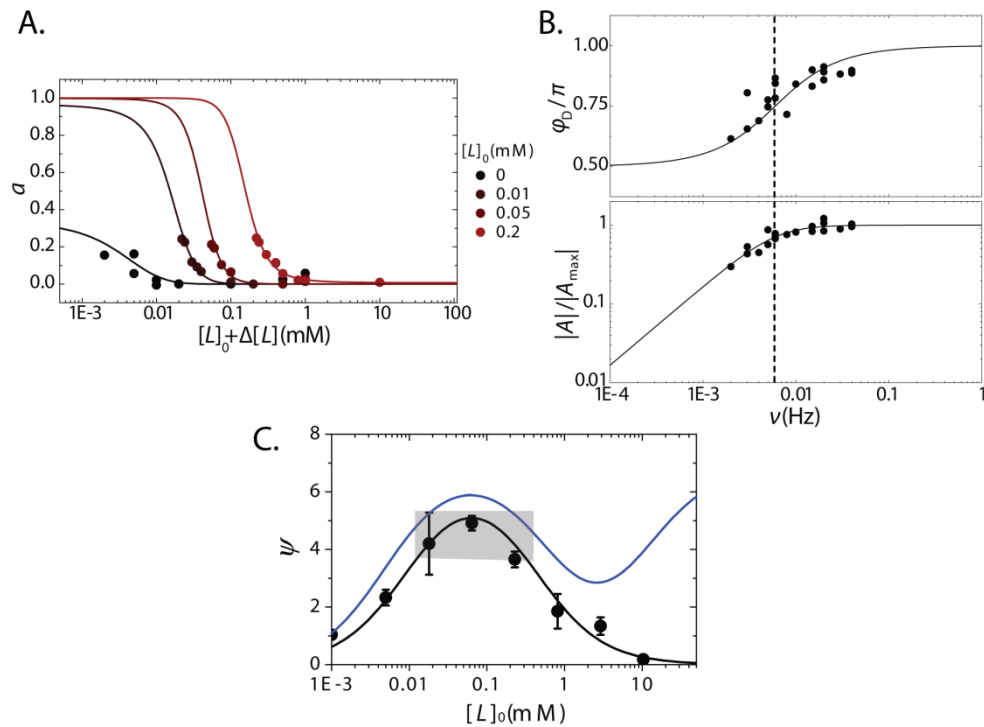


Figure 6.3. Kinase response of ECOR51. (A) Dose-response data of the kinase activity (a) to steps of MeAsp, applied to ECOR51 cells, adapted at different background concentrations of MeAsp, $[L]_0$. Fits using the MWC model²⁶⁰ are shown with parameters $N = 2$, $K_I = 0.018$ mM and $K_A = 0.239$ mM. (B) Bode plot for ECOR51, showing the phase delay (top) and the normalized amplitudes (bottom) of the output sinusoids as a function of the driving frequency ν (see Chapter 3). The characteristic frequency for ECOR51 chemotactic signaling response ($\nu_m = 0.006$ Hz) is indicated with a dashed line. (C) Sensitivity modulation profile $\psi([L]_0)$ for ECOR51 in response to inputs of the type shown on Figure 3.8A (the fitted parameters are $N = 7$, $K_I = 0.01$ mM and $K_A = 0.4$ mM, see Chapter 3). $\psi([L]_0)$ for wild type *E. coli* (blue) is shown for comparison (see Chapter 3). The plateau of invariant responses of ECOR51 is indicated by the shaded rectangle. Error bars represent standard deviation from 2-5 repeats.

6.3. Opposite responses to a redox pair

We discovered a redox pair, cystine / cysteine, which elicited chemotactic signaling responses of opposite signs in *S. typhimurium*. The reduced form, cysteine, is sensed as an attractant, and the response is Tsr / Tar-dependent¹³⁸ (Chapter 4, Appendix A). The oxidized form, cystine, elicits a repellent response over a broad concentration range (20 nM – 500 μ M), and the amplitude of the response scales linearly with the logarithm of cystine concentration over more than four orders of magnitude, which is not typical for a response that is based on receptor-ligand interactions (Appendix A). In Chapter 4, we showed that deletion of *mcpB* and *mcpC* genes in *S. typhimurium* 14028 abolishes the repellent response to cystine, indicating that McpB and McpC are involved in cystine sensing¹³⁸. However, Δ *mcpB* Δ *mcpC* *S. typhimurium* LT2 is able to sense cystine even at nanomolar concentrations, suggesting that in this strain there is also an McpB / C-independent pathway of cystine response. The strain-based differences of *S. typhimurium*'s response to cystine could be a subject of further investigations.

Based on the similarity of the time series and the dose-dependent response to cystine and another oxidized compound, benzoquinone, as well as the observation that the response to cystine-cysteine mixtures can have either a positive or a negative sign, depending on the redox potential of the mixtures, we hypothesized that the chemotaxis responses to cystine / cysteine pair are likely to be mediated by a redox-dependent pathway (Appendix A). Cystine / cysteine redox gradients are likely to be formed in nature in the presence of oxidizing agents¹⁴². Oxidative environments generate reactive oxygen species, which are responsible for damage to all macromolecules (DNA, lipids and proteins)²⁰⁵. Thus, redox-sensing mechanisms that allow the bacteria to sense and avoid oxidative conditions might facilitate *S. typhimurium* survival.

We sought to understand how the observed modes for cystine and cysteine sensing aid *S. typhimurium* to orient in gradients, formed by cystine / cysteine redox pair. We performed pilot experiments using the microfluidics platform⁷, described in Chapter 3 (see Figure 3.7A). By injecting cystine / cysteine in the flanking channels of the platform (source

Chapter 6

and sink channels), we created spatial gradients of cystine and cysteine. Using a video microscopy, we recorded the time evolution of the distribution of *S. typhimurium* populations within the test channel. To estimate the strength of the chemotactic response, we computed the chemotaxis migration coefficient (CMC), which represents the mean displacement of the population from the center of the test channel ¹⁵⁶, *i.e.* $CMC(t) \equiv (\langle x \rangle(t) - W/2)/(W/2)$, where W is the width of the test channel, and $\langle x \rangle(t)$ is the mean position of the bacterial population along the gradient. Negative CMC indicates a displacement of the population towards the sink channel, and positive CMC : displacement of the population towards the source channel.

Although bacteria accumulate towards increasing concentrations of cysteine in cysteine gradients, as expected from the attractant response observed in the FRET experiments, no response is observed for populations of *S. typhimurium* placed in a gradient of cystine (Figure 6.4A). However, when the cysteine and cystine were mixed together and used to create a gradient by injecting the mixture in the source channel and flowing only motility buffer through the sink channel, *S. typhimurium* populations moved in opposite directions depending on the cystine / cysteine ratio. When we injected a mixture of 10 mM cysteine and 0.5 mM cystine in the source channel, the bacteria moved towards the source, *i.e.* showed an attractant response to the mixture (Figure 6.4B). On the contrary, when we injected a mixture of 10 mM cysteine and 1 mM cystine in the source channel, the bacteria moved away from the source channel, *i.e.* showed a repellent response to the mixture (Figure 6.4B). Moreover, if we inject cysteine and cystine in the opposing flanking channels (source and sink respectively), the attractant response is stronger than that elicited by a gradient formed by the same concentration of cysteine in the source channel versus a motility buffer only in the sink channel (Figure 6.4).

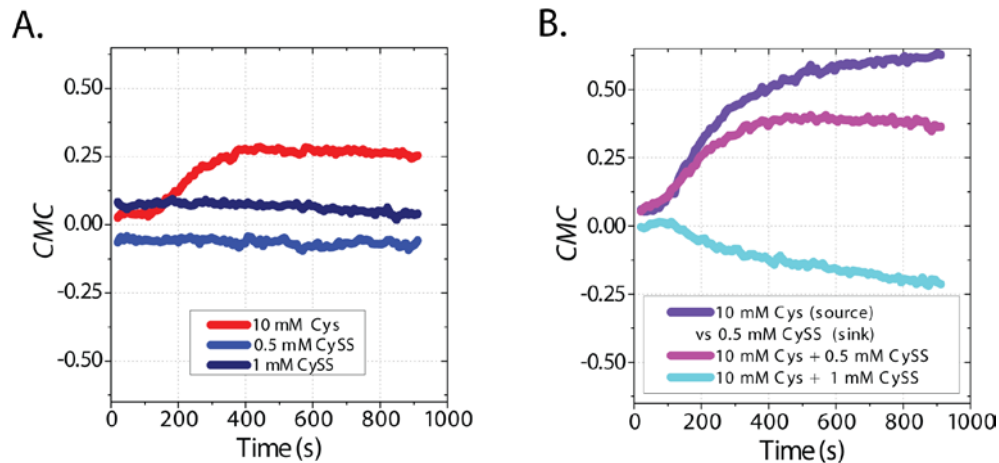


Figure 6.4. Response of *S. typhimurium* LT2 to spatial gradients of the cystine / cysteine redox pair. Steady linear gradients were created in microfluidic platforms with parallel source, test and sink channels (see Figure 3.7A). **(A)** 10 mM cysteine, 0.5 mM cystine or 1 mM cystine was injected in the source channel. Only motility buffer was flown through the test channel. For each of the three gradients, CMC of wild type *S. typhimurium*, injected in the test channel, is shown. **(B)** Mixtures of 10 mM cysteine and 0.5 mM or 1 mM cystine were injected in the source channel, whereas only motility buffer was flown through the test channel. The third gradient (purple) was created by flowing 10 mM cysteine in the test channel and 0.5 mM cystine in the sink channel. For each of the three gradients, CMC of wild type *S. typhimurium*, injected in the test channel, is shown.

These preliminary experiments with cystine / cysteine spatial gradients demonstrate that these compounds invoke a motile chemotactic response under certain conditions. Whether this response is dominated by the redox conditions or cysteine concentration, the reason for the lack of response to cystine-only gradients, and how cystine affects the response to cysteine gradients could be a subject of further investigations. Further experiments probing the response of receptor-mutant *S. typhimurium* strains in cystine / cysteine gradients could also be used to address the contribution of the individual receptors to the cystine / cysteine response.

Cystine / cysteine responses could be relevant for survival and spreading of the pathogen *S. typhimurium* in the host. Although little is

Chapter 6

known about the habitat of the enteric bacteria in the gut, it is unlikely that steady amino acid / redox gradients are formed in the lumen. However, close to the wall of the intestine, there is a mucus layer, consisting of glycoprotein (mucin), proteins, carbohydrates and lipids ^{59,253}. The composition and rapid turnover of the mucus suggests the formation of amino acid / peptide gradients. The role of the mucus layer in protecting the underlying epithelial cells from contact with the luminal gut bacteria is largely unknown ⁶⁰.

We hypothesize that chemotaxis response to cystine / cysteine might guide bacteria through the mucus layer towards the epithelial layer, facilitating systemic infections. Some of the mucins are cysteine rich, and cysteines get crosslinked by disulfide bridges, giving the gel structure of the mucus layer, which prevents bacteria from entering the layer ¹²⁵. Defects in the crosslinking of the mucus, e.g created by locally reducing conditions, might provide a path for systemic invasion of the bacteria. The opposite responses to the cystine / cysteine redox pair might improve the ability of the pathogenic *S. typhimurium* strains to find such crosslinking defects in the structure of the mucus layer, and facilitate systemic infections ¹⁴⁵.

6.4. Phosphorylation-dependent feedbacks in bacterial chemotaxis

The activity of the methylesterase enzyme CheB of *E. coli* is feedback-regulated via phosphorylation by the kinase CheA on its regulatory (REC) domain: the phosphorylation induces a conformational change in the REC domain, which activates the methylesterase activity of CheB ⁶⁹, which in turn enhances the deactivation of the receptor-kinase complexes ¹⁵. In Appendix C, we probed whether the sharp transition of the methylation-dependent feedback transfer function $F(a)$ at high values of a is a consequence of the phosphorylation feedback on CheB activity. We used *E. coli* mutants that cannot be phosphorylated because the REC domain of CheB is knocked out or the phosphorylation site of CheB is disrupted. The shape of $F(a)$ in the mutant strains, lacking the REC domain and having a steady-state kinase activity >0.40 , followed Michaelis-Menten kinetics, suggesting that the phospho-regulation of CheB activity might cause the sharp decrease of $F(a)$ in wild type cells (Figure C.2, Appendix C).

Concluding remarks and outlook

Another phosphorylation-dependent feedback might exist in the chemotaxis system of *S. typhimurium*, which has a scaffolding protein CheV that contains a REC domain¹⁰. Our experiments with methylation deficient *S. typhimurium* suggested that a partial methylation-dependent adaptation to MeAsp exist in CheV⁺ but not in CheV⁻ cells (Chapter 5), and this adaptation might be phosphorylation-dependent: CheV mutant with genetically disrupted phosphorylation site does not complement the defect of $\Delta cheV$ methylation-deficient cells. Furthermore, using a fluorescent marker for the chemoreceptor clusters (YFP-CheR) we revealed that the number of lateral clusters decreases in CheV⁻ cells, suggesting that CheV plays role in chemoreceptor clustering (Chapter 4).

The role of CheV in *S. typhimurium* chemoreceptor clustering and adaptation could be investigated in future studies of bacteria with altered chemoreceptor species composition. These studies might reveal that only part of the chemoreceptor species in *S. typhimurium* are coupled to the kinase via CheV. Identification of chemoreceptors, which couple to CheA in CheV-dependent manner will facilitate further physiological studies of CheV function, using chemoeffectors that are sensed specifically by these chemoreceptors.

6.5. Acknowledgements

The microfluidics experiments with cystine / cysteine were performed in the lab of Prof. Dr. Roman Stocker (Massachusetts Institute of Technology).

Chapter 6

Appendix A

Multiple pathways of opposite chemotactic responses to the cystine / cysteine redox pair in *Salmonella typhimurium*

The chemotaxis system enables motile bacteria to search for an optimum level of environmental factors. Different chemoreceptor species in *Salmonella typhimurium* sense the amino acid cysteine as an attractant and its oxidized dimeric form cystine as a repellent. We investigated the dose-dependent response to cystine and cysteine of *S. typhimurium* using *in vivo* fluorescence resonance energy transfer measurements. Tsr / Tar-mediated response to cysteine has a sigmoidal shape, typical for receptor-ligand interactions. However, the magnitude of the repellent response to cystine scales linearly with the logarithm of cystine concentration over more than four orders of magnitude (20 nM – 500 μ M). In contrast to *S. typhimurium* 14028, where we previously observed no response in absence of the McpB / C chemoreceptors, McpB / C-independent responses exist in *S. typhimurium* LT2 even at the very low concentrations in the nanomolar range. We provide a plausible explanation of the linear dependence of the response on the logarithm of cystine concentrations, based on a McpB / C-independent redox-sensing pathway.

Appendix A

A.1. Introduction

Chemotaxis allows bacteria to navigate in gradients of physiologically relevant stimuli, e.g. moving towards higher concentration of nutrients ^{2,4}, lower concentration of toxins ⁷⁷, or an optimal value of pH ¹²³, oxygen ³¹, temperature ²¹⁰ or redox potential ²⁸. The chemoeffector stimuli are detected by transmembrane receptors, forming allosteric complexes associated with histidine kinase molecules via scaffolding proteins ^{243,266}. The chemotaxis signaling system has been thoroughly studied in the enteric bacteria *Escherichia coli* and *Salmonella typhimurium*. The receptor-associated kinase CheA's autophosphorylation activity is altered by binding of chemoeffectors to the chemoreceptor clusters. CheA transfers phosphoryl groups to the response regulator CheY, and phosphorylated CheY (CheY-P) interacts with the flagellar motors and alters their rotational bias. The phosphatase CheZ accelerates the dephosphorylation of CheY, and the activity of the receptor-kinase complex is feedback-regulated by a pair of enzymes, CheR and CheB, which add and remove, respectively, methyl groups to specific glutamyl residues of the chemoreceptors.

Chemoreceptors, also called methyl-accepting chemotaxis proteins (MCPs) ¹, form homodimers, which in turn assemble into allosteric arrays in the membrane ¹⁰². Chemoreceptor dimers interact at their distal cytoplasmic tips forming trimers of dimers ^{93,102}, which arrange into hexagonal arrays, responsible for the high sensitivity and cooperative nature of chemotaxis signaling ⁴³. Chemoeffector ligands reversibly bind to the periplasmic domains of the chemoreceptors either directly or via periplasmic binding proteins ¹⁸⁵. Chemoeffector binding induces a conformational change in the periplasmic domain, which is transmitted across the membrane through the regulatory HAMP domain ²⁹¹, the methyl-accepting domain, and the signal-output domain that regulates the activity of the kinase CheA. Five chemoreceptor species exist in *E. coli*, whereas nine chemoreceptor species exist in *S. typhimurium* (see Table 3.1, Chapter 3). A subset of these MCP species contains a conserved C-terminal pentapeptide motif (NWE^T/sF) that reversibly binds CheR and CheB, facilitating efficient methylation-dependent adaptation ¹⁴⁴. MCPs have different substrate specificities, with some responding to multiple

Opposite responses to the cystine / cysteine redox pair

chemoeffectors. Conversely, some chemoeffectors are sensed by multiple MCPs (see Table 3.1, Chapter 3). Some chemoreceptor species respond to stimuli via mechanisms other than ligand binding, e.g. Tar and Tsr sense temperature ²¹⁰. The relative abundance of each chemoreceptor species depends on the growth conditions and population density ^{210,284}.

The amino acid *L*-cysteine and its oxidized dimeric form *L*-cystine are chemoeffectors of opposing sign for *S. typhimurium* ¹³⁸ (see Chapter 4). The oxidized and reduced forms are also sensed by different subsets of chemoreceptors: in Chapter 4 ¹³⁸, we showed that the repellent response to the oxidized form (cystine, abbreviated as CySS) is mediated by McpB and McpC, and the attractant response to the reduced form (cysteine, abbreviated as Cys) is mediated by Tsr and Tar ^{103,138}. The relative mRNA levels of cystine-sensing receptors McpB and McpC fall between those of the high abundance receptor Tsr and low-abundance receptor Trg, and are similar to those of Tar ²⁶⁷. McpC does not contain the conserved C-terminal pentapeptide, whereas the C-terminal pentapeptide motif EWVSF in McpB conserves two key residues of the NWE^T/sF motif ²²⁸, and hence is likely to serve as a docking site for the methylation enzymes. The adaptive recovery upon cystine step stimulation has been shown to be incomplete, and the imperfect adaptation has been suggested to promote spreading in motility-plate chemotaxis assays ¹³⁸.

The opposite responses to cystine and cysteine might provide a mechanism for *S. typhimurium* to find optimal redox conditions and assist the escape of *S. typhimurium* from damage-inducing oxidative environments. Migration to optimal redox conditions, in contrast to movement towards increasing concentration of attractant or decreasing concentration of repellent, cannot be achieved by a monotonic response by a single receptor species, as recently demonstrated for pH taxis and thermotaxis in *E. coli* ^{210,284}. *E. coli* avoids both highly acidic and highly alkaline conditions by opposing responses of Tar and Tsr: increase of pH elicits an attractant response via Tsr and a repellent response via Tar, and the relative strength of the response is modulated by receptor methylation ^{122,131,235,259,284}. The sign of the net response is inverted at a well-defined value of pH, which is adjusted in response to changes in cell density. In the motile response to temperature gradients, the opposing responses of Tar

Appendix A

and Tsr lead to accumulation at a preferred point in a temperature gradient: Tsr is responsible for the attraction to warmth and Tar – for the attraction to cold ^{84,192,210}.

Here we investigate the dose-dependent response of *S. typhimurium* to the cystine / cysteine redox pair using *in vivo* fluorescence resonance energy transfer (FRET) measurements. The dose-dependent response to the reduced form, cysteine, is sigmoidal and Tsr / Tar-dependent. However, we show that the oxidized form is sensed by wild type *S. typhimurium* even at very low concentrations (10-20 nM), and the magnitude of the response scales linearly with the logarithm of cystine concentration over more than four orders of magnitude (20 nM – 500 μ M). Surprisingly, we detected McpB / C-independent responses to cystine in *S. typhimurium* LT2 strain even at the very low concentrations in the nanomolar range. We observed repellent response in the nanomolar concentration range for another oxidized compound, benzoquinone, and propose an explanation of the linear dependence of the response on the logarithm of cystine concentrations, based on a McpB / C-independent redox-sensing pathway.

A.2. Dose-response relation of the Tar / Tsr -mediated attractant response to cysteine

To characterize the chemotactic signaling response to the reduced form, cysteine, we applied sequential steps of cysteine with increasing concentrations to populations of *S. typhimurium* LT2 cells, immobilized in a flow cell. We measured the output of the chemotaxis system using a fluorescence resonance energy transfer (FRET) assay that utilizes a donor-acceptor pair between the phosphatase CheZ and the response regulator CheY, fused to yellow and cyan fluorescent proteins (YFP and CFP) respectively ^{226,240-242}. CheY phosphorylation by CheA and its dephosphorylation by CheZ have equal rates at steady state. Thus, the FRET efficiency is proportional to the concentration of the CheZ·CheY-P complex, and this FRET assay provides a measure of the kinase (CheA) activity on time scales longer than the relaxation time of the CheY phosphorylation cycle (~100 ms) ²⁴². A typical FRET response time series to cysteine is shown on Figure A.1A (cysteine is added and removed at times 0

Opposite responses to the cystine / cysteine redox pair

on the left and right panels respectively; note that it takes ~25 s for the cysteine solution to reach the cells after flipping the switch; see Materials and methods). The initial decrease of the FRET level upon addition of cysteine, indicates an attractant response, which is followed by a perfect adaptation to the prestimulus level (see Chapter 4)¹³⁸. Upon removal of cysteine, transient increase in the FRET level followed by a perfect adaptation is observed.

We applied steps of cysteine with increasing concentrations and measured the FRET response in order to characterize the dose-response relation for cysteine in wild type, Δtar , Δtsr , and $\Delta tar \Delta tsr$ *S. typhimurium* LT2 strains (Figure A.1B). The dose-response curve for cysteine in wild type *S. typhimurium* shows a sigmoidal shape, with a threshold < 20 μ M, half-maximum at ~40 μ M and saturation after ~100 μ M. Knocking out *tar* does not decrease the amplitude of the response (the slight increase in the amplitudes could be due to experiment-to-experiment variation). However, the amplitude of the saturating response is greatly diminished in the Δtsr strain, confirming that Tsr is the dominant receptor for cysteine at zero cysteine background.

The $\Delta tar \Delta tsr$ strain does not show an attractant response to cysteine for any of the tested concentrations. Instead, the FRET level increases upon stimulation by dissolved cysteine (Figure A.1B). A plausible explanation for this repellent-like response to cysteine of the $\Delta tar \Delta tsr$ cells is that under the aerobic conditions of our experiments, part of the cysteine oxidizes to cystine (see Section A.2). This effect is not noticeable in wild type cells, where the attractant response to cysteine dominates, but a response in the repellent direction is clearly observed in the cysteine-insensitive $\Delta tar \Delta tsr$ cells.

Appendix A

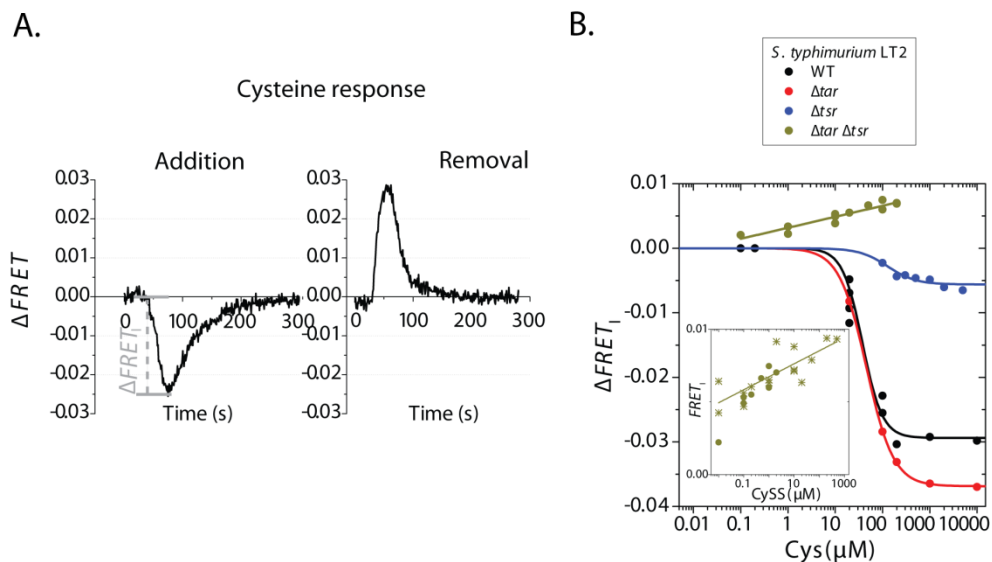


Figure A.1. Attractant response to cysteine of *S. typhimurium* LT2. (A) Typical time series of addition (left) and removal (right) of cysteine (100 μM) in WT *S. typhimurium*. Cysteine is added and removed at times 0 (B) Initial amplitudes of the FRET response ($\Delta FRET_i$) to cysteine of WT, Δtar , Δtsr , and $\Delta tar \Delta tsr$ strains are plotted as a function of the cysteine concentration. The respective Hill equation fits with half maximum of 38, 46, and 128 μM , and Hill coefficients of 2.1, 1.5, 1.5 are shown for the first three strains. An apparent linear fit with a slope of 0.017 is shown for the $\Delta tar \Delta tsr$ strain. Inset: Comparison of the measured response of the $\Delta tar \Delta tsr$ strain to cysteine (stars) and the expected response to cysteine upon stimulation with cysteine solutions in which 1% of the cysteine is oxidized to cystine.

A.3. The magnitude of the repellent response to cystine is proportional to the logarithm of cystine concentration

Cystine, the oxidized molecule in the cystine / cysteine redox pair, elicits a repellent kinase response in *S. typhimurium*: the FRET ratio transiently decreases, followed by a partial (imperfect) adaptation to the prestimulus level (Figure A.2A left) ¹³⁸. Upon removal of cystine, the FRET level returns to the prestimulus level in 200-300 s (Figure A.2A right).

We measured the initial amplitudes of the FRET response to a cystine step increase, $\Delta FRET_i$, and plotted them as a function of the added cystine concentration (Figure A.2B). We detected responses to cystine for concentrations as low as 20 nM. For the tested range, 20 nM – 500 μ M, the amplitude of the response scales linearly with the logarithm of cystine concentration. We have not explored the response to concentrations of cystine greater than 500 μ M because cystine solutions become acidic, and the low pH itself can elicit a chemotaxis response ²⁸⁴.

The shape of the dose-dependent response to cystine is atypical for receptor-ligand binding interactions, which are characterized by linear mass action kinetics or positively cooperative binding, i.e. Hill coefficients $n_H \geq 1$ ^{80,240,241,248}. Fits with a Hill equation of the cystine dose-response data give Hill coefficients $n_H = 0.50 \pm 0.15$ (these fits were not well constrained, explaining the large fitting error). The atypical shape of the dose-response curve could be a result of multiple receptors with different affinities binding cystine, leading to lower apparent cooperativity of the cystine response ¹⁹⁹. Alternatively, a mechanism that does not involve receptor binding might explain the observed dose-response dependence.

The repellent response to cysteine solutions of the cysteine-insensitive $\Delta tar \Delta tsr$ strain scales linearly with the logarithm of cysteine concentration, similar to response to cystine of *S. typhimurium*. The magnitude of the measured responses to cysteine solutions of the cysteine insensitive strain is very similar to the one to cystine solutions with 50-times lower concentration (see Figure A.1, *Inset*). Thus, we conclude that 1% of cysteine in our cysteine solutions might be oxidized to cystine under the aerobic conditions of our experiments (note that two cysteine molecules get oxidized to form one cystine molecule).

Appendix A

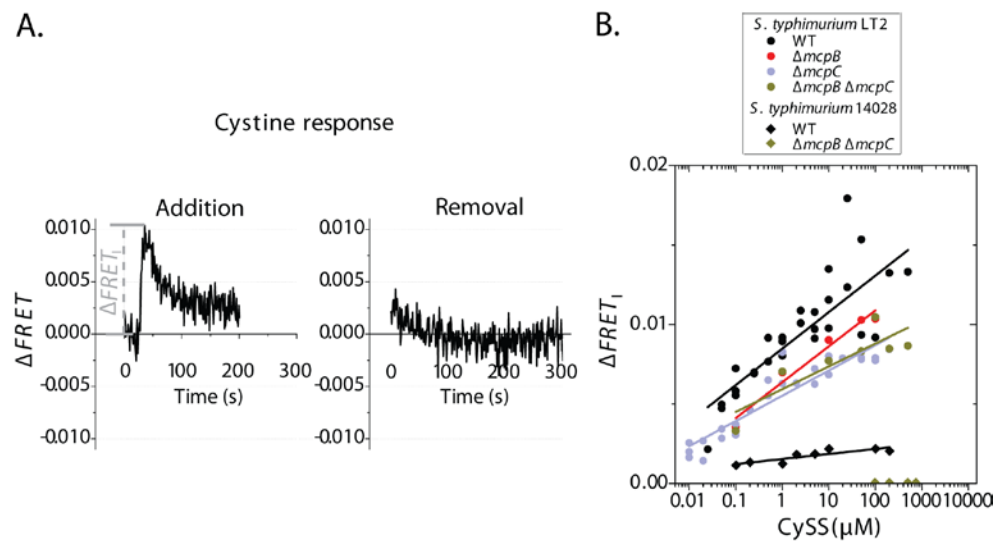


Figure A.2. Repellent response to cystine of *S. typhimurium*. (A) Typical time series of addition (*left*) and removal (*right*) of cystine (100 μM) in wild type (WT) *S. typhimurium* LT2. Cystine is added and removed at times 0. (B) Initial amplitudes of the FRET response (ΔFRET_i) of WT LT2, $\Delta mcpB$ LT2, $\Delta mcpC$ LT2, $\Delta mcpB \Delta mcpC$ LT2, WT 14028, and $\Delta mcpB \Delta mcpC$ 14028 strains are plotted as a function of the cystine concentration. The apparent linear fits for the first four strains have slopes of 0.0023, 0.0023, 0.0016, 0.0014, and 0.0006 respectively. $\Delta mcpB \Delta mcpC$ 14028 does not respond to cystine in the tested concentration range.

A.4. McpB / C knockouts do not affect the shape of cystine dose-response curve in *S. typhimurium* LT2

We showed previously¹³⁸ (Chapter 4) that two chemoreceptors of *S. typhimurium*, McpB and McpC, sense cystine as a repellent: deletion of both receptors in *S. typhimurium* 14028 completely abolished the repellent response to cystine (see Figure 4.5, Chapter 4). If there are two receptors that bind ligand independently with different affinities, the net response might be characterized with apparent negative cooperativity, *i.e.* Hill coefficient $n_H < 1$ ¹⁹⁹. The receptors with higher affinity ligand-binding sites will bind the ligand first, but as the concentration of ligand is increased, the receptors with lower affinity binding sites will also bind the ligand, producing an apparent $n_H < 1$. Thus, cystine binding to McpB and McpC with different affinities might explain the shape of the observed dose-response curve. To test this hypothesis, we measured the dependence of $\Delta FRET_i$ on the cystine concentration in $\Delta mcpB$, $\Delta mcpC$, and $\Delta mcpB \Delta mcpC$ *S. typhimurium* LT2 mutant strains. Unexpectedly, the thresholds of cystine response for all tested strains are < 100 nM, and a linear dependence of the amplitude of their response with the logarithm of cystine concentration is observed (Figure A.2B).

The responses of the $\Delta mcpB \Delta mcpC$ *S. typhimurium* LT2 strain to cystine contrasts with our previous finding that a $\Delta mcpB \Delta mcpC$ *S. typhimurium* 14028 strain does not respond to cystine¹³⁸ (Figure A.2B). This finding suggests that a McpB / C-independent mechanism of cystine sensing exists in *S. typhimurium* LT2, which might not exist in *S. typhimurium* 14028. We tested the response to cystine of wild type *S. typhimurium* 14028. Despite the fact that the amplitudes of the cystine response are smaller than those of LT2, we also observe in wild type 14028 a linear scaling of the response with the logarithm of cystine concentration (Figure A.1B). We also observed responses to cystine at concentrations below < 100 nM in both LT2 and 14028 wild type strains.

Unlabeled *cheY* and *cheZ* are present on the genome of the 14028 strains used in our studies, in addition to the *cheY-yfp* and *cheZ-cfp* genes on the plasmid for expression of the FRET pair, and competitive interactions of labeled and unlabeled CheY and CheZ might explain the smaller

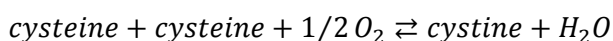
Appendix A

amplitudes of the response of the 14028 strains (see Figure 4.6, Chapter 4). Another explanation of the smaller amplitudes of the response of *S. typhimurium* 14028 might be different expression levels of some of the chemotaxis network components between LT2 and 14028 strains¹³⁸. Since the amplitudes of the FRET response of the 14028 strain are in general much smaller than those of the LT2 strain (Figure A.2B) we cannot exclude the possibility that there are small-amplitude responses in the $\Delta mcpB \Delta mcpC$ 14028 strain that we are unable to detect at the finite signal-to-noise ratio of these FRET experiments.

A.5. The response to another oxidized redox component, benzoquinone, is similar to the cystine response at low concentrations

The dose-response measurements in *S. typhimurium* LT2 *mcpB/C* knockout strains (Figure A.2) suggest the existence of an McpB/C-independent cystine-sensing mechanism in *S. typhimurium*, which magnitude scales linearly with the logarithm of cystine concentration over the whole tested range of concentrations (100 nm – 500 μ M for the $\Delta mcpB \Delta mcpC$ strain). The latter observation precludes mechanisms in which the response is dependent on ligand-binding to chemoreceptors by linear mass action kinetics or positively cooperative binding^{80,240,241,248}.

Cystine is a dimeric amino acid, formed by oxidation of the sulfhydryl (-SH) groups of two cysteine monomers, leading to the formation of a disulfide bridge (-S-S-) by a redox reaction



It has been shown previously that redox molecules, such as substituted quinones, elicited redox taxis responses: in a spatial redox gradient, bacteria migrate towards a preferred redox potential, and these responses depend mainly on the Aer receptor in *E. coli*^{28,202}. Under aerobic conditions, the oxidized forms in the tested quinone redox pairs were sensed as repellents²⁸. Our FRET experiments, which were also performed under aerobic conditions, confirmed the latter observation: the oxidized compound benzoquinone elicited a repellent response (note that the reduced form, hydroquinone, also elicited repellent responses, but only for concentrations $\geq 100 \mu$ M; because of its toxicity at high concentrations²⁵⁸ we

Opposite responses to the cystine / cysteine redox pair

have not explored the hydroquinone response further). Figure A.3A shows a typical time series of a response to benzoquinone. The response to benzoquinone is similar to the repellent response to cystine: both components elicit a repellent response upon a step addition (the FRET level increases), followed by an imperfect adaptation (Figure A.2A and A.3A). Moreover, responses to both compounds were detected at very low concentrations: 1 nM for benzoquinone and 10-20 nM for cystine, and the dose-response dependences for both cystine and benzoquinone appear to scale proportionately with the logarithm of the concentration over the tested range (Figures A.2B and A.3B). We were not able to test benzoquinone concentrations larger than 1 μM because the compound is toxic to the bacteria at high concentrations ²⁵⁸ and its optical activity interferes with the fluorescence levels of the FRET sensors.

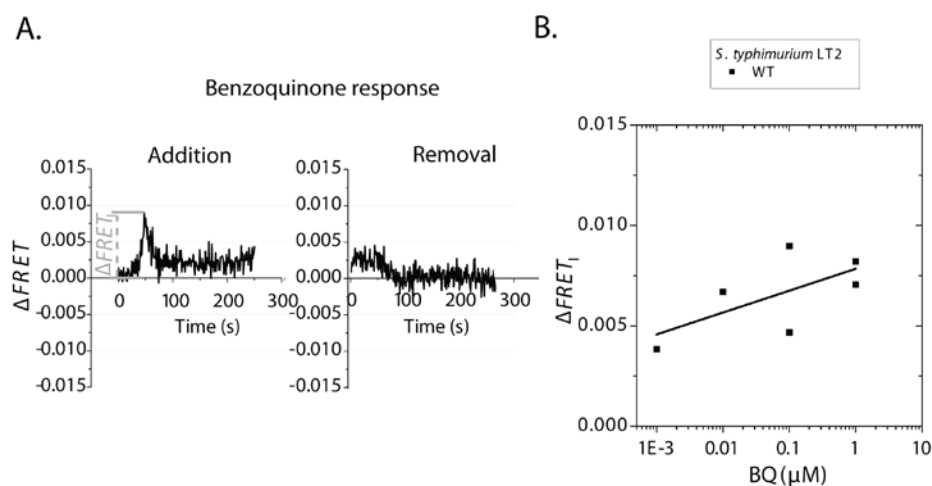


Figure A.3. Repellent response to benzoquinone of *S. typhimurium* LT2. (A) Typical time series of addition (left) and removal (right) of benzoquinone (0.1 μM) in WT *S. typhimurium* LT2. Benzoquinone is added and removed at times 0. **(B)** Initial amplitudes of the FRET response (ΔFRET_i) to benzoquinone of WT *S. typhimurium* are plotted as a function of the benzoquinone concentration. The apparent linear fit has a slope of 0.0011.

Appendix A

A.6. The sign of the response to mixed cystine / cysteine solutions depends on their redox potential

In order to evaluate the redox-dependence of the chemotactic response to cystine / cysteine redox pair, we probed the response of wild type *S. typhimurium* LT2 to defined mixtures of cysteine and cystine at different ratios. (We accounted for 1% interconversion of cysteine to cystine in all cysteine solutions; see Section A.2 and Figure A.1, *Inset*).

We plotted the initial amplitude of the FRET response, $\Delta FRET_i$, for each mixture against $\log Q$, where Q is the reaction quotient of Cys / CySS interconversion reaction, *i.e.* $Q = [CySS]/[Cys]^2$ (Figure A.4; cysteine concentration is squared because two molecules participate in each oxidation reaction). The values of $\log Q$ are proportional to the changes in the redox potentials of the cystine / cysteine solutions, which can be determined by the Nernst equation:

$$E_h = E_0 + 2.3 \frac{RT}{nF} \log Q,$$

where E_h is the redox potential of the solution, E_0 is the standard redox potential of the cystine / cysteine redox reaction, R is the gas constant, T is the absolute temperature, n is the number of moles of electrons transferred in the half redox reaction, F is the Faraday constant and Q is the reaction quotient of the redox reaction. For the cystine / cysteine redox pair under the conditions of our experiments (room temperature, neutral pH), the redox potential (V) is

$$E_h = -250 + 30 \log Q$$

For values of $\log Q < 100$ the FRET efficiency was found to decrease, indicating an attractant response. For values of $\log Q > 100$ the FRET efficiency was found to increase, indicating a repellent response. Thus, cystine / cysteine mixtures appear to elicit either an attractant or a repellent response depending on the value of $\log Q$, *i.e.* the redox potential of the solutions. Attractant response is observed for more reducing conditions, and repellent response is observed for more oxidizing conditions. Further experiments with defined cystine / cysteine mixtures with $\log Q$ within the range 10 – 1000 could be performed to confirm that the transition between attractant and repellent responses is redox-dependent.

Opposite responses to the cystine / cysteine redox pair

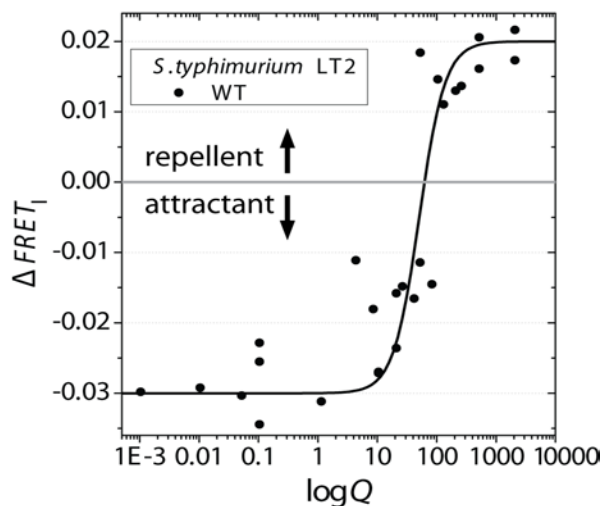


Figure A.4. Response of *S. typhimurium* to cystine / cysteine mixtures. Dependence of the initial amplitude of the FRET response, $\Delta FRET_i$, of wild type (WT) *S. typhimurium* LT2 to the redox potential, expressed in units of $\log Q$, where Q is the reaction quotient of Cys / CySS interconversion. A Hill equation fit (with Hill coefficient of 2 and half-maximum of 51) is shown for guidance of the eye. The grey line at 0 divides attractant (negative) and repellent (positive) responses.

A.7. Discussion

Motile bacteria often implement more than one pathway of sensing in order to orient in a gradient and find an optimal environmental niche. For example, thermotaxis and pH taxis responses both implement different receptors for sensing positive or negative changes from the optimal temperature and pH, respectively ^{210,284}. We found that the response of *S. typhimurium* to the cystine / cysteine redox pair is mediated by different pathways. Tsr / Tar sense the reduced form (cysteine) as an attractant (Figure A.1). Our earlier measurements of the FRET response of *S. typhimurium* 14028 strain showing that the response is abolished in $\Delta mcpB \Delta mcpC$ cells suggested that the cystine response is McpB / C-dependent ¹³⁸ (Chapter 4). However, our FRET measurements in

Appendix A

S. typhimurium LT2 showed that McpB / C-independent responses exist even at concentrations as low as 100 nM (Figure A.2B).

A plausible explanation for the observed discrepancy of the cystine response of $\Delta mcpB \Delta mcpC$ cells is that here and in Chapter 4¹³⁸ we used different *S. typhimurium* strains to evaluate the role of McpB / C in the cystine response: the commonly used lab strain LT2 and the ATCC strain 14028 respectively. LT2 and 14028 shared a common ancestor about 3000 to 9000 years ago, and the 14028 strain is more virulent^{89,112}. Their genomes are very similar (>98%) and the alignment of chemotaxis receptor nucleotide sequences show no difference between the two strains. However, it is possible that the McpB / C-independent pathway has different properties in the two strains: since its divergence, the highly virulent 14028 strain accumulated 10% more base substitutions (spread genome-wide, primarily in non-synonymous sites) compared to the virulence-attenuated LT2 strain¹¹². The apparent loss of the cystine response in the 14028 strain¹³⁸ but not in the LT2 strain upon deletion of both *mcpB* and *mcpC* might also be an artefact resulting from the finite signal-to-noise ratio of our FRET assay: the generally low amplitude of the FRET response of 14028 strains might render responses in the $\Delta mcpB \Delta mcpC$ 14028 strain indistinguishable from the noise floor of the FRET measurement.

The shape of the dose-response dependence of *S. typhimurium*'s response to cystine is atypical for receptor-ligand binding: the magnitude of the response scales linearly with the logarithm of the cystine concentration over a very broad concentration range (20 nM – 500 μ M). We propose that these responses are part of a redox-sensing pathway, based on our observations of similar responses to another oxidized compound, benzoquinone (Figure A.3). Redox-dependent inversion of the sign of the response to mixtures of cystine and cysteine (Figure A.4) further suggests that a redox-dependent cystine-sensing pathway might exist. However, the results shown on Figure A.4 should be complemented with further measurements of the response to cystine /cysteine mixtures with $\log(Q) = (10 - 1000)$ in order to confirm that the inversion of the response is caused by the redox potential of the mixtures.

The redox responses in *S. typhimurium* could be mediated by Aer as shown for *E. coli*²⁰², or other redox-sensing receptors might exist: there are

Opposite responses to the cystine / cysteine redox pair

five *S. typhimurium* chemoreceptors that do not exist in *E. coli* (McpB, McpC, Tcp, Tip and the cytosolic receptor McpA, where the function of McpA and Tip is unknown; see Table 3.1, Chapter 3).

What could be the physiological relevance of the multiple pathways of response to the cystine / cysteine redox pair in *S. typhimurium*? Redox potential is an environmental factor that strongly affects cellular metabolism, and it has been hypothesized that redox taxis could guide bacterial species to niches with optimal redox conditions for different metabolic processes, such as hydrogen utilization and nitrogen fixation²⁸. Moreover, highly oxidizing conditions lead to a production of free oxygen radicals and oxidative stress, *i.e.* damage to DNA, lipids and proteins²⁰⁵, and therefore can be detrimental for cells. Creating an oxidative microniche surrounding the macrophage cells is a strategy commonly used by the immune system of the host^{111,162}, and an active mechanism of avoiding such microenvironments could promote the survival of *S. typhimurium* in the host.

Detection of cysteine as an attractant could also be beneficial for the cells, as cystine is a sulphur-containing nutrient source, and participates in various metabolic pathways. Another advantage of having several pathways for cystine / cysteine sensing is that it could allow bacteria to adjust their “preference” to match the requirements of the cells, by changing the expression levels of some of the chemoreceptors, as observed *e.g.* for pH taxis and thermotaxis^{210,284}. Future studies of the behaviour of *S. typhimurium* in defined cystine / cysteine microenvironments (see Chapter 6) and animal models could shed light on the relevance cystine / cysteine sensing for *S. typhimurium* survival and pathogenesis.

A.8. Materials and methods

Bacterial strains, plasmids and growth conditions

All strains and plasmids used in this work are listed in Table A.1.

CheY-YFP and CheZ-CFP fusions for the FRET experiments were expressed from a plasmid pVS88²⁴⁰, induced with 150 μ M isopropyl β -D-1-thiogalactopyranoside (IPTG). In the strains used in FRET experiments,

Appendix A

except the strains from R. Harshey's lab (Table A.1), chromosomal *cheY* and *cheZ* were deleted, in order to prevent a competitive interaction between labelled CheY-YFP and CheZ-CFP, and unlabelled CheY and CheZ, expressed from the chromosome, which would lead to a smaller amplitude of the FRET response¹³⁸.

| Strain | Relevant genotype | | | Source |
|---------|--|------------|-----------|---|
| LT2 | <i>Salmonella enterica</i> serovar Typhimurium strain LT2 (wild type <i>S. typhimurium</i> LT2) | | | <i>Salmonella</i> Genetic Stock Center (SGSC) |
| TSS500 | LT2 $\Delta cheY \Delta cheZ$ | | | 138 |
| TSS878 | LT2 $\Delta tar \Delta cheY \Delta cheZ$ | | | 138 |
| TSS868 | LT2 $\Delta tsr \Delta cheY \Delta cheZ$ | | | 138 |
| TSS866 | LT2 $\Delta tar \Delta tsr \Delta cheY \Delta cheZ$ | | | 138 |
| TSS941 | LT2 $\Delta mcpB \Delta cheY \Delta cheZ$ | | | This work |
| TSS942 | LT2 $\Delta mcpC \Delta cheY \Delta cheZ$ | | | This work |
| TSS958 | LT2 $\Delta mcpB \Delta mcpC \Delta cheY \Delta cheZ$ | | | This work |
| 14028 | wild type <i>S. typhimurium</i> ATCC strain 14028 | | | R.M. Harshey |
| SM542 | 14028 $\Delta mcpB \Delta mcpC$ | | | 138 |
| Plasmid | Gene(s) | Resistance | Induction | Source |
| pVS88 | <i>cheZ-ecfp / cheY-eyfp</i> | ampicillin | IPTG | 240 |

Table A.1. Strains and plasmids used in this study.

In-frame deletion of genes in the strains designed for this study was achieved by allele-replacement procedure based on Datsenko and Wanner's method⁶². The initial deletion step involved an insertion of a cassette that provides kanamycin resistance, and also contains the lethal gene *ccdB* under the control of *L*-rhamnose inducible promoter, allowing the cassette to be removed by positive selection on *L*-rhamnose-minimal plates²⁸⁸. *Salmonella*'s resident plasmid pSLT contains a *ccdA ccdB* operon that interferes with the deletion strategy. Thus, pSLT was displaced prior to allele replacements using Kit10 from *Salmonella* Genetics Stock Collection (SGSC): a plasmid pLL6, which is from the same compatibility group as pSLT, was transformed in the strains of interest, pSLT was cured, and pLL6 was subsequently removed using temperature selection¹¹⁸.

Opposite responses to the cystine / cysteine redox pair

In all experiments cells were grown at 33.5° C to mid-exponential phase ($OD_{600} \sim 0.5$) in tryptone broth (TB) (1% Bacto tryptone, 0.5% NaCl, pH 7.0), supplemented with appropriate antibiotics and inducers (Table A.1). Bacteria were harvested by centrifugation, washed and resuspended twice in motility buffer (10 mM potassium phosphate buffer pH 7.0, 0.1 mM EDTA, 1 μ M *L*-methionine, 10 mM lactic acid, pH 7.0), and stored at 4° C 1-5 h prior to the experiment.

Chemoeffector preparation

Chemoeffector solutions were prepared as follows. A stock solution of 500 mM cystine (*L*-cystine, Calbiochem, 99.1%, with a certified synthetic origin) was prepared in 1 M HCl because of the poor solubility of cystine in water. Working dilutions were prepared in motility buffer. It has been reported previously that cystine dissolved directly in motility buffer (without using HCl) also elicits a repellent response¹³⁸. Cysteine (*L*-cysteine, Sigma Aldrich, from non-animal source) 100 mM stock and dilutions were prepared directly in motility buffer. The stocks of all other chemoeffectors were made directly in motility buffer. The stock solutions and dilutions of all chemoeffectors were freshly prepared on the day of the FRET experiment (1-3 h prior to the experiment).

Fluorescence resonance energy transfer (FRET) experiments and data analysis

In vivo FRET microscopy on live bacterial populations was performed as described previously²⁴². Bacteria, expressing the FRET donor-acceptor pair CheZ-CFP / CheY-YFP, were immobilized on a poly-*L*-lysine-coated microscope coverslip, attached to the top surface of a flow cell²⁷, and kept under constant flow of motility buffer, generated by a syringe pump (Harvard Apparatus, PHD2000). During the experiment chemoeffectors were added and removed by continuous flow, alternating between solutions using a switch valve (Hamilton). There is a nearly constant delay of ~25 s between the time in which the change of solutions is induced by switching the valve (indicated as time 0 in the figures) and the time, when the new solution reaches the bacteria at the flow cell.

Appendix A

FRET microscopy on bacterial populations was performed on an upright microscope (Nikon FN1), equipped with an oil immersion objective (Nikon CFI Plan Fluor, 40x/1.3). The bacteria in the flow cell were illuminated by a metal halide arc lamp with closed-loop feedback (EXFO X-Cite *exacte*) through an excitation bandpass filter (Semrock, FF01-438/24-25) and a dichroic mirror (Semrock, FF458-Di01). The epifluorescent emission was split by a second dichroic mirror (Semrock, FF509-FDi01) into donor (cyan, C) and acceptor (yellow, Y) channels. The signals from the C and Y channels, passed through emission bandpass filters Semrock FF01-483/32 and FF01-542/27 respectively, were collected by photon-counting photomultipliers (Hamamatsu H7422P-40). Signal intensities were recorded through a data acquisition card (National Instruments) installed on a PC, running custom-written software.

The ratio R between the coverslip background-corrected Y and C fluorescence signal intensities: $R = Y/C$, provided an indicator of FRET activity, robust to fluctuations in the intensity of the light. The change in FRET activity upon stimulation, $\Delta FRET$, can be expressed as a function of the change in the ratio ΔR ,

$$\Delta FRET = \frac{R_{pre} + \Delta R - R_0}{R_{pre} + \Delta R + |\Delta Y/\Delta C|} - \frac{R_{pre} - R_0}{R_{pre} + |\Delta Y/\Delta C|}$$

where R_{pre} is the pre-stimulus acceptor to donor ratio, $\Delta R = R - R_{pre}$ is the ratio change, R_0 is the acceptor to donor ratio in absence of FRET, and $|\Delta Y/\Delta C|$ is the constant absolute ratio between the changes in the acceptor and donor signals per FRET pair (for the setup in this study, $|\Delta Y/\Delta C| \approx 0.6$)²⁴². Under the measurement conditions $R_{pre} + |\Delta Y/\Delta C| \gg \Delta R$; thus $\Delta FRET \sim \Delta R$. ($\Delta FRET$ is expressed in arbitrary units of ΔR throughout the study).

A.9. Acknowledgements

The FRET experiments were performed by Bob Rosier (MSc student, VU University Amsterdam). Prof. Dr. Rasika Harshey (University of Texas, Austin) provided 14028 strains and helpful discussions.

Appendix B

Comparative analysis of the chemotaxis system of natural *Escherichia coli* isolates

The chemotaxis system of *Escherichia coli* is a paradigmatic signaling circuit, characterized by multiple experimental and theoretical studies. However, these research efforts have been concentrated on understanding the chemotactic signaling of a limited number of laboratory strains. Here we study the chemotactic behavior of a subset of natural *E. coli* isolates that represent the genotypic diversity of the species. We demonstrate variability in chemotactic performance and swimming speed, even in closely related strains. We compare the nucleotide sequence of the chemotaxis operon *meche* between strains with different chemotactic performance and demonstrate that the evolution of the chemotaxis operon closely matches that of a set of housekeeping genes. We observe genetic variation resulting from mutations and possibly horizontal gene transfer, and find *E. coli* strains with reduced chemoreceptor species composition. We discuss the possibility that a comparison of the chemotactic traits of natural *E. coli* strains could allow us to uncover quantitative features of chemotaxis that have undergone changes in the recent evolution of this species.

Appendix B

B.1. Introduction

The *Escherichia coli* chemotaxis network, which allows bacteria to orient in gradients of chemical stimuli, is a paradigmatic signaling circuit that represents many general features of signaling systems, such as adaptation, signal amplification and wide dynamic range^{12,171,241}. Each of these characteristics has been a subject of numerous quantitative modeling, theoretical and experimental studies^{35,120,127,128,137,222,225,226,260}, and the behavioral consequences of chemotactic signaling has also been evaluated using a number of standard assays^{2,171,276} as well as microfluidics technology^{7,8,156}. The chemotaxis network, like other biological signaling systems¹⁹⁸, is a subject of evolutionary optimization¹²⁶, as exemplified by the finding that clinical and natural isolates of *E. coli* vary in their chemotactic performance^{133,262}. The extensive knowledge about the molecular-level mechanisms of the chemotaxis system of *E. coli* present a rare opportunity to study the design principles involved in evolutionary optimization¹²⁷, which requires generation of phenotypic variability while preserving the important functional features of the chemotactic signaling. However, the vast majority of the experimental work and the information about the properties of *E. coli* chemotactic signaling and behavior have been derived from only a small number of laboratory strains¹⁰⁴, which do not represent the genetic and ecological diversity of *E. coli*^{150,189}.

E. coli is ubiquitous in nature, with an estimated total population of $\sim 10^{20}$ bacteria²⁷³. Its primary habitat is the vertebrate gut, where it is the predominant aerobic commensal organism²⁵⁶. Some *E. coli* strains also represent intractintestinal or extraintestinal pathogens^{130,133}. Secondary habitats of *E. coli* are water, sediments and soil^{70,110}. The population genetic structure is defined by the balance between recombination and mutation²⁵⁶. Low recombination levels define a clonal structure, whereas high recombination levels define a panmictic structure²³⁶. In the pre-sequencing era, studies using multilocus enzyme electrophoresis (MLEE) analysis²¹⁹ suggested that the population structure of *E. coli* is predominantly clonal^{173,220}. MLEE analysis of thousands of natural and clinical isolates allowed the assembly of a set of 72 reference strains, the ECOR collection, that represented the known genetic diversity of *E. coli*¹⁸⁹ (Table B.1). The ECOR

Chemotaxis system of natural *Escherichia coli* isolates

collection was subdivided into four groups: A, B1, B2, and D, plus a minor group E ²⁷⁵, where group D diverged first and the sister groups A and B1 separated later ¹⁸²⁻¹⁸⁴. More recent studies suggest that group B2 is the ancestral one ^{79,139}.

| ECOR strain | Location | Host | MLEE group | Spreading in TB soft-agar | Swimming in motility buffer | Doubling time (h) |
|-------------|----------------|--------------|------------|---------------------------|-----------------------------|-------------------|
| 1 | Iowa | Human (F) | A | L | F | |
| 2 | New York | Human (M) | A | L | F | 0.67 |
| 3 | Massachusetts | Dog | A | L | F | |
| 4 | Iowa | Human (F) | A | L | F | |
| 5 | Iowa | Human (F) | A | L | S | |
| 6 | Iowa | Human (M) | B1 | NM | NM | |
| 7 | Washington zoo | Orangutan | A | L | F | |
| 8 | Iowa | Human (F) | A | L | F | |
| 9 | Sweden | Human (F) | A | NM | NM | |
| 10 | New York | Human (F) | A | L | F | |
| 11 | Sweden | Human (F) | A | NM | NM | |
| 12 | Sweden | Human (F) | A | L | F | 0.73 |
| 13 | Sweden | Human (F) | A | L | S | 0.77 |
| 14 | Sweden | Human (F) | A | L | F | |
| 15 | Sweden | Human (F) | B1 | L | S | |
| 16 | Washington zoo | Leopard | A | L | S | |
| 17 | Indonesia | Pig | A | NM | NM | |
| 18 | Washington zoo | Celebese ape | A | D | S | 1.05 |
| 19 | Washington zoo | Celebese ape | A | L | F | 0.73 |
| 20 | Bali | Steer | A | L | F | |
| 21 | Bali | Steer | A | L | F | 0.74 |
| 22 | Bali | Steer | A | L | F | |
| 23 | Washington zoo | Elephant | A | S | S | |
| 24 | Sweden | Human (F) | A | NM | NM | |
| 25 | New York | Dog | A | D | NM | |
| 26 | Massachusetts | Human Infant | B1 | L | F | |
| 27 | Washington zoo | Giraffe | B1 | L | S | 0.67 |
| 28 | Iowa | Human (F) | B1 | NM | NM | |
| 29 | Nevada | Kangaroo rat | B1 | L | S | 0.72 |
| 30 | Alberta | Bison | B1 | L | S | |
| 31 | Washington zoo | Leopard | E | L | S | 0.67 |
| 32 | Washington zoo | Giraffe | B1 | D | S | 0.63 |
| 33 | California | Sheep | B1 | L | F | 0.67 |
| 34 | Massachusetts | Dog | B1 | NM | NM | |
| 35 | Iowa | Human (M) | D | NM | NM | |
| 36 | Iowa | Human (F) | D | NM | NM | |
| 37 | Washington zoo | Marmoset | E | D | S | 0.59 |
| 38 | Iowa | Human (F) | D | NM | NM | |

Appendix B

| | | | | | | |
|----|----------------|--------------|----|----|----|------|
| 39 | Sweden | Human (F) | D | NM | NM | |
| 40 | Sweden | Human (F) | D | NM | NM | |
| 41 | Tonga | Human (M) | D | NM | NM | |
| 42 | Massachusetts | Human (M) | E | L | F | |
| 43 | Sweden | Human (F) | E | NM | NM | |
| 44 | Washington zoo | Cougar | D | L | S | |
| 45 | Indonesia | Pig | B1 | L | F | 0.76 |
| 46 | Washington zoo | Celebese ape | D | NM | NM | |
| 47 | New Guinea | Sheep | D | L | F | |
| 48 | Sweden | Human (F) | D | L | F | 0.76 |
| 49 | Sweden | Human (F) | D | S | F | |
| 50 | Sweden | Human (F) | D | D | F | 0.67 |
| 51 | Massachusetts | Human infant | B2 | L | F | 0.75 |
| 52 | Washington zoo | Orangutan | B2 | L | S | |
| 53 | Iowa | Human (F) | B2 | L | F | |
| 54 | Iowa | Human | B2 | L | F | |
| 55 | Sweden | Human (F) | B2 | L | F | |
| 56 | Sweden | Human (F) | B2 | L | F | |
| 57 | Washington zoo | Gorilla | B2 | S | S | |
| 58 | Washington zoo | Lion | B1 | L | F | |
| 59 | Massachusetts | Human (M) | B2 | L | F | |
| 60 | Sweden | Human (F) | B2 | D | S | |
| 61 | Sweden | Human (F) | B2 | L | F | |
| 62 | Sweden | Human (F) | B2 | S | F | 0.55 |
| 63 | Sweden | Human (F) | B2 | NM | NM | |
| 64 | Sweden | Human (F) | B2 | NM | NM | |
| 65 | Washington zoo | Celebese ape | B2 | L | F | |
| 66 | Washington zoo | Celebese ape | B2 | L | F | |
| 67 | Indonesia | Goat | B1 | L | F | |
| 68 | Washington zoo | Giraffe | B1 | S | S | 0.66 |
| 69 | Washington zoo | Celebese ape | B1 | NM | NM | |
| 70 | Washington zoo | Gorilla | B1 | NM | NM | |
| 71 | Sweden | Human (F) | B1 | D | M | |
| 72 | Sweden | Human (F) | B1 | L | S | |

Table B.1. Standard reference collection of *E. coli* strains (ECOR collection) ¹⁸⁹. Color-coding represents phylogenetic groups A (green), B1 (red), B2 (yellow), D (blue), and E (black) ²⁷⁵. Strains are categorized according to their spreading as non-motile (NM), strains spreading diffusely (D), strains forming small but distinct rings (S), and strains forming large rings (L) (see text). Strains are categorized according to their swimming speed as non-motile (NM), slow (S; swimming speeds <10 $\mu\text{m/s}$), and fast (F; swimming speeds $\geq 10 \mu\text{m/s}$) (see text). The doubling time (h) of a selected subset of ECOR strains in TB at 33.5° C is shown at the last column.

Chemotaxis system of natural *Escherichia coli* isolates

The subsequent development of DNA sequencing techniques led to the discovery that *E. coli* populations are actually seldom clonal, with frequent recombination events revealing themselves as clustered third-base substitutions¹⁷⁴. The genetic diversity among members of the ECOR collection was attributed to recombination rather than to mutation⁹⁵. Phylogenetic analysis of concatenated sequences of ECOR housekeeping genes revealed the existence of four clades, largely in agreement with the MLEE groups A, B1, B2 and D, although hybrid groups such as AxB1 and ABD, a result of recombination, also exist within the global *E. coli* population²⁷⁵. Thus *E. coli* is more diverse than previously appreciated, although some data suggest population contractions and bottlenecks reduced the diversity 10-30 million years ago²⁷⁵. During population expansions in the last five million years the descendants of the four major lineages A, B1, B2 and D have become predominant and represent the majority of the contemporary strains²⁷⁵.

Here we study the diversity of *E. coli* with respect to their chemotaxis and motility. To largely cover the existing natural diversity in behavior, we selected a subset of ECOR strains, which represent the variations in chemotactic spreading and swimming motility in soft-agar plates. The selected strains contain representatives of each of the phylogenetic lineages of *E. coli*, and also cover strains from different geographic locations, animal and human hosts, as well as pathogens and commensals. We show variability of the chemotactic performance even in strains that are closely related phylogenetically. We observe mutation- and recombination-based changes in the chemotaxis operon *meche*, and compare the genetic diversity of this chemotaxis operon with that of a subset of housekeeping genes. We discuss how further physiological studies on chemotactic signaling in the selected subset of strains could reveal which features of *E. coli* chemotactic signaling and behavior are conserved, and which features have undergone changes in the recent past.

Appendix B

B.2. Diversity of soft-agar plate phenotypes of natural *E. coli* isolates

To observe the natural variations of chemotactic performance of *E. coli*, we tested the spreading of all 72 strains from the ECOR collection, using the classical soft-agar assay for chemotaxis² (Figure B.1). Bacteria were inoculated in tryptone-broth (TB) soft-agar plates, and incubated at 30° C. Growing bacteria consume nutrients in the media and the motile and chemotactic strains swim outwards in concentric bands, which form due to chemotactic responses to the spatial gradients, resulting from metabolic consumption. In TB (the nutrient tryptone is a casein hydrolysate), the first band consumes serine and most of the oxygen, the second band aspartate, and the third band threonine^{2,276}. Motile but non-chemotactic strains also spread outwards due to bacterial growth and motility, but the spreading is slower and do not produce distinct bands²⁷⁶. Non-motile strains only expand around the inoculation point due to growth of the bacteria.

Figure B.1A and B.1B show the spreading of the 72 strains of the ECOR collection after 4h and 7.5 h of incubation, respectively. ~25% of the ECOR strains do not spread even after prolonged incubation (Table B.1), suggesting that they are immotile, which was confirmed after performing phase-contrast microscopy of these strains in liquid medium (Materials and methods). Non-motile strains were observed in each of the phylogenetic groups, with the lowest percent in group B2 (13%) and the highest percent in group D (58%). The rest of the strains spread in TB soft-agar plates and swim in liquid medium; however, both the spreading patterns and the motility strongly differ between strains. Spreading strains either spread diffusely or form most often two rings at the time of observation (Table B.1). The swimming speed varies between a few microns per second and >30 µm/s (Table B.1 shows a rough approximation of the swimming speed for the strains of the ECOR collection, see Section B.3). Variations in the spreading patterns and swimming speeds are observed in each of the phylogenetic groups, although there are more fast-spreading strains in groups A and B1 than in B2 and D.

Chemotaxis system of natural *Escherichia coli* isolates

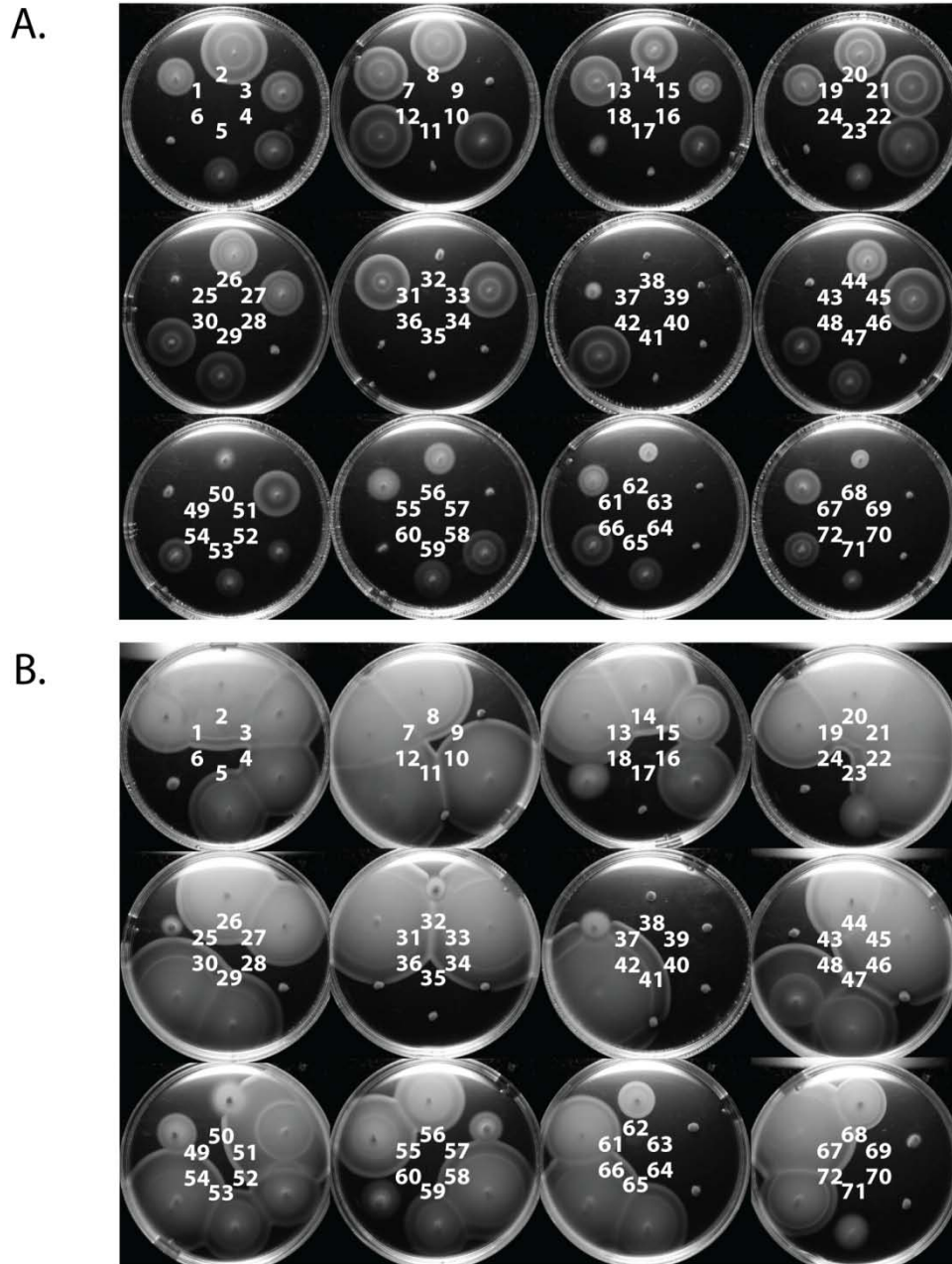


Figure B.1. Soft-agar assays of all 72 strains of the ECOR collection. The numbers correspond to the numbers of the strains in the ECOR collection. The plates were incubated at 30° C and imaged after 4 h (A) and 7.5 h (B).

Appendix B

B.3. *E. coli* isolates with distinct chemotaxis characteristics and motility

To analyze the observed diversity of spreading pattern, accounting for the contributions of chemotaxis and other factors, such as differences in growth and random motility²⁷⁶, we selected for further characterization a quarter of the ECOR strains that show different spreading and belong to different phylogenetic groups and measured their growth in TB and swimming speed in liquid medium. Three groups of strains were selected based on their spreading pattern: strains forming large rings, small but distinct rings, and strains that spread diffusely in TB soft agar. The 18 selected strains have comparable growth rates in TB at 33.5° C with an average doubling time of 0.7±0.1 h (Table B.1). Thus, the observed differences in spreading in TB soft agar are not due to differences in growth, but other factors: mostly chemotactic performance and random motility. Swimming speeds, however, differed between the strains (Table B.1): we labeled the strains to be “fast” if they swim at ≥10 μm/s, and “slow” if they swim at <10 μm/s. Table B.2 summarizes the characteristics of the selected subset of ECOR strains.

| ECOR strains | Large rings | Small rings | Diffuse spreading |
|---------------|-------------------------------------|-------------|-------------------|
| Fast swimming | 2, 12, 19, 21 33, 45 48 51 | 62 | 50 |
| Slow swimming | 13 27, 29 31 | 68 | 18 32 37 |

Table B.2. Selected subset of ECOR strains, grouped by their spreading patterns and swimming speed. The doubling times in TB at 33.5° C of the selected strains are comparable. The MLEE groups are color-coded: A (green), B1 (red), B2 (yellow), D (blue), and E (black).

B.4. Sequence analysis of the *meche* operon

The canonical chemotactic signaling system of *E. coli* consists of six soluble chemotaxis proteins: the kinase CheA, the scaffolding protein CheW, the adaptation enzymes CheR (methyltransferase) and CheB (methyl-esterase / deamidase), the response regulator CheY and its phosphatase CheZ²⁶⁶. Chemical and physical stimuli are detected by five chemoreceptors: Tar, Tap, Tsr, Trg and Aer²⁶⁶. Most of the chemotaxis genes are organized into two polycistronic transcriptional units (operons)¹⁴⁸: *meche*, encoding Tar, Tap, CheR, CheB, CheY, and CheZ, and *mocha*, encoding CheA, CheW, and the flagellar motor proteins MotA and MotB. Tsr, Trg and Aer are encoded elsewhere on the genome.

To understand the differences in the chemotactic behavior of the selected ECOR strains at the genetic level, we sequenced the major chemotaxis operon *meche* of each of these strains (Figure B.2A). The total length of the *meche* operon is conserved in 16 of the 18 strains; the other two strains (ECOR51 and ECOR62), which are both from group B2, have a truncation of the gene of the chemoreceptor Tap. The truncated region is flanked on both sides by the same sequence GAATCAGG, likely a site of homologous recombination that led to the deletion of part of the gene. The truncated *tap* gene nevertheless is in-frame and may produce a 75-amino acid peptide (42 amino acids from the start and 33 amino acids from the end of the gene; Figure B.2A), in which the first transmembrane domain is preserved.

We observed also a truncation of gene product due to a mutation in the start codon. The *cheB* gene of ECOR62 had a reading frame starting at the 43rd base pair of the *cheB* gene of the rest of the strains. This truncation might affect the CheB expression level²⁰⁸. The truncated amino acids 4 – 42 belong to the regulatory (REC) domain of CheB (see Appendix C). However, according to a domain prediction using the SMART database^{141,217}, the two-domain structure of CheB is preserved in ECOR62.

We analyzed the polymorphic sites at the nucleotide and amino acid sequences of the ECOR *meche* genes, compared with the *meche* genes from the model strain for chemotaxis, *E. coli* K12. For the selected subset of strains, 4.1% of polymorphic sites exist at the nucleotide sequence of the

Appendix B

whole *meche* operon, ranging from 2.8% (for *cheY*) to 5.8% (for *cheB*) per gene (Figure B.2B). At the amino acid level, polymorphic sites make up 1.9% of all sequences, ranging from 0.5% (for CheZ) to 2.8% (for Tap) per protein (Figure B.2B, polymorphic sites at the amino acid level are indicated as “informative sites”). The group D strain ECOR48 stands out with the highest number of polymorphisms at the nucleotide level but not at the amino acid level. The high rate of third-base (non-coding) substitutions, *i.e.* different codon usage, might indicate the occurrence of horizontal gene transfer of the *meche* operon in the evolutionary past of this strain ¹⁷⁴. However, ECOR48 also shows high occurrence of substitutions on nucleotide level and amino acid level in other parts of the genome (in the fragments of housekeeping genes discussed below).

To compare the evolution of the chemotaxis genes with the evolution of the rest of the genome, we performed an identical analysis of nucleotide and amino acid polymorphisms in concatenated fragments of seven housekeeping genes of the selected ECOR strains (the sequences of *recA*, *purA*, *mdh*, *icd*, *gyrB*, *fumC*, and *adk* gene fragments for 492 *E. coli* isolates are publicly available in the MSLT database ²⁷⁵) (Figure B.2B). These genes are distributed over the *E. coli* chromosome, and a previous study showed that their concatenated sequences fell largely into four phylogenetic clades in good agreement with the MLEE groups A, B1, B2 and D ²⁷⁵. Polymorphisms at the nucleotide level for the selected subset of ECOR strains were found to be 4.2% (from 2.3% to 7.0% per gene fragment), very similar to the nucleotide polymorphism level of the *meche* operon (4.1%). At the amino acid level, the percentage of polymorphic sites for the housekeeping genes is lower (0.7%, ranging from 0.6 to 1.7% per fragment); however, a larger sequence sample might be needed to confirm the significance of this difference.

We used the sequence information for the *meche* operon to construct a phylogenetic tree (see Materials and methods) of the selected subset of ECOR strains (Figure B.3). Strains are clustered in a very good agreement with the MLEE phylogenetic groups (color-coded on Figure B.3). The laboratory strain *E. coli* K12 and a closely related species, *Salmonella typhimurium* LT2, are included for comparison. As expected, *E. coli* K12 clusters with the group A strains. However, we do not observe a

Chemotaxis system of natural *Escherichia coli* isolates

pronounced correlation between the chemotactic spreading and random motility characteristics with the sequence divergence of the *meche* operon, as illustrated in Figure B.3.

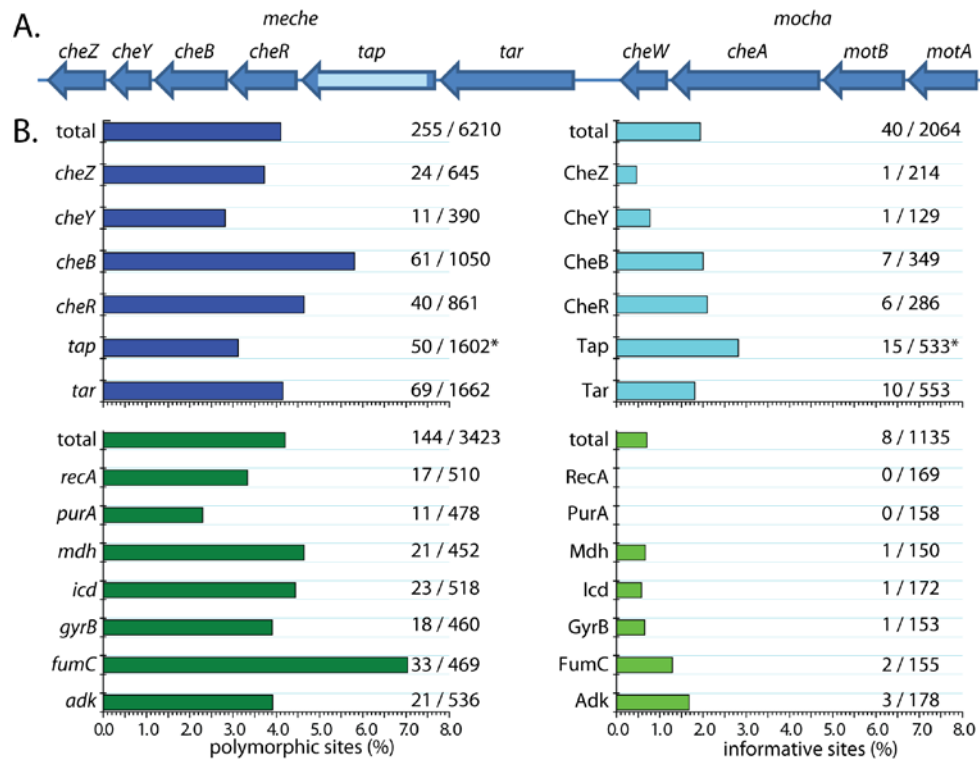


Figure B.2. Genetic diversity of chemotaxis genes in the selected ECOR strains. (A) Structure of the *meche* operon and the adjacent *mocha* operon of *E. coli*. The light blue box indicates the truncation at the *tap* gene of ECOR51 and ECOR62. (B) Histograms of the polymorphic sites for *meche* operon genes (top left) and housekeeping genes from MSTL database ²⁷⁵ (bottom left). Histograms of the polymorphic sites at the respective amino acid sequences (“informative sites”), are shown for the proteins expressed from the *meche* operon (top right) and housekeeping genes (bottom right). The number of substitutions over the total number of base pairs or amino acids respectively is shown. The first rows (labeled as “total”) show the total number of polymorphic sites at all the sequences.

Appendix B

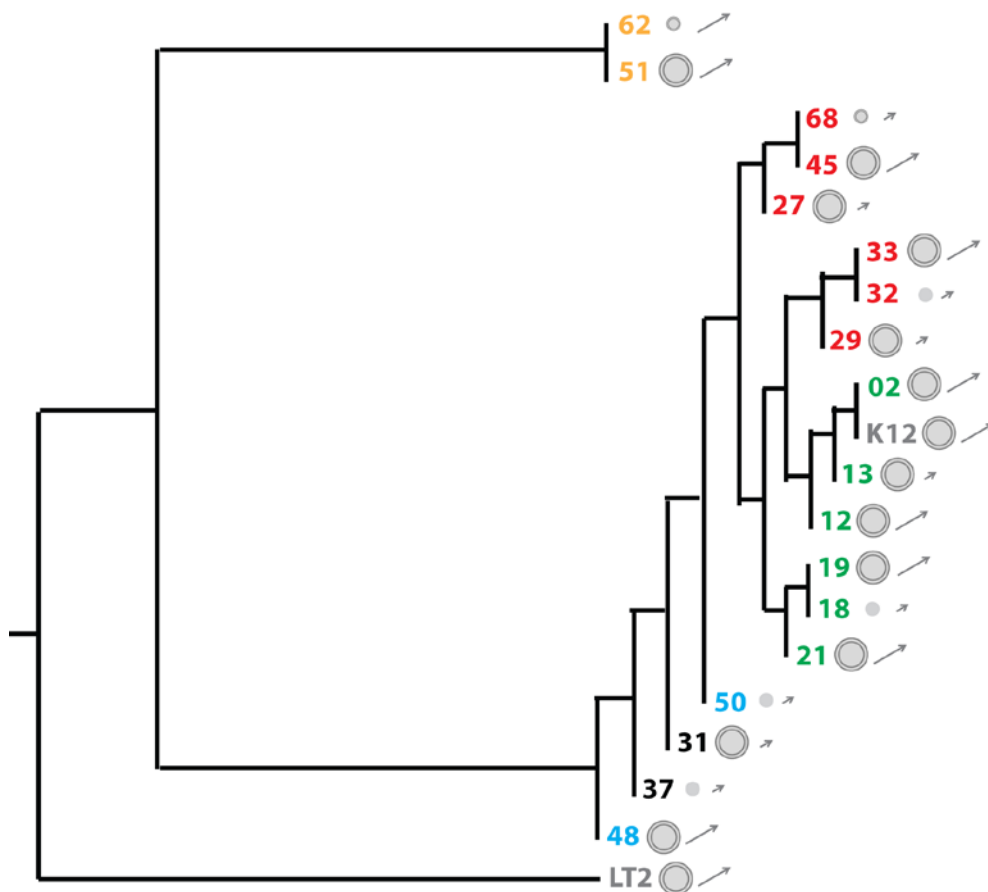


Figure B.3. Phylogenetic tree of the selected subset of ECOR strains, including the laboratory strain *E. coli* K12 and its closely related species *S. typhimurium* LT2. The tree was constructed using the concatenated sequences of *meche* genes of the selected strains and an algorithm, implemented into the BioEdit software (Fitch-Margoliash and least squares methods with evolutionary clock-based algorithm). The MLEE phylogenetic groups are color coded as in Tables B.1 and B.2. Spreading and swimming motility are indicated next to each strain as following: large circles – a strain forming large rings, small circles – a strain forming small but distinct rings, one circle – a strain that do not form distinct rings but spread diffusely; a large arrow – a strain that swims fast (swimming speed $\geq 10 \mu\text{m/s}$), a small arrow – a strain that swims slow (swimming speed $< 10 \mu\text{m/s}$) (see Table B.2).

B.5. Discussion

We explored the natural variation in the chemotactic behavior of *E. coli*, using a subset of the strains from the ECOR collection that represents much of the contemporary genetic diversity of the species, and covers strains from different locations and host origins. The chemotactic performance differs largely between the strains, even between those that are close phylogenetic relatives, and have comparable swimming speeds. Our observations suggest that after the divergence from their common ancestor and a major historical bottleneck ~30 million years ago that removed most of the extant diversity^{57,275}, the chemotaxis system of *E. coli* strains has evolved, likely improving the fitness (chemotactic performance) of the bacteria in the various environmental niches that different strains inhabit^{70,256,273}.

We analyzed sequences of the major genes of the chemotactic signaling system, which are part of the *meche* operon: the genes of the chemoreceptors Tar and Tap, the adaptation enzymes CheR and CheB, the response regulator CheY, and its phosphatase CheZ. Overall, the nucleotide substitution frequencies were found to be similar to those reported for housekeeping genes²⁷⁵. The adaptive evolution in prokaryotes is driven by mutation and recombination¹⁰⁷, the latter underlying the process of horizontal gene transfer³⁸. We observed examples for sequence variations in the chemotaxis genes that likely result from mutation or recombination processes. For example, a mutation in the start codon of the *cheB* gene of ECOR62 creates a truncated open reading frame. Mutations in a close proximity to the start codon might affect the translational expression^{208,209}, therefore the expression levels of the methyltransferase CheB might be altered in ECOR62, which can affect the methylation / demethylation balance and, in turn, the modification states of the chemoreceptors²¹⁵.

Recombination-based changes are the likely cause of the truncation of the *tap* gene in ECOR51 and ECOR62, and the high level of third-base substitutions (*i.e.* different codon usage) in the *meche* operon of ECOR48. Truncations of the genes of Tap and Trg chemoreceptors were previously reported to be prevalent in uropathogenic *E. coli* strains¹³³; ECOR62 is also

Appendix B

an isolate from a pyelonephritis patient ¹⁸⁹. The truncation has occurred between the same flanking sequences, GAATCAGG, in the *tap* gene. The *tap* reading frame is preserved, as well as the first transmembrane domain, suggesting that the resulting 75-amino acid peptide might integrate into the membrane. The occurrence of clustered third-base substitutions might also indicate genetic changes due to recombination ¹⁷⁴. We observed multiple third-base substitutions in the strain ECOR48. This strain also contains a F1-like plasmid ¹⁵⁹, which could take part in a conjugative horizontal gene transfer.

Our analyses of the chemotactic behavior and the genetic variation of the chemotaxis operon *meche* of *E. coli* provide a basis for future physiological studies that could assess which quantitative features of chemotaxis have undergone changes in the recent evolution of this species. We have used *in vivo* fluorescence resonance energy transfer (FRET) ²⁴² to perform a detailed comparison between the quantitative features of the chemotactic signaling of *E. coli* K12 and the closely related species *S. typhimurium* LT2, and we have identified differences in the transfer functions of chemotactic signaling ²⁶⁰ that affect the sensitivity to chemoeffectors, the receptor-receptor cooperativity, and the adaptation kinetics (Chapter 3). The chemotactic transfer functions of *S. typhimurium* could serve as an outgroup for a similar comparison of the chemotactic transfer functions of the selected *E. coli* strains (we have engineered genetically a subset of these strains for future FRET experiments; see Materials and methods and Chapter 6). The fitness (chemotactic performance) of the compared strains can be evaluated quantitatively in defined gradients created in microfluidic devices ⁸. Such future studies could reveal design principles underlying the evolution of the bacterial chemotaxis system, and improve our understanding for the design of signaling circuits in nature.

B.6. Materials and methods

Bacterial strains

The ECOR collection (Table B.1) is described in reference ¹⁸⁹.

Some of the ECOR strains (listed below) were engineered genetically for future FRET experiments in the following manner. In-frame chromosomal gene deletions of *cheY* and *cheZ* genes were created using an allele replacement procedure, based on a modification of Datsenko and Wanner's method ⁶², that does not leave a scar. It is based on an insertion cassette that contains the lethal *ccdB* gene under the control of a L-rhamnose-inducible promoter. This cassette can be removed later by positive selection on rhamnose-minimal plates ²⁸⁸. Then the plasmid pVS88 ²⁴⁰ used for expression of the FRET fusion proteins CheY-YFP and CheZ-CFP was transformed in the selected strains.

ECOR strains 13, 18, 19, 21, 27, 29, 32, 33, 48, 51, 62 and 68 were engineered for FRET in the way described above. ECOR strains 2, 12, 45 and 50 were engineered in a similar manner, but the *ccdB* cassettes were not removed because of problems with false positive colonies that have occurred with the rhamnose positive selection strategy. The strains ECOR31 and 37 are resistant to ampicillin and kanamycin and chloramphenicol and kanamycin respectively, and thus these strains have not been engineered for FRET experiments (the plasmids used in the knockout strategy have ampicillin and kanamycin resistances, and pVS88 has an ampicillin resistance, thus the native resistances of ECOR31 and 37 should be removed prior to knock out or transformation procedures).

All strains engineered for FRET should be tested to determine the optimal levels of induction of the FRET fluorescent fusions. The pilot experiments with ECOR13, 18, 29, and 68 showed that the same amount of inducer (IPTG) led to ~two-fold lower level of fluorescence for both yellow and cyan channels. The fluorescence levels in ECOR51 were similar to that of *E. coli* HCB33 (wild type for chemotaxis). The attachment of the strains to the coverslips in the FRET experiments should also be optimized (e.g. ECOR18 do not stick well to polylysine-coated coverslips).

Appendix B

Soft-agar plate experiments

The bacterial cultures were grown overnight to saturation in tryptone broth (TB, 1% Bacto tryptone, 0.5% sodium chloride, pH 7.0). The soft-agar plates were prepared using 25 ml TB per plate, solidified with 0.26% Bacto agar. The plates were left to solidify overnight under a humidity chamber. 5 μ l of the tested cultures were inoculated in the plates. Six strains were tested per plate, and two independent replicates were performed for each strain. The plates were incubated at 30° C for 4 h, and imaged using MultiDoc-It™ digital imaging system, equipped with Olympus camera. After an additional 3.5 h of incubation, the plates were imaged again.

Plate reader experiments

The growth in TB at 33.5° C was evaluated for the strains of interest by measuring the optical density of the cultures at 600 nm (OD_{600}) in a multilabel plate reader (Perkin Elmer 2030). The temperature of the plate reader was set to 33.5° C. The saturated overnight cultures were diluted 100 times in TB. 200 μ l of the diluted cultures were placed in the wells of a 96-well plate (OptiPlate-96). The OD_{600} was measured and recorded at 35 min intervals. After every third measurement, 11 μ l of water was dispensed in each well to compensate for the evaporation of water and maintain the volume in each well constant. One of the rows in the 96-well plate was filled with a sterile TB and the averaged OD_{600} measured in this row was used for a background correction. At least four wells were allocated for each strain and the averaged results were used to plot a growth curve for each strain. The doubling times of the strains were calculated by fitting to the log phase of the growth curves an exponential function $OD_{600} = OD_{600}^0 2^{\tau}$, where OD_{600}^0 is the OD_{600} in the beginning of the log phase and τ is the doubling time of the strain.

Chemotaxis system of natural *Escherichia coli* isolates

Swimming motility experiments

The overnight cultures were diluted 100x in TB and grown at 33.5° C on a rotary shaker, until the cultures reached mid-exponential phase ($OD_{600} \sim 0.5$). Then the bacteria were harvested by centrifugation (5 min, 5000 rpm), washed twice and carefully resuspended (by shaking the tube, without pipetting) in motility buffer (10 mM potassium phosphate buffer pH 7.0, 0.1 mM EDTA, 1 μ M *L*-methionine, 10 mM lactic acid, pH 7.0). The cultures were imaged immediately or stored at 4° C up to 5 h prior to the experiment.

The swimming behavior of the bacteria was observed on a Nikon Eclipse inverted microscope using a 20x phase-contrast objective and an additional 1.5x magnification. The tested bacterial strain, diluted 3 - 5x in motility buffer was placed in tunnel slides, in which the distance between the glass and the cover slip was ~ 1.5 mm. The bacteria were imaged at mid-depth, close to the liquid-air border of the tunnel slide to ensure that oxygen was available to the bacteria. The temperature during the microscopy observation was maintained at 33.5° C using a temperature-control plastic chamber covering the microscope.

A Roper Scientific (Photometrics CoolSNAP HQ) camera was used to record movies with 7.6 frames per second. Movies with a higher frame rate (30 frames per second) were also recorded for some of the strains using a smaller field of view. The bacterial trajectories were extracted using BacTrack cell tracking software⁹. First, each frame was subtracted from the following one to remove the background; then, the bacteria in each frame were located as peaks in a monochrome intensity field; finally, the bacteria were tracked between the frames using the particle tracking algorithm "Conservative search radius" (also called "Roman1") implemented in the BacTrack software. This algorithm utilizes a user-defined hard cutoff radius that corresponds to the maximum distance that an object (bacterium) can move between successive frames. The objects in a frame n are called "parent particles" and the objects in the consecutive frame, $n+1$, are called "children particles". The basic rule is that each child comes from one parent and each parent begets one child. The algorithm does the following:

Appendix B

1. locates parent and children particles in frames n and $n+1$
2. accepts an user-defined cutoff radius R
3. computes the distances for all pairs of parents and children; throw out all pairs whose distance $> R$
4. considers for one parent particle at a time whether the parent has
 - (a) no children (no child particle within R): the trajectory ends
 - (b) a single child (only one child particle within R); if the child has
 - a single parent, the child-parent pair is considered a match (the child and the parent are the same particle)
 - >1 parent: the trajectory ends
 - (c) >1 child (>1 child particle within R): the trajectory ends
5. the children that have no parent start new trajectories
6. the process is repeated from step 2 for the next pair of frames

The post-processing of trajectories was performed in MATLAB to yield the 2D population-averaged run velocity (the MATLAB code that was used has been published in the B.Sc. thesis of M. D. Sekora, MIT, 2005).

The tracking algorithm has worked only for a subset ($\sim 1/4$ of the total number) of the movies of swimming ECOR strains. The main problems were the density of the cells (too high or too low) and drift of the liquid in the tunnel slides. Fast / slow categories (Table B.1) are thus approximate, strains that seemed (by eye) to swim similar to strains with swimming speed $< 10 \mu\text{m/s}$ were labeled as "slow", and strains that seemed to swim similar to strains with swimming speed $\geq 10 \mu\text{m/s}$ were labeled as "fast".

Sequencing and genetic analysis

Sequencing primers for the *meche* region were designed using the Primer 3 program and the genomic sequence of the *E. coli* K12 substrain MG1655 (NCBI accession number: NC_000913.2). PCR products of length 700-800 base pairs were obtained for the whole length of the *meche* operon, including its flanking regions, and the samples were sent for sequencing to ServiceXS. Results were analyzed using BioEdit and Mutalin programs. Multiple sequence alignments were obtained using CLUSTALW algorithm. ExPASy translate tool was used obtain the amino acid sequences.

Chemotaxis system of natural *Escherichia coli* isolates

The concatenated sequences of the genes of *meche* operon from the selected subset of ECOR strains, *E. coli* K12 substrain MG1655, and *S. typhimurium* LT2 were used to construct a neighbor-joining tree using KITSCH© algorithm by Joseph Felsenstein in Bioedit, which estimates phylogenies from distance matrix data, assuming that the distances are equal to the sums of branch lengths between the strains. It assumes an evolutionary clock and uses the Fitch-Margoliash criterion.

B.7. Acknowledgements

Michel de Vries provided help with the sequencing of the chemotaxis operon of ECOR strains.

Appendix B

Appendix C

Effect of CheB phosphorylation feedback on adaptation kinetics in bacterial chemotaxis

The chemotactic signaling network of bacteria provides a model system for testing the effect of altering network topology on the function of signaling pathways. Here we studied how the disruption of the phosphorylation-dependent feedback via the activity of the methylesterase CheB affects the adaptation kinetics in *Escherichia coli* chemotaxis. Using *in vivo* fluorescence resonance energy transfer (FRET) measurements coupled with temporal step and exponential ramp stimuli, we determined the shape of the transfer function $F(a)$, describing the methylation kinetics of the chemoreceptors, in populations of cells that express a mutant CheB lacking the phosphorylatable N-terminal regulatory domain (CheBc) or having a mutation in the phosphorylation site (CheB^{D56E}). We showed that the shape of $F(a)$ differs between wild type cells and cells that express CheBc or CheB^{D56E}. $F(a)$ for cells expressing CheBc and having a steady-state kinase activity > 0.40 follows Michaelis-Menten kinetics, whereas a nonlinearity in $F(a)$ of at high values of kinase activity was observed for wild type cells. Our observations suggest that the strong nonlinearity of $F(a)$ could be a consequence of the specific topology of the chemotaxis network of *E. coli*.

Appendix C

C.1. Introduction

Changes in the topology of signaling and regulatory networks can have a strong effect on cellular responses and ultimately the cell fate ^{134,245}. The simple and thoroughly characterized chemotaxis circuit of *E. coli* ^{243,266}, provides an ideal system for studying the effects of genetic changes of the network topology on the cellular response. In this thesis we have studied the response of a natural chemotaxis network with a different topology by looking at the response functions of the close relative to *E. coli*, *S. typhimurium*, which has an additional scaffolding protein that can be phosphorylated ¹⁰ (Chapter 3 and 5). Here, we change the structure of the *E. coli* signaling network by genetic modifications, and using sensitive physiological measurements of the network response, study the consequences of the altered topology *in vivo*.

The bacterial chemotaxis network has a modular structure describable by a coarse-grained model with three dynamic variables: $[L]$ – input (ligand concentration), m – memory (receptor methylation level), and a – output (kinase activity), linked by two transfer functions ²⁶⁰, which have been characterized using FRET experiments ²²⁶. One of the two transfer functions, $G([L], m)$, representing the receptor module, is well described by an MWC model of receptor interactions ²⁶⁰ (see Chapter 3). The second transfer function, $F(a)$, represents the integrand of negative feedback within the adaptation module. It represents the rate of change of receptor methylation, catalyzed by a methyltransferase CheR and methylesterase / deamidase CheB. Assuming that CheR binds only the inactive receptors and CheB – only the active receptors, $F(a)$ can be expressed by an enzymatic reaction model

$$F(a) = V_R \frac{1-a}{K_R+1-a} - V_B(a) \frac{a}{K_B+a}, \quad (1)$$

where K_R and K_B are the Michaelis constants, and V_R and $V_B(a)$ are the maximal velocities for methylation and demethylation respectively. However, it has been shown experimentally that $F(a)$ could not be fit by a simple mechanistic model of enzyme kinetics ²²⁶, as explained below.

$F(a)$ has been mapped experimentally in *E. coli*, using FRET measurements coupled with exponential ramp inputs, $[L](t) = [L]_0 e^{rt}$, where r is the ramp rate, and $[L]_0$ is the ligand concentration, to which the

Effect of CheB phosphorylation feedback on adaptation kinetics

cells are adapted before applying the ramp ²²⁶. During exponential ramp inputs the kinase activity reaches a new constant steady-state level, a_c , which can be used to infer the shape of $F(a)$ ²²⁶ (see Chapter 3, Figure 3.4). For $a < 0.74$, the shape of $F(a)$ can be fit by Michaelis-Menten kinetics, with a constant V_B . As the kinase activity, a , approaches unity, there is a sharp increase in $V_B(a)$, which can be fit by a piecewise linear form (see Chapter 3, equation 22). However, this phenomenological fit does not provide a mechanistic explanation for the strongly non-linear behavior of $V_B(a)$ and $F(a)$ respectively.

One hypothesis for the nonlinearity of $F(a)$ is that it is a consequence of the specific topology of the *E. coli* chemotaxis network, in which CheB activity is controlled by phosphorylation ²²⁶. The methyltransferase CheR and methylesterase / deamidase CheB regulate the level of methylation of the chemoreceptors, which modulates the activity of the receptor-kinase complexes. CheB has a two-domain structure (Figure C.1A). The N-terminal domain is a regulatory (REC) domain, which is phosphorylated by the active kinase (CheA) molecules. The REC domain regulates the activity of the C-terminal domain, which has a methylesterase activity: upon phosphorylation at position D56 in the REC domain, the methylesterase activity is stimulated. The mechanistic explanation of this phenomenon is that in the unphosphorylated CheB, the REC domain packs against the active site of the methylesterase domain, inhibiting its activity (Figure C.1A *left*). Upon its phosphorylation, the REC domain changes its conformation, disrupting the domain interface, which allows access to the methylesterase active site, activating the methylesterase activity of CheB ⁶⁹ (Figure C.1A *right*). Demethylation of the receptors leads to the deactivation of the receptor-kinase complex, which provides a phosphorylation-dependent negative feedback loop in the chemotaxis system of *E. coli* ¹⁵.

To test whether the sharp transition of $F(a)$ around $a = 0.74$ is a result of the phosphorylation-dependent feedback, we transformed $\Delta cheB$ *E. coli* cells with plasmids used for expression of mutant CheB variants CheB^{D56E} and CheBc. CheB^{D56E} (Figure C.1B *left*) bears a mutation at the phosphorylation site (D56), which prevents phosphorylation by CheA, *i.e.* the methylesterase activity of CheB^{D56E} cannot be stimulated by

Appendix C

phosphorylation. CheBc (Figure C.1B *right*) is a truncated version of CheB, in which only the methylesterase domain is preserved. It has been shown that CheBc has a much lower methylesterase activity than the phosphorylated intact CheB⁶⁹, implying that the phosphorylation of the REC domain has a role not only in the relief of the methylesterase inhibition, but also in the stimulation of the methylesterase activity¹⁵. If the phosphorylation-dependent feedback on CheB activity is responsible for sharp transition in $F(a)$ at high values of kinase activity, a , observed in wild type *E. coli*, such a sharp transition should not be observed in the CheB^{D56E}- and CheBc-expressing strains where the phosphorylation-dependent feedback is disrupted. We describe below our efforts to test this hypothesis using *in vivo* FRET experiments.

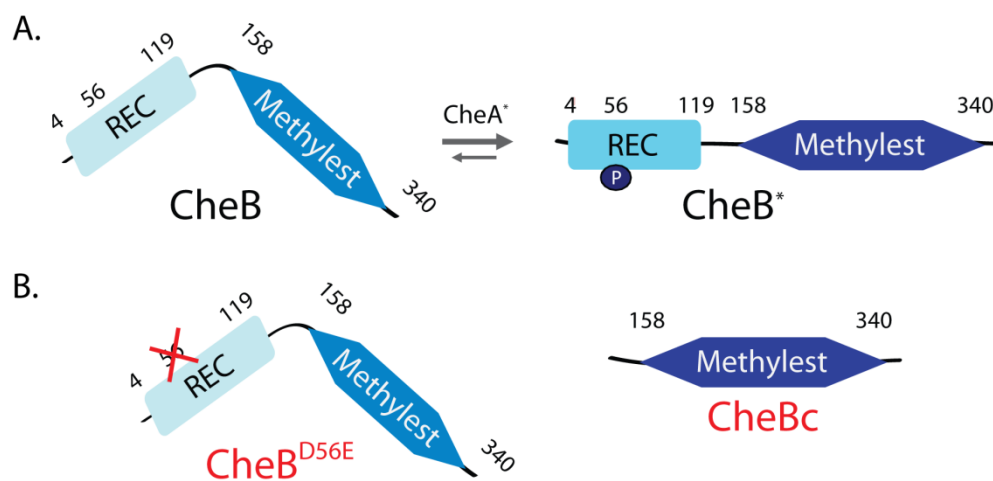


Figure C.1. Domain structure of CheB. (A) CheB has two domains: regulatory (REC) N-terminal domain and methylesterase C-terminal domain. CheB changes its conformation from inactive (*left*) to active (*right*) after phosphorylation of D56 in the REC domain. (B) *Left*: CheB^{D56E} is a mutant of CheB, in which the phosphorylation position in the REC domain is mutated and therefore it cannot be phosphorylated. *Right*: CheBc is a truncated mutant of CheB, which lacks the N-terminal REC domain.

C.2. Shape of $F(a)$ in *E. coli* with disrupted phosphorylation feedback, characterized using temporal step stimuli

We characterized the shape of $F(a)$ in $\Delta cheB$ cells expressing either wild type CheB, CheB^{D56E} or CheBc from an *L*-arabinose-inducible plasmid (see Materials and methods). To measure the rate of change of the methylation level $\frac{dm}{dt} = F(a)$, as a function of the kinase activity a , we used a recently developed experimental strategy, which employs simple step addition and removal of chemoeffector²⁸⁷. During adaptation to a step change, in the input ligand concentration, $[L]$, is constant and the methylation level of the receptors, m , changes. Thus, using the model of reference²⁶⁰, the kinase activity a can be expressed as $\frac{da}{dt} = \frac{da}{dm} \frac{dm}{dt} = \alpha Na(1-a) \frac{dm}{dt}$, where N is the number of ligand binding units in a receptor-kinase complex ($N=6$ for *E. coli*²⁶⁰), and α is the free energy change per methylation increment ($\alpha \approx 2 k_B T$ for *E. coli*²⁶⁰). Therefore $F(a)$ can be expressed as $F(a) = (da/dt)/(aNa(1-a))$, and $F(a)$ can be reconstructed experimentally as described below²⁴².

We applied saturating (1 or 5 mM) steps of α -methyl-aspartate (MeAsp) to wild type cells and $\Delta cheB$ cells expressing either wild type CheB, CheB^{D56E} or CheBc. We allowed the cells to adapt completely after both addition and removal of MeAsp. We converted the FRET response into units of kinase activity a (see Materials and methods), and calculated da/dt at each point in time by fitting a line to a segment of 31 data points centered at the current time and extracting the slope (the number of data points is consistent with the analysis performed in reference²⁸⁷). Using the constants $N=6$ and $\alpha=2 k_B T$ determined previously^{226,260}, we calculated $\frac{dm}{dt} = F(a)$ and plotted the values as a function of a (Figure C.2A).

In the wild type cells, we observed a steep linear decrease of $F(a)$ at large a , similar to that observed previously in wild type *E. coli* using exponential ramp stimuli^{226,287} (Figure C.2A, B). Wild type cells in our measurements had a steady-state kinase activity $a_0 = 0.38$, whereas those in the experiments of reference²²⁶ had $a_0 = 0.33$. The difference in the steady-state kinase activity and the position in which the kink in $F(a)$ occurs ($a \approx 0.62$ in our measurements and $a \approx 0.74$ in the measurements of

Appendix C

reference ²²⁶) might be explained by variations in the expression level of CheB, e.g. due to subtle differences in the growth conditions ¹⁹².

In the $\Delta cheB$ cells expressing CheB from *L*-arabinose-inducible plasmid we controlled a_0 by changing the amount of inducer. By increasing CheB expression level using higher concentration of inducer, we achieved lower a_0 due to the higher demethylation rate at constant expression of CheR. Figure C.2A *left* shows a comparison between wild type *E. coli*, and $\Delta cheB$ *E. coli*, complemented with CheB using 0.0001% and 0.0003% *L*-arabinose as an inducer, having a_0 of 0.38, 0.46 and 0.34 respectively. For all three strains we could not fit the entire $F(a)$ using the Michaelis-Menten model of equation (1) with a constant maximal rate of demethylation V_B : a steep linear decrease occurs at $a \approx 0.62$, 0.60 and 0.72 respectively (Figure C.2A *left*).

We measured the shape of $F(a)$ in $\Delta cheB$ cells expressing CheBc and CheB^{D56E}. Cells expressing CheBc with a kinase activity of 0.48 and 0.42 (CheB expression induced with 0.0001% and 0.0003% *L*-arabinose respectively) can be fit by equation (1) with a constant V_B (Figure C.2A *middle*). $\Delta cheB$ cells expressing CheB^{D56E} (0.00015% *L*-arabinose, $a_0 = 0.42$), as well as cells, expressing larger amounts of CheBc (0.001% *L*-arabinose, $a_0 = 0.20$), both showed a kink in $F(a)$ at $a \approx 0.85$ (Figure C.2A *right* and *middle*) and thus cannot be fit by equation (1) with a constant V_B .

C.3. Shape of $F(a)$ in *E. coli* with disrupted phosphorylation feedback, characterized using exponential ramp stimuli

We confirmed the difference in the shape of $F(a)$ in cells that express CheBc by measuring the constant kinase a_c activity reached during temporal exponential ramp stimulation, and converting the obtained gradient sensitivity curve to $F(a)$ (see Chapter 3). Figure C.2B shows the results obtained using FRET measurements in CheBc-expressing cells (0.0003% *L*-arabinose, $a_0 = 0.42$), in comparison to results from the same type of measurements in wild type cells taken from reference ²²⁶. Similar to the result from the analysis of the response to a step, $F(a)$ for CheBc-expressing cells could be fit by equation (1) with a constant V_B (Figure C.2B). Thus, we conclude that the phosphorylation-dependent feedback in wild

Effect of CheB phosphorylation feedback on adaptation kinetics

type *E. coli*, which is disrupted in CheBc cells, affects the shape of $F(a)$ at high levels of kinase activity.

Table C.1 summarizes the fitted parameters for the Michaelis-Menten model (equation (1)) for all strains shown of Figure C.2A and B.

| Strain | a_0 | V_R (s ⁻¹) | V_B (s ⁻¹) | K_R | K_B | a in which a kink in $F(a)$ occurs |
|----------------------|-------|-----------------------------|-----------------------------|-------|-------|--------------------------------------|
| WT | 0.38 | 0.008 | 0.007 | 0.32 | 0.30 | 0.62 |
| CheB | 0.46 | 0.008 | 0.006 | 0.32 | 0.30 | 0.72 |
| CheB | 0.34 | 0.008 | 0.008 | 0.32 | 0.30 | 0.60 |
| CheBc | 0.46 | 0.008 | 0.007 | 0.32 | 0.08 | - |
| CheBc | 0.42 | 0.008 | 0.006 | 0.32 | 0.08 | - |
| CheBc | 0.20 | 0.008 | 0.008 | 0.32 | 0.08 | 0.85 |
| CheB ^{D56E} | 0.42 | 0.014 | 0.009 | 0.32 | 0.01 | 0.85 |
| WT | 0.33 | 0.010 | 0.013 | 0.32 | 0.30 | 0.74 |
| CheBc | 0.42 | 0.014 | 0.013 | 0.32 | 0.08 | - |

Figure C.1. Fitted parameters to the data shown on Figure C.2, using equation (1). Fits to equation (1) end at the value of a , shown in the last column. CheB, CheB and CheB^{D56E} refer to $\Delta cheB$ strains, expressing the respective CheB variant from a plasmid. The last two rows refer to the strains, used in Figure C2.B. Note that the fits are not well constrained.

Appendix C

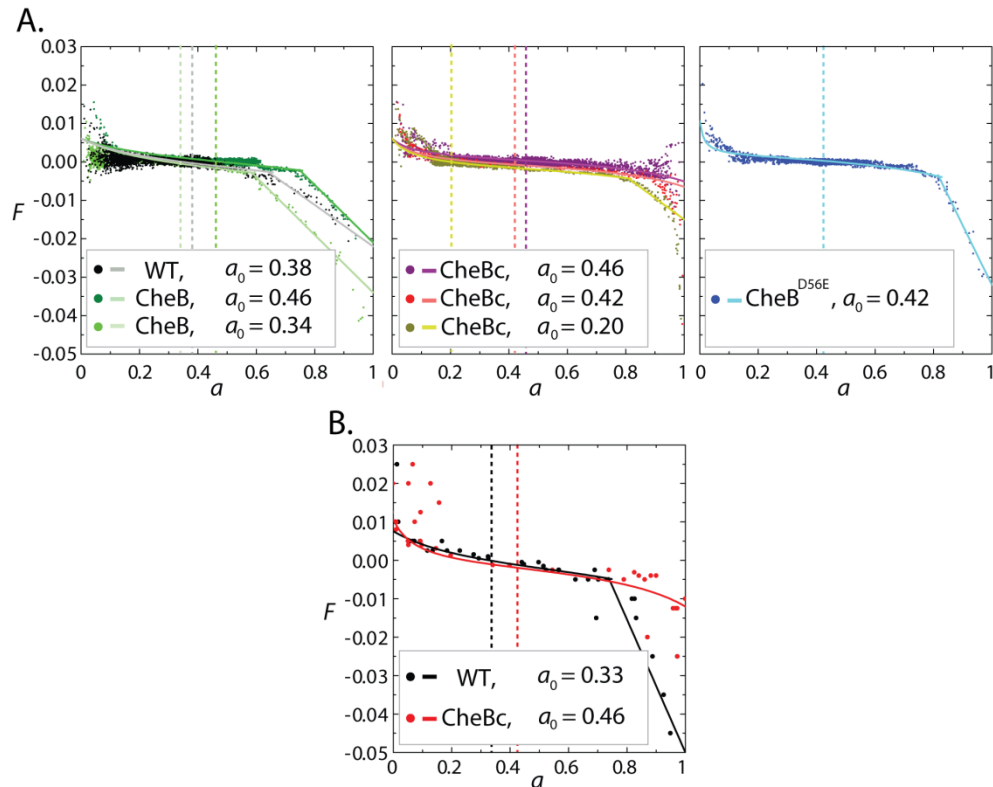


Figure C.2. Effect of disruption of the phosphorylation-dependent feedback in bacterial chemotaxis on the shape of $F(a)$. The shape of $F(a)$ was determined using step stimuli (A), and exponential ramp stimuli (B). Results for strains expressing CheB (left), CheBc (middle), and CheB^{D56E} (right) are shown with the name of the CheB variant within each panel. Different colors of each panel in (A) correspond to different induction levels of the CheB variants, leading to different a_0 (indicated within the key of each panel, and with a vertical dashed line). The result for wild type (WT) *E. coli* is shown for comparison in the left panel of (A). The data for wild type *E. coli* shown in (B) is taken from reference ²²⁶. Fits with Michaelis-Menten model are shown for all strains with parameters, indicated in Table C.1. Linear fits are shown for the segments that could not be fit by the Michaelis-Menten model.

C.4. Discussion

A fundamental question in systems biology is how the topologies of biochemical networks affect their input-output relationships, *i.e.* transfer functions^{22,280}. We have shown an example of how *in vivo* FRET measurements can be used to elucidate the effect of topological changes in a biological signaling circuit. We used *E. coli* cells in which the chemotaxis system was genetically altered in such a way that removes the phosphorylation feedback on the methylesterase activity of CheB, *i.e.* cells, expressing a CheB mutant with a disrupted phosphorylation site (CheB^{D56E}) or lacking the phospho-receiver domain (CheBc). Using FRET measurements coupled with temporal step and exponential ramp stimuli, we demonstrated that in contrast to wild type cells, the transfer function $F(a)$ of CheBc-expressing cells with a steady-state kinase activity > 0.40 can be fit by Michaelis-Menten kinetics with a constant maximal rate of demethylation V_B (Figure C.2). CheBc-expressing cells with lower steady-state kinase activity ($a_0 = 0.20$), as well as CheB^{D56E}-expressing cells (with $a_0 = 0.42$) showed a steep linear decrease of $F(a)$ at high values of a similar to that observed in wild type cells (Figure C.2). CheBc has a much lower methylesterase activity than the phosphorylated intact CheB⁶⁹, and CheB^{D56E} cannot be activated by phosphorylation, implying that the higher activity of CheB induced by the phosphorylation feedback leads to the nonlinearity of $F(a)$ at large a .

The mechanistic event that determines the characteristic kink of $F(a)$ in wild type *E. coli* cells is still to be identified. Clausznitzer et al.⁵⁶ propose that the fast demethylation at high a could be due to cooperative action of two phosphorylated CheB (CheB-P) molecules: one CheB-P molecule could bind to a C-terminal tether of a chemoreceptor to allosterically activate the group of surrounding chemoreceptors, while another CheB-P molecule demethylates the activated chemoreceptors^{23,56}. A plausible explanation of the effect of the phosphorylation feedback is that the phosphorylation of CheB affects its association with the receptor-kinase clusters, and its proximity with its substrate (chemoreceptors) and phosphorylation enzyme (CheA) respectively. Imaging of fluorescently labelled CheB and CheBc showed that they both localize to the cell poles but CheBc localizes to a

Appendix C

lesser extent ²⁰. The dynamic localization of CheB with the receptor clusters can be further assessed using superresolution microscopy imaging in living cells, such as photoactivated localization microscopy (PALM) ⁹⁴.

A form of CheB similar to CheBc might exist in wild type bacteria. Simms et al. ²³³ reported that purified CheB from *S. typhimurium* contains two forms of CheB: the intact full-length product of *cheB* gene and a C-terminal fragment, starting at residue 147 of the intact CheB, *i.e.* containing the full methylesterase domain (see Figure C.1). The C-terminal fragment could be a result of proteolysis of the full-length CheB, which is a common mechanism for turning on enzymatic activities ^{53,108,187}. This fragment itself could target to the receptor-kinase clusters ²⁰. The ratio of full-length to C-terminal fragment of CheB in wild type cells could affect the shape of $F(a)$ and the position, in which the steep decrease of $F(a)$ occurs.

Another explanation could lie in the cell-to-cell variation of the expression of CheR and CheB in *E. coli* cells (Ned Wingreen, personal communication; Michael Salazar's B.Sc. thesis, 2010). The net rate of receptor methylation is proportional to the methylation rate of CheR, v_R , minus the demethylation rate of CheB, v_B , assuming for simplicity linear, rather than Michaelis-Menten kinetics, and that only the inactive receptors are methylated and only the active receptors are demethylated:

$$F(a) = \frac{dm}{dt} = v_R(1 - a) - v_B a, \quad (2)$$

where v_R and v_B are the rate constants of CheR and CheB respectively. For temporal exponential ramp stimuli with ramp rates r , it has been shown that $F(a) = r/\alpha$, where α is the free energy added to the free energy of the receptor-kinase complex per methylation increment ²²⁶ (see Chapter 3). Thus, for equation (2) it follows that

$$a_c = \frac{v_R}{v_R + v_B} - \frac{1}{\alpha(v_R + v_B)} r, \quad (3)$$

where a_c is the constant kinase activity reached during ramp stimulation. Assuming that for individual cells v_R and v_B are constants, for $0 < a < 1$ the gradient-sensitivity curve $a_c(r)$ is a straight line, and it becomes constant when a_c reaches 0 or 1, its minimum and maximum respectively. However, different cells in a bacterial population produce different amounts of CheR and CheB: it has been reported that the steady-state distributions of protein concentration in a population of cells generally follow a gamma

Effect of CheB phosphorylation feedback on adaptation kinetics

distribution as a consequence of the stochastic protein expression⁸⁵. The v_R and v_B values will be large for cells producing large amounts of CheR and CheB, therefore the slope of $a_c(r)$ will be shallow (see equation (3)), and a_c will reach 1 at large values of r . The opposite will be observed for cells expressing small amounts of CheR and CheB, therefore a_c will reach 1 at small values of r . Salazar et al. simulated the effects of such variability in adaptation kinetics at the population level, and found that the cell-to-cell variations in v_R and v_B values can lead to the sharp nonlinearity in $a_c(r)$ observed experimentally²²⁶ even if $F(a)$ for each cell is a linear function of a . The shape of the feedback transfer function $F(a)$ can be obtained from the $a_c(r)$ curve by inverting $a_c(r) = F^{-1}(r/\alpha)$ ^{226,260}, thus the strong nonlinearity in $a_c(r)$ could explain the kink in $F(a)$. This hypothesis could be tested experimentally by observing the shape of $F(a)$ in single cells.

Future developments of sensitive physiological assays comparable to these FRET measurements of the chemotaxis pathway, for other biological signaling systems could shed light on the function of regulatory motifs that can be genetically altered. Considering biological sensory systems as modular structures, knowledge of the function of particular cellular regulatory motifs could accelerate the development of bioengineering and synthetic biology^{51,200}.

C.5. Materials and methods

Bacterial strains and plasmids

The FRET donor-acceptor pair (CheZ-CFP and CheY-YFP) was expressed from a plasmid pVS88²⁴⁰ in a $\Delta cheB \Delta cheY \Delta cheZ$ *E. coli* RP437 (*i.e.* VS124, gift from Victor Sourjik). Wild type *cheB*, non-phosphorylatable mutant *cheB*^{D56E} and truncated mutant *cheBc* (containing the last 612 base pairs of *cheB*) were cloned into pBAD33 vector using SacI and XbaI cloning sites (pVS91, pVS97 and pVS112 plasmids respectively, gifts from Victor Sourjik). The expressions of wild type CheB, CheB^{D56E} and CheBc were induced with *L*-arabinose (the percentages of *L*-arabinose that we used for the different plasmids and experiments are indicated in the text). Wild type

Appendix C

E. coli refers to $\Delta cheY \Delta cheZ$ *E. coli* RP437 expressing CheY-YFP and CheZ-CFP from pVS88.

In vivo FRET measurements and data analysis

Cells were grown at 250 rpm at 33.5°C in a rotary shaker to mid-exponential phase ($OD_{600} \sim 0.5$) in tryptone broth (TB; 1% tryptone, 0.5% NaCl, pH 7.0) supplemented with appropriate antibiotics and inducers. Cells were harvested by centrifugation, washed twice and resuspended in motility buffer (10 mM potassium phosphate, 0.1 mM EDTA, 1 μ M methionine, 10 mM lactic acid, pH 7), and stored at 4°C for 1-5 h prior to the experiment.

FRET microscopy of bacterial populations was performed as described previously²⁴². Cells, attached to a poly-*L*-lysine-coated coverslip, were situated at the top face of a bespoke flow cell²⁷, and kept under constant flow of motility buffer, generated by a peristaltic pump (Rainin Dynamax RP1) or syringe pump (Harvard Apparatus, PHD2000). Exponential ramp stimuli were generated by mixing a concentrated solution of the chemoeffector α -methyl-*DL*-aspartate (MeAsp; Sigma Aldrich) and motility buffer by a fluid mixer of a type described before^{35,226} (see Chapter 3). An upright microscope (Nikon FN1) was equipped with an oil immersion objective (Nikon CFI Plan Fluor, 40x/1.3). The sample was illuminated by a metal halide arc lamp with closed-loop feedback (EXFO X-Cite *exacte*) through an excitation bandpass filter (Semrock, FF01-438/24-25) and a dichroic mirror (Semrock, FF458-Di01). The epifluorescent emission was split by a second dichroic mirror (Semrock, FF509-FDi01) into donor (cyan, C) and acceptor (yellow, Y) channels and collected by two photon-counting photomultipliers (Hamamatsu H7422P-40) through bandpass filters (Semrock FF01-483/32 and FF01-542/27 for the C and Y channels, respectively). Detector output from the two channels were recorded through a data acquisition card (National Instruments) installed on a PC running custom-written software.

After background subtraction, the ratio between the acceptor and donor channel ($R = Y/C$) was used to compute the change in FRET efficiency upon stimulation (see Chapter 3). Under the conditions of the

Effect of CheB phosphorylation feedback on adaptation kinetics

measurements, $\Delta FRET \sim \Delta R$, and we expressed $\Delta FRET$ for simplicity in arbitrary units of ΔR .

$\Delta FRET(t)$ was normalized to the absolute magnitude of the response to addition of a saturating attractant step, $|\Delta FRET_{sat}^{add}|$, to compensate for variations due to different absolute levels of signal between the experiments. The steady-state kinase activity, a_0 , was calculated as $a_0 = \frac{|\Delta FRET_{sat}^{add}|}{|\Delta FRET_{sat}^{add}| + |\Delta FRET_{sat}^{remove}|}$, where $\Delta FRET_{sat}^{remove}$ is the response to removal of a saturating attractant step after the cells have been completely adapted. The kinase activity $a = a_0 + \Delta a$, where $\Delta a = \frac{\Delta FRET}{|\Delta FRET_{sat}^{add}| + |\Delta FRET_{sat}^{remove}|}$ is the kinase activity change in every point in time.

C.6. Acknowledgements

The work with CheB mutant strain was performed by Quyen Le, a M.Sc. student (University of Twente).

Appendix C

Bibliography

- 1 Adler, J., Chemoreceptors in bacteria. *Science* **166** (3913), 1588 (1969).
- 2 Adler, J., Chemotaxis in bacteria. *Science* **153** (3737), 708 (1966).
- 3 Adler, J., A method for measuring chemotaxis and use of the method to determine optimum conditions for chemotaxis by *Escherichia coli*. *J Gen Microbiol* **74** (1), 77 (1973).
- 4 Adler, J., Hazelbauer, G. L., and Dahl, M. M., Chemotaxis toward sugars in *Escherichia coli*. *J Bacteriol* **115** (3), 824 (1973).
- 5 Adler, J. et al., Osmotaxis in *Escherichia coli*. *Cold Spring Harb Symp Quant Biol* **53 Pt 1**, 19 (1988).
- 6 Adler, J. and Shi, W., Galvanotaxis in bacteria. *Cold Spring Harb Symp Quant Biol* **53 Pt 1**, 23 (1988).
- 7 Ahmed, T., Shimizu, T. S., and Stocker, R., Bacterial chemotaxis in linear and nonlinear steady microfluidic gradients. *Nano Lett* **10** (9), 3379 (2010).
- 8 Ahmed, T., Shimizu, T. S., and Stocker, R., Microfluidics for bacterial chemotaxis. *Integr Biol (Camb)* **2** (11-12), 604 (2010).
- 9 Ahmed, T. and Stocker, R., Experimental verification of the behavioral foundation of bacterial transport parameters using microfluidics. *Biophys J* **95** (9), 4481 (2008).
- 10 Alexander, R. P., Lowenthal, A. C., Harshey, R. M., and Ottemann, K. M., CheV: CheW-like coupling proteins at the core of the chemotaxis signaling network. *Trends Microbiol* **18** (11), 494 (2010).
- 11 Alexandre, G. and Zhulin, I. B., More than one way to sense chemicals. *J Bacteriol* **183** (16), 4681 (2001).
- 12 Alon, U., Surette, M. G., Barkai, N., and Leibler, S., Robustness in bacterial chemotaxis. *Nature* **397** (6715), 168 (1999).
- 13 Amann, E., Ochs, B., and Abel, K. J., Tightly regulated *tac* promoter vectors useful for the expression of unfused and fused proteins in *Escherichia coli*. *Gene* **69** (2), 301 (1988).
- 14 Amin, D. N. and Hazelbauer, G. L., Chemoreceptors in signalling complexes: shifted conformation and asymmetric coupling. *Mol Microbiol* **78** (5), 1313 (2010).
- 15 Anand, G. S., Goudreau, P. N., and Stock, A. M., Activation of methylesterase CheB: evidence of a dual role for the regulatory domain. *Biochemistry* **37** (40), 14038 (1998).

Bibliography

- 16 Anderson, J. D., Galvanotaxis of slime mold. *J Gen Physiol* **35** (1), 1 (1951).
- 17 Aoki, K., Kiyokawa, E., Nakamura, T., and Matsuda, M., Visualization of growth signal transduction cascades in living cells with genetically encoded probes based on Forster resonance energy transfer. *Philos Trans R Soc Lond B Biol Sci* **363** (1500), 2143 (2008).
- 18 Asquith, R. S. and Hirst, L., The photochemical degradation of cystine in aqueous solution in the presence of air. *Biochimica et biophysica acta* **184** (2), 345 (1969).
- 19 Baker, M. D., Wolanin, P. M., and Stock, J. B., Systems biology of bacterial chemotaxis. *Curr Opin Microbiol* **9** (2), 187 (2006).
- 20 Banno, S., Shiomi, D., Homma, M., and Kawagishi, I., Targeting of the chemotaxis methyltransferase/deamidase CheB to the polar receptor-kinase cluster in an *Escherichia coli* cell. *Mol Microbiol* **53** (4), 1051 (2004).
- 21 Baptist, E. W. and Kredich, N. M., Regulation of L-cystine transport in *Salmonella typhimurium*. *Journal of bacteriology* **131** (1), 111 (1977).
- 22 Barkai, N. and Leibler, S., Robustness in simple biochemical networks. *Nature* **387** (6636), 913 (1997).
- 23 Barnakov, A. N., Barnakova, L. A., and Hazelbauer, G. L., Allosteric enhancement of adaptational demethylation by a carboxyl-terminal sequence on chemoreceptors. *J Biol Chem* **277** (44), 42151 (2002).
- 24 Barnakov, A. N., Barnakova, L. A., and Hazelbauer, G. L., Efficient adaptational demethylation of chemoreceptors requires the same enzyme-docking site as efficient methylation. *Proceedings of the National Academy of Sciences of the United States of America* **96** (19), 10667 (1999).
- 25 Berg, H. C., How to track bacteria. *Rev Sci Instrum* **42** (6), 868 (1971).
- 26 Berg, H. C., The rotary motor of bacterial flagella. *Annu Rev Biochem* **72**, 19 (2003).
- 27 Berg, H. C. and Block, S. M., A miniature flow cell designed for rapid exchange of media under high-power microscope objectives. *J Gen Microbiol* **130** (11), 2915 (1984).
- 28 Bespalov, V. A., Zhulin, I. B., and Taylor, B. L., Behavioral responses of *Escherichia coli* to changes in redox potential. *Proc Natl Acad Sci U S A* **93** (19), 10084 (1996).
- 29 Bhalla, U. S. and Iyengar, R., Emergent properties of networks of biological signaling pathways. *Science* **283** (5400), 381 (1999).
- 30 Bibikov, S. I., Miller, A. C., Gosink, K. K., and Parkinson, J. S., Methylation-independent aerotaxis mediated by the *Escherichia coli* Aer protein. *J Bacteriol* **186** (12), 3730 (2004).

Bibliography

- 31 Bibikov, S.I., Biran, R., Rudd, K.E., and Parkinson, J.S., A signal transducer
for aerotaxis in *Escherichia coli*. *J Bacteriol* **179** (12), 4075 (1997).
- 32 Biemann, H. P. and Koshland, D. E., Jr., Aspartate receptors of *Escherichia*
coli and *Salmonella typhimurium* bind ligand with negative and half-of-the-
sites cooperativity. *Biochemistry* **33** (3), 629 (1994).
- 33 Blat, Y. and Eisenbach, M., Phosphorylation-dependent binding of the
chemotaxis signal molecule CheY to its phosphatase, CheZ. *Biochemistry* **33**
(4), 902 (1994).
- 34 Blattner, F. R. et al., The complete genome sequence of *Escherichia coli* K-12.
Science **277** (5331), 1453 (1997).
- 35 Block, S. M., Segall, J. E., and Berg, H. C., Adaptation kinetics in bacterial
chemotaxis. *J Bacteriol* **154** (1), 312 (1983).
- 36 Block, S. M., Segall, J. E., and Berg, H. C., Impulse responses in bacterial
chemotaxis. *Cell* **31** (1), 215 (1982).
- 37 Booth, I. R., The regulation of intracellular pH in bacteria. *Novartis Found*
Symp **221**, 19 (1999).
- 38 Boucher, Y. and Baptiste, E., Revisiting the concept of lineage in
prokaryotes: a phylogenetic perspective. *Bioessays* **31** (5), 526 (2009).
- 39 Boukhvalova, M. S., Dahlquist, F. W., and Stewart, R. C., CheW binding
interactions with CheA and Tar. Importance for chemotaxis signaling in
Escherichia coli. *J Biol Chem* **277** (25), 22251 (2002).
- 40 Bourret, R. B., Receiver domain structure and function in response
regulator proteins. *Curr Opin Microbiol* **13** (2), 142 (2010).
- 41 Bray, D., Levin, M. D., and Lipkow, K., The chemotactic behavior of
computer-based surrogate bacteria. *Curr Biol* **17** (1), 12 (2007).
- 42 Bray, D., Levin, M. D., and Morton-Firth, C. J., Receptor clustering as a
cellular mechanism to control sensitivity. *Nature* **393** (6680), 85 (1998).
- 43 Briegel, A. et al., Bacterial chemoreceptor arrays are hexagonally packed
trimers of receptor dimers networked by rings of kinase and coupling
proteins. *Proc Natl Acad Sci U S A* **109** (10), 3766 (2012).
- 44 Burkart, M., Toguchi, A., and Harshey, R. M., The chemotaxis system, but
not chemotaxis, is essential for swarming motility in *Escherichia coli*. *Proc*
Natl Acad Sci U S A **95** (5), 2568 (1998).
- 45 Burrows, L. L., *Pseudomonas aeruginosa* twitching motility: type IV pili in
action. *Annu Rev Microbiol* **66**, 493 (2012).
- 46 Butler, J. D. et al., Amino acid composition and N-terminal sequence of
purified cystine binding protein of *Escherichia coli*. *Life Sci* **52** (14), 1209
(1993).

Bibliography

- 47 Butler, S. M. and Camilli, A., Both chemotaxis and net motility greatly
influence the infectivity of *Vibrio cholerae*. *Proc Natl Acad Sci U S A* **101** (14),
5018 (2004).
- 48 Caetano-Anolles, G. et al., Role of Motility and Chemotaxis in Efficiency of
Nodulation by *Rhizobium meliloti*. *Plant Physiol* **86** (4), 1228 (1988).
- 49 Cardozo, M. J., Massazza, D. A., Parkinson, J. S., and Studdert, C. A.,
Disruption of chemoreceptor signalling arrays by high levels of CheW, the
receptor-kinase coupling protein. *Mol Microbiol* **75** (5), 1171 (2010).
- 50 Celani, A. and Vergassola, M., Bacterial strategies for chemotaxis response.
Proc Natl Acad Sci U S A **107** (4), 1391 (2010).
- 51 Chau, A. H. et al., Designing synthetic regulatory networks capable of self-
organizing cell polarization. *Cell* **151** (2), 320 (2012).
- 52 Cheng, S. Y. et al., A hydrogel-based microfluidic device for the studies of
directed cell migration. *Lab Chip* **7** (6), 763 (2007).
- 53 Chock, P. B., Rhee, S. G., and Stadtman, E. R., Interconvertible enzyme
cascades in cellular regulation. *Annu Rev Biochem* **49**, 813 (1980).
- 54 Christian, F. et al., Small molecule AKAP-protein kinase A (PKA)
interaction disruptors that activate PKA interfere with compartmentalized
cAMP signaling in cardiac myocytes. *J Biol Chem* **286** (11), 9079 (2011).
- 55 Clark, D. A. and Grant, L. C., The bacterial chemotactic response reflects a
compromise between transient and steady-state behavior. *Proc Natl Acad
Sci U S A* **102** (26), 9150 (2005).
- 56 Clausznitzer, D. et al., Chemotactic response and adaptation dynamics in
Escherichia coli. *PLoS Comput Biol* **6** (5), e1000784 (2010).
- 57 Cohan, F. M., What are bacterial species? *Annu Rev Microbiol* **56**, 457 (2002).
- 58 Cohen-Saidon, C. et al., Dynamics and variability of ERK2 response to EGF
in individual living cells. *Mol Cell* **36** (5), 885 (2009).
- 59 Corazziari, E. S., Intestinal mucus barrier in normal and inflamed colon. *J
Pediatr Gastroenterol Nutr* **48 Suppl 2**, S54 (2009).
- 60 Corfield, A. P. et al., Mucins and mucosal protection in the gastrointestinal
tract: new prospects for mucins in the pathology of gastrointestinal disease.
Gut **47** (4), 589 (2000).
- 61 Danino, T. et al., In Vivo Gene Expression Dynamics of Tumor-Targeted
Bacteria. *ACS Synth Biol* **1** (10), 465 (2012).
- 62 Datsenko, K. A. and Wanner, B. L., One-step inactivation of chromosomal
genes in *Escherichia coli* K-12 using PCR products. *Proc Natl Acad Sci U S A*
97 (12), 6640 (2000).
- 63 de Gennes, P. G., Chemotaxis: the role of internal delays. *Eur Biophys J* **33**
(8), 691 (2004).

Bibliography

- 64 de Hemptinne, A., Marrannes, R., and Vanheel, B., Influence of organic
acids on intracellular pH. *Am J Physiol* **245** (3), C178 (1983).
- 65 de Pina, K. et al., Purification and characterization of the periplasmic
nickel-binding protein NikA of *Escherichia coli* K12. *Eur J Biochem* **227** (3),
857 (1995).
- 66 DeFranco, A. L., Parkinson, J. S., and Koshland, D. E., Jr., Functional
homology of chemotaxis genes in *Escherichia coli* and *Salmonella*
typhimurium. *J Bacteriol* **139** (1), 107 (1979).
- 67 Delong, E. F., Frankel, R. B., and Bazylynski, D. A., Multiple evolutionary
origins of magnetotaxis in bacteria. *Science* **259** (5096), 803 (1993).
- 68 Diehn, B., Phototaxis and sensory transduction in *Euglena*. *Science* **181**
(4104), 1009 (1973).
- 69 Djordjevic, S. et al., Structural basis for methylesterase CheB regulation by
a phosphorylation-activated domain. *Proc Natl Acad Sci U S A* **95** (4), 1381
(1998).
- 70 Doran, J. W. and Linn, D. M., Bacteriological quality of runoff water from
pastureland. *Appl Environ Microbiol* **37** (5), 985 (1979).
- 71 Drews, G., Contributions of Theodor Wilhelm Engelmann on phototaxis,
chemotaxis, and photosynthesis. *Photosynth Res* **83** (1), 25 (2005).
- 72 Duke, T. A. and Bray, D., Heightened sensitivity of a lattice of membrane
receptors. *Proc Natl Acad Sci U S A* **96** (18), 10104 (1999).
- 73 Ehrenberg, L., Harmsringdahl, M., Fedorcsak, I., and Granath, F., Kinetics
of the Copper-Catalyzed and Iron-Catalyzed Oxidation of Cysteine by
Dioxygen. *Acta Chem Scand* **43** (2), 177 (1989).
- 74 Eisenbach, M., Sperm chemotaxis. *Rev Reprod* **4** (1), 56 (1999).
- 75 Eisenbach, M. and Adler, J., Bacterial cell envelopes with functional
flagella. *J Biol Chem* **256** (16), 8807 (1981).
- 76 Endres, R. G. et al., Variable sizes of *Escherichia coli* chemoreceptor
signaling teams. *Mol Syst Biol* **4**, 211 (2008).
- 77 Englert, D. L., Adase, C. A., Jayaraman, A., and Manson, M. D., Repellent
taxis in response to nickel ion requires neither Ni²⁺ transport nor the
periplasmic NikA binding protein. *J Bacteriol* **192** (10), 2633 (2010).
- 78 Erbse, A. H. and Falke, J. J., The core signaling proteins of bacterial
chemotaxis assemble to form an ultrastable complex. *Biochemistry* **48** (29),
6975 (2009).
- 79 Escobar-Paramo, P. et al., Decreasing the effects of horizontal gene transfer
on bacterial phylogeny: the *Escherichia coli* case study. *Mol Phylogenet Evol*
30 (1), 243 (2004).

Bibliography

- 80 Falke, J. J., Cooperativity between bacterial chemotaxis receptors. *Proc Natl Acad Sci U S A* **99** (10), 6530 (2002).
- 81 Fechner, G. T., *Elements of Psychophysics*. (Holt, Rinehart and Winston, New York, 1966).
- 82 Feng, X., Baumgartner, J. W., and Hazelbauer, G. L., High- and low-abundance chemoreceptors in *Escherichia coli*: differential activities associated with closely related cytoplasmic domains. *Journal of bacteriology* **179** (21), 6714 (1997).
- 83 Feng, X., Lilly, A. A., and Hazelbauer, G. L., Enhanced function conferred on low-abundance chemoreceptor Trg by a methyltransferase-docking site. *Journal of bacteriology* **181** (10), 3164 (1999).
- 84 Frank, V., Koler, M., Furst, S., and Vaknin, A., The physical and functional thermal sensitivity of bacterial chemoreceptors. *J Mol Biol* **411** (3), 554 (2011).
- 85 Friedman, N., Cai, L., and Xie, X. S., Linking stochastic dynamics to population distribution: an analytical framework of gene expression. *Phys Rev Lett* **97** (16), 168302 (2006).
- 86 Frye, J. et al., Identification of new flagellar genes of *Salmonella enterica* serovar Typhimurium. *J Bacteriol* **188** (6), 2233 (2006).
- 87 Gao, R., Mack, T. R., and Stock, A. M., Bacterial response regulators: versatile regulatory strategies from common domains. *Trends Biochem Sci* **32** (5), 225 (2007).
- 88 Gao, R. and Stock, A. M., Molecular strategies for phosphorylation-mediated regulation of response regulator activity. *Curr Opin Microbiol* **13** (2), 160 (2010).
- 89 Garcia-Quintanilla, M. and Casadesus, J., Virulence plasmid interchange between strains ATCC 14028, LT2, and SL1344 of *Salmonella enterica* serovar Typhimurium. *Plasmid* **65** (2), 169 (2011).
- 90 Gegner, J. A., Graham, D. R., Roth, A. F., and Dahlquist, F. W., Assembly of an MCP receptor, CheW, and kinase CheA complex in the bacterial chemotaxis signal transduction pathway. *Cell* **70** (6), 975 (1992).
- 91 Goentoro, L. and Kirschner, M. W., Evidence that fold-change, and not absolute level, of beta-catenin dictates Wnt signaling. *Mol Cell* **36** (5), 872 (2009).
- 92 Goentoro, L., Shoval, O., Kirschner, M. W., and Alon, U., The incoherent feedforward loop can provide fold-change detection in gene regulation. *Mol Cell* **36** (5), 894 (2009).

Bibliography

- 93 Gosink, K. K., Buron-Barral, M. C., and Parkinson, J. S., Signaling
interactions between the aerotaxis transducer Aer and heterologous
chemoreceptors in *Escherichia coli*. *J Bacteriol* **188** (10), 3487 (2006).
- 94 Greenfield, D. et al., Self-organization of the *Escherichia coli* chemotaxis
network imaged with super-resolution light microscopy. *PLoS Biol* **7** (6),
e1000137 (2009).
- 95 Guttman, D. S. and Dykhuizen, D. E., Clonal divergence in *Escherichia coli*
as a result of recombination, not mutation. *Science* **266** (5189), 1380 (1994).
- 96 Guzman, L. M., Belin, D., Carson, M. J., and Beckwith, J., Tight regulation,
modulation, and high-level expression by vectors containing the arabinose
PBAD promoter. *J Bacteriol* **177** (14), 4121 (1995).
- 97 Hader, D. P., Lebert, M., and Richter, P., Gravitaxis and graviperception in
Euglena gracilis. *Adv Space Res* **21** (8-9), 1277 (1998).
- 98 Hart, Y., Mayo, A. E., Shoval, O., and Alon, U., Comparing apples and
oranges: fold-change detection of multiple simultaneous inputs. *PLoS One*
8 (3), e57455 (2013).
- 99 Hartwell, L. H., Hopfield, J. J., Leibler, S., and Murray, A. W., From
molecular to modular cell biology. *Nature* **402** (6761 Suppl), C47 (1999).
- 100 Hayashi, T. et al., Complete genome sequence of enterohemorrhagic
Escherichia coli O157:H7 and genomic comparison with a laboratory strain
K-12. *DNA Res* **8** (1), 11 (2001).
- 101 Hazelbauer, G. L., Bacterial chemotaxis: the early years of molecular
studies. *Annu Rev Microbiol* **66**, 285 (2012).
- 102 Hazelbauer, G. L., Falke, J. J., and Parkinson, J. S., Bacterial chemoreceptors:
high-performance signaling in networked arrays. *Trends Biochem Sci* **33** (1),
9 (2008).
- 103 Hedblom, M. L. and Adler, J., Chemotactic response of *Escherichia coli* to
chemically synthesized amino acids. *J Bacteriol* **155** (3), 1463 (1983).
- 104 Hobman, J. L., Penn, C. W., and Pallen, M. J., Laboratory strains of
Escherichia coli: model citizens or deceitful delinquents growing old
disgracefully? *Mol Microbiol* **64** (4), 881 (2007).
- 105 Hong, C. B., Fontana, D. R., and Poff, K. L., Thermotaxis of *Dictyostelium*
discoideum amoebae and its possible role in pseudoplasmodial thermotaxis.
Proc Natl Acad Sci U S A **80** (18), 5646 (1983).
- 106 Hood, M. A. and Ness, G. E., Survival of *Vibrio cholerae* and *Escherichia coli*
in estuarine waters and sediments. *Appl Environ Microbiol* **43** (3), 578 (1982).
- 107 Ibarra, R. U., Edwards, J. S., and Palsson, B. O., *Escherichia coli* K-12
undergoes adaptive evolution to achieve in silico predicted optimal
growth. *Nature* **420** (6912), 186 (2002).

Bibliography

- ¹⁰⁸ Inoue, M., Kishimoto, A., Takai, Y., and Nishizuka, Y., Studies on a cyclic nucleotide-independent protein kinase and its proenzyme in mammalian tissues. II. Proenzyme and its activation by calcium-dependent protease from rat brain. *J Biol Chem* **252** (21), 7610 (1977).
- ¹⁰⁹ Insall, R. and Andrew, N., Chemotaxis in *Dictyostelium*: how to walk straight using parallel pathways. *Curr Opin Microbiol* **10** (6), 578 (2007).
- ¹¹⁰ Ishii, S., Ksoll, W. B., Hicks, R. E., and Sadowsky, M. J., Presence and growth of naturalized *Escherichia coli* in temperate soils from Lake Superior watersheds. *Appl Environ Microbiol* **72** (1), 612 (2006).
- ¹¹¹ Ishii, T., Itoh, K., Sato, H., and Bannai, S., Oxidative stress-inducible proteins in macrophages. *Free Radic Res* **31** (4), 351 (1999).
- ¹¹² Jarvik, T., Smillie, C., Groisman, E. A., and Ochman, H., Short-term signatures of evolutionary change in the *Salmonella enterica* serovar typhimurium 14028 genome. *J Bacteriol* **192** (2), 560 (2010).
- ¹¹³ Jiang, L., Ouyang, Q., and Tu, Y., A mechanism for precision-sensing via a gradient-sensing pathway: a model of *Escherichia coli* thermotaxis. *Biophys J* **97** (1), 74 (2009).
- ¹¹⁴ Jiang, L., Ouyang, Q., and Tu, Y., Quantitative modeling of *Escherichia coli* chemotactic motion in environments varying in space and time. *PLoS Comput Biol* **6** (4), e1000735 (2010).
- ¹¹⁵ Kalinin, Y. V., Jiang, L., Tu, Y., and Wu, M., Logarithmic sensing in *Escherichia coli* bacterial chemotaxis. *Biophys J* **96** (6), 2439 (2009).
- ¹¹⁶ Karatan, E., Saulmon, M. M., Bunn, M. W., and Ordal, G. W., Phosphorylation of the response regulator CheV is required for adaptation to attractants during *Bacillus subtilis* chemotaxis. *J Biol Chem* **276** (47), 43618 (2001).
- ¹¹⁷ Karsten, V. et al., Chemotaxis activation of peritoneal murine macrophages induced by the transplantation of free and encapsulated pancreatic rat islets. *Cell Transplant* **9** (1), 39 (2000).
- ¹¹⁸ Kelln, R. A. and Lintott, L. G., Construction of plasmid-free derivatives of *Salmonella typhimurium* LT2 using temperature-sensitive mutants of pKZ1 for displacement of the resident plasmid, pSLT. *Mol Gen Genet* **222** (2-3), 438 (1990).
- ¹¹⁹ Kentner, D., Thiem, S., Hildenbeutel, M., and Sourjik, V., Determinants of chemoreceptor cluster formation in *Escherichia coli*. *Mol Microbiol* **61** (2), 407 (2006).
- ¹²⁰ Keymer, J. E. et al., Chemosensing in *Escherichia coli*: two regimes of two-state receptors. *Proc Natl Acad Sci U S A* **103** (6), 1786 (2006).

Bibliography

- 121 Khan, S., Macnab, R. M., DeFranco, A. L., and Koshland, D. E., Jr.,
Inversion of a behavioral response in bacterial chemotaxis: explanation at
the molecular level. *Proc Natl Acad Sci U S A* **75** (9), 4150 (1978).
- 122 Khan, S., Spudich, J. L., McCray, J. A., and Trentham, D. R., Chemotactic
signal integration in bacteria. *Proc Natl Acad Sci U S A* **92** (21), 9757 (1995).
- 123 Kihara, M., Homma, M., Kutsukake, K., and Macnab, R. M., Flagellar
switch of *Salmonella typhimurium*: gene sequences and deduced protein
sequences. *J Bacteriol* **171** (6), 3247 (1989).
- 124 Kihara, M. and Macnab, R. M., Cytoplasmic pH mediates pH taxis and
weak-acid repellent taxis of bacteria. *Journal of bacteriology* **145** (3), 1209
(1981).
- 125 Kim, Y. S. and Ho, S. B., Intestinal goblet cells and mucins in health and
disease: recent insights and progress. *Curr Gastroenterol Rep* **12** (5), 319
(2010).
- 126 Kirschner, M. and Gerhart, J., Evolvability. *Proc Natl Acad Sci U S A* **95** (15),
8420 (1998).
- 127 Kollmann, M. et al., Design principles of a bacterial signalling network.
Nature **438** (7067), 504 (2005).
- 128 Kollmann, M. and Sourjik, V., In silico biology: from simulation to
understanding. *Curr Biol* **17** (4), R132 (2007).
- 129 Kondoh, H., Ball, C. B., and Adler, J., Identification of a methyl-accepting
chemotaxis protein for the ribose and galactose chemoreceptors of
Escherichia coli. *Proc Natl Acad Sci U S A* **76** (1), 260 (1979).
- 130 Kosek, M., Bern, C., and Guerrant, R. L., The global burden of diarrhoeal
disease, as estimated from studies published between 1992 and 2000. *Bull
World Health Organ* **81** (3), 197 (2003).
- 131 Krikos, A. et al., Chimeric chemosensory transducers of *Escherichia coli*.
Proc Natl Acad Sci U S A **82** (5), 1326 (1985).
- 132 Lan, G., Schulmeister, S., Sourjik, V., and Tu, Y., Adapt locally and act
globally: strategy to maintain high chemoreceptor sensitivity in complex
environments. *Mol Syst Biol* **7**, 475 (2011).
- 133 Lane, M. C. et al., Uropathogenic *Escherichia coli* strains generally lack
functional Trg and Tap chemoreceptors found in the majority of *E. coli*
strains strictly residing in the gut. *J Bacteriol* **188** (15), 5618 (2006).
- 134 Larremore, D. B., Shew, W. L., Ott, E., and Restrepo, J. G., Effects of
network topology, transmission delays, and refractoriness on the response
of coupled excitable systems to a stochastic stimulus. *Chaos* **21** (2), 025117
(2011).

Bibliography

- 135 Laughlin, S., A simple coding procedure enhances a neuron's information
capacity. *Z Naturforsch C* **36** (9-10), 910 (1981).
- 136 Lawrence, J. G. and Ochman, H., Molecular archaeology of the *Escherichia*
coli genome. *Proc Natl Acad Sci U S A* **95** (16), 9413 (1998).
- 137 Lazova, M. D. et al., Response rescaling in bacterial chemotaxis. *Proc Natl*
Acad Sci U S A **108** (33), 13870 (2011).
- 138 Lazova, M. D., Butler, M. T., Shimizu, T. S., and Harshey, R. M., *Salmonella*
chemoreceptors McpB and McpC mediate a repellent response to L-cystine:
a potential mechanism to avoid oxidative conditions. *Mol Microbiol* **84** (4),
697 (2012).
- 139 Lecointre, G., Rachdi, L., Darlu, P., and Denamur, E., *Escherichia coli*
molecular phylogeny using the incongruence length difference test. *Mol*
Biol Evol **15** (12), 1685 (1998).
- 140 Lertsethtakarn, P., Ottemann, K. M., and Hendrixson, D. R., Motility and
chemotaxis in *Campylobacter* and *Helicobacter*. *Annu Rev Microbiol* **65**, 389
(2011).
- 141 Letunic, I., Doerks, T., and Bork, P., SMART 7: recent updates to the
protein domain annotation resource. *Nucleic Acids Res* **40** (Database issue),
D302 (2012).
- 142 Levring, T. B. et al., Activated human CD4 T cells express transporters for
both cysteine and cystine. *Sci Rep* **2**, 266 (2012).
- 143 Li, J., Li, G., and Weis, R. M., The serine chemoreceptor from *Escherichia coli*
is methylated through an inter-dimer process. *Biochemistry* **36** (39), 11851
(1997).
- 144 Li, M. and Hazelbauer, G. L., The carboxyl-terminal linker is important for
chemoreceptor function. *Mol Microbiol* **60** (2), 469 (2006).
- 145 Linden, S. K., Florin, T. H., and McGuckin, M. A., Mucin dynamics in
intestinal bacterial infection. *PLoS One* **3** (12), e3952 (2008).
- 146 Liu, J. D. and Parkinson, J. S., Role of CheW protein in coupling membrane
receptors to the intracellular signaling system of bacterial chemotaxis. *Proc*
Natl Acad Sci U S A **86** (22), 8703 (1989).
- 147 Liu, J. et al., Molecular architecture of chemoreceptor arrays revealed by
cryoelectron tomography of *Escherichia coli* minicells. *Proc Natl Acad Sci U S*
A **109** (23), E1481 (2012).
- 148 Lovdok, L. et al., Role of translational coupling in robustness of bacterial
chemotaxis pathway. *PLoS Biol* **7** (8), e1000171 (2009).
- 149 Lowenthal, A. C. et al., A fixed-time diffusion analysis method determines
that the three *cheV* genes of *Helicobacter pylori* differentially affect motility.
Microbiology **155** (Pt 4), 1181 (2009).

Bibliography

- 150 Luo, C. et al., Genome sequencing of environmental *Escherichia coli*
expands understanding of the ecology and speciation of the model
bacterial species. *Proc Natl Acad Sci U S A* **108** (17), 7200 (2011).
- 151 Lux, R. et al., Coupling the phosphotransferase system and the methyl-
accepting chemotaxis protein-dependent chemotaxis signaling pathways
of *Escherichia coli*. *Proc Natl Acad Sci U S A* **92** (25), 11583 (1995).
- 152 Macnab, R. M., How bacteria assemble flagella. *Annu Rev Microbiol* **57**, 77
(2003).
- 153 Maddock, J. R. and Shapiro, L., Polar location of the chemoreceptor
complex in the *Escherichia coli* cell. *Science* **259** (5102), 1717 (1993).
- 154 Manson, M. D., Blank, V., Brade, G., and Higgins, C. F., Peptide
chemotaxis in *E. coli* involves the Tap signal transducer and the dipeptide
permease. *Nature* **321** (6067), 253 (1986).
- 155 Manson, M. D., Boos, W., Bassford, P. J., Jr., and Rasmussen, B. A.,
Dependence of maltose transport and chemotaxis on the amount of
maltose-binding protein. *J Biol Chem* **260** (17), 9727 (1985).
- 156 Mao, H., Cremer, P. S., and Manson, M. D., A sensitive, versatile
microfluidic assay for bacterial chemotaxis. *Proc Natl Acad Sci U S A* **100** (9),
5449 (2003).
- 157 Marcos, Fu, H. C., Powers, T. R., and Stocker, R., Bacterial rheotaxis. *Proc
Natl Acad Sci U S A* **109** (13), 4780 (2012).
- 158 Masson, J. B. et al., Noninvasive inference of the molecular chemotactic
response using bacterial trajectories. *Proc Natl Acad Sci U S A* **109** (5), 1802
(2012).
- 159 Mazel, D., Dychinco, B., Webb, V. A., and Davies, J., Antibiotic resistance
in the ECOR collection: integrons and identification of a novel *aad* gene.
Antimicrob Agents Chemother **44** (6), 1568 (2000).
- 160 McClelland, M. et al., Complete genome sequence of *Salmonella enterica*
serovar Typhimurium LT2. *Nature* **413** (6858), 852 (2001).
- 161 McEvoy, M. M., Bren, A., Eisenbach, M., and Dahlquist, F. W.,
Identification of the binding interfaces on CheY for two of its targets, the
phosphatase CheZ and the flagellar switch protein *fliM*. *J Mol Biol* **289** (5),
1423 (1999).
- 162 McGhie, E. J. et al., *Salmonella* takes control: effector-driven manipulation
of the host. *Curr Opin Microbiol* **12** (1), 117 (2009).
- 163 Meir, Y. et al., Precision and kinetics of adaptation in bacterial chemotaxis.
Biophys J **99** (9), 2766 (2010).
- 164 Meister, M., Lowe, G., and Berg, H. C., The proton flux through the
bacterial flagellar motor. *Cell* **49** (5), 643 (1987).

Bibliography

- 165 Mello, B. A. and Tu, Y., An allosteric model for heterogeneous receptor
complexes: Understanding bacterial chemotaxis responses to multiple
stimuli. *Proc Natl Acad Sci U S A* **102** (48), 17354 (2005).
- 166 Mello, B. A. and Tu, Y., Effects of adaptation in maintaining high
sensitivity over a wide range of backgrounds for *Escherichia coli* chemotaxis.
Biophys J **92** (7), 2329 (2007).
- 167 Mello, B. A. and Tu, Y., Perfect and near-perfect adaptation in a model of
bacterial chemotaxis. *Biophys J* **84** (5), 2943 (2003).
- 168 Mello, B. A. and Tu, Y., Quantitative modeling of sensitivity in bacterial
chemotaxis: the role of coupling among different chemoreceptor species.
Proc Natl Acad Sci U S A **100** (14), 8223 (2003).
- 169 Melton, T. et al., Chemotaxis of *Salmonella typhimurium* to amino acids and
some sugars. *Journal of bacteriology* **133** (2), 708 (1978).
- 170 Mesibov, R. and Adler, J., Chemotaxis toward amino acids in *Escherichia*
coli. *J Bacteriol* **112** (1), 315 (1972).
- 171 Mesibov, R., Ordal, G. W., and Adler, J., The range of attractant
concentrations for bacterial chemotaxis and the threshold and size of
response over this range. Weber law and related phenomena. *J Gen Physiol*
62 (2), 203 (1973).
- 172 Miki, K. and Clapham, D. E., Rheotaxis guides Mammalian sperm. *Curr*
Biol **23** (6), 443 (2013).
- 173 Milkman, R., Electrophoretic variation in *Escherichia coli* from natural
sources. *Science* **182** (4116), 1024 (1973).
- 174 Milkman, R. and Crawford, I. P., Clustered third-base substitutions among
wild strains of *Escherichia coli*. *Science* **221** (4608), 378 (1983).
- 175 Miller, L. D., Russell, M. H., and Alexandre, G., Diversity in bacterial
chemotactic responses and niche adaptation. *Adv Appl Microbiol* **66**, 53
(2009).
- 176 Monod, J., Wyman, J., and Changeux, J. P., On the Nature of Allosteric
Transitions: A Plausible Model. *J Mol Biol* **12**, 88 (1965).
- 177 Mori, I., Genetics of chemotaxis and thermotaxis in the nematode
Caenorhabditis elegans. *Annu Rev Genet* **33**, 399 (1999).
- 178 Morrison, D. K. and Davis, R. J., Regulation of MAP kinase signaling
modules by scaffold proteins in mammals. *Annu Rev Cell Dev Biol* **19**, 91
(2003).
- 179 Moszer, I., The complete genome of *Bacillus subtilis*: from sequence
annotation to data management and analysis. *FEBS Lett* **430** (1-2), 28 (1998).

Bibliography

- 180 Mowbray, S. L. and Koshland, D. E., Jr., Additive and independent
responses in a single receptor: aspartate and maltose stimuli on the tar
protein. *Cell* **50** (2), 171 (1987).
- 181 Nakamura, T. and Matsuda, M., In vivo imaging of signal transduction
cascades with probes based on Forster Resonance Energy Transfer (FRET).
Curr Protoc Cell Biol **Chapter 14**, Unit 14 10 (2009).
- 182 Nelson, K. and Selander, R. K., Evolutionary genetics of the proline
permease gene (*putP*) and the control region of the proline utilization
operon in populations of *Salmonella* and *Escherichia coli*. *J Bacteriol* **174** (21),
6886 (1992).
- 183 Nelson, K., Wang, F. S., Boyd, E. F., and Selander, R. K., Size and sequence
polymorphism in the isocitrate dehydrogenase kinase/phosphatase gene
(*aceK*) and flanking regions in *Salmonella enterica* and *Escherichia coli*.
Genetics **147** (4), 1509 (1997).
- 184 Nelson, K., Whittam, T. S., and Selander, R. K., Nucleotide polymorphism
and evolution in the glyceraldehyde-3-phosphate dehydrogenase gene
(*gapA*) in natural populations of *Salmonella* and *Escherichia coli*. *Proc Natl
Acad Sci U S A* **88** (15), 6667 (1991).
- 185 Neumann, S., Grosse, K., and Sourjik, V., Chemotactic signaling via
carbohydrate phosphotransferase systems in *Escherichia coli*. *Proc Natl Acad
Sci U S A* **109** (30), 12159 (2012).
- 186 Neumann, S., Hansen, C. H., Wingreen, N. S., and Sourjik, V., Differences
in signalling by directly and indirectly binding ligands in bacterial
chemotaxis. *EMBO J* **29** (20), 3484 (2010).
- 187 Neurath, H. and Walsh, K. A., Role of proteolytic enzymes in biological
regulation (a review). *Proc Natl Acad Sci U S A* **73** (11), 3825 (1976).
- 188 O'Toole, R. et al., The chemotactic response of *Vibrio anguillarum* to fish
intestinal mucus is mediated by a combination of multiple mucus
components. *J Bacteriol* **181** (14), 4308 (1999).
- 189 Ochman, H. and Selander, R. K., Standard reference strains of *Escherichia
coli* from natural populations. *J Bacteriol* **157** (2), 690 (1984).
- 190 Ochman, H. and Wilson, A. C., Evolution in bacteria: evidence for a
universal substitution rate in cellular genomes. *J Mol Evol* **26** (1-2), 74 (1987).
- 191 Ohtsu, I. et al., The L-cysteine/L-cystine shuttle system provides reducing
equivalents to the periplasm in *Escherichia coli*. *The Journal of biological
chemistry* **285** (23), 17479 (2010).
- 192 Oleksiuk, O. et al., Thermal robustness of signaling in bacterial chemotaxis.
Cell **145** (2), 312 (2011).

Bibliography

- 193 Olszewski, J., Haehnel, M., Taguchi, M., and Liao, J. C., Zebrafish larvae
exhibit rheotaxis and can escape a continuous suction source using their
lateral line. *PLoS One* **7** (5), e36661 (2012).
- 194 Parkinson, J. S., Ames, P., and Studdert, C. A., Collaborative signaling by
bacterial chemoreceptors. *Curr Opin Microbiol* **8** (2), 116 (2005).
- 195 Parkinson, J. S. and Houts, S. E., Isolation and behavior of *Escherichia coli*
deletion mutants lacking chemotaxis functions. *J Bacteriol* **151** (1), 106
(1982).
- 196 Pineda-Molina, E. et al., Evidence for chemoreceptors with bimodular
ligand-binding regions harboring two signal-binding sites. *Proc Natl Acad
Sci U S A* **109** (46), 18926 (2012).
- 197 Pittman, M. S., Goodwin, M., and Kelly, D. J., Chemotaxis in the human
gastric pathogen *Helicobacter pylori*: different roles for CheW and the three
CheV paralogues, and evidence for CheV2 phosphorylation. *Microbiology*
147 (Pt 9), 2493 (2001).
- 198 Poelwijk, F. J., de Vos, M. G., and Tans, S. J., Tradeoffs and optimality in
the evolution of gene regulation. *Cell* **146** (3), 462 (2011).
- 199 Prinz, H., Hill coefficients, dose-response curves and allosteric
mechanisms. *J Chem Biol* **3** (1), 37 (2010).
- 200 Rafelski, S. M. and Marshall, W. F., Building the cell: design principles of
cellular architecture. *Nat Rev Mol Cell Biol* **9** (8), 593 (2008).
- 201 Rao, C. V., Kirby, J. R., and Arkin, A. P., Design and diversity in bacterial
chemotaxis: a comparative study in *Escherichia coli* and *Bacillus subtilis*.
PLoS Biol **2** (2), E49 (2004).
- 202 Rebbapragada, A. et al., The Aer protein and the serine chemoreceptor Tsr
independently sense intracellular energy levels and transduce oxygen,
redox, and energy signals for *Escherichia coli* behavior. *Proc Natl Acad Sci U
S A* **94** (20), 10541 (1997).
- 203 Rieke, F. and Rudd, M. E., The challenges natural images pose for visual
adaptation. *Neuron* **64** (5), 605 (2009).
- 204 Rosario, M. M., Fredrick, K. L., Ordal, G. W., and Helmann, J. D.,
Chemotaxis in *Bacillus subtilis* requires either of two functionally
redundant CheW homologs. *J Bacteriol* **176** (9), 2736 (1994).
- 205 Rosner, J. L. and Storz, G., Regulation of bacterial responses to oxidative
stress. *Curr Top Cell Regul* **35**, 163 (1997).
- 206 Russo, A. F. and Koshland, D. E., Jr., Identification of the tip-encoded
receptor in bacterial sensing. *J Bacteriol* **165** (1), 276 (1986).

Bibliography

- 207 Sabariego, R. et al., Fluorescence resonance energy transfer-based assay
for characterization of hepatitis C virus NS3-4A protease activity in live
cells. *Antimicrob Agents Chemother* **53** (2), 728 (2009).
- 208 Salis, H. M., The ribosome binding site calculator. *Methods Enzymol* **498**, 19.
209 Salis, H. M., Mirsky, E. A., and Voigt, C. A., Automated design of synthetic
ribosome binding sites to control protein expression. *Nat Biotechnol* **27** (10),
946 (2009).
- 210 Salman, H. and Libchaber, A., A concentration-dependent switch in the
bacterial response to temperature. *Nat Cell Biol* **9** (9), 1098 (2007).
- 211 Sanders, D. A., Mendez, B., and Koshland, D. E., Jr., Role of the CheW
protein in bacterial chemotaxis: overexpression is equivalent to absence. *J*
Bacteriol **171** (11), 6271 (1989).
- 212 Sano, G. et al., Flagella facilitate escape of *Salmonella* from oncotic
macrophages. *Journal of bacteriology* **189** (22), 8224 (2007).
- 213 Schmidt, J. et al., The *Pseudomonas aeruginosa* chemotaxis
methyltransferase CheR1 impacts on bacterial surface sampling. *PLoS One*
6 (3), e18184 (2011).
- 214 Schnitzer, M. J., Block, S. M., Berg, H. C., and Purcell, E. M., Strategies for
chemotaxis. *Symp Soc Gen Microbiol* **46**, 15 (1990).
- 215 Schulmeister, S., Grosse, K., and Sourjik, V., Effects of receptor
modification and temperature on dynamics of sensory complexes in
Escherichia coli chemotaxis. *BMC Microbiol* **11**, 222 (2011).
- 216 Schulmeister, S. et al., Protein exchange dynamics at chemoreceptor
clusters in *Escherichia coli*. *Proc Natl Acad Sci U S A* **105** (17), 6403 (2008).
- 217 Schultz, J., Milpetz, F., Bork, P., and Ponting, C. P., SMART, a simple
modular architecture research tool: identification of signaling domains.
Proc Natl Acad Sci U S A **95** (11), 5857 (1998).
- 218 Segall, J. E., Block, S. M., and Berg, H. C., Temporal comparisons in
bacterial chemotaxis. *Proc Natl Acad Sci U S A* **83** (23), 8987 (1986).
- 219 Selander, R. K. et al., Methods of multilocus enzyme electrophoresis for
bacterial population genetics and systematics. *Appl Environ Microbiol* **51** (5),
873 (1986).
- 220 Selander, R. K. and Levin, B. R., Genetic diversity and structure in
Escherichia coli populations. *Science* **210** (4469), 545 (1980).
- 221 Seymour, J. R., Simo, R., Ahmed, T., and Stocker, R., Chemoattraction to
dimethylsulfoniopropionate throughout the marine microbial food web.
Science **329** (5989), 342 (2010).

Bibliography

- 222 Shimizu, T. S., Aksenov, S. V., and Bray, D., A spatially extended stochastic
model of the bacterial chemotaxis signalling pathway. *J Mol Biol* **329** (2),
291 (2003).
- 223 Shimizu, T. S. and Bray, D., Modelling the bacterial chemotaxis receptor
complex. *Novartis Found Symp* **247**, 162 (2002).
- 224 Shimizu, T. S., Delalez, N., Pichler, K., and Berg, H. C., Monitoring
bacterial chemotaxis by using bioluminescence resonance energy transfer:
absence of feedback from the flagellar motors. *Proc Natl Acad Sci U S A* **103**
(7), 2093 (2006).
- 225 Shimizu, T. S. et al., Molecular model of a lattice of signalling proteins
involved in bacterial chemotaxis. *Nat Cell Biol* **2** (11), 792 (2000).
- 226 Shimizu, T. S., Tu, Y., and Berg, H. C., A modular gradient-sensing
network for chemotaxis in *Escherichia coli* revealed by responses to time-
varying stimuli. *Mol Syst Biol* **6**, 382 (2010).
- 227 Shinohara, K. and Kilpatrick, M., The stability of cystine in acid solution.
Journal of Biological Chemistry **105**, 241 (1934).
- 228 Shiomi, D., Okumura, H., Homma, M., and Kawagishi, I., The aspartate
chemoreceptor Tar is effectively methylated by binding to the
methyltransferase mainly through hydrophobic interaction. *Mol Microbiol*
36 (1), 132 (2000).
- 229 Shiomi, D., Zhulin, I. B., Homma, M., and Kawagishi, I., Dual recognition
of the bacterial chemoreceptor by chemotaxis-specific domains of the CheR
methyltransferase. *J Biol Chem* **277** (44), 42325 (2002).
- 230 Shoal, O., Alon, U., and Sontag, E., Symmetry invariance for adapting
biological systems. *SIAM J Appl Dyn Syst* **In Press** (2011).
- 231 Shoal, O. et al., Fold-change detection and scalar symmetry of sensory
input fields. *Proc Natl Acad Sci U S A* **107** (36), 15995 (2010).
- 232 Si, G., Wu, T., Ouyang, Q., and Tu, Y., Pathway-based mean-field model
for *Escherichia coli* chemotaxis. *Phys Rev Lett* **109** (4), 048101 (2012).
- 233 Simms, S. A., Keane, M. G., and Stock, J., Multiple forms of the CheB
methyltransferase in bacterial chemosensing. *J Biol Chem* **260** (18), 10161 (1985).
- 234 Slivka, P. F. and Falke, J. J., Isolated bacterial chemosensory array
possesses quasi- and ultrastable components: functional links between
array stability, cooperativity, and order. *Biochemistry* **51** (51), 10218 (2012).
- 235 Slonczewski, J. L., Macnab, R. M., Alger, J. R., and Castle, A. M., Effects of
pH and repellent tactic stimuli on protein methylation levels in *Escherichia*
coli. *J Bacteriol* **152** (1), 384 (1982).
- 236 Smith, J. M., Smith, N. H., O'Rourke, M., and Spratt, B. G., How clonal are
bacteria? *Proc Natl Acad Sci U S A* **90** (10), 4384 (1993).

Bibliography

- 237 Sourjik, V., Receptor clustering and signal processing in *E. coli* chemotaxis. *Trends Microbiol* **12** (12), 569 (2004).
- 238 Sourjik, V. and Armitage, J. P., Spatial organization in bacterial chemotaxis. *EMBO J* **29** (16), 2724 (2010).
- 239 Sourjik, V. and Berg, H. C., Binding of the *Escherichia coli* response regulator CheY to its target measured in vivo by fluorescence resonance energy transfer. *Proc Natl Acad Sci U S A* **99** (20), 12669 (2002).
- 240 Sourjik, V. and Berg, H. C., Functional interactions between receptors in bacterial chemotaxis. *Nature* **428** (6981), 437 (2004).
- 241 Sourjik, V. and Berg, H. C., Receptor sensitivity in bacterial chemotaxis. *Proc Natl Acad Sci U S A* **99** (1), 123 (2002).
- 242 Sourjik, V., Vaknin, A., Shimizu, T. S., and Berg, H. C., In vivo measurement by FRET of pathway activity in bacterial chemotaxis. *Methods Enzymol* **423**, 365 (2007).
- 243 Sourjik, V. and Wingreen, N. S., Responding to chemical gradients: bacterial chemotaxis. *Curr Opin Cell Biol* **24** (2), 262 (2012).
- 244 Soyer, O. S., The promise of evolutionary systems biology: lessons from bacterial chemotaxis. *Sci Signal* **3** (128), pe23 (2010).
- 245 Steuer, R., Waldherr, S., Sourjik, V., and Kollmann, M., Robust signal processing in living cells. *PLoS Comput Biol* **7** (11), e1002218 (2011).
- 246 Stevens, R., Stevems, L., and Price, N.C., The stabilities of various thiol compounds used in protein purifications. *Biochemical Education* **11**, 70 (1983).
- 247 Stevens, S. S., Neural events and the psychophysical law. *Science* **170** (3962), 1043 (1970).
- 248 Stock, J., Sensitivity, cooperativity and gain in chemotaxis signal transduction. *Trends Microbiol* **7** (1), 1 (1999).
- 249 Stock, J. B., Maderis, A. M., and Koshland, D. E., Jr., Bacterial chemotaxis in the absence of receptor carboxymethylation. *Cell* **27** (1 Pt 2), 37 (1981).
- 250 Stock, J., Kersulis, G., and Koshland, D. E., Jr., Neither methylating nor demethylating enzymes are required for bacterial chemotaxis. *Cell* **42** (2), 683 (1985).
- 251 Stocker, R., Reverse and flick: Hybrid locomotion in bacteria. *Proc Natl Acad Sci U S A* **108** (7), 2635 (2011).
- 252 Stocker, R. et al., Rapid chemotactic response enables marine bacteria to exploit ephemeral microscale nutrient patches. *Proc Natl Acad Sci U S A* **105** (11), 4209 (2008).
- 253 Swidsinski, A. et al., Comparative study of the intestinal mucus barrier in normal and inflamed colon. *Gut* **56** (3), 343 (2007).

Bibliography

- 254 Szurmant, H. and Ordal, G. W., Diversity in chemotaxis mechanisms
among the bacteria and archaea. *Microbiol Mol Biol Rev* **68** (2), 301 (2004).
- 255 Taylor, B. L., Zhulin, I. B., and Johnson, M. S., Aerotaxis and other energy-
sensing behavior in bacteria. *Annu Rev Microbiol* **53**, 103 (1999).
- 256 Tenaillon, O., Skurnik, D., Picard, B., and Denamur, E., The population
genetics of commensal *Escherichia coli*. *Nat Rev Microbiol* **8** (3), 207 (2010).
- 257 Tomb, J. F. et al., The complete genome sequence of the gastric pathogen
Helicobacter pylori. *Nature* **388** (6642), 539 (1997).
- 258 Trevors, J. T. and Basaraba, J., Toxicity of benzoquinone and hydroquinone
in short-term bacterial bioassays. *Bull Environ Contam Toxicol* **25** (4), 672
(1980).
- 259 Tso, W. W. and Adler, J., Negative chemotaxis in *Escherichia coli*. *J Bacteriol*
118 (2), 560 (1974).
- 260 Tu, Y., Shimizu, T. S., and Berg, H. C., Modeling the chemotactic response
of *Escherichia coli* to time-varying stimuli. *Proc Natl Acad Sci U S A* **105** (39),
14855 (2008).
- 261 Turner, L., Ryu, W. S., and Berg, H. C., Real-time imaging of fluorescent
flagellar filaments. *J Bacteriol* **182** (10), 2793 (2000).
- 262 Ulrich, L. E. and Zhulin, I. B., The MiST2 database: a comprehensive
genomics resource on microbial signal transduction. *Nucleic Acids Res* **38**
(Database issue), D401 (2010).
- 263 Vaknin, A. and Berg, H. C., Osmotic stress mechanically perturbs
chemoreceptors in *Escherichia coli*. *Proc Natl Acad Sci U S A* **103** (3), 592
(2006).
- 264 Vaknin, A. and Berg, H. C., Physical responses of bacterial chemoreceptors.
J Mol Biol **366** (5), 1416 (2007).
- 265 Vladimirov, N. and Sourjik, V., Chemotaxis: how bacteria use memory.
Biol Chem **390** (11), 1097 (2009).
- 266 Wadhams, G. H. and Armitage, J. P., Making sense of it all: bacterial
chemotaxis. *Nat Rev Mol Cell Biol* **5** (12), 1024 (2004).
- 267 Wang, Q. et al., Uncovering a large set of genes that affect surface motility
in *Salmonella enterica* serovar Typhimurium. *J Bacteriol* **188** (22), 7981 (2006).
- 268 Wang, Q. et al., Sensing wetness: a new role for the bacterial flagellum.
Embo J **24** (11), 2034 (2005).
- 269 Ward, S., Chemotaxis by the nematode *Caenorhabditis elegans*: identification
of attractants and analysis of the response by use of mutants. *Proc Natl
Acad Sci U S A* **70** (3), 817 (1973).

Bibliography

- 270 Watts, K. J., Ma, Q., Johnson, M. S., and Taylor, B. L., Interactions between
the PAS and HAMP domains of the *Escherichia coli* aerotaxis receptor Aer. *J*
Bacteriol **186** (21), 7440 (2004).
- 271 Weerasuriya, S., Schneider, B. M., and Manson, M. D., Chimeric
chemoreceptors in *Escherichia coli*: signaling properties of Tar-Tap and Tap-
Tar hybrids. *Journal of bacteriology* **180** (4), 914 (1998).
- 272 Whitesides, G. M. et al., Soft lithography in biology and biochemistry.
Annu Rev Biomed Eng **3**, 335 (2001).
- 273 Whitman, W. B., Coleman, D. C., and Wiebe, W. J., Prokaryotes: the unseen
majority. *Proc Natl Acad Sci U S A* **95** (12), 6578 (1998).
- 274 Winfield, M. D. and Groisman, E. A., Role of nonhost environments in the
lifestyles of *Salmonella* and *Escherichia coli*. *Appl Environ Microbiol* **69** (7),
3687 (2003).
- 275 Wirth, T. et al., Sex and virulence in *Escherichia coli*: an evolutionary
perspective. *Mol Microbiol* **60** (5), 1136 (2006).
- 276 Wolfe, A. J. and Berg, H. C., Migration of bacteria in semisolid agar. *Proc*
Natl Acad Sci U S A **86** (18), 6973 (1989).
- 277 Wouters, F. S. and Bastiaens, P. I., Imaging protein-protein interactions by
fluorescence resonance energy transfer (FRET) microscopy. *Curr Protoc Cell*
Biol **Chapter 17**, Unit 17 1 (2001).
- 278 Wright, S., Walia, B., Parkinson, J. S., and Khan, S., Differential activation
of *Escherichia coli* chemoreceptors by blue-light stimuli. *J Bacteriol* **188** (11),
3962 (2006).
- 279 Wu, K. et al., Attractant binding induces distinct structural changes to the
polar and lateral signaling clusters in *Bacillus subtilis* chemotaxis. *J Biol*
Chem **286** (4), 2587 (2011).
- 280 Wu, Y., Zhang, X., Yu, J., and Ouyang, Q., Identification of a topological
characteristic responsible for the biological robustness of regulatory
networks. *PLoS Comput Biol* **5** (7), e1000442 (2009).
- 281 Wuichet, K. and Zhulin, I. B., Origins and diversification of a complex
signal transduction system in prokaryotes. *Sci Signal* **3** (128), ra50 (2010).
- 282 Yamamoto, K. and Imae, Y., Cloning and characterization of the *Salmonella*
typhimurium-specific chemoreceptor Tcp for taxis to citrate and from
phenol. *Proc Natl Acad Sci U S A* **90** (1), 217 (1993).
- 283 Yamamoto, Y. et al., NEXAFS studies on the structure of perfluoroalkyl
carbonic acid Langmuir Blodgett films. *J Synchrotron Radiat* **6** (Pt 3), 796
(1999).

Bibliography

- 284 Yang, Y. and Sourjik, V., Opposite responses by different chemoreceptors
set a tunable preference point in *Escherichia coli* pH taxis. *Mol Microbiol*
(2012).
- 285 Yaryura, P. M. et al., Assessment of the role of chemotaxis and biofilm
formation as requirements for colonization of roots and seeds of soybean
plants by *Bacillus amyloliquefaciens* BNM339. *Curr Microbiol* **56** (6), 625
(2008).
- 286 Yi, T. M., Huang, Y., Simon, M. I., and Doyle, J., Robust perfect adaptation
in bacterial chemotaxis through integral feedback control. *Proc Natl Acad*
Sci U S A **97** (9), 4649 (2000).
- 287 Yuan, J. and Berg, H. C., Characterization of the adaptation module of the
signaling network in bacterial chemotaxis by measurement of step
responses. *Biophys J* **103** (6), L31 (2012).
- 288 Yuan, J. and Berg, H. C., Resurrection of the flagellar rotary motor near
zero load. *Proc Natl Acad Sci U S A* **105** (4), 1182 (2008).
- 289 Yuan, J., Branch, R. W., Hosu, B. G., and Berg, H. C., Adaptation at the
output of the chemotaxis signalling pathway. *Nature* **484** (7393), 233 (2012).
- 290 Zeke, A., Lukacs, M., Lim, W. A., and Remenyi, A., Scaffolds: interaction
platforms for cellular signalling circuits. *Trends Cell Biol* **19** (8), 364 (2009).
- 291 Zhou, Q., Ames, P., and Parkinson, J. S., Biphasic control logic of HAMP
domain signalling in the *Escherichia coli* serine chemoreceptor. *Mol*
Microbiol **80** (3), 596 (2011).

Summary

The chemotaxis signaling circuit that enables enteric bacteria to sense and respond to chemicals and physical changes in their environment is one of the best characterized signaling networks in biology. The detailed molecular knowledge about this system has enabled quantitative experimental and theoretical studies that have explained the characteristics of chemotaxis response, such as precise adaptation and high signal amplification. Many of the properties of the chemotactic signaling in bacteria are also observed in the more complex sensory systems of multicellular organisms. Thus, insights from studies of the bacterial chemotaxis system could facilitate the understanding of fundamental properties of sensory systems in biology.

In this thesis, the chemotactic signaling of enteric bacteria was investigated from a functional point of view. Quantitative experiments measuring the chemotactic signaling response of *Escherichia coli* and *Salmonella typhimurium* were used to characterize the properties of the receptor response and adaptation at the systems level. Behavioral strategies were predicted from the transfer functions of the signaling response and confirmed experimentally. The roles of previously uncharacterized chemotaxis proteins were explored using physiological measurements and quantitative imaging.

Physiological studies of sensory responses have highlighted that the threshold of response to a stimulus is proportional to the magnitude of the original stimulus: a property, known as Weber's law. However, Weber's law addresses only the instantaneous response to small step stimuli. In Chapter 2, we provide the first demonstration that an adaptive sensory system rescales the entire dynamics of its response to time-varying inputs. We show for the chemotaxis response of *E. coli* to α -methylaspartate (MeAsp) that the entire shape of the output depends only on the fold changes in the input and not on its absolute levels, a property recently described as fold-change detection (FCD). We used fluorescence resonance energy transfer (FRET) to probe this rescaling of the signaling response in *E. coli*, and we found two ranges of background concentrations, in which

Summary

FCD holds, i.e. “FCD regimes”. The amplitude of the response differed between the two regimes; however, the adaptation timescale was invariant. We identified three sufficient conditions for FCD in bacterial chemotaxis. FCD was also observed for the distributions of *E. coli* swimming in spatial gradients of MeAsp created in microfluidic platforms.

Input-output relationships of the chemotaxis response have been thoroughly characterized in the model strain *E. coli* K12. FRET-based studies showed high receptor sensitivity and cooperativity and explored the properties of the adaptation system, using time-varying stimuli. However, even within the species *E. coli*, there is a great variety in the chemotactic performance between different strains, as we showed in Appendix B. In Chapter 3 we performed a detailed comparison of the physiological response of *E. coli* K12 and the closely related species *S. typhimurium* LT2 that share homologous chemotactic networks. We revealed that adaptation to MeAsp in *S. typhimurium* is three-fold faster and the apparent cooperativity of the receptor response is three-fold lower than that of *E. coli*. Moreover, the response-rescaling properties differed between the two species: in contrast to *E. coli*, *S. typhimurium* showed a single FCD regime. Using the obtained parameters for the chemotactic signaling transfer functions of both species, we explained the differences in the sensitivity modulation of the response.

In Chapter 4 we study two chemoreceptors of *S. typhimurium*, McpB and McpC, with hitherto unknown functions. The radial migration in soft-agar plates suggested that these receptors sense the amino acid cysteine and its oxidized dimeric form cystine as chemoattractants. However, our FRET measurements of the chemotactic kinase response showed that cells expressing only McpB / C chemoreceptors respond only to the oxidized form, and the response was unexpectedly in the repellent direction. Furthermore, we showed that the reduced form, cysteine, is an attractant sensed by Tsr and Tar. We showed that the adaptation to both cystine and cysteine is methylation dependent, and the adaptation to cystine is incomplete, i.e. imperfect adaptation. We discuss that cystine-cysteine interconversion and imperfect adaptation to cystine could explain the attractant-like responses to both components in the soft-agar assays. We explore the dose-response dependence of the opposite responses to

cystine / cysteine redox pair in Appendix A. We observed linear scaling of the magnitude of the response to cystine with the logarithm of cystine concentration. Unexpectedly, we detected McpB / C independent responses to cystine in *S. typhimurium* LT2, which might represent a redox response. In Chapter 6, we present our preliminary results on testing the responses of *S. typhimurium* to redox gradients.

Another chemotaxis protein with previously uncharacterized function in *S. typhimurium* is CheV: a hybrid protein consisting of a scaffolding domain and a phosphorylatable receiver domain. CheV plays a role in receptor-kinase scaffolding and adaptation to chemoeffectors in some bacterial species. The distinctive phenotype of knocking out *cheV* in *S. typhimurium* strains incapable of methylation-dependent adaptation suggested that CheV has a function in *S. typhimurium*'s chemotactic response. Our FRET measurements presented in Chapter 5 revealed methylation-independent partial adaptation to MeAsp, which is CheV-dependent. To understand the mechanistic origin of this partial adaptation, we performed quantitative image analysis of receptor clusters and showed that the number of detectable clusters decreases in *cheV* knockout cells. In particular there are less clusters that are not localized at the poles, *i.e.* lateral clusters, in the *cheV* knockout cells. We speculate that a phosphorylation-dependent feedback on the receptor cluster stability might explain the role of CheV in *S. typhimurium*.

We explored another phosphorylation-dependent feedback mechanism: the negative feedback loop introduced by phosphorylation of the methyltransferase CheB in *E. coli* chemotaxis in Appendix C. Using FRET, we characterized the adaptation kinetics of genetically modified cells with disrupted CheB phosphorylation site. We showed that the strong nonlinearity in the transfer function characterizing the rate of change of methylation as a function of the kinase activity could be a consequence of the phosphorylation feedback on CheB activity.

In summary, we have studied the input-output relationships of the chemotaxis response in *E. coli* and *S. typhimurium* using *in vivo* experiments. We have demonstrated the fold-change detection strategy in both species at both the signaling and behavioral levels. We have shown differences in the chemotactic performance of bacteria with homologous chemotaxis

Summary

networks, and explained the observed differences in terms of the underlying control physiology. We have used the existing experimental tools to probe the functions of uncharacterized chemotaxis components. Future functional studies of signaling responses could further advance our understanding how biological systems are designed.

Samenvatting

(Translated in Dutch by Johannes Keegstra)

Het chemotaxis netwerk is het systeem welke bacterien in staat stelt fysische en chemische veranderingen omgeving waar te nemen en op deze te reageren. Het is een van de best gekarakteriseerde signaalnetwerken in de biologie. De gedetailleerde kennis van dit systeem op moleculair niveau heeft kwantitatief onderzoek mogelijk gemaakt, zowel theoretisch als experimenteel. Dit onderzoek heeft geleid tot een uitgebreide karakterisatie van het chemotaxis systeem, waaronder het effect van volledige aanpassing en de hoge signaalversterking. Veel van de eigenschappen van het chemotaxis systeem in bacterien spelen ook een rol bij complexere sensorische systemen bij meercellige organismen. Zo kan inzicht uit studies van de bacteriele chemotaxis het begrip van fundamentele eigenschappen van sensorische systemen binnen de biologie vergemakkelijken.

In het onderzoek beschreven in dit proefschrift werd het chemotaxis systeem van bacterien onderzocht vanuit het perspectief van functionaliteit. Metingen aan de chemotaxis respons van *Escherichia coli* en *Salmonella typhimurium* werden gebruikt om de eigenschappen van de receptorrespons en -aanpassing te karakteriseren op het niveau van de informatieverwerking. Uit de overdrachtsfuncties van de signaalverwerking werden strategieën van de bacterien voorspeld en met behulp van experimenten werden deze voorspellingen bevestigd. De functie van eerder ongekaracteriseerde eiwitten van het chemotaxis systeem werden onderzocht met behulp van fysiologische metingen en kwantitatieve beeldverwerking.

Fysiologische studies van zintuiglijke reacties geven aan dat de drempelwaarde van de reactie op een stimulus evenredig is met de grootte van de oorspronkelijke stimulus, wat bekend staat als de wet van Weber. Echter, de wet van Weber beschrijft de respons van een systeem op stimuli met een kleine stapgrootte op een bepaald tijdstip. In Hoofdstuk 2 tonen wij voor het eerst aan dat een adaptief zintuiglijk systeem voor het gehele

Samenvatting

tijdsinterval van zijn reactie hetingangssignaal herschaalt. We laten zien dat de chemotaxis respons van *E. coli* op α -methylaspartate (MeAsp) dat het uitgangssignaal gelijk is voor veelvouden van hetzelfde ingangssignaal en dus niet afhankelijk is van het absolute niveau, een eigenschap welke recent beschreven is als detectie veelvoudverandering (Fold-change detection - FCD). We gebruikten een fysische techniek gebaseerd op energieoverdracht door resonantie van verschillende fluorescerende deeltjes (Fluorescence resonance energy transfer - FRET) om de herschaling van het ingangssignaal in *E. coli* te bestuderen, en we hebben twee reeksen van achtergrondconcentraties gevonden voor waar FCD geldt, zogenaamde "FCD regimes". De amplitude van de respons verschilde tussen de twee regimes, maar de tijdschaal van de aanpassing was hetzelfde. We identificeerden drie voldoende voorwaarden voor FCD in bacteriële chemotaxis. FCD werd ook waargenomen voor de verdelingen van zwemmende *E. coli* in de ruimtelijke gradiënten van MeAsp welke tot stand kwamen in vloeistofcellen op micrometerschaal.

Ingang-uitgangs relaties van de chemotaxis respons zijn grondig gekarakteriseerd in de modelstam *E. coli* K12. Onderzoek met FRET toonde een hoge gevoeligheid van, alsmede een hoge cooperativiteit tussen, de receptoren. Ook de eigenschappen van het aanpassingssysteem werden onderzocht, met behulp van de tijd variërende stimuli. Echter, zelfs binnen de soort *E. coli* is er een grote variatie in de chemotactische prestaties van verschillende stammen, zoals is te zien in Appendix B. In Hoofdstuk 3 maken we een gedetailleerde vergelijking van de fysiologische respons van *E. coli* K12 en de nauw verwante species *S. typhimurium* LT2, welke homologe chemotactische netwerken bezitten. Het bleek dat de aanpassing aan MeAsp in *S. typhimurium* driemaal sneller is en de gemeten cooperativiteit van de receptor respons driemaal lager dan die van *E. coli*. Bovendien is de respons herschaling verschillend tussen de twee soorten: in tegenstelling tot *E. coli*, toonde *S. typhimurium* een FCD regime. Met behulp van de verkregen parameters voor de signaaloverdrachtsfuncties van beide soorten konden we de verschillen in de modulatie van de gevoeligheid van de reactie verklaren.

In Hoofdstuk 4 bestuderen we twee chemoreceptors van *S. typhimurium*, McpB en McpC, met tot nu toe onbekende functies. Radiale

migratie in halfzachte agar platen gesuggereert dat deze receptoren reageren op het aminozuur cysteine en zijn geoxideerde dimeer cystine als stoffen met een aantrekkende functie. Onze FRET metingen van de chemotactische kinase reactie toonden echter aan dat cellen met alleen McpB / C chemoreceptors slechts reageren op de geoxideerde vorm, en de respons was onverwacht in de afstotende richting. Verder toonden we aan dat de gereduceerde vorm, cysteine, als een aantrekkende stof wordt waargenomen door Tsr en Tar. We toonden aan dat de aanpassing aan zowel cystine en cysteine methylering afhankelijk is, en dat de aanpassing aan cystine onvolledig is, dat wil zeggen dat de adaptatie het signaal niet terugbrengt naar het niveau voor de stimulus. We bespreken dat cysteine-cysteine omzetting en de onvolledige aanpassing aan cystine de aantrekkend-achtige reacties aan beide componenten in de halfzachte agar assays kunnen uitleggen. De dosis-respons afhankelijkheid van de tegenovergestelde reacties op het cystine / cysteine redoxsysteem wordt besproken in Appendix A. We observeerden lineaire schaling van de omvang van de respons op cystine met de logaritme van cystine concentratie. Onverwacht, we ontdekten enkele McpB / C onafhankelijke reacties op cystine in *S. typhimurium* LT2, welke een redox respons zou kunnen representeren. In Hoofdstuk 6 presenteren wij onze voorlopige resultaten over het testen van de reacties van *S. typhimurium* aan redox gradienten.

Een ander chemotaxis eiwit zonder eerder gekenmerkte functie *S. typhimurium* is CheV: een hybride eiwit dat bestaat uit een structuurdomein en een fosforyleerbare ontvangdomein. CheV speelt een rol in receptor-kinase structuur en aanpassing aan chemo-effectoren in sommige bacteriesoorten. Het kenmerkende fenotype van cellen zonder het *cheV* gen in stammen van *S. typhimurium* welke niet in staat waren tot methylering suggereert dat CheV een andere functie heeft binnen het chemotaxis netwerk van *S. typhimurium*'s. Onze FRET metingen gepresenteerd in Hoofdstuk 5 toonden gedeeltelijke aanpassing aan MeAsp onafhankelijk van methylering en afhankelijk van CheV. Voor een mechanistisch begrip van deze gedeeltelijke aanpassing voerden we een kwantitatieve beeldanalyse van de receptorclusters uit, en daarmee toonden we aan dat het aantal detecteerbare clusters afneemt bij cellen

Samenvatting

waarin het *cheV* gen is verwijderd. Er is met name minder laterale clusters, dwz clusters die niet gelokaliseerd bij de polen van de bacterie, in de cellen zonder het *cheV* gen. We speculeren dat een fosforylatie-afhankelijke terugkoppeling op de stabiliteit van de receptorclusters de rol van CheV bij *S. typhimurium* zou kunnen verklaren.

We verkenden een andere fosforylatie-afhankelijke terugkoppelingsmechanisme: de negatieve terugkoppeling geïntroduceerd door fosforylering van de methylesterase CheB in *E. coli* chemotaxis, hetgeen is beschreven in Appendix C. Met behulp van FRET hebben we de adaptatiekinetica van cellen met genetisch gemodificeerde CheB fosforylatieposities onderzocht. We hebben laten zien dat de sterke niet-lineariteit in de overdrachtsfunctie die de methylatiesnelheid als een functie van de kinase activiteit een gevolg zou kunnen zijn van de fosforylatie terugkoppeling van CheB activiteit.

Samengevat hebben we de overdrachtsfunctie van het chemotaxis systeem in *E. coli* en *S. typhimurium* met *in vivo* experimenten onderzocht. We hebben de FCD eigenschap aangetoond in zowel soorten op zowel de signalering en gedragsniveau. We hebben verschillen aangetoond in de functionaliteit van chemotaxis netwerken in homologe bacteriën, en legde de waargenomen verschillen in de onderliggende fysiologie. We hebben bestaande experimentele technieken gebruikt om de functies van niet eerder gekenmerkte chemotaxis componenten in kaart te brengen. Toekomstige studies van signaalverwerking in functioneel perspectief kunnen leiden tot een beter begrip van de vraag hoe biologische systemen zijn ontworpen.

Acknowledgements

I find it hard to believe that it is my time to thank to all the people that changed my perception for science and life in my way towards my PhD-dream. I certainly cannot be exhaustive, thus I would like first to thank to all that I are not mentioned below but played a role in my journey.

I cannot be grateful enough to Baba. She triggered my life-long, I believe, love to biology, which turned into my hobby and profession. Dqdo, the German-summer together were my first touch to experimental biology. Polki, you ideated the two-Dutch-years, who would imagine that they will expand into six. Mitko, we make it together on the way upwards. Nadejda, keep being a good follower. Rodi, you showed me what is to be a scientist. Darq, Nicki, Danche – thank you for being with me all that time.

It was fascinating to be a part of the BF and BDZP crowds. From watching migration in the Bulgarian sky, to watching migration under the microscope, I truly enjoyed being surrounded by people, sharing the same fascination to life. Dali, Iva, Mila, Yana, all the people that stayed with me throughout the years – thank you for the good times.

Ewa, you have been next to me from my start in Leiden. You have been an example and a guide for me. Thomas, your guidance and advice definitely had a big impact to my decision to continue with biophysics, and to join AMOLF. Freek, I enjoyed my time in the Leiden-team and in the Dicty world, learning how to become a scientist. Erika and Wiestke, I have enjoyed our visits in Leiden and in Amsterdam. Marileen, you were the first to show me AMOLF.

Tom, your fascination for science is contagious. I have learned a ton from you. It has been an invaluable experience to participate in building your lab, and it has been truly inspirational to navigate and observe the bacteria in action.

Michel, you made the lab a happier place. Francois, it has been great to share the joy and frustration of experimental life with you. Simone, you structured the lab chaos. Quyen, it was a memorable Mixer-summer. Katja and Sebastian, you injected life in our group. Pieter and Istvan, I was fascinated to see you entering the world of science. Bob, I learned from you

Acknowledgements

more than you learned from me. Stephen, I am impressed by your drive to create and develop. Johannes and Jacopo, I am glad to witness the new-lab generation – I am sure you will keep the lab spirit high.

My AMOLF-experiences expanded well beyond our group. From coffee breaks, lunches and Polder-times, to pre-submission dramas, complaints of the day and discussions of the meaning of life, I was lucky to have the AMOLFeers around me. The long hours in the office would never be so enjoyable without my officemates Alireza and Chris. Florian and Dimitry – keep the office atmosphere. The bacterial masters – Manjunatha, Alexandre, Marjon, Vanda – it was a privilege to have them to ask for advice, or just to share the joy of lab work. Feng, we have so many memories together. Ioana, I hope we will meet also in New York soon. Jeanette, I will remember the Saturday lab fun. Jose, I am looking forward to see each other on the other coast. Tomek, amazingly I have learned from you facts about my own country. Marjon, I miss your high-adrenaline spirit. Iza, your words were always wise. Pierre, Sophie, Filipe, Sarah, Philippe, Noreen, Maga, Andrew, Joris, Eva, Nils, Simona and many others – the good memories will last.

Sharing journal clubs with both Sander's and Pieter Rein's people, the discussions with Ron and Andras, working with Roman, Tanvir, and Filippo, Rasika and Mitch – all these interactions enriched me, I enjoyed seeing different points of view. The Cold Spring Harbor course was a turning point: I discovered the fun of genetics.

The MIT-time was memorable - great city, fantastic university, seminars, incredible people. I am grateful to Tom, Roman and Eduardo that they made it possible. Filippo, you were a great support in the lab-frustration times. I enjoyed also the meetings with, Vicente, Maja, and Abdulah, and working with the people from Roman's team. Thank you for sharing lab-resources Mike and Linda. Jane, it was great to share with you the Saturdays. Corinna, it was great to meet you and keep in touch. Eve, I remember our conversations. Françoise and Hans, it was a pleasure to be in your house. I have enjoyed the communication there and after. Giovanni, your reality talks changed my attitude to life. The time flight was an experience to remember. Dora, I felt at home with you.

Acknowledgements

Tomek, Sarah, Jose, and Eva – I am so happy that we are all graduating together. It was such a relief to share the thesis-creation hurdles with you, and also to celebrate with you our steps towards success. Thank you, Ioana and Feng, for joining me in the defense day.

Hearing the shape of a dream, explosions, random walks, bright green, merging day / night cycles, full of pictures, ups and downs - my AMOLF years were anything but boring. Without all the people in my life, I will most likely never be here. Now I am ready to follow my dreams – I am looking forward to the future.

Acknowledgements

Curriculum Vitae

Milena D. Lazova was born on October 29, 1984 in Sofia, Bulgaria. She obtained her secondary education at Sofia High School of Mathematics in 2003. In the same year she started her undergraduate studies in Molecular Biology at Sofia University. In August 2007 she moved to The Netherlands to start a Master's program in Molecular and Cellular Biology in Leiden University. Under the supervision of Dr. B. Ewa Snaar-Jagalska from Leiden Institute of Biology and Prof. Dr. Thomas Schmidt from Leiden Institute of Physics, she used single-molecule microscopy to study the G protein mobility in chemotactic social amoeba *Dictyostelium discoideum*. After graduating with honors, in May 2009 she joined FOM Institute AMOLF as the first PhD student in the group of Dr. Tom Shimizu. During the summer of 2012 she worked as a visiting student in the group of Prof. Dr. Roman Stocker at the Massachusetts Institute of Technology. Her research on chemotactic signaling and behavior of bacteria is presented in this thesis. Upon receipt of her PhD, Milena will investigate the control of bacterial replication cycle as a postdoctoral researcher with Prof. Dr. Alan Grossman at the Massachusetts Institute of Technology.

